UNIVERSITÉ DE NANTES

FACULTÉ DE MÉDECINE

ÉCOLE DOCTORALE BIOLOGIE-SANTÉ

Année 2015   N° attribué par la bibliothèque   11

Etude de Maladies du Rythme Cardiaque à l'aide de Cellules Souches Pluripotentes Induites

THÈSE DE DOCTORAT

Discipline : Biologie

Spécialité : Biologie des Organismes

Présentée

et soutenue publiquement par

Mariam JOUNI

Le 28 septembre 2015 devant le jury ci-dessous

Président :   M. Vincent PROBST, PU-PH, *Université de Nantes*

Rapporteurs   M. Stéphan HATEM, PU-PH, *Université Pierre et Marie Curie*

                          M. Marwan REFAAT, PU-PH, *Université Américaine de Beyrouth*

Examinateurs   M. Patrick BOIS, PU, *Université de Poitiers*

Directeur de thèse   Mme. Patricia LEMARCHAND, PU-PH, *Université de Nantes*

                          M. Kazem ZIBARA, PU, *Université Libanaise*

Co-Directeur de thèse   Mme. Nathalie GABORIT, CR2, *Université de Nantes*

Acknowledgments

First I would like to extend my sincere thanks to the jury members Drs Stéphane Hatem, Marwaan Refaat and Patrick Bois for their kind acceptance to be evaluators for this work. I would also like to thank Dr. Vincent Probst for agreeing to be the president of this jury.

I want to thank Professor Hervé Le Marec for welcoming me at the institute. Thank you for your time, your help and your important advices for the advance of this work.

I arrived at institut du thorax on 15th January 2013, three years have passed and I am at the end of my thesis. This thesis represents not only my work; it is the sum of contributions done by many people, a work that was launched before my arrival. I would like to thank everybody contributed to the accomplishment of this work, even those who I do not know.

I have been given a unique opportunity to be a part of institut du thorax. For my thesis director, Prof. Patricia Lemarchand, I would like to express my deepest gratitude. Thank you for trusting me throughout my thesis. Thank you for bringing me your support in the ups and downs both personal and professional. You taught me a lot, I am proud to have you as my thesis director.

For my Lebanese director, Prof. Kazem Zibara, there are a lot of things I want to thank you for. Thanks for your trust, your encouragement, your time, your advices and your passion. You taught me tons of things that I cannot even count. You were always there, in good and bad. Without you, things would be much harder. For my both directors, I am so thankful for the amazing chance you gave me!

Nathalie, my co-director, for everything you taught me, thanks! Thank you, for all the amazing funny time we spend, for the discussions that we had, for your support in ups and downs and for your advices. Thank you, for you believed in me; none of this work would be possible without you, it was a pleasure for me to work with such a kind person like you, I wish I would stay your PhD student for my whole life! But unfortunately this is not possible!! My precious amazing funniest co-director, thank you!

Flavien, Gildas and Isabelle, being a student in this lab gave me a great chance to meet amazing people like you. Flavien, I am so grateful for all your help, your time, your support, your amazing discussions and your kindness. You trusted me; you were always by my side, you taught me a lot, and the most important thing you were always there, in good and bad.

Table of Contents

List of Abbreviations

A

AIDS: acquired immunodeficiency syndrome

AKAP9: A-Kinase Anchor Protein 9

AP: action potential

ATP: adenosine triphosphate

AV: atrioventricular

B

BrS: Brugada syndrome

BMP4: Bone morphogenetic protein 4

C

CACNA1C: Calcium Channel, Voltage-Dependent, L Type, Alpha 1C Subunit

CaM: calmoduline

CaMKII: calmodulin-dependent protein kinase type II

cAMP: cyclic adenosine monophosphate

CASQ2: calsequestrin

CAV3: caveolin-3

cDNA: complementary deoxyribo nucleic acid

CMs: cardiomyocytes

cNBD: cyclic nucleotide binding domain

Cx43: connexin 43

D

DNA: deoxyribo nucleic acid

E

EB: embryoid body

ECG: electrocardiogram

Endo: Endocardial cells

Epi: Epicardial cells

ESC: embryonic stem cells

F

FGF2: Fibroblast Growth Factor 2

G

GFP: Green fluorescence protein

H

hERG: encoded human-ether-a-go-go-related gene

HIV: human immune deficiency virus

hiPS: human induced pluripotent stem cells

hiPS-CMs: human induced pluripotent stem cell-derived cardiomyocytes

I

$I_{Ca,L}$: inward depolarizing Ca^{2+} current (through L-type Ca^{2+} channels)

$I_{Ca,T}$ inward depolarizing Ca^{2+} current (through T-type Ca^{2+} channels)

I_f: inward-rectifier mixed Na^+ and K^+ funny current

I_{KACh}: The G-protein-gated K^+ current

I_{KATP}: ATP-sensitive K^+ current

I_{K1}: inward-rectifier K^+ current

I_{Kr}: rapid component of the delayed-rectifier K^+ current

I_{Ks}: slow component of the delayed-rectifier K^+ current

I_{Na}: inward depolarizing sodium current

iPS: induced pluripotent stem cells

I_{to}: transient outward potassium current

K

KCNE1: Potassium Channel, Voltage Gated Subfamily E Regulatory Beta Subunit 1

KCNE2: Potassium Channel, Voltage Gated Subfamily E Regulatory Beta Subunit 2

KCNH1: Potassium voltage-gated channel subfamily H member 1

KCNH2: Potassium voltage-gated channel subfamily H member 2

KCNJ1: Potassium Channel, Inwardly Rectifying Subfamily J, Member 1

KCNJ5: Potassium Channel, Inwardly Rectifying Subfamily J, Member 2

KCNQ1: potassium channel, voltage gated KQT-like subfamily Q, member 1

L

LQT: long QT syndrome

LQT-1: long QT syndrome type 1

LQT-2: long QT syndrome type 2

LQT-3: long QT syndrome type 3

LTR: long terminal repeat

M

MHC: myosin heavy chain

MOG1: Ran guanine nucleotide release factor

mRNA: messenger ribonucleic acid

N

Na^+/K^+/ATPase: Sodium potassium pump

NCX: sodium-calcium exchanger

P

PAS: Per-Arnt-Sim domain

PKC: protein kinase C

PLN: cardiac phospholamban

PVT: polymorphic ventricular tachycardia

Q

QTc: corrected QT

R

RNA: ribonucleic acid

RVOT: right ventricular outflow tract

RyR: ryanodine receptor

RyR2: ryanodine receptor type II

S

SA: sinoatrial

SCD: sudden cardiac death

SCN5A: sodium channel, voltage gated, type V alpha subunit

SCN4B: Sodium Channel, Voltage Gated, Type IV Beta Subunit

SERCA: sarco/endoplasmic reticulum calcium-ATPase

SNP: single nucleotide polymorphism

SNTA1: Syntrophin, Alpha 1

SOICR: store overload-induced Ca^{2+} release

SR: sarcoplasmic reticulum

T

Tat: trans-activator of transcription

TdP: torsades de pointes

TGFβ: Transforming Growth Factor-Beta

V

VF: ventricular fibrillation

W

WNT: Wingless/Integrated

List of Figures

List of Tables

I. INTRODUCTION

I – Cardiac cycle within the heart

Ion channels are essential membrane proteins found in all cell types, including cardiomyocytes. By allowing the regulated flux of ions across the plasma membrane, these ion channels produce electrical currents and play major roles in cell function (Abriel and Zaklyazminskaya, 2013). In the heart, cardiac ionic channels and the currents they generate are essential for the ability of the heart to coordinate cardiac contraction to distribute blood efficiently throughout the body, which also depends on the coordination of nodal, atrial, and ventricular cardiomyocytes.

In healthy individuals, the cardiac cycle is initiated by the spontaneous depolarization of specialized pacemaker cells in the sinoatrial node located within the right atrium. Electrical coupling via intercellular gap junctions allows the rapid conduction of depolarizing electrical impulses to nearby atrial cardiomyocytes, which triggers the excitation and subsequent contraction of the atria that is reflected by the P-wave on the surface electrocardiogram (ECG). The electrical impulse is then conducted from the atria to the atrioventricular node which, after a brief delay, propagates through the Purkinje fibers to the apex of the heart and then into the cardiomyocytes of the right and left ventricles. The excitation of ventricular cardiomyocytes results in the contraction of the ventricles and is represented by the QRS complex on the surface ECG and their repolarization is represented by the T wave (Giudicessi and Ackerman, 2012) (Figure 1).
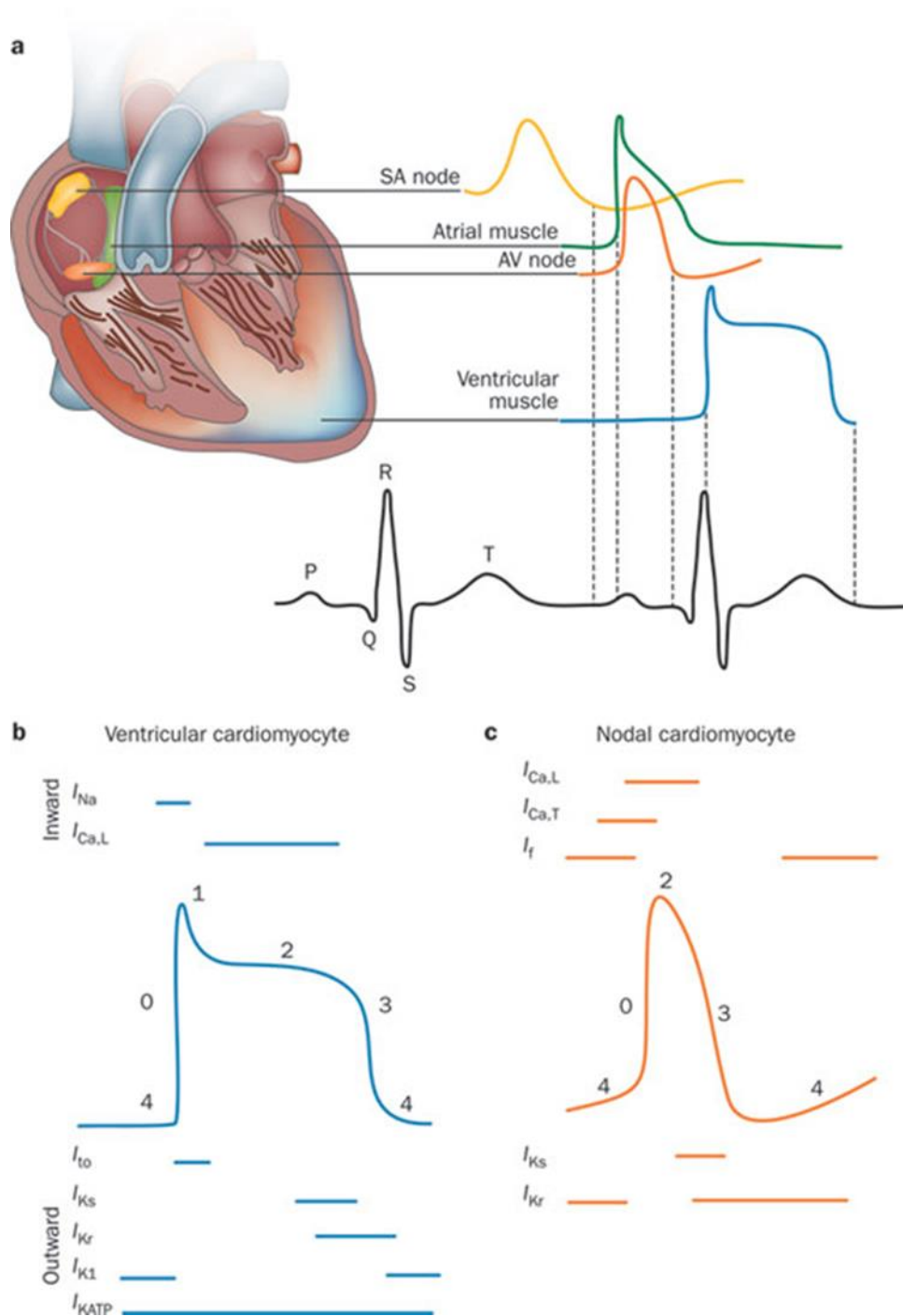
Figure 1: Normal electrical activity of the heart. a. Schematic representation of the cardiac conduction system and the correlation between the action potentials of cardiomyocytes in distinct regions of the heart and the surface electrocardiogram. b. Temporal relationship between the inward and outward currents that contribute to the distinct phases (0-4) of the ventricular cardiomyocyte action potential. c. Temporal relationship between the inward and outward currents that contribute to the distinct phases (0-4) of the nodal cardiomyocyte action potential (which lacks a defined phase 1). Abbreviations: AV, atrioventricular; $I_{Ca,L}$, inward depolarizing Ca^{2+} current (through L-type Ca^{2+} channels); $I_{Ca,T}$, inward depolarizing Ca^{2+} current (through T-type Ca^{2+} channels); I_f, inward-rectifier mixed Na^+ and K^+ 'funny' current; I_{K1}, inward-rectifier K^+ current; I_{KATP}, ATP-sensitive K^+ current; I_{Kr}, rapid component of the delayed-rectifier K^+ current; I_{Ks}, slow component of the delayed-rectifier K^+ current; I_{Na}, inward depolarizing Na^+ current; I_{to}, transient outward K^+ current; SA, sinoatrial (Giudicessi and Ackerman, 2012).

At the cellular level, the electrical impulses that drive the cardiac cycle are dependent on the generation of action potentials within individual cardiomyocytes, via the sequential opening and closing of ion channels that conduct the depolarizing inward (Na^+ and Ca^{2+}) and repolarizing outward (K^+) currents (Figure 2, Figure 3) (Giudicessi and Ackerman, 2012).
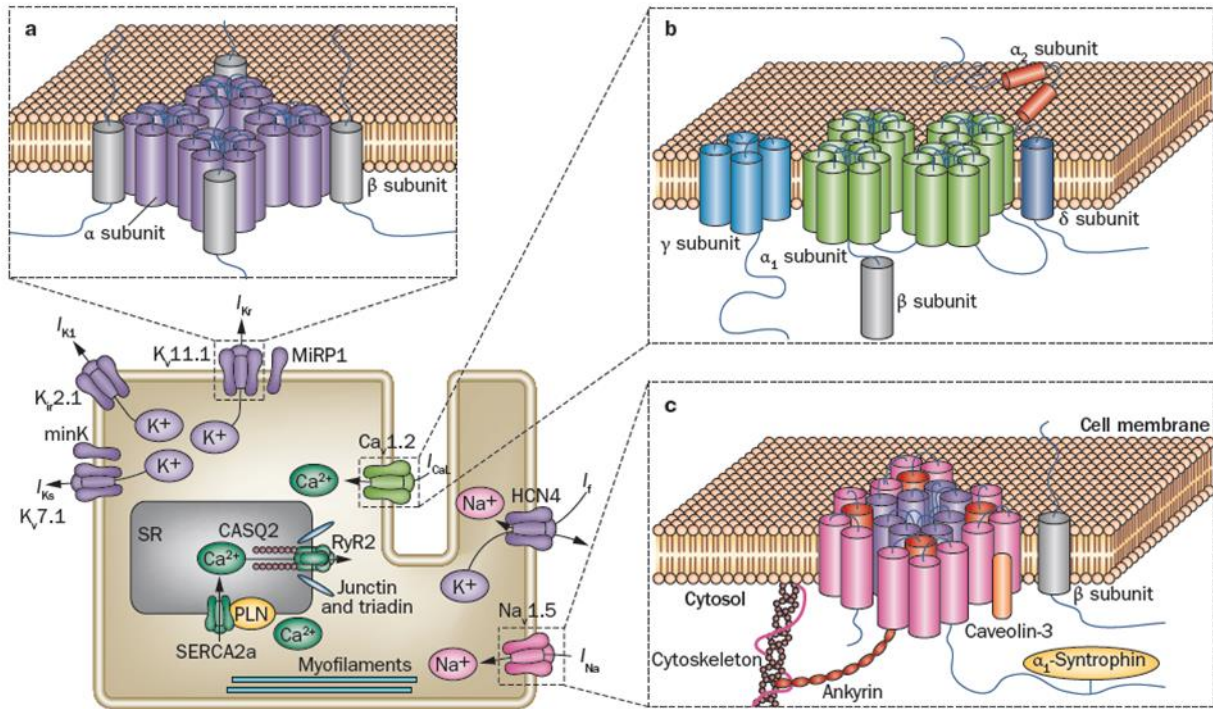
Figure 2: The main channels found in the heart. a. Potassium (I_{Kr}), b. calcium (I_{CaL}), and c. sodium (I_{Na}) channel structures and subunits are shown. Abbreviations: CASQ2, calsequentrin-2; PLN, cardiac phospholamban; RyR2, ryanodine receptor 2; SERCA2a, sarcoplasmic/endoplasmic reticulum calcium ATPase 2a; SR, sarcoplasmic reticulum (Wilde and Behr, 2013).
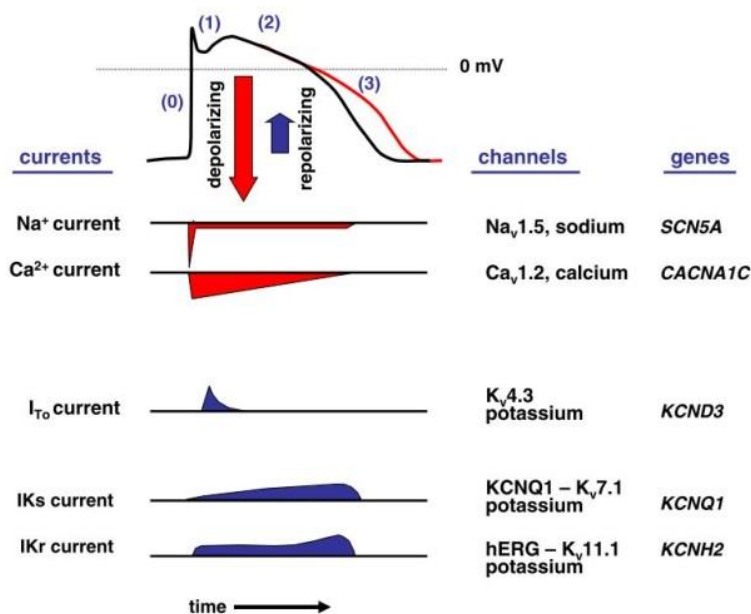
Figure 3: Schematic representation of the main ionic currents responsible for the different phases of the cardiac action potential. Red (depolarizing) and blue (repolarizing) shapes indicate relative current amplitude, duration and direction (Abriel and Zaklyazminskaya, 2013).

Mutations in genes encoding cardiac ion channel subunits or proteins that interact with and regulate these channels leads to channelopathies. Dysfunctional ion channels cause abnormalities in the electrical properties of the heart, resulting in arrhythmia (Marsman et al., 2014).

II – Cardiac Arrhythmic Diseases

Cardiac arrhythmias are a group of primary electrical disorders associated with a risk of sudden cardiac death. These include long QT syndrome (LQT) and Brugada syndrome (BrS). These electrical disorders are often characterized by specific ECG abnormalities either at baseline or during particular conditions, such as exercise (LQT), fever or pharmacological challenge (BrS) (Marsman et al., 2014).

II.1. – Long QT syndrome

LQT is the most investigated primary cardiac rhythm disorder. A genetic defect can be identified in ~70% of definitive LQT patients (Bhuiyan et al., 2013). A rapidly changing balance of inward and outward ionic currents through ionic channels and transporters produces the prototypical cardiac action potential (AP) demonstrated in Figure 4. LQT has been generally divided into congenital or acquired types. Congenital LQT occurs when a genetic defect tips the balance of inward and outward currents to delay repolarization of the ventricular action potential. The resulting increase in action potential duration is reflected by a prolongation of the QT interval on the surface electrocardiogram (Marsman et al., 2014) (Kamp, 2011). On the other hand, acquired LQT is most commonly due medications which are known to prolong the QTc (Puri et al., 2009). An example of acquired LQT is observed in HIV/AIDS infected patients that could be directly due to the presence of the virus and/or to the treatment. In the next part congenital LQT will be further described, and following that, acquired LQT in the case of HIV/AIDS patients, with the possible mechanisms underlying the cardiac complications will be further discussed.
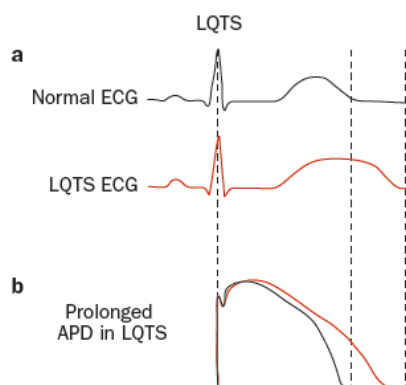
Figure 4: Pathophysiological mechanisms of K-channel-mediated arrhythmias at the ionic and cellular level. a. Schematic representation of a normal ECG (black) and typical ECGs for potentials (black) and tracings that display epicardial action potential prolongation in LQT patients. b. Tracings of normal ventricular action potential (Giudicessi and Ackerman, 2012).

II.1.1 – Congenital LQT

II.1.1.1 – Clinical presentation

Patients with all forms of LQT are predisposed to the ventricular tachyarrhythmia, torsades de pointes (TdP) leading to recurrent syncope, or sudden cardiac death (SCD). In many instances, syncope or sudden death could be the first and the only manifestation. LQT affects an estimated 1 in 2,000 people world-wide (Bhuiyan et al., 2013). Mutations in at least 12 genes encoding different ion channels or channel-associated proteins have been linked to congenital LQT. These mutations can cause a gain of function, which increases depolarizing currents, or a loss of function, leading to reduced repolarizing currents (Kamp, 2011).

II.1.1.2 – Cellular pathophysiology

LQT is the result of delayed repolarization of ventricular cells due to either a reduction in repolarizing (outward) currents or an increase in depolarizing (inward) currents (Lu and Kass, 2010). Loss-of-function mutations in the genes coding for K^+ channel subunits, and gain-of-function mutations in the genes coding for Na^+ and Ca^{2+} channel subunits and their regulatory proteins have been found in patients with congenital LQT. The mechanisms by which ion channel mutations lead to a loss or gain of function are very diverse. Mutations in K^+ channel gene subunits have been shown to either decrease the number of channels at the cardiac cell surface, through the alteration of trafficking, or reduce the K^+ current via mutation-induced alterations in the intrinsic biophysical properties of the K^+ channels (Delisle et al., 2004). For the Nav1.5 channel, most of the mutations have been shown to increase the late sodium current due to late channel re-openings or bursts (Terrenoire et al., 2007), which results in delayed AP repolarization (Abriel and Zaklyazminskaya, 2013).

II.1.1.3 – Inheritance and molecular genetics

Inheritance can be oligogenic in approximately 5% of patients. Incomplete penetrance is common, and up to 40% of genetic carriers have a normal corrected QT (QTc) interval. The three most common forms of LQT are long QT syndrome type 1 (LQT-1), long QT syndrome type 2 (LQT-2), and long QT syndrome type 3 (LQT-3), each of which is caused by genetic mutations in a different ion channel. These LQT subtypes are typically associated with particular symptoms; however, the symptoms associated with one subtype are sometimes seen in patients with other forms of LQT. Loss-of-function mutations in α-subunit of the slow rectifier current (I_{Ks}), encoded by the *KCNQ1* gene, cause LQT-1. LQT-2 arises from mutations in *KCNH2* that cause loss of function in α- subunit of the rapid rectifier current

(I_{Kr}). Trafficking defects are more common in LQT-2 than in LQT-1. Mutations in *SCN5A* cause LQT-3 by a gain of function that result in increased late sodium current. Mutations in genes encoding ion channel β-subunits and channel-interacting proteins can also prolong repolarization by causing loss of function in I_{Kr} or I_{Ks}, or gain of function in I_{Na} (Wilde and Behr, 2013). Mutations in different ion channels or channel-associated proteins linked to congenital LQT are summarized in Table 1.

Table 1: Genetic basis of congenital long-QT syndromes (Sinnecker et al., 2013).

Syndrome	Affected gene	Gene Product	Known functions of the gene
LQT-1	*KCNQ1*	Kv7.1 α (KVLQT1)	α- subunit of sodium channel for I_{Ks}
LQT-2	*KCNH2*	Kv11.1(hERG)	α- subunit of sodium channel for I_{Kr}
LQT-3	*SCN5A*	Nav1.5 α	α- subunit of sodium channel for I_{Na}
LQT-4	*ANK2*	Ankyrin-B	Adaptor protein involved in membrane targeting of sodium/potassium ATPase and sodium/calcium exchanger
LQT-5	*KCNE1*	MinK β	β- subunit of sodium channel for I_{Ks}
LQT-6	*KCNE2*	MiRP1 B	β- subunit of sodium channel for I_{Kr}
LQT-7	*KCNJ1*	Kir2.1 α	α- subunit of sodium channel for I_{K1}
LQT-8	*CACNA1C*	Cav1.2 a_{1c}	α- subunit of sodium channel for $I_{Ca,L}$
LQT-9	*CAV3*	Caveolin-3	Membrane protein presumably binding to sodium channels
LQT-10	*SCN4B*	Nav1.5 β4	β- subunit of sodium channel for I_{Na}
LQT-11	*AKAP9*	YOTIAO (AKAP9)	A-kinase anchoring protein mediating regulation of I_{Ks} by protein kinase A
LQT-12	*SNTA1*	Syntrophin- $α_1$	Cytoskeletal protein interacting with channel responsible for I_{Na}
LQT-13	*KCNJ5*	Kir3.4 (GIRK4)	Subunit channel responsible for I_{KACh}
LQT-14	*CALM1*	Calmodulin-1	calcium binding protein which is one of the four subunits of phosphorylase kinase
LQT-15	*CALM2*	Calmodulin-2	calcium binding protein which is one of the four subunits of phosphorylase kinase

During the thesis I focused on LQT-2 study. As mentioned before, LQT-2 is caused by loss-of-function mutations in the *KCNH2* encoded human-ether-a-go-go-related gene K^+ channel 1 (hERG1 or Kv11.1) and is responsible for an estimated 25-30% of all LQT cases. The assembly of four full-length hERG1a α-subunits, or a combination of hERG1a and the shorter, alternatively spliced hERG1b isoform, form the tetramer Kv11.1 channel that conducts I_{Kr} (Figure 5). This current is differentiated from other K^+ currents by the unique structural features of the inner mouth of its channel pore that leave the channel prone to

blockade by an array of drugs, leading to acquired, drug-induced LQT (Giudicessi and Ackerman, 2012).
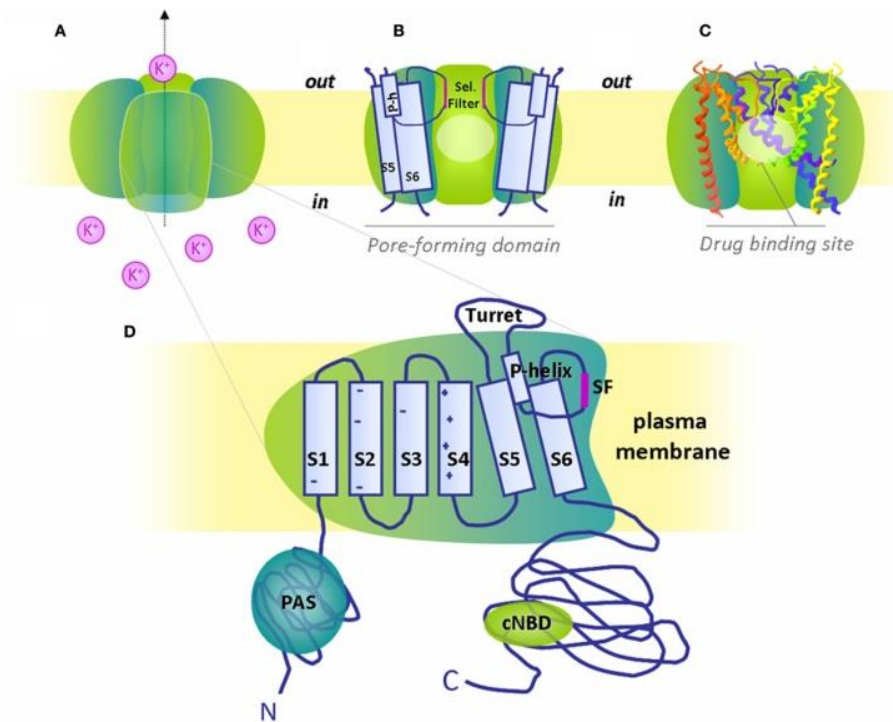
Figure 5: The hERG1 channel structure and putative binding region for blocking drugs. A. Schematized hERG1 tetramer channel at the plasma membrane and B. pore-forming region in schematic and C. ribbon representation D. Magnification of one α-subunit with six trans membrane domains (S1-S6), S5-P linker or turret loop, pore-helix (P-helix) and selectivity filter (SF). Both N- and C-termini are intracellular with respectively identified Per-Arnt-Sim (PAS) domain and cyclic nucleotide binding domain (cNBD) (Grilo et al., 2010)

KCNH2 genes encodes for the α-subunit of the Kv11.1 channel that generates the rapid rectifier current (I_{Kr}). Kv11.1 channels can exist in closed, open, or inactivated states (Figure 6). The inactivation process of Kv11.1 channels, however, exhibits a number of unusual features. Most notably, the kinetics of inactivation is much more rapid than the kinetics of activation, and second, the inactivation process is voltage-dependent. This unique combination of properties underlies the physiological role I_{kr} plays in cardiac repolarization by its disproportionately rapid rate of inactivation compared with its activation (Vandenberg et al., 2012).
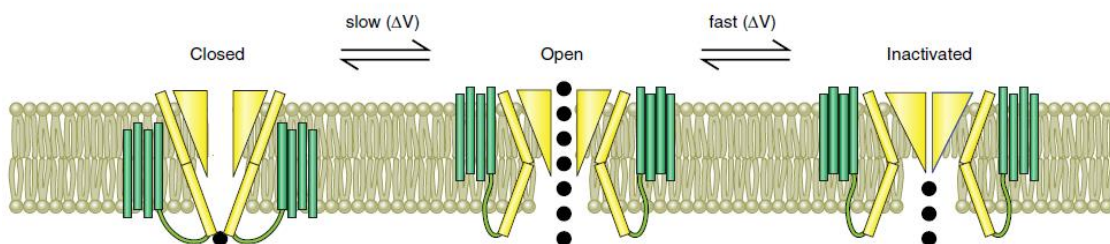
Figure 6: Gating of Kv11.1 channels. Kv11.1 channels can exist in closed, open, or inactivated states. Transitions between them are voltage dependent, with the transition between the closed and open states being slower than transitions between open and inactivated states (Vandenberg et al., 2012).

The functional characterization of a small percentage of known *KCNH2* mutations has elucidated multiple mechanisms responsible for I_{Kr} loss-of-function in LQT-2, including nonsense-mediated decay, defective Kv11.1 protein synthesis, impaired Kv11.1 protein trafficking, and kinetic alterations in channel gating and K^+ selectivity or K^+ permeation. Defective Kv11.1 protein trafficking, which encompasses defective protein folding, retention in the endoplasmic reticulum, and disrupted trafficking to the Golgi apparatus or to the cell surface represents the dominant molecular mechanism in LQT-2 and is thought to underlie the functional consequences of an estimated 80-90% of *KCNH2* missense mutations (Giudicessi and Ackerman, 2012).

II.1.2 – Acquired LQT-2 in HIV/AIDS patients

Incidence of cardiovascular events has been shown to be increased in AIDS patients, including QT prolongation (Reinsch et al., 2009). Several studies have been done in order to investigate the pathological QT prolongation observed in HIV patients, and to determine the origin of this pathological condition.

LQT may be directly due to the presence of the virus and/or to the treatment. On one hand, various drugs that are currently prescribed to HIV-infected patients, have also been associated with a QT prolongation, such as macrolides, pentamidine, azole antifungals fluoroquinolones (Fantoni et al., 2001), and methadone (Vallecillo et al., 2013). Thus, many drugs and combinations of drugs could be potential triggers of LQT through the inhibition of a major cardiac repolarizing current I_{Kr}, conducted by the voltage gated potassium channel hERG (Haverkamp et al., 2000). On the other hand, a clinical study suggests that QT prolongation is correlated to the duration of the infection rather than to the anti-HIV treatment, in particular protease inhibitors (Charbit et al., 2009). In addition, another study shows that among 42 HIV patients, 9 presented with QTc prolongation in absence of any treatment or electrolyte abnormality (Kocheril et al., 1997). In addition, several works using animal models suggested a rather direct implication of the virus in the long QT syndrome. A mouse model expressing the whole HIV-1 genome showed prolonged cardiac repolarization and decreased repolarizing potassium currents, in absence of pharmacological treatment (Hanna et al., 1998) (Brouillette et al., 2007). However, mice are not the most appropriate models to study LQT syndrome since molecular entities conducting repolarizing potassium currents are different from human (Nerbonne, 2004).

Tat, one of the 19 proteins encoded by the virus, is a major regulator of HIV virus replication; it acts as a trans-activator of viral transcription, and has many other effects. This 86 to 101 amino-acid protein is massively secreted by infected cells (Rayne et al., 2010), and serum Tat concentration can reach hundreds of ng/ml in patients (Poggi et al., 2004). Noteworthy, serum levels of Tat remain high in treated patients, which could explain the lack of correlation between LQT and antiretroviral therapies (Poggi et al., 2004). From the serum, Tat enters various cell types and acts as a viral toxin that triggers various cell responses (Debaisieux et al., 2012). Ventricular cardiomyocytes are potentially one of the targets, but this remains to be tested in human cells. In the guinea pig, Tat has been shown to prolong the action potential of ventricular cardiomyocytes (Bai et al., 2011) through a reduction in the hERG associated I_{Kr} current (Sanguinetti et al., 1995). Furthermore, Bai et al. showed that incubating HEK293 cells stably expressing hERG channels, with Tat protein for 24 hrs. led to a decrease in the hERG protein level combined with a decrease in the generated current. In addition, Tat also promotes bradycardia as observed in a rat model (Brailoiu et al., 2014). This bradycardia may be related to the dysregulation of the autonomic nervous system, as observed in some HIV patients (Chow et al., 2011), which may. Such dysautonomia favors LQT (Villa et al., 1995). Thus, Tat protein is a part of several arrhythmic mechanisms involving I_{Kr} and changes in calcium levels in different cell types (Satoh, 1999), and these mechanisms may be involved in the LQT associated with HIV-infected patients.

Whether LQT is resulting from a congenital or acquired cause, modeling and understanding the underlying pathological mechanisms is a must and in turn will improve patients' treatment.

The other arrhythmic disease we are interested in is the BrS. It was first described by Drs. Pedro and Josep Brugada in 1992. The cellular basis for the life-threatening abnormal heart rhythms associated with this syndrome was discovered in the early 1990's (Campuzano et al., 2010). Full description of BrS is discussed below.

II.2. – Brugada Syndrome (BrS)

BrS is a cardiac disorder characterized by ST-segment elevations in the right precordial leads (Figure 7) and susceptibility to ventricular arrhythmias and sudden cardiac death. It affects young subjects with structurally normal hearts. The prevalence varies with ethnicity ranging

from 1 to 5 per 10 000 persons in different parts of the world (Steinfurt et al., 2015). The syndrome has a genetic basis, and several mutations have been identified in genes encoding subunits of cardiac sodium, potassium, and calcium channels, as well as in genes involved in the trafficking or regulation of these channels. Despite this, approximately 70% of BrS cases cannot be explained genetically with the current knowledge (Nielsen et al., 2013) (Brugada et al., 2014).
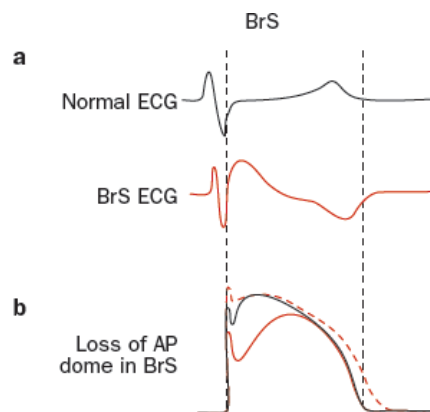
Figure 7: Pathophysiological mechanisms of BrS. A. Schematic representation of a normal ECG (black) and typical ECGs for patients with BrS. B. Tracings of normal ventricular action potentials (black) and tracings that display the transmural gradient between the epicardial action potential (solid red line) and endocardial action potential (dotted red line) (Giudicessi and Ackerman, 2012).

II.2.1 – Clinical presentation of BrS

BrS is associated with a high risk of sudden cardiac death. Currently, it is believed to be responsible for 12% of sudden cardiac death cases and 20% of sudden cardiac death in patients with structurally normal hearts. Patients may suffer syncope or sudden cardiac death secondary to polymorphic ventricular tachycardia (PVT)/ventricular fibrillation (VF). However, the majority of patients remain completely asymptomatic. Some of the arrhythmias may occur after large meals, during rest, or while sleeping. The symptoms usually appear around 40 years of age; however, there are reports of patients affected from ages 1 to 84. Males are more often symptomatic than females, probably due to the influence of hormones and gender distribution of ion channels across the heart. There is little information regarding the pediatric population, but studies performed in children have failed to identify a male predominance, perhaps due to low levels of testosterone in children of both genders. The prevalence of the disease is difficult to estimate because the pattern is not always recognized. Nevertheless, global prevalence varies from 5 to 20 in every 10,000 (Brugada et al., 2014).

II.2.2 – Diagnosis and risk stratification

Crucially, a diagnosis of the BrS requires not only a Brugada-type ECG but also clear clinical features. The presence of ECG features alone is not sufficient. With regards to diagnosis, three distinct ECG patterns are characteristic as outlined in Figure 8.
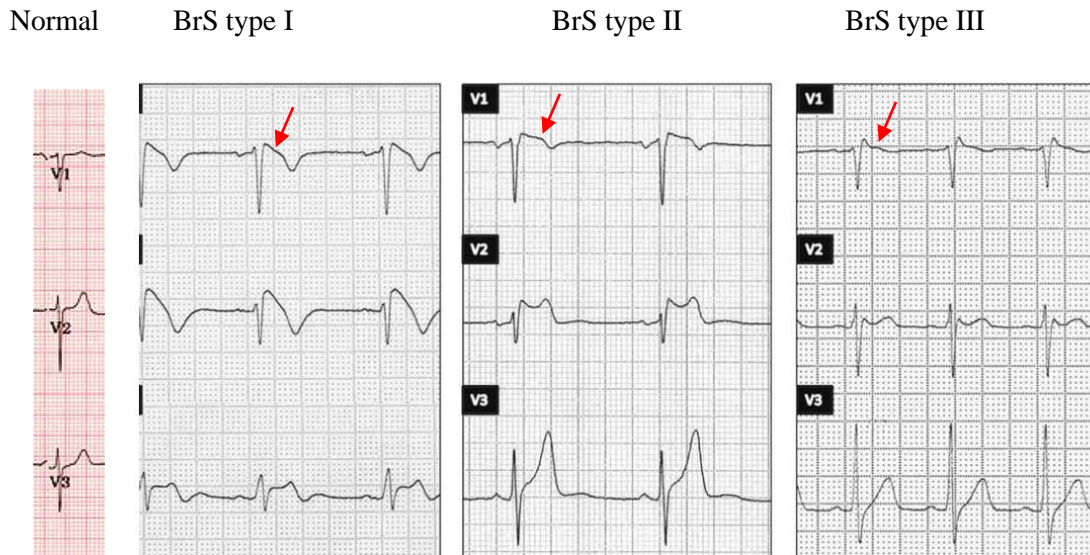
Figure 8: Three types of BrS ECG patterns. Type 1 is a coved-type pattern and type 2 is a saddleback-type, which has ST elevation ≥2 mm without T-wave inversion. Type 3 pattern shows a J-point elevation without ST elevation≥1 mm (Veerakul G1, 2012) (Benito et al., 2009).

Diagnosis is considered in those with a type 1 ECG pattern and any of the following clinical features:

1. Documented ventricular fibrillation (VF)
2. Polymorphic ventricular tachycardia (VT) or inducibility of VT with programmed electrical stimulation
3. A family history of sudden cardiac death under 45 years old
4. Coved-type ECGs in family members
5. Unexplained syncope
6. Nocturnal agonal respiration

Patients with a type 2 or 3 ECG pattern at baseline which transform to a type 1 pattern on drug challenge are also considered for a diagnosis. Drug challenge involves administration of a sodium channel blocker such as flecainide or ajmaline. The sensitivity of the drug challenge remains a somewhat controversial point (Brugada et al., 2000) (Priori et al., 2000). Moreover, other drugs, including tricyclic antidepressants, lithium, fluoxetine and cocaine, are known to

induce a Brugada-like ECG pattern, often without a concomitant risk of arrhythmia (Yap et al., 2009).

Risk stratification remains difficult. Clinically, the combination of ST elevation at baseline and syncope may constitute the strongest predictor of risk (Priori et al., 2002). Male sex is clearly another risk factor, though this does not mean that female patients are necessarily at low risk of arrhythmia (Brugada et al., 2002) Interestingly, it has been suggested that family history of SCD is not a strong predictor of a patient's risk (Probst et al., 2010). Finally, while genetic testing is often requested, it is not particularly helpful as regards risk stratification. Such tests usually performed to identify mutation in *SCN5A*, the gene most commonly implicated in the BrS. However, the presence of such mutation does not in itself confer an increased risk of arrhythmic events (Priori et al., 2002) nor does its absence eliminate risk of arrhythmia, given that mutations in other genes may be present (Mashar et al., 2014).

II.2.3 – Pathophysiological mechanisms underlying BrS phenotype

The key electrophysiological abnormality in the BrS is a decrease in the net depolarizing current, specifically affecting the right ventricular epicardium where channels carrying key repolarizing currents are most prominent. Consequent voltage gradients give rise both to the characteristic ECG features which is an ST segment elevation. This compromised net depolarizing current can lead to loss of the epicardial action potential (AP) dome, markedly shortening the epicardial AP duration along with its refractory period. The AP dome is maintained in the endocardium and midmyocardium, leading to marked transmural heterogeneity in repolarization. The electro-pathophysiology of BrS continues to be debated. Two main hypotheses have been proposed based on defects in the repolarization or the depolarization.

II.2.3.1 – The repolarization theory

The repolarization theory described in Figure 9 is based on an imbalance between repolarizing ionic currents contributing to the phase 1 of AP, I_{to}, and depolarizing ionic current, I_{Na} (Bébarová, 2013).

This model revolves around unequal amount of the transient outward potassium current (I_{to}) between epicardium and other transmural layers. I_{to} drives the early repolarization of the phase 1 of the AP. Stronger I_{to} expression in epicardium than in endocardium renders epicardium more susceptible to the effects of reduced depolarizing force. Thus, in epicardium,

when I_{Na} is reduced (e.g., when mutant Na channels produce reduced I_{Na} in the presence or absence of I_{Na} blockers), a ''spike-and-dome'' AP shape arises, manifesting as saddle-back ST elevation on the ECG (Figure 9B). To account for the negative T wave in coved-type ST elevation, prolongation of epicardial AP dome is invoked, which causes AP duration to become longer than in endocardium (Figure 9C). With further I_{Na} reduction, I_{to} repolarizes the membrane beyond the voltage at which L-type Ca channels ($I_{Ca,L}$) are activated, resulting in loss of the AP dome. This loss is, however, heterogeneous, generating epicardial dispersion of repolarization (Figure 9D). The phase 2 reentry, which was proved as the likely mechanism of ventricular arrhythmias in BrS, might appear under these conditions (Figure 9E). These hypotheses require that AP shape in endocardium remain unaltered by I_{Na} reduction; this is explained by less I_{to} current in endocardium as compared to epicardium in many species, including humans (Meregalli et al., 2006) (Gaborit et al., 2007).
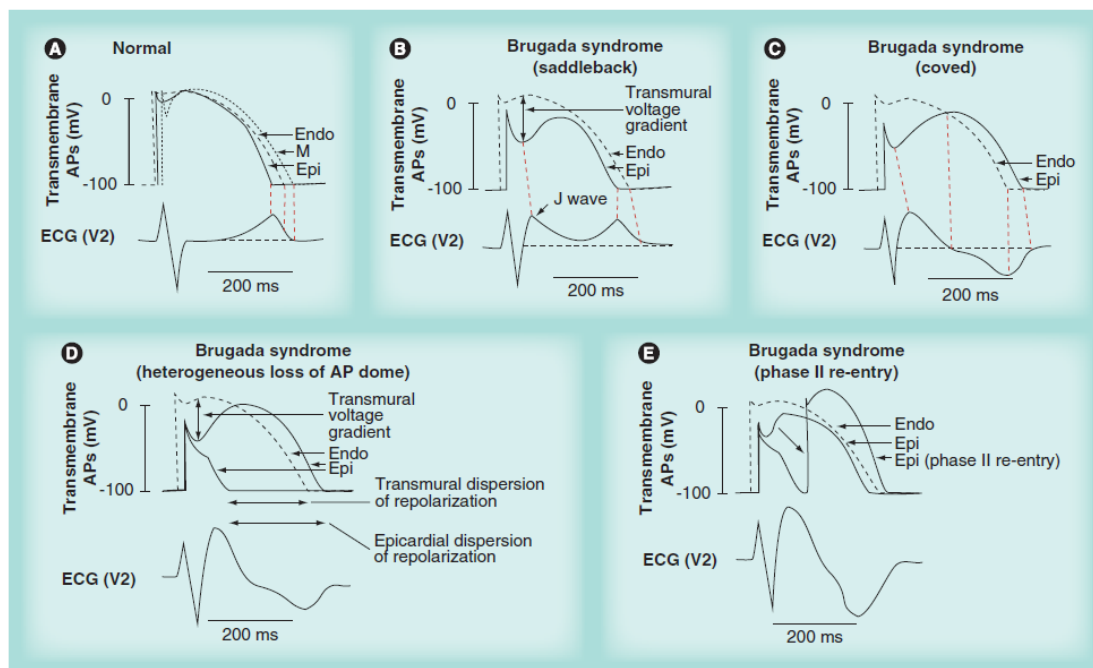
Figure 9: Representation of the repolarization disorder hypothesis. (A) Normal transmembrane APs showing a prominent phase I AP notch in epicardial and myocardial cells due to preferential transient outward current channel expression. (B) Reduction in sodium current channel function augments the phase I AP notch, leading to a steep transmural voltage gradient, inscribing an elevated J wave on the surface ECG. (C) Prolongation of epicardial cell repolarization resulting in a negative T wave on the surface ECG. (D) Further reduction in sodium current channel function leads to loss of the AP dome in some epicardial cells, but not others, leading to transmural and epicardial cell dispersion of repolarization. (E) Phase II re-entry leads to short coupled extrasystoles, triggering ventricular fibrillation. AP: Action potential; Endo: Endocardial cells; Epi: Epicardial cells; M: M cells (Li et al., 2013).

II.2.3.2 – Depolarization theory

The depolarization hypothesis is mainly related to conduction delay. It suggests that there are structural abnormalities within the myocardium that cause delayed conduction within the right

ventricular outflow tract. This in turn leads to abnormal gradients of depolarization and repolarization between the right ventricle and right ventricular outflow, inscribing ST elevation and T-wave inversion on the ECG in the right precordial leads (Figure 10). This may be especially relevant in *SCN5A*-associated BrS where mutations may lead to conduction slowing owing to slowed upstroke to the action potential and further decreasing intraventricular conduction velocities (Meregalli et al., 2006). An alternative explanation for the ECG signature in BrS, which does not invoke fundamentally different AP shapes, is based on conduction delay in right ventricular outflow tract (RVOT; Figure 10). The RVOT AP (Figure 10B, top) is delayed with respect to the RV AP (Figure 10B, bottom). During the hatched phase of the cardiac cycle in Figure 10D, the membrane potential in RV is more positive than in RVOT, thus acting as a source, and driving intercellular current to RVOT, which acts as a sink (Figure 10C, a). To ensure a closed-loop circuit, current passes back from RVOT to RV in the extracellular space (Figure 10C, c), and an ECG electrode positioned over the RVOT ($V2_{IC3}$) inscribes a positive signal, as it records the limb of this closed-circuit which travels towards it (Figure 10C, b). Thus, this electrode inscribes ST elevation during this phase of the cardiac cycle (Figure 10D, bottom, bold line). Reciprocal events are recorded in the left precordial leads, as demonstrated using body surface mapping. Here, current flowing from the extracellular space into RV (Figure 10C, d) causes ST depression. In the next phase of the cardiac cycle (following the upstroke (Figure 10F, hatched phase) of the delayed AP in RVOT), the potential gradients between RV and RVOT are reversed, as membrane potentials are now more positive in RVOT than RV. Thus, RVOT now acts as the source, driving the closed-loop circuit in the opposite direction (Figure 10E), with current now passing away from lead $V2_{IC3}$ (Figure 10E, d), thus resulting in the negative T wave (Figure 10F, bottom, bold line). Note that in Figure 10D and F, the delayed AP of RVOT is abbreviated in comparison to RV AP (and in comparison to Figure10B, where APs of isolated cells are shown), as electro-tonic interaction between RV and RVOT (which is present when RV and RVOT are electrically well-coupled) accelerates repolarization of RVOT AP (the mass of RV strongly exceeding that of RVOT). In fact, it is possible that all mechanisms may operate in the causation of the phenotype (Meregalli et al., 2006).
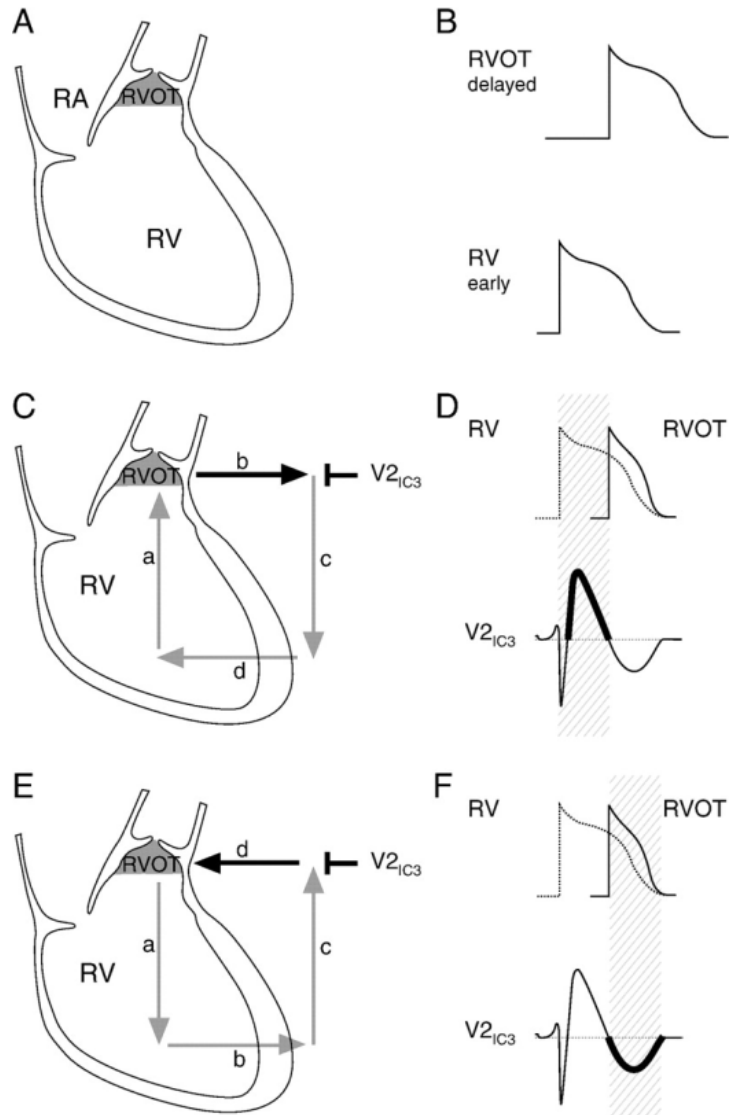
Figure 10: Representation of the depolarization disorder hypothesis (Meregalli et al., 2005).

In summary, the cellular basis of the BrS is still not completely understood (Morita et al., 2009). The repolarization theory claims that the ECG manifestations of BrS are a direct consequence of a shift in the balance between the ionic currents active during the end of the depolarization phase of the action potential generating a remarkable dispersion of epicardial and transmural repolarization (Naseef et al., 2015) (Berne and Brugada, 2012). This theory was initially promoted on the basis of experimental studies (Morita et al., 2009) (Yan et al., 1998) (Yan and Antzelevitch, 1999), and was later supported by clinical studies (Nagase et al., 2008). In addition this theory has been supported by studies on animal models, as well as in human tissues (Yan and Antzelevitch, 1999) (Gussak et al., 1999) (Antzelevitch, 2005). On the other hand, the depolarization theory explains the Brugada ECG type solely by a delay of the RVOT activation relative to the rest of the RV (Meregalli et al., 2005). There is also mounting evidences, from experimental (Aiba et al., 2006) (Gussak et al., 1999), histo-

pathological (Coronel et al., 2005), computational, clinical electrophysiological (Lambiase et al., 2009) (Nagase et al., 2002), and imaging (Tukkie et al., 2004) studies, to show the presence of conduction abnormalities in the RVOT and their importance for the genesis of ventricular arrhythmias in BrS. In addition, Zhang et al have recently showed that both discontinuous conduction and dispersion of repolarization are seen in the right ventricular outflow tract of BrS patients (Zhang et al., 2015).

A third hypothesis unifying the above two explains the BrS with abnormal expression of the neural crest cells during the embryological development of the RVOT. This defect leads to both abnormally augmented electrical gradients during repolarization as well as to delayed activation of the RVOT (Elizari et al., 2007).

II.2.4 – Genetic basis of BrS

BrS is inherited in an autosomal dominant pattern with incomplete penetrance. It is genetically heterogeneous with an increasing number of mutations in genes encoding proteins involved in regulation of sodium, potassium and calcium currents. To date, 17 genes have been associated with BrS (Campuzano et al., 2010) (Table 2) (Nielsen et al., 2013). The most frequent mutation is located in the Na^+ channel gene, *SCN5A*, which has been shown to be present in 20% to 30% of patients. The other involved genes represent rare sporadic cases or individual BrS families (Potet et al., 2003). In functional terms, the mutations show either a loss-of-function effect on depolarizing currents (I_{Na} or $I_{Ca,L}$) or a gain-of-function effect on repolarizing currents (I_{to} and ATP-sensitive potassium current, I_{K-ATP}) (Mizusawa and Wilde, 2012). Whether these gene mutations are actually causative of BrS or only have a modifying role is a matter of ongoing debate (Mizusawa and Wilde, 2012) (Probst et al., 2009). In addition, Béziau et al reported a rare *CACNA1C* mutation causing BrS and/or shortened QT interval in a family also carrying a *SCN5A* stop mutation, but which does not segregate with BrS (Béziau et al., 2014). This study underlies the complexity of BrS and pointed the difficult interpretation of BrS genetic testing. More recent data show frequent genetic variants (single nucleotide polymorphisms, SNPs) in *SCN5A*, *SCN10A*, and *HEY2* (*SCN5A* encodes for the alpha subunit of the voltage-gated Na^+ channel Nav1.5; *SCN10A* encodes for the voltage-gated Nav1.8; *HEY2* encodes for the transcription factor HEY2) (Bezzina et al., 2013). These gene polymorphisms influence individual disease risk and may in the future allow the development of a genetic risk score that could be of practical clinical use (Nielsen et al., 2013).

Table 2: Mutations in genes associated with BrS (Nielsen et al., 2013)

BrS Subtype	Gene	Protein	Ionic current	Functional effect	References
BrS1	*SCN5A*	Nav1.5	I_{Na}	Loss of function	(Chen et al., 1998)
BrS 2	*GPD1L*	G3PD1L	I_{Na}	Loss of function	(London et al., 2007)
BrS 3	*CACNA1C*	$Ca_v1.2$	$I_{Ca,L}$	Loss of function	(Antzelevitch et al., 2007)
BrS 4	*CACNB2*	Cavβ2	$I_{Ca,L}$	Loss of function	(Antzelevitch et al., 2007)
BrS 5	*SCN1B*	Navβ1	I_{Na}	Loss of function	(Watanabe et al., 2008)
BrS 6	*KCNE3*	MiRP2	I_{to} / I_{Ks}	Gain of function	(Delpon et al., 2008)
BrS 7	*SCN3B*	Navβ3	I_{Na}	Loss of function	(Hu et al., 2009)
BrS 8	*KCNH2*	hERG	I_{Kr}	Loss of function	(Itoh et al., 2009; Verkerk et al., 2005)
BrS 9	*KCNJ8*	$K_{ir}6.1$	$I_{K,ATP}$	Gain of function	(Medeiros-Domingo et al., 2010)
BrS 10	*CACNA2D1*	Cavα2δ1	$I_{Ca,L}$	Not available	(Burashnikov et al., 2010)
BrS 11	*RANGRF*	MOG1	I_{Na}	Loss of function	(Kattygnarath et al., 2011)
BrS 12	*KCNE5*	MiRP4	I_{to} / $I_{Ks\ a}$	Gain of function	(Ohno et al., 2011)
BrS 13	*KCND3*	Kv4.3	I_{to}	Gain of function	(Giudicessi et al., 2011)
BrS 14	*HCN4*	HCN4	I_f	Not available	(Crotti et al., 2012)
BrS 15	*SLMAP*	SLMAP	I_{Na}	Loss of function	(Ishikawa et al., 2013)
BrS 16	*TRMP4*	TRMP4	NSC_{Ca}	Both	(Liu et al., 2013)
BrS 17	*SCN2B*	Navβ2	I_{Na}	Loss of function	(Riuró et al., 2013)

Subtypes listed chronologically, NSC_{Ca} Calcium activated Non Selective Cation channel.

Two of the individual genes associated with BrS, *SCN5A* and *CACNA1C* are further discussed. Starting with *SCN5A*, this gene was the first to be associated with BrS and still represents the major gene in BrS pathogenesis (Nielsen et al., 2013).

II.2.4.1 – Sodium channel type 5 α-subunit (SCN5A)

Mutations in the *SCN5A* gene, which encodes the α-subunit of the Nav1.5 sodium channel, result in loss of function and have been identified in 21% of probands. Some of these variants have mixed biophysical properties and have been associated with overlapping phenotypes between BrS and premature cardiac conduction disease or long QT syndrome (Wilde and Behr, 2013). Sodium channels are dynamic transmembrane proteins in excitable cells (e.g., cardiomyocytes, skeletal muscle cells, neurons) that open and close to conduct ions. They are large molecular complexes containing a pore forming ion-conducting α-subunit and ancillary β-subunits, and several regulatory proteins. It is organized into a cytoplasmic N terminus, four homologous transmembrane domains (DI-DIV) that are connected to each other by cytoplasmic linkers, and a cytoplasmic C terminus. Each domain consists in six transmembrane α-helical segments (S1-S6), connected to each other by alternating extracellular and cytoplasmic loops. The four domains fold around an ion conducting pore, which is lined by the extracellular loops (P-loops) between S5 and S6 segments (Figure 11). Some amino acids in the P-loops confer the selectivity for sodium ions (Amin et al., 2010).
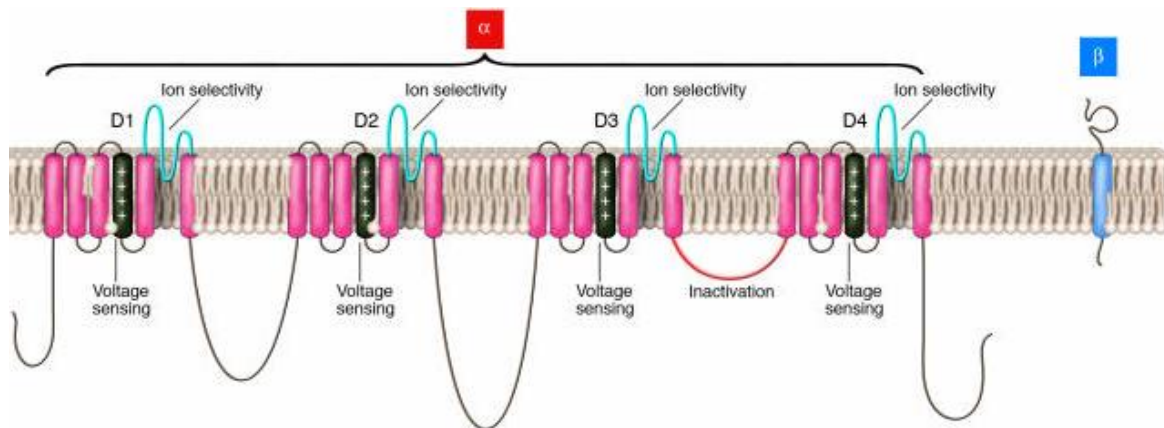
Figure 11: Structure of human Nav1.5 channel Simple model representing transmembrane topology of α and β Nav1.5 channel subunits. Structural domains mediating key functional properties are labeled.(Li et al., 2013).

Gating represents time-dependent transitions between distinct conformational states of the channel protein due to molecular movements in response to membrane potential changes (voltage-dependent gating). When cardiomyocytes are excited by electrical stimuli from adjacent cells or by artificially applied stimuli during patch-clamp experiments, their resting membrane potential (approximately -85 mV) depolarizes. This triggers an outward movement of the positively charged S4 segments (voltage sensors), which leads to channel activation (opening of the pore). Inactivation (closing of the pore) starts simultaneously with activation, but since inactivation is slower than activation, channels remain transiently open to conduct I_{Na} during phase 0 of the action potential (Figures 12, 13). Inactivation comprises different conformational states, including fast, intermediate, and slow inactivation (Amin et al., 2010).
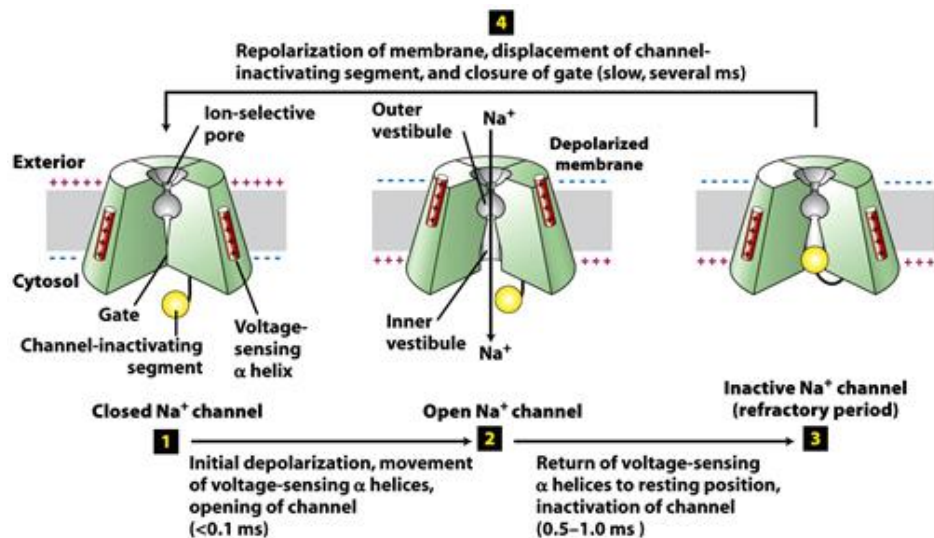
Figure 12: Biophysical properties of *SCN5A* channel (Amin et al., 2010).
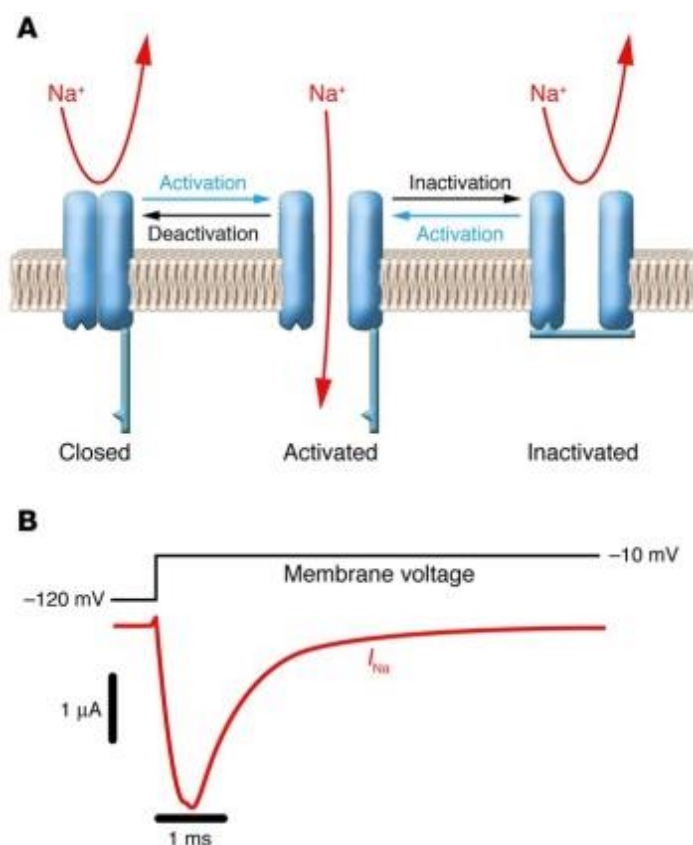
Figure 13: Functional properties of sodium channel. (A) Schematic representation of sodium channel undergoing the major gating transitions. (B) Voltage-clamp recording in response to membrane depolarization. Downward deflection of the current trace (red) corresponds to inward movement of Na^+ (George, 2005).

II.2.4.1.b – Mutations affecting SCN5A and/or its interacting protein

Mutations that affect Nav1.5 function in BrS could be located in the *SCN5A* gene, or in the proteins interacting with the Nav1.5 for a functional or a regulatory task (Amin et al., 2010) (Keller et al., 2005) (Petitprez et al., 2008). Mutations in *SCN5A* include missense mutations, nonsense mutations, and nucleotide deletions or insertions The latter may alter mRNA splicing or create a premature stop codon by shifting the open reading frame, and result in truncated Nav1.5 proteins [66]. More than 300 mutations in this gene have been associated with BrS. Functional studies of many different mutations in the gene have been performed and they all lead to a reduction in net sodium current due to one or more of following reasons (Antzelevitch et al., 2005) (1) reduced current density due to failure of the sodium channel to express or defect trafficking of the channel (Baroudi et al., 2001) (Valdivia et al., 2004) (Pfahnl et al., 2007) (2) a shift in the voltage-and time-dependence of sodium channel current activation, inactivation or reactivation (Keller et al., 2005) (Chiang et al., 2009) (Calloe et al., 2013) or (3) entry of the sodium channel into an intermediate state of inactivation from which it recovers more slowly than normal (Nielsen et al., 2013) (Chiang et al., 2009) (Bezzina et al., 1999) (Veldkamp et al., 2000).

In the same context, Nav1.5 proteins may also directly interact with several regulatory proteins. At the translational level, many modifiers regulate Nav1.5 protein synthesis, folding, trafficking, and assembly with accessory subunits and interacting proteins. For example, activated mitogen-activated protein kinases (MAPKs), such as p38-MAPK and MAPK8 (Cook et al., 1999) (Muslin, 2008), can affect translation of the Nav1.5 channel and gap junction α1 protein connexin 43 (Cx43) and contribute to arrhythmia (Muslin, 2008) (Ursitti et al., 2007) (van Bemmelen et al., 2004) (Yanagita et al., 2003).

Furthermore, the loss of Cx43, together with increased collagen deposition and decreased expression of the cardiac sodium channel Nav1.5, is thought to impair the proper conduction of the electrical impulse, increasing the risk for fatal ventricular arrhythmias which is a common mechanism in BrS (Maury et al., 2013). Besides a decreased expression, a more inhomogeneous distribution of Cx43 has been found in remodeled hearts, resulting in a more dispersed conduction, which is also correlated with an increased susceptibility for arrhythmias. Previous studies have shown that a 50% reduction in Cx43 expression in mice did not affect impulse conduction. However, an additional 5% reduction of Cx43 levels by conditional deletion of the Cx43 gene resulted in a high vulnerability for arrhythmias owing to slowed and dispersed conduction (van Rijen et al., 2004). It was then proposed as shown in a genetic model of heterogeneous Cx43 expression (Gutstein et al., 2001) that the decreased and heterogeneous expression of Cx43 protein levels allowed for the occurrence of ventricular arrhythmias (Petitprez et al., 2011) (Jansen et al., 2012).

Moreover, after *SCN5A* is translated to protein and assembled in the endoplasmic reticulum, the channel is transited to the Golgi complex, where Nav1.5 channel trafficking begins. A Golgi vesicle containing the Nav1.5 channel is then transported to the plasma membrane area. Modifiers such as cAMP-dependent protein kinase (also known as protein kinase A; PKA) and protein kinase C (PKC) regulate channel trafficking to the plasma membrane. For instance, PKC activation can decrease Nav1.5 channel trafficking, whereas PKA can have the opposite effect (Zhou et al., 2002) (Hallaq et al., 2012). In addition to that, Nav1.5 α-subunit interacts with accessory proteins (β-subunits and interacting proteins) to form a macromolecular complex (Figure 14). Mutations of these accessory proteins have been reported to cause BrS. For example, patients with BrS and mutations in the sodium channel β1 and β3-subunits show impaired Nav1.5 channel function [65] (Watanabe et al., 2008) (Hu et al, 2009). The expression level of the β4-subunit is reported to affect the severity of cardiac conduction disease in mice by modulating Nav1.5 channel activation (Remme et al., 2009).

Nav1.5 interacting proteins, such as ankyrin, Ran guanine nucleotide release factor (MOG1), and syntrophin, interact with α and β-subunits of the sodium channel. Mutations and mis-regulation of these proteins can disturb Nav1.5 membrane expression and function (Liu et al., 2014).
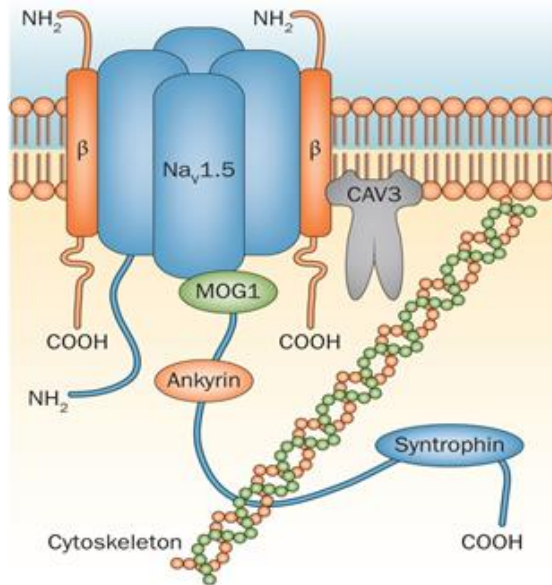
Figure 14: The channel α-subunit interacts with multiple cellular proteins, including accessory proteins such as β subunits, ankyrin, CAV3, MOG1, syntrophin, and cytoskeleton at the cell membrane, forming a macromolecular complex. Nav1.5channel activity can be modified by the altered expression or function of the components of the macromolecular protein complex. Abbreviations: CAV3, caveolin-3; MOG1, Ran guanine nucleotide release factor (Liu et al., 2014).

Although mutations in *SCN5A* are identified in approximately 20% to 30% of probands affected by BrS, the relationship between these mutations and BrS remains poorly understood. A group of studies aimed to investigate the association of *SCN5A* mutations and BrS. Probst et al showed that *SCN5A* mutations are not directly causal of the occurrence of a BrS-positive ECG in a cohort of 115 mutation carriers and that genetic background may play a powerful role in the pathophysiology of BrS (Probst et al., 2009). On the other hand, a multi-center study based on data collected on demographics, clinical history, family history and electrocardiogram (ECG) parameters, showed that BrS patients with, and those without, an *SCN5A* mutation can be differentiated by phenotypical differences (Smits et al., 2002).

These findings add further complexity to concepts regarding the causes of BrS, and are consistent with the emerging notion that the pathophysiology of BrS includes various actors beyond mutated sodium channels.

In addition to mutations in *SCN5A*, mutations in *CACNA1C* have also been linked to BrS [19].

II.2.4.2 – BrS and Cav1.2

Two different types of calcium channel are present in the heart: L‑type and T‑type. L-type Ca^{2+} channels are expressed at high levels throughout the heart (Mohamed et al., 2006), and so far they are the main Ca^{2+} channels that have been linked to cardiac channelopathies (Napolitano and Antzelevitch, 2011). L-type Ca^{2+} channel activation is voltage dependent with maximal activation around 0 mV (Yuan et al., 1996). Inactivation is dependent on both voltage and Ca^{2+} concentration. The latter mechanism enables the cell to modulate Ca^{2+} influx in response to cytoplasmic Ca^{2+} concentration and prevents Ca^{2+} overload. $I_{Ca,L}$ has two major functions: modulation of action-potential duration, and triggering the release of Ca^{2+} from the SR. Cardiac L−type Ca^{2+} channels are composed of one pore-forming subunit α1, and two accessory subunits α2δ and β (Figure 15) (Bers and Perez-Reyes, 1999). Four isoforms of the α1 subunit exist: α1s, α1c, α1d, and α1f. In the heart, only the α1c and α1d isoforms are expressed. The α1c subunit is the main isoform expressed in the atria and the ventricles, and is also expressed in the nodes. The α1d isoform is predominantly expressed in the sinus and atrioventricular nodes, and to a lesser extent in the atria (Zhang et al., 2002). Only mutations of the α1c isoform, encoded by the *CACNA1C* gene, have been linked to cardiac channelopathies (Napolitano and Antzelevitch, 2011).
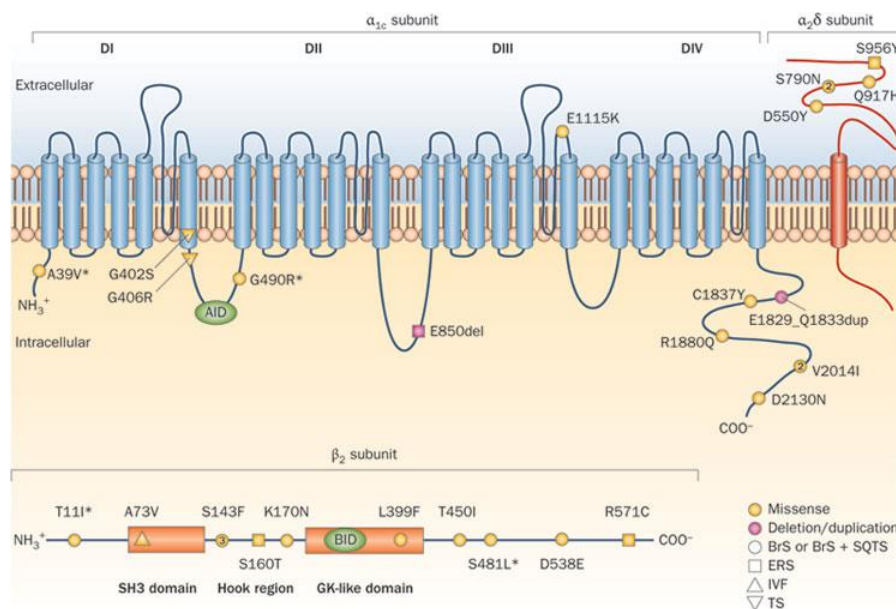
Figure 15: The L-type Ca^{2+} channel is formed by the assembly of three subunits: α1c, β2, and α2δ. The α1c subunit forms the channel pore and is comprised of four homologous domains (DI to DIV) that co4ntain six trans membrane segments. These domains are linked by cytoplasmic loops. The loop between DI and DII contains the binding site for the β2 subunit (AID) (Venetucci et al., 2012).

To date, 25 mutations affecting three genes encoding components of the L-type Ca^{2+} channel macromolecular complex (*CACNA1C*, *CACNB2*, and *CACNA2D1*) have been reported to be associated with BrS, BrS with short QT duration, short QT syndrome, early repolarization syndrome, and cardiac arrest without ECG abnormalities (Napolitano and Antzelevitch, 2011). Functional studies suggest a loss-of-function effect of these mutations. The behavior of this group of mutations looks similar to what has been described for loss-of-function mutations in *SCN5A*, which can cause various phenotypes, such as BrS, progressive conduction disease, sick sinus syndrome, dilated cardiomyopathy, atrial fibrillation, and overlapping phenotypes (Venetucci et al., 2012) (Ruan et al., 2009) (Napolitano and Antzelevitch, 2011).

Up to date, over 300 mutations in 17 genes have been associated with BrS. Thanks to genetic screening, the knowledge about BrS associated mutations is therefore rapidly increasing. The intention would be to use this knowledge in risk stratification, as some asymptomatic BrS patients have an appreciable risk of arrhythmia [28]. A study by Meregalli et al. reveals an association between the type of *SCN5A* mutation and the clinical severity (Meregalli et al., 2009). They compared groups having either missense mutations or mutations leading to premature truncation of the protein. They found that the disease phenotype was more severe in the patients with large I_{Na} reduction than in those with small I_{Na} reduction (truncation versus missense), as evidenced by larger proportions of patients with syncope and SCD. Furthermore, Sommariva et al. demonstrated that *SCN5A* mutation carriers had a significantly increased risk of major arrhythmic event compared with non-carriers in a BrS cohort (Sommariva et al., 2013). In addition, Gaborit et al. showed that BrS patients exhibit a common ion-channel molecular expression signature, irrespective of the culprit gene (Gaborit et al., 2008). They performed transcriptional profiling on biopsies from unrelated BrS probands. The molecular profile of BrS patients with *SCN5A* mutations did not differ from BrS patients without *SCN5A* mutations, suggesting that all BrS patients display a common and specific expression patterns for ion channels regulating cardiac conduction, excitability, and repolarization.

Even though over 300 mutations in 17 genes have been associated with BrS, approximately 70% of BrS incidents cannot be explained genetically at present. For example, many families that carry a *SCN5A* mutation contain clinically affected members with BrS who are not genetic carriers. Thus, there is a need for an alternative strategy to further understand the pathophysiological mechanisms associated with BrS (Nielsen et al., 2013).

III – Cellular basis underlying arrhythmogenic incidents in LQT and BrS syndromes

As mentioned before BrS and LQT are associated with a high risk of sudden cardiac death. SCD is a consequence of the immediate and complete inability of the heart to maintain its contraction. The most likely SCD causes are cardiac arrhythmias like ventricular tachycardia (VT) or ventricular fibrillation. However, the underlying mechanisms of these life-threatening ventricular tachyarrhythmia are manifold (Huikuri et al., 2001). They can occur as a consequence of isolated channelopathies in a structurally normal heart, such as in the case of BrS and LQT. However, more frequently, they are secondary to substantial dysregulation of intracellular Ca^{2+} and Na^+ handling. Patients with acquired dysfunction in many ion channels and transporters exhibit profound dysregulation of Na^+ and Ca^{2+} handling and are especially prone to arrhythmias. Thus understanding the mechanisms linking Ca^{2+} and Na^+ handling to arrhythmogenesis will help clarify pathophysiological mechanisms associated with BrS and LQT syndromes (Wagner et al., 2015).

III.1. – Early afterdepolarizations (EADs)

EADs are classically bradycardia dependent. Mechanisms by which they promote tachyarrhythmia such as torsades de pointes and ventricular fibrillation are not fully understood. Recent evidence suggests that EADs also may occur at rapid heart rates as a result of spontaneous sarcoplasmic reticulum (SR) Ca^{2+} release related to intracellular Ca^{2+} overload (Huffaker et al., 2004).

EADs occur during the AP and is a consequence of increased inward currents or reduced repolarization reserve (reduced outward K^+ currents) (Bers, 2002). The plateau phase of the AP is especially vulnerable because repolarizing and depolarizing currents are small and nearly balanced. During this phase, small alterations in the amplitude of even one ionic current can result in the generation of an EAD. The fundamental mechanisms of triggered activity were explained by studying familial disorders with prolonged repolarization. For example, congenital long QT syndrome 3 is characterized by profound AP prolongation because of increased persistent or late Na current (late I_{Na}) (Song et al., 2006) (Wagner et al., 2011).

EADs are strongly associated with ventricular arrhythmias in LQT. Both phase 2 and phase 3 EADs have been described in LQT. Phase 2 EADs result from the reactivation *of* $I_{Ca,L}$ and/or spontaneous Ca^{2+} release from the sarcoplasmic reticulum (SR) (Volders et al., 2000) (Choi et al., 2002). It has been suggested that spontaneous SR Ca^{2+} release may underlie phase 3

EADs because they may occur concurrently with delayed afterdepolarizations (Patterson et al., 1990), are facilitated by intracellular Ca (Ca$_i$) loading, and are suppressed by inhibition of Na$^+$/Ca^{2+}exchanger current (I$_{NCX}$). Alternatively, it is possible that most phase 3-EADs observed in tissue, are not genuine cellular-level phenomena but are a consequence of "prolonged repolarization-dependent re-excitation." It is reported that if dispersion of repolarization is enhanced in LQT, a voltage gradient between long and short action potential duration (APD) regions could create a "boundary" current that electronically depolarizes the short APD region as it tries to repolarize, generating triggered activity as long as a large voltage gradient is maintained (Maruyama et al., 2011) (January and Riddle, 1989) (Antoons et al., 2007). Interestingly, pathological AP prolongation is a prominent feature of a pro-arrhythmic electric remodeling (Kääb et al., 1996) (Beuckelmann et al., 1993) but can also occur in response to gene mutations or drugs that inhibit K$^+$ channels, especially I$_{Kr}$ (Burashnikov and Antzelevitch, 1998) (Volders et al., 2000) (Edwards et al., 2014) (Figure 16).
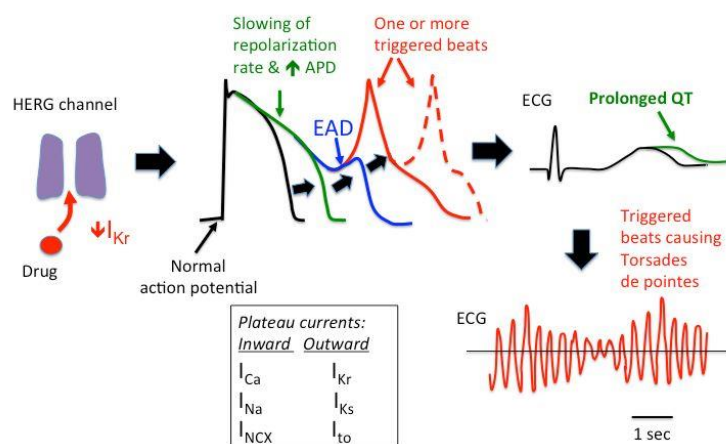
Figure 16: Mechanism of EAD formation & initiation of Torsade de pointes. Drug-induced blockade of the hERG channel reduces I$_{Kr}$ amplitude, which in turn reduces net outward current during the plateau, and prolongation of the ventricular APD and QT interval in the ECG (green). If net inward currents during phase 3 become larger than outward currents, this can form an EAD (blue). These changes are typically heterogeneous and can create a substrate for producing triggered beats in multiple locations, resulting in a multifocal ventricular tachycardia. (Adapted from Kannankeril et al, 2010) (Kannankeril et al., 2010).

III.2. – Delayed afterdepolarizations (DADs)

DADs are a consequence of cytosolic and SR Ca^{2+} overload. Both cytosolic and SR luminal Ca^{2+} increase the diastolic open probability of cardiac ryanodine receptor 2 (RyR2) (Bers, 2002). Ca^{2+} sparks are elementary SR Ca^{2+} release events that occur when a cluster of RyR2 opens. During systolic Ca^{2+} -induced Ca^{2+} release, Ca^{2+} sparks are synchronized within the cell and summate to form the Ca^{2+} transient. Spontaneous Ca^{2+} sparks are mainly responsible for diastolic SR Ca^{2+} release and diastolic SR Ca^{2+} leak via RyR2 (Bassani and Bers, 1995) (Bers, 2014). Because RyR2 is in relatively close proximity to the NCX, this localized [Ca^{2+}]i

elevation drives inward I_{NCX}. Note that due to the stoichiometry of Na^+/Ca^{2+} exchange ($3Na^+:1Ca^{2+}$), one Ca^{2+} extrusion is accompanied by a net inward movement of three positive charges, which is almost entirely responsible for what transient inward current I_{ti}. If this I_{NCX} is large enough, it can cause an appreciable DAD, which can trigger an arrhythmic AP. Individual Ca^{2+} sparks normally do not produce enough I_{NCX} to produce a measurable DAD because they are isolated unsynchronized events. However, at higher SR Ca^{2+} content, the Ca^{2+} sparks are larger in amplitude and nearby RyR2 clusters are more sensitive to activation, resulting in a cell-wide Ca^{2+} wave with sufficient I_{NCX} to cause DADs and triggered APs.

In the intact heart, the I_{NCX} produced by a Ca^{2+} wave in a single myocyte is insufficient to trigger an appreciable DAD or AP because all of the neighboring cells can effectively clamp that single cell at the diastolic voltage. However, when these Ca^{2+} waves and consequent I_{NCX} are synchronized regionally among many cells (by the prior AP and similar RyR2 recovery kinetics), that region can initiate triggered beats and premature ventricular contractions(Xie et al., 2010) (Myles et al., 2012). The heart is relatively protected from these triggered arrhythmias initiated via EADs and DADs, but under pathological conditions caused by either genetic ion channel/transporter mutations or acquired diseases, both the cellular propensity for EADs and DADs and their ability to cause whole heart premature ventricular contractions can be greatly increased (Myles et al., 2015) (Pogwizd et al., 2001) (Figure 17).
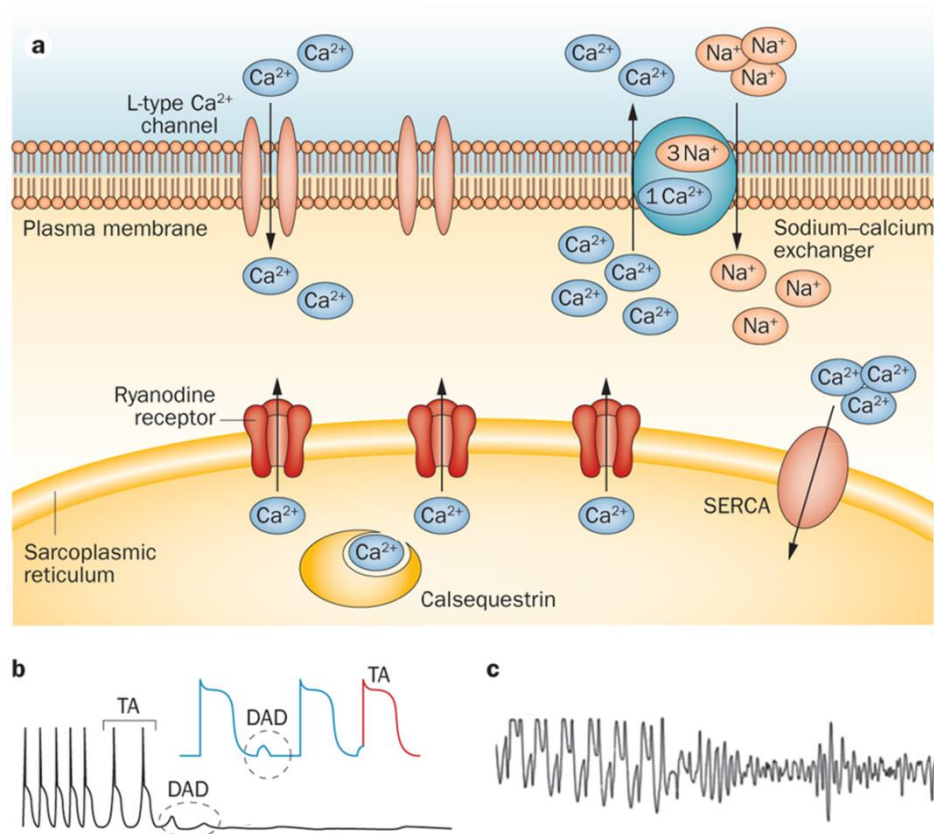
Figure 17: a. Calcium overload in the cytosol increase the activity of the sodium-calcium exchanger generates DADs. b. a schematic representation and an actual recording from a cardiac cell of a mouse. DADs (blue) and TA (red) are elicited by isoproterenol superf usion. c. these cellular abnormalities are the cause of the ventricular arrhythmias observed in the clinical setting. Abbreviations: DAD, delayed afterdepolarization; SERCA, sarcoplasmic/endoplasmic reticulum calcium ATPase; SOICR, store overload-induced calcium release; TA, triggered activity; VT, ventricular tachycardia modified form (Bongianino and Priori, 2015).

III.3. – Repolarization alternans

Alternation in APD is called repolarization alternans and it can be clinically observed as T-wave alternans (TWA) (Pastore et al., 1999). TWA has been shown to be associated with cardiac arrhythmias and SCD (Rosenbaum et al., 1994) (Narayan, 2006) (Armoundas et al., 2002). TWA is not restricted to a specific underlying disease but can be observed in many cardiac disease including BrS and LQT (Qu et al., 2010).

TWA can result from changes in sarcolemma ion current recovery (typically of I_{Na} or $I_{Ca,L}$) manifested by a steep slope of cellular APD restitution (Pruvot et al., 2004). This type of TWA typically occurs at high heart rates with reduced diastolic intervals (Pastore et al., 1999) (Christini et al., 2006; Mironov et al., 2008). The dependence of APD and conduction velocity (CV) on the preceding diastolic interval, are called APD restitution and CV restitution, respectively. Shorter diastolic intervals result in shorter APD and slower CV. Both APD and CV restitution critically depend on the speed of recovery from inactivation of sarcolemmal ion channels. Nevertheless, other mechanisms, for instance SR Ca^{2+} release, can also

contribute to APD restitution changes. Intracellular Ca^{2+} released from the SR inactivates $I_{Ca,L}$. A large SR Ca^{2+} release could, therefore, result in a more pronounced Ca^{2+}-dependent inactivation of $I_{Ca,L}$, which would influence APD restitution.

CV restitution, on the other hand, mainly depends on Na^+ channel recovery (Qu et al., 2004). This is because CV depends on AP upstroke velocity, and the latter is determined by the magnitude of I_{Na}. Na channel recovery is usually fast; thus, CV restitution occurs only at high heart rates, as would be the influence of Na^+ channel recovery on APD restitution. However, under conditions of slowed Na^+ channel recovery, the impact on CV restitution (and also APD restitution) may already occur at much lower heart rates. This is important because slowed Na channel recovery has been shown to be a feature of many cardiac diseases like BrS (Wang et al., 2000).

As mentioned above, APD restitution depends on sarcolemma ion channel recovery. Among them, L-type Ca^{2+} channels are very important. $I_{Ca,L}$ generates the major inward current during the AP plateau. AP plateau is the most vulnerable phase of the AP. This explains why inhibition of $I_{Ca,L}$ has been shown to reduce the slope of the APD restitution curve. In addition, the recovery of Ca^{2+} channels is slower compared with, for instance, Na^+ channels. Therefore, Ca^{2+} channels influence APD restitution already at lower heart rates. Interestingly, because $I_{Ca,L}$ also determines SR Ca^{2+} load, and vice versa, APD alternans and Ca^{2+} alternans are functionally linked.

III.4. – Calcium alternans

It has been shown that Ca^{2+} and APD alternans usually coexist, are mechanistically linked, and that Ca^{2+}-driven alternans seem to be more clinically relevant in the setting of heart disease (Pruvot et al., 2004). Several factors contribute to alternans, and they seem to follow a sequence. The first step seems to be an abnormal RyR2 recovery so that SR Ca^{2+} release decreases, despite unaltered APD, $I_{Ca,L}$, and $[Ca^{2+}]_{SR}$. This is because RyR2 restitution is much slower than normal $I_{Ca,L}$ restitution (Hüser et al., 2000) (Florea and Blatter, 2010) (Belevych et al., 2009). The partial failure of SR Ca^{2+} release at this first small beat allows improved RyR2 recovery at the next large beat, but then the cycle repeats. SR Ca^{2+} release alternans can appear at heart rates where the consequent APD alternans are not yet detectable (Figure 18B). As Ca^{2+} release alternans grow, they are amplified by alternating changes in SR Ca^{2+} load (Figure 18C). The small release limits Ca^{2+}-dependent inactivation of $I_{Ca,L}$, thereby increasing Ca^{2+} influx and load for the next (large) beat. The small Ca^{2+} transient also drives less Ca^{2+} extrusion via NCX, which limits Ca^{2+} loss at the small beat. Then at the large beat,

there is greater Ca^{2+}-dependent $I_{Ca,L}$ inactivation and greater Ca^{2+} efflux via NCX, which reduces cell and SR Ca^{2+} load, setting the scene for stable alternans, (Figure 18C). At even higher stimulation rates, shorter diastolic intervals or more depolarized diastolic voltage, one can encroach on $I_{Ca,L}$ (or even I_{Na}) restitution, which may also exacerbate a sort of Ca^{2+}-driven alternans (smaller $I_{Ca,L}$ causes smaller Ca^{2+} transient and APD) (Qu et al., 2013) (Aistrup et al., 2009) (Figure 18).
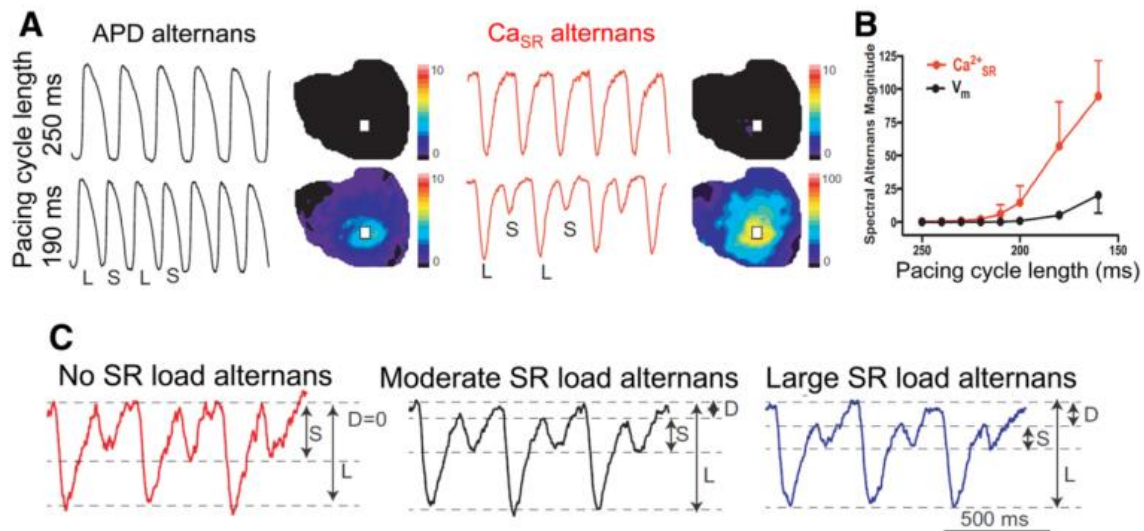
Figure 18: Characteristics of cardiac alternans. A, Simultaneous recordings of action potential (AP) and intra-sarcoplasmic reticulum (SR) free $[Ca^{2+}]$ in isolated Langendorff-perfused rabbit hearts by optical mapping. At shorter pacing intervals (190 ms), alternans of the AP duration as well as SR Ca^{2+}release alternans was observed. B, SR Ca^{2+}release alternans can occur at heart rates where action potential duration (APD) alternans is not yet detectable. C, Ca^{2+}release alternans can be amplified by alternating changes in SR Ca^{2+} load, that is, SR Ca^{2+}load alternans (Wagner et al., 2015).

III.5. – Late sodium current

Late I_{Na} is generated by dysfunctional inactivation of cardiac voltage-gated Na^+ channels Nav1.5 (Maltsev and Undrovinas, 2006). The detailed molecular mechanism is not fully understood (Moreno and Clancy, 2012). Although late I_{Na} has a small amplitude compared with peak I_{Na}, it persists for hundreds of milliseconds during the cardiac AP, providing a source for increasing $[Na^+]_i$ (Saint et al., 1992). Increased $[Na^+]_i$ is a well-known feature of LQT3 syndrome or other conditions and contribute to contractile dysfunction and arrhythmias (Pieske et al., 2002) (Despa et al., 2002) (Sossalla et al., 2008). The late I_{Na}-dependent prolongation of the AP plateau renders the membrane potential vulnerable for EADs (Figure 19). Mutations in the gene encoding for Nav1.5 (*SCN5A*) have been shown to increase late I_{Na}, leading to AP prolongation and EADs. Transmural differences in late I_{Na} might also increase dispersion of repolarization, which underlies the development of torsade de pointes

tachyarrhythmia (Antzelevitch and Belardinelli, 2006). Beside AP prolongation, late I_{Na}-dependent Na^+ overload leads to intracellular Ca^{2+} accumulation either by reduced Ca^{2+} exit, because of limitations to Ca^{2+} extrusion by NCX, or by additional Ca^{2+} Entry via the reverse mode of NCX. Intracellular Ca^{2+} accumulation is associated with increased diastolic SR Ca^{2+} leak and DADs (Figure 19) (Wagner et al., 2011) (Fredj et al., 2006).
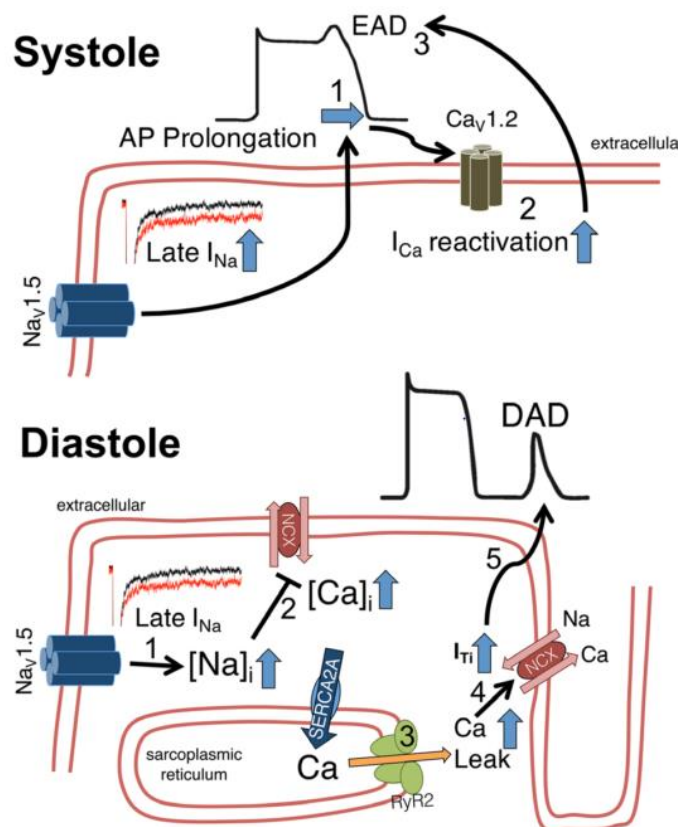
Figure 19: Proarrhythmogenic mechanisms of enhanced late I_{Na}. In I_{Na} leads to action potential (AP) prolongation (1). The longer AP plateau phase increases the likelihood of I_{Ca} reactivation (2), which may lead to early afterdepolarizations (EAD, 3). Lower panel, the increased amount of Na influx also results in increased intracellular Na (1), which impairs Ca elimination (2) by the Na/Ca exchanger (either less forward or even increased reverse mode activity). In diastole, the increased intracellular Ca facilitates SR Ca leak (3), which could lead to transient inward current (I_{Ti}) by the Na/Ca exchanger (4). The latter can result in delayed afterdepolarizations (DAD) (Wagner et al., 2015).

In brief, investigators in the field of cardiac channelopathies have evolved a complex understanding of the pathophysiological basis of cardiac diseases such as LQT and BrS. A lot of work has been done in the field of diagnosis, genetic testing and mutations characterization in various models. Despite that, some common problems still exist: the variable penetrance and expressivity of genetic disease, and the difficulty of assessing the functional and clinical effects of novel mutations. Indeed, a different approach to fully characterize these channelopthies is required. In the next part I will describe the current status of cardiac channelopathies modeling using human induced pluripotent stem cells derived cardiomyocytes that may offer a different approach for modeling these diseases.

IV – Modeling of cardiac arrhythmic diseases

Much progress has been made in identifying the clinical phenotypes, the genetic background and the cellular mechanisms underlying various arrhythmic syndromes, including LQT and BrS. Genotype-phenotype relationship studies have uncovered important gene-specific aspects of these diseases, and indicated that patient management must take into consideration the nature of the affected gene(s). However, there is considerable variation in phenotypic expression of arrhythmia syndromes even within families carrying the same mutation (Addis and Epstein, 2013) (Scicluna et al., 2008).

Studying the electrophysiological and molecular consequences of a mutation associated with cardiac arrhythmia should be ideally performed in the native cardiomyocytes environment. However, obtaining ventricular cardiac biopsies from patients is a highly invasive procedure and not without significant risk. Consequently the majority of functional studies on specific mutations associated with the arrhythmia disorders have made using heterologous expression systems, primarily Xenopus oocytes, human embryonic kidney (HEK) cells, and Chinese Hamster Ovary (CHO) cells, and COS-7 cells (Watanabe et al., 2008), in which the mutated ion channel of interest is expressed. Such cellular models have significant shortcomings since they lack important constituents of cardiac ion channel macromolecular complexes that might be required to reproduce the exact molecular and electrophysiological phenotype of the mutation. For example, the behavior of the Na^+ channel in cell expression systems seems to be different from that in CMs (Remme and 2008). One way of overcoming this has been to generate transgenic mice carrying specific mutations (Sabir et al., 2008). However, the costly generation of such mouse models is not practical for high-throughput screening of rare inherited arrhythmia mutations. Moreover, there remain crucial differences between mouse and human cardiac electrophysiological characteristics, such as the high basal heart rate (>500 bpm), the very negative action potential (AP) plateau phase, and the short AP duration of the mouse compared to human CM. These differences are amongst others due to the different biophysical properties in the transient outward currents (I_{to}) in human and mouse CMs (Nerbonne and Kass, 2005).

The discovery of somatic cell reprogramming to generate induced pluripotent stem cells has created much excitement because of the possibility of producing unique patient- and disease-specific human induced pluripotent stem cells (hiPS cells) lines (Takahashi and Yamanaka, 2006). With this technique, somatic cells can be turned into embryonic stem cell-like cells

which can differentiate into all cell types of the human body and be propagated indefinitely in culture. Human iPS cells preserve the integrity of the patient's genome and the complete set of genes that resulted in the disease is present. Thus, hiPS cells can provide genetically diverse human models to study mechanisms of diseases and identify strategies for potential new therapies (Marsman et al., 2014). Zhang et al were the first to show that hiPS cells can differentiate to functional CMs, making it possible to generate patient-specific human CMs with its own genetic background. The usual approach is to obtain somatic cells (classically skin fibroblasts) from selected patients with genetic diseases, to derive them into stem cells, and then to differentiate them into cardiomyocytes. After a number of weeks in culture, the cardiomyocytes will develop disease features such as abnormal contractile function, dysregulated calcium movements, altered electrical activity and can serve as a platform to model the disease. hiPS cells-derived CMs (hiPS-CMs) therefore represent a new model system for studying inherited arrhythmia disorders (Hoekstra et al., 2012). Since 2011, as a proof of concept, CM differentiated from patient-specific induced pluripotent stem cells (hiPS-CM) have been shown to provide valuable models of heritable cardiac arrhythmias, including catecholaminergic polymorphic ventricular tachycardia (Marsman et al., 2014) (Jung et al., 2012) and LQT (Moretti et al., 2010) (Itzhaki et al., 2011a) (Yazawa et al., 2011), and several other diseases (Table 3). They indeed recapitulated the predicted phenotypes of these well-described syndromes. It is now time to use human iPS cells as a primary experimental system to decipher unknown mechanism of more complex cardiac diseases.

Table 3: Heart Arrhythmic disorders analyzed using iPS cells.

Heart Arrhythmic Diseases	Phenotype observed / recapitulated in vitro	References
LQT-1	Cardiac action potential prolongation, irregularities in potassium gated voltage channel (KCNQ1) localization	(Gherghiceanu et al., 2011)
LQT-1	Drug-induced prolongation of field potential duration	(Egashira et al., 2012)
LQT-2	Prolonged field and action potential, drug-induced early after depolarization	(Matsa et al., 2011)
LQT-2	hiPS cells technology is able to model the abnormal functional phenotype of an inherited cardiac disorder and to identify potential new therapeutic agents	(Itzhaki et al., 2011a)
LQT-2	Electrophysiological abnormalities can be detected in hiPS-CM, even when derived from asymptomatic carriers of KCNH2 mutations	(Lahti et al., 2012)
LQT-2	Precise genetic modification of pluripotent stem cells provided a physiologically and functionally relevant human cellular context to reveal the pathogenic mechanism underlying this specific disease phenotype	(Bellin et al., 2013)
LQT-2	Modulation of chaperones proteins could be therapeutic in LQT-2 treatment	(Mehta et al., 2014)
LQT-3	Prolonged action potential duration, early after depolarization, sodium current irregularities	Malan D et al.,2011
LQT-3	hiPS cells could be useful to characterize LQT disease as well as drug responses in the LQT patient with a novel mutation	(Egashira et al., 2012)
LQT-3	Sodium current irregularities, prolonged QT interval	(Terrenoire et al., 2013)
Overlap Syndrome (OLS)	iPS-CM can recapitulate the characteristics of a combined gain- and loss-of-function Na^+ channel mutation and that the electrophysiological immaturity does not preclude their usage	(Davis et al., 2012)

IV.1. – Derivation of hiPS cells models

IV.1.1 – Cell origin

Although the first hiPS cells lines were derived from dermal fibroblasts (Takahashi and Yamanaka, 2006), hiPS cells can now be generated from a wide variety of somatic cells. It is important to consider easily accessible sources, which are efficient to reprogram and give minimal burden to the patient. Easily accessible sources used successfully for reprogramming include keratinocytes from skin or plucked hair (Aasen et al., 2008), peripheral blood (Loh et al., 2009) mesenchymal cells in fat (Sun et al., 2009), dental pulp (Tamaoki et al., 2010), oral mucosa (Miyoshi et al., 2010) and urine (Zhou et al., 2012).

IV.1.2 – Cell reprogramming

Somatic cells can be reprogrammed to a pluripotent state by introducing pluripotency-associated genes. The first reported iPS cells generated by transducing mouse fibroblasts with four retroviral vectors OCT4, SOX2, KLF4, and C-MYC (Takahashi and Yamanaka, 2006). The first human iPS cells were generated using the same four retroviral vectors (Takahashi et al, 2007) al or OCT4, SOX2, LIN28, and NANOG (Yu et al., 2007). Later studies reported reprogramming with other combinations and numbers of pluripotency factors. The hiPS cells thus generated can be kept in culture indefinitely either on feeder cells, mouse embryonic fibroblasts, and fetal calf serum-based medium or using defined mTESr/Matrigel-based protocols. Transplantation of hiPS cells into immune-compromised mice leads to the formation of teratomas with derivation of the three embryonic germ layers, demonstrating the pluripotent potential of these cells. In addition, differentiation of hiPS cells *in vitro* also results in derivation of the three germ layers (Figure 20).
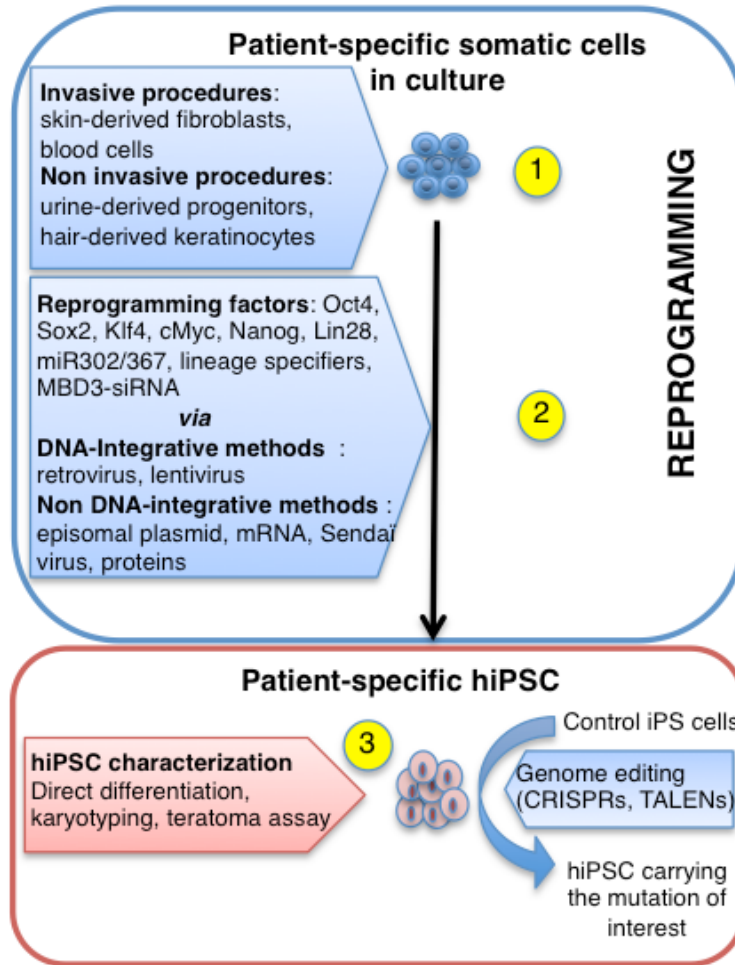
Figure 20: Type of procedures related to the source of human somatic cells. (2) Methods for reprogramming human somatic cells toward hiPS cells. (3) hiPS cells characterization for validation (Gerbal-Chaloin et al., 2014).

IV.1.3 – Generation of hiPS cells-derived cardiomyocytes

The ability to differentiate hiPS cells in a directed manner has progressed considerably in the past 8 years. The most reproducible and efficient strategies involve stage-specific activation of different signaling pathways in defined culture conditions, recapitulating key steps in cardiac development in the early embryo . There is consensus that the cardiac differentiation process is very delicate, and the variability in each individual component of the cardiac differentiation strategy must be carefully optimized to reliably produce cardiomyocytes from human pluripotent stem cells. One of the first directed differentiation methods involved human embryonic stem cells (hES cells) co-cultured with mouse visceral endoderm-like cells (END-2) (Mummery et al., 2003), which is relatively inefficient but has been shown to generate mostly (~85%) ventricular-like cardiomyocytes. This protocol provided early insight into methods for improving differentiation efficiency, such as removing fetal bovine serum (FBS), adding L-ascorbic acid (Passier et al., 2005), and removing insulin between d_0 and d_4 (Freund et al., 2008). Directed differentiation toward the cardiac lineage is mainly achieved by one of the following strategies: (1) the first involves the formation of EBs in the presence

of growth factors and repressors known to influence heart development (Kehat et al., 2001); (2) the second relies on the influence of endoderm on cardiac differentiation during embryogenesis (Mummery et al., 2003); (3) the third involves monolayer culture at high density of iPS cells seeded on matrigel with sequential treatment with Activin A and BMP4 (Laflamme et al., 2007).This method was developed using hES cells and has then been transferred to hiPS cells culture. Beating areas usually appear in 7-10 days. These areas can be microscopically dissected and dissociated in single cells. For electrophysiological and immunofluorescence analysis, the dissociated cells can be seeded onto glass coverslips. Figure 21 summarizes the principles of the reported strategies used for cardiomyocytes differentiation from human pluripotent stem cells
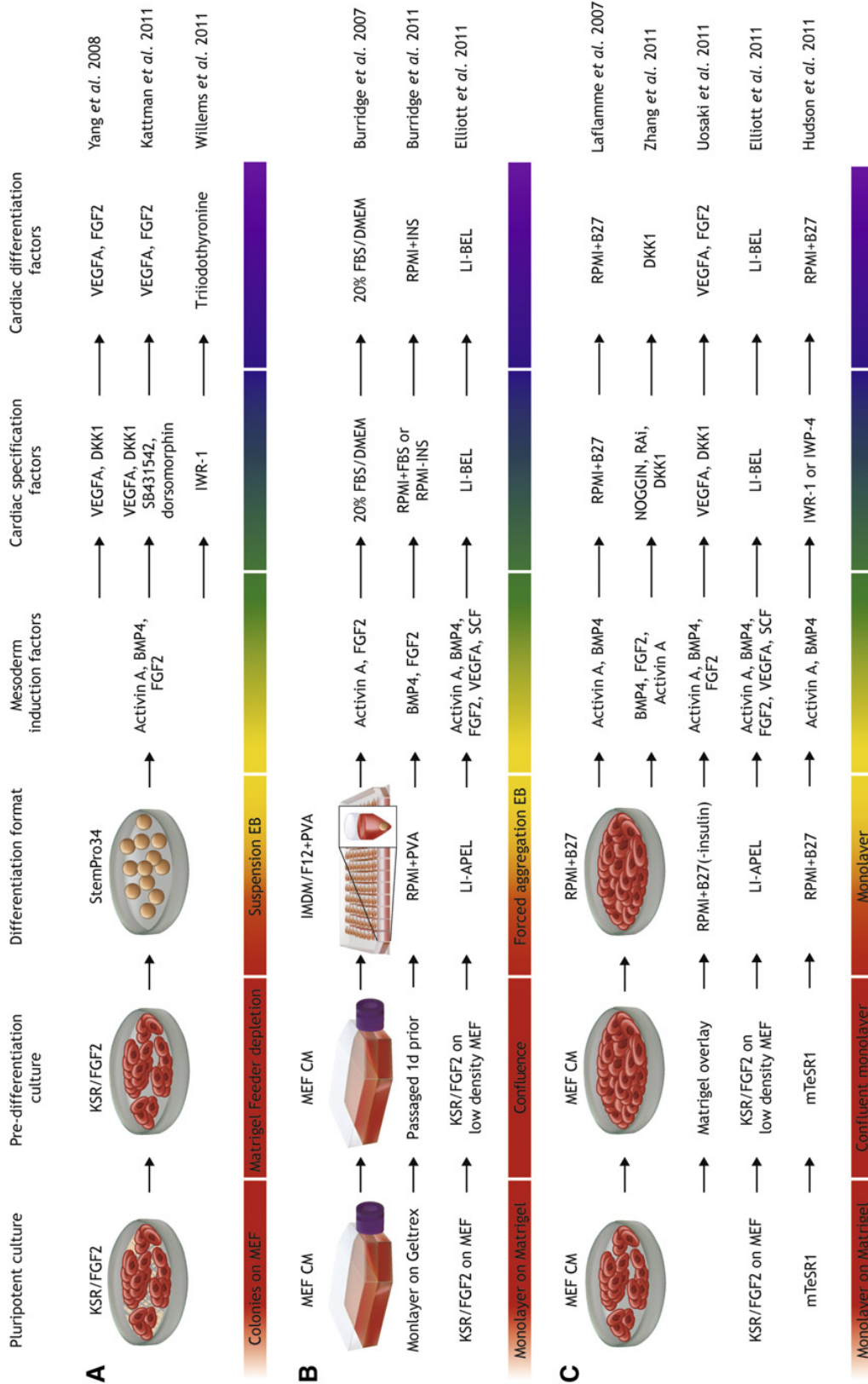
Figure 21: Methods for the Differentiation of Human Pluripotent Stem Cells. Three methods for differentiating hiPS cells, highlighting commonalities at each of the six steps: pluripotent culture, pre-differentiation culture, differentiation format, and treatment with mesoderm induction factors, cardiac specification factors, and cardiac differentiation factors. A. Yang et al. (2008) suspension EBs in StemPro34; B. Burridge et al. (2007) forced aggregation; C. Laflamme et al. (2007) monolayer differentiation (Burridge et al., 2012).

Collectively, these studies demonstrate that the importance of exposure of hiPS cells to various growth factors at specific times and in specific doses is essential for directing differentiation from early meso-endoderm to a specific cardiac state, via mesoderm state. Data collected from experiments using both the EB and monolayer methodologies show that four major signaling pathways are involved in early cardiac differentiation of hiPS cells: BMP pathway, TGFB/Activin/NODAL pathway, WNT pathway, and FGF pathway, with highly specific temporal windows for effectiveness (Figure 22) (Burridge and 2012).
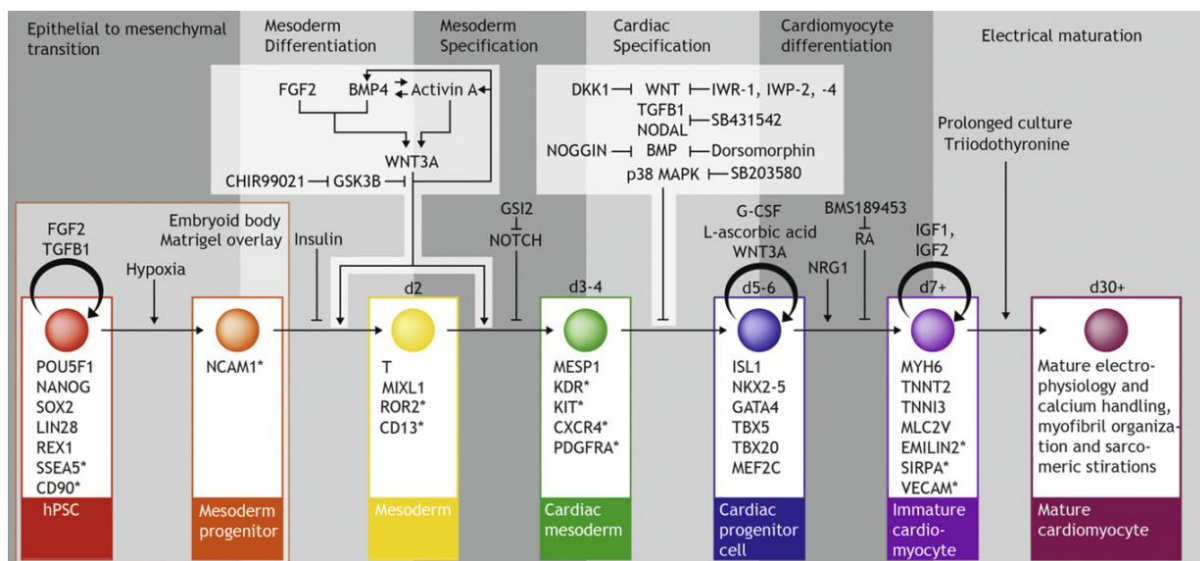
Figure 22: Schematic of Current Knowledge of Factors Involved in hiPS cells cardiac differentiation factors that influence the progression through each of the six major steps of hiPS cells cardiomyogenesis: epithelial to mesenchymal transition, mesoderm differentiation, mesoderm speciation, cardiac specification, cardiomyocytes differentiation, and electrical maturation. Data shown are derived from developmental biology models that have been directly assessed and proved functional in hiPS cells cardiac differentiation, along with knowledge gained directly from hiPS cells differentiation. Below are the markers associated with each of the seven cell types during differentiation; surface markers are marked with an asterisk (Burridge and 2012).

IV.2. – Characteristics of hiPS cells-derived cardiomyocytes

IV.2.1 – Molecular and structural characteristics

The first hiPS-CMs were generated by Zhang et al. (Zhang et al., 2009). In these cells the investigators examined the gene expression of the transcription factor Nkx2.5, the myofilament proteins cardiac troponin T, the α-myosin heavy chain, the α-Actinin, the atrial and ventricular isoforms of myosin light chain 2, the atrial natriuretic factor and the phospholamban (PLN). Low levels of cardiac troponin T and the atrial isoform of myosin light chain 2 were found in undifferentiated hiPS cells and high expression of all the cardiac genes were found in the hiPS-CMs, which was comparable to the expression of these genes in adult ventricular myocardium. Immunohistochemistry showed a typically striated pattern for

α-Actinin and myosin light chain. However, these cells had multi-angular morphologies and relatively disorganized sarcomeres (Dick et al., 2010) (Marsman et al., 2014) (Figure 23).
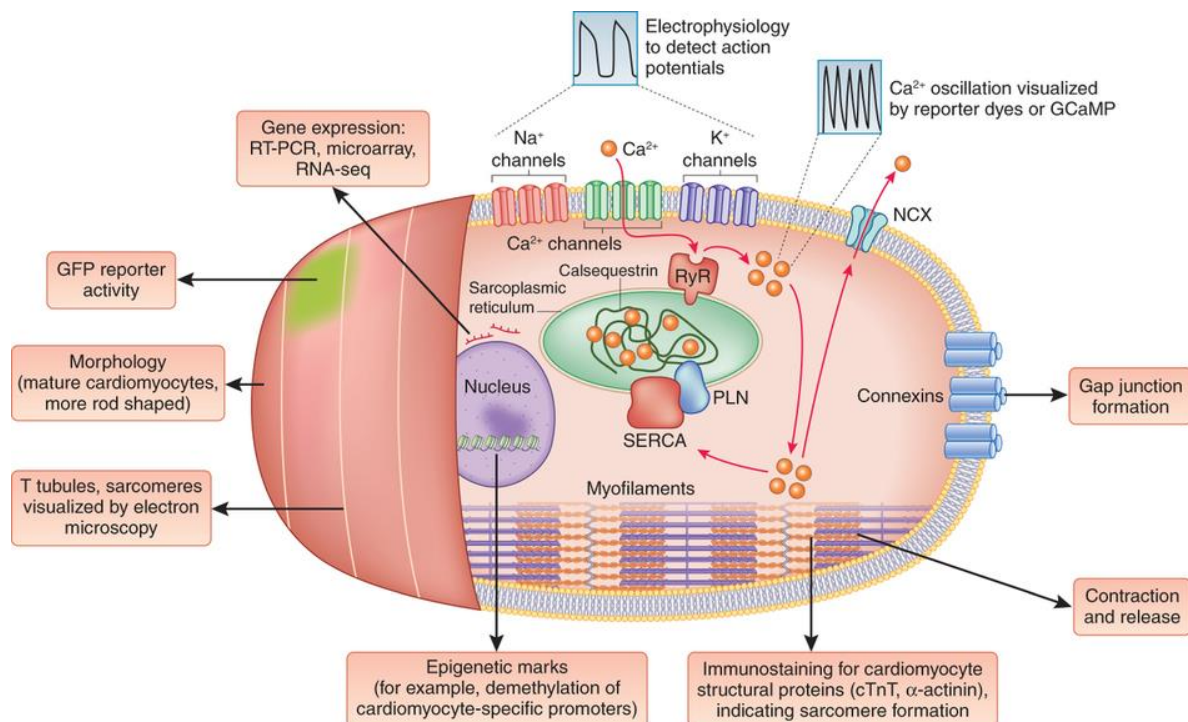
Figure 23: Defining cardiomyocyte identity. A wide range of phenotypic features can be assayed to determine whether a reprogrammed cell is a cardiomyocyte. These range from expression of a panel of genes or the activation of a reporter transgene (such as α-MHC–GFP) to more complex functional characteristics, such as the ability to fire action potentials and show calcium oscillation (Addis and Epstein, 2013).

IV.2.2 – Action potentials

Using the patch clamp technique, Zhang et al. were the first to measure the APs in spontaneously contracting cells isolated from hiPS cells-EBs (Zhang et al., 2009). The majority of the cells showed ventricular-like APs (70–74% of cells for two distinct hiPS cell lines), but atrial-like and nodal-like APs were also observed.

The distinction was made on AP phenotype, with a negative diastolic membrane potential, a rapid AP upstroke and a long plateau phase for ventricular-like APs. The absence of a prominent plateau phase was a characteristic of atrial-like APs, resulting in shorter AP duration compared to ventricular-like APs. Nodal-like APs showed a more positive maximum diastolic potential (MDP), a slower AP upstroke and a prominent phase 4 depolarization. Many studies were also published describing ventricular-like, atrial-like, and sometimes nodal-like APs (Moretti et al., 2010) (Itzhaki et al., 2011a) (Fatima et al., 2011) (Ma et al., 2011) (Matsa et al., 2011) (Jung et al., 2012) (Lahti et al., 2012), with the ventricular-like

phenotype being the most prominent AP form (76-48%) (Zhang et al., 2009) (Itzhaki et al., 2011a).

Table 4 summarizes the reported AP characteristics of hiPS-CMs, hES-CMs, and native ventricular CMs. The APs measured in hiPS-CMs differ from APs measured in freshly isolated native CMs (Table 4). The first remarkable difference is that most of the hiPS-CMs studied, including the ventricular-like and atrial-like cells, are spontaneously active, with beating rates between 28 and 108 bpm.

Table 4: Action potential characteristics in hiPS-CMs and human ventricular cardiomyocytes (Hoekstra et al., 2012).

Cell type	BMP	APD$_{90}$ (ms)	dv/dt$_{max}$ (V/s)	APA (mV)	MDP/RMP (mV)	Refernces
iPS-CMs V IMR90C4	43.8±2.7	320±17	40.5±4.6	87.7±2.6	-63.5±1.7	(Zhang et al., 2009)
iPS-CMs V Foreskin C$_1$	44.2±3.5	312.5±11.2	27.2±3.7	87.9±2.4	-63.3±1.5	(Zhang et al., 2009)
iPS-CMs V	68.2±2.7	381.3±35.3	9±0.2	107.8±2.1	-6..5±2.1	(Moretti et al., 2010)
iPS-CMs V	72±1.2	314.4±17.6	26.8±6.3	113±2.4	-63.4±1.3	(Lahti et al., 2012)
iPS-CMs V	35.5±2.1	414.7±21.8	27.8±4.8	101.5±2.5	-75.6±1.2	(Ma et al., 2011)
iPS-CMs V	28±5	495±36	9.5±1.8	109±3	-57±1	(Itzhaki et al., 2011a)
iPS-CMs V* ns	60	173.5±12.2	115.7±18.4	106±3.2	-72.4±0.9	(Davis et al., 2012)
hES-CMs V	47.1±23.3	247.2±66.7	13.2±6.2	85.4±9.3	-53.9±8.6	(He et al., 2003)
hES-CMs V		285.8±52.6	11.4±2.8	86.8±52.6	-62.3±8.6	(Zhang et al., 2011)
VM*	50	213±7	215±33	106.7±1.4	-81.8±3.3	(Magyar et al., 2000)
VM endo*	60	330±16	234±28	105±2	-87.1±1	(Drouin et al., 1998)
VM epi*	60	351±14	28±11	104±2	-86±1	(Drouin et al., 1998)

*iPS-CMs V: iPS-CM of ventricular like phenotype, iPS-CMs ns: not specified to action potential type, VM: native human ventricular myocytes, endo: endocardial, epi: epicardial, BMP: beats per minute, APD$_{90}$: action potential duration at 90% of repolarization, dv/dt$_{max}$: maximum upstroke velocity, APA: action potential amplitude, MDP: maximum diastolic potential, RMP: resting membrane potential, *: non spontaneous beating cells, hES-CMs V: hES-CMs of ventricular like phenotype.*

IV.2.3 – Ionic currents

The shape of the AP is the result of the various inwardly and outwardly directed ionic currents present in the CMs. Because of the clear differences in AP shape between native CMs and hiPS-CMs, one can assume that differences exist in the content and function of the various cardiac ion channels between the two cell types. In this part there is a detailed comparison between the cardiac ionic currents in hiPS-CMs with those in native CMs.

IV.2.3.1 – Sodium current

The cardiac Na^+ current (I_{Na}) is responsible for the AP upstroke in ventricular CMs. Mutations in the genes encoding the α and β-subunits of the cardiac Na^+ channel can alter the kinetics and amount of the cardiac Na^+ current (Remme and 2008). The upstroke velocity in hiPS-CMs APs is low compared to the AP upstroke of freshly isolated human ventricular CMs. In hiPS-CMs, I_{Na} was studied in detail in two reports. Ma et al. reported a half-maximal potential ($V_{1/2}$) of activation and inactivation of -34.1 and -96.1 mV , respectively. Davis et al. reported a $V_{1/2}$ of activation of ~42 mV (Davis et al., 2012). The findings of these studies are consistent with values reported for native human ventricular CMs. The low temperature and reduced Na^+ concentration used to study the maximal peak I_{Na} in native human ventricular CM prevents comparison with the maximal peak I_{Na} measured in hiPS-CMs. Other I_{Na} characteristics, such as recovery from inactivation and slow inactivation kinetics have been reported (Davis et al., 2012). In the presence of the Na^+ channel blocker tetrodotoxin (TTX) the upstroke of the AP in hiPS-CMs is delayed and the dv/dt_{max} is reduced (Ma et al., 2011). Whether I_{Na} plays a role in spontaneous activity in hiPS-CMs is unknown. However, hiPS-CMs have prominent Na^+ currents with characteristics close to that of native human ventricular CMs. Despite lack of information to compare maximal peak I_{Na}, it seems that the low dv/dt_{max} of spontaneously active ventricular-like hiPS-CMs APs is due to lower functional availability of Na^+ channels (due to the relative positive value of the RMP) rather than differences in I_{Na} density.

IV.2.3.2 – Calcium current

Two types of Ca^{2+} currents exist in the mammalian heart, the L-type (I_{CaL}) and T-type (I_{CaT}) Ca^{2+} current. Patch clamp studies have demonstrated the presence of the I_{CaL} in hiPS-CMs with a $V_{1/2}$ of activation and inactivation of -15 and -29 mV, respectively (Ma et al., 2011). These values are more comparable to those found in native atrial CMs (-12 and -27 mV, for $V_{1/2}$ of activation and inactivation, respectively) than native ventricular myocytes (-4.2 and -4.7 mV and -23.5 and -19.3 mV) (Ma et al., 2011).

IV.2.3.3 – Transient outward current

Two transient outward current components are found in native mammalian cardiac cells, one carried by K^+ (I_{to1}), the other by Cl^- ions (I_{to2}). I_{to1} has been found in hiPS-CMs (Moretti et al., 2010) (Ma et al., 2011), but data about its gating properties have not been published.

IV.2.3.4 – The delayed rectifier potassium current

In the mammalian heart, the delayed rectifier K^+ current (I_K) is composed of three different components: the ultra-rapid (I_{Kur}), the rapid (I_{Kr}), and the slow (I_{Ks}) components. I_{Kr} has been reported in hiPS-CMs with a maximal I_{Kr} density varying between 0.55 and 1.9 pA/pF(Moretti et al., 2010) (Ma et al., 2011) (Lahti et al., 2012) (Itzhaki et al., 2011a). In hiPS-CMs, blockade of I_{Kr} by E4031 resulted in a significant AP prolongation. In addition, E4031 induced early after-depolarizations (EADs) (Itzhaki et al., 2011a) (Ma et al., 2011) (Matsa et al., 2011). These data show that I_{Kr} plays a prominent role in the repolarization phase of hiPS-CMs APs.

The presence of I_{Ks} in hiPS-CMs has been reported in two studies. Ma et al. found I_{Ks} in 5 out of 16 cells studied, and when present the average I_{Ks} density was 0.31 pA/pF (Ma et al., 2011). In contrast, Moretti et al. measured I_{Ks} in all studied cells and the average density was around 2.5 pA/pF (Moretti et al., 2010). In hiPS-CMs, blockade of I_{Ks} by chromanol 293B results only in minimal prolongation of the AP (Ma et al., 2011) This is consistent with the relative small number of cells exhibiting I_{Ks} and the small I_{Ks} densities found in their study, but contrast with the effects of a loss-of-function I_{Ks} mutation which results in a prominent AP prolongation.

IV.2.3.5 – Excitation-Contraction coupling

hiPS-CMs display visible contractions. Calcium Induced Calcium Release (CICR) is the key mechanism underlying excitation-contraction coupling. The key Ca^{2+} handling proteins, RyR2, sarcoplasmic reticulum Ca^{2+} -ATPase (SERCA), junctin (Jun), triadin (TRDN), Na^+/Ca^{2+} exchanger (NCX), calsequestrin (CASQ2), L-type Ca^{2+}channel (Cav1.2), inositol-1,4,5-trisphosphate receptor (IP3R2) and PLN are expressed in hiPS-CMs (Itzhaki et al., 2011b) (Lee et al., 2011) Spontaneous rhythmic Ca^{2+} transients are present in hiPS-CMs, and blocking of the $I_{Ca,L}$ by nifedipine, abolishes Ca^{2+} transients (Itzhaki et al., 2011b). The presence of functional SR and RyRs was proven by application of caffeine, which induced a large Ca^{2+} transients (Itzhaki et al., 2011b), consistent with findings in human ventricular

CMs (Piacentino et al., 2003). In addition, ryanodine caused a reduction in the amplitude of the Ca^{2+} transients (Itzhaki et al., 2011b) (Lee et al., 2011). The pattern of Ca^{2+} transients in hiPS-CMs was studied by transverse line-scan images and revealed a U-shape Ca^{2+} wavefront (the rise of Ca^{2+} in the periphery is faster than in the center of the cell), which is typical for t-tubule deficient cells (Lee et al., 2011). This suggests that hiPS-CMs lack t-tubuli, an observation in line with that of Novak and co-workers who did not find t-tubuli using transmission electron microscopy (Novak et al., 2012). This would mean that hiPS-CMs likely have poor coupling between Ca^{2+} influx through L-type Ca^{2+} channels and Ca^{2+} release from the SR through RyRs.

V – Conclusion

Cardiac arrhythmic diseases are of variable complexity, and various genes and distinct mutations are associated with the pathophysiology of these diseases. In my thesis I am interested in two examples of these diseases. The first example is LQT-2; LQT-2 was one of the first cardiac diseases extensively studied in hiPS-CMs because of the low genetic complexity associated with this disease. LQT-2 was modeled using hiPS-CMs of various origins except urine cells. In this context, we aimed to model congenital LQT-2 using hiPS-CMs of urine-derived cellular origin. We also investigated whether acquired LQT2, in the context of HIV infection, could be modeled and studied using hiPS-CMs.

BrS is the other disease we are interested in. A high complexity is associated with this disease as despite the extensive genetic studies, no common genetic variant has been identified in BrS patients. Despite all the work that has been developed since the identification of the syndrome in 1992, many questions remain unresolved. Compared with advances that have been conducted in other arrhythmic diseases such as long QT syndrome, knowledge on BrS pathophysiological bases is progressing more slowly. One of the major limitations in understanding BrS is probably the weakness in modeling this pathology. In this issue, hiPS-CMs may provide another brick in the wall of the mechanistic bases of this pathology.

II. HYPOTHESIS AND OBJECTIVES

Channelopathies are electrical disorders that are due to gene mutations that affect the function of ion channels responsible for the generation of action potentials (AP). There has been a substantial progress in understanding the genetic basis of these disorders, allowing improvement of diagnostic and preventive strategies in the management of patients. However, the less understood relationship between the genotype and phenotype of these diseases limits accurate prediction of clinical manifestations of disease, assessment of prognosis, and selection of appropriate preventive measures and therapeutic approaches.

Although heterologous expression systems and animal models have provided important insights into cardiac arrhythmic syndromes pathogenesis, the lack of in vitro sources for human cardiomyocytes and the inability to model patient-specific disease variations has significantly hampered the study of these diseases. In the past 10 years, Dr. Yamanaka's revolutionary discovery of how to transform ordinary adult skin cells into stem cells that can develop into any cell in the human body has fundamentally altered the fields of developmental biology and stem cell research. In opposition to animal models, human iPS cells preserve the integrity of the patient's genome and the complete set of genes that resulted in the disease is present. In order to make proof of concept, so far iPS studies in the cardiovascular field have been used for diseases that were already mechanistically well understood, such as Long QT syndromes. These studies showed that iPS cell-derived cardiomyocytes successfully validate data previously obtained using other models. It is now time to use human iPS cells as a primary experimental system to decipher unknown mechanism of cardiac diseases, such as Brugada syndrome. We hypothesized that **hiPS-CMs may provide novel insights into cardiac arrhythmia pathophysiology and offer a unique approach to improve understanding of patient-specific genotype-phenotype relationships.**

Objective 1: To validate the use of cardiomyocytes differentiated from urine-derived pluripotent stem cells as a new cellular model to study patient's specific arrhythmia mechanism.

Objective 2: To use cardiomyocytes derived from hiPS-CMs to decipher the mechanism of a non-genetic disease, such as cardiac arrhythmias in HIV patients.

Objective 3: To characterize and explore functional characteristics of hiPS-derived cardiomyocytes from BrS patients carrying different genetic backgrounds in order to unveil their common phenotype

III.   MATERIALS AND METHODS

I – Molecular Biology

I.1 – Site directed mutagenesis

I.1.1 – Principle

Site directed mutagenesis allows the introduction of one or more specific mutations in a gene. Initially, the sequence to be modified is inserted into a plasmid. PCR pair of primers containing desired mutation(s) is used; parental plasmids are the template to amplify the mutated plasmid.

Site-directed mutagenesis based on PCR has several advantages: (i) high yield; (ii) low risk to form secondary structures (thanks to high temperatures) that may reduce the effectiveness of DNA. polymerization The main limitations of this technique are: (i) the risk that some polymerases make mistakes; (ii) PCR conditions should be developed for each new primer pair for each new matrix; (iii) long fragments are sometimes difficult to amplify (> 2-3 kb).

I.1.2 - Protocol

Directed mutagenesis experiments were performed to obtain N1722D-*SCN5A* point mutation. The point mutation N1722D (1859G>A) in *SCN5A* was introduced using mutated oligonucleotide extension (QuikChange II XL Site-Directed Mutagenesis Kit) in *SCN5A* isoform 2 cDNA (GenBank Acc. No. NM_000335). The mutated plasmid was verified by complete DNA sequencing of the cDNA insert by the genomics core facility (genomics platform Nantes, SFR Health Bonamy F).

II – Cell models used

II.1 – COS-7 cell line and transfection

For the BrS study, I used COS-7 line. COS-7 cell line is derived from African Green Monkey kidney fibroblasts. Because of the absence or very low level of sodium currents of endogenous potential, this line is used as a heterologous expression system for Na^+ channels.

II.1.1 – Culture media

COS-7 cell line was maintained in 25 cm² plastic flasks in a humidified incubator at 37 ° C in the presence of 5% CO2. The culture medium for the COS-7 line is composed of DMEM (Dulbecco's Modified Eagle Medium, Gibco BRL) supplemented with 10% fetal calf serum 2 mM L-Glutamine, 100 U / ml penicillin and 100 ug / ml streptomycin The culture medium is changed every 2 days.

II.1.2 – Transfection

Cells were transfected with 2 µg *SCN5A* plasmid (wild type or mutant) together with 2 µg of beta subunit (SCN1B) plasmid. Transfections were performed using JetPI reagents (Polyplus Transfections, France) according to the manufacturer's instructions. Enhanced green fluorescent protein GFP encoding plasmid (1.2 µg) was included to identify transfected cells

II.2 – Human induced pluripotent stem cells maintenance

Human induced pluripotent stem cells (hiPS cells) were generated by Karim Si-Tayeb team for the LQT-2 study and by the iPSC platform in Nantes for the BrS study. Following that, hiPS were kept on mitotically-inactivated feeder cells (mouse embryonic feeder cells (MEFs) For maintenance and amplification, cells were kept in DMEM/F12 medium supplemented with 2 mmol/L L-glutamine, 0.07% β-mercaptoethanol, 20% knockout serum replacement, 5 ng/mL bFGF and 1% NEAA under low oxygen atmosphere (4% O2). Cells were passaged by manual dissection of cell clusters every 6-7 days.

II.3 – Human induced pluripotent stem cells-derived cardiomyocytes

II.3.1 – Principle

The second important step in my thesis after reprogramming was to establish an efficient differentiation protocol. After the discovery of human induced pluripotent stem cells by Yamanaka et al (Takahashi and Yamanaka, 2006), a lot of groups worked on establishing various differentiation protocols for different types of cells including cardiomyocytes. Many protocols were already used for generating cardiomyocytes form embryonic stem cells (Anderson et al., 2007)

In our lab, human iPS cells were differentiated into cardiomyocytes using the established matrix sandwich method with modifications. Cardiomyocytes differentiation protocols use cytokines that mimics the developmental environment which lead to the formation of cardiomyocytes. Growth factors including Activin A, BMP4 and FGF2 have been shown to enhance the cardiac specification of hiPS cells, in a time- and dose-dependent manner [7] [8].

II.3.2 – Protocol

Briefly, 6 days before initiating differentiation, hiPS cell colonies were passaged on hESC-qualified matrigel-coated plates (0.05 mg/ml, using Gentle Cell Dissociation Buffer and cultured as a monolayer in StemMACS (iPS-Brew XF) (Miltenyi), human with 1x Y-27632 Rock inhibitor (Miltenyi) under normal oxygen atmosphere. Rock inhibitor reduces cell

apoptosis prior to differentiation. When cells reached 80% confluence, cold StemMACS with Growth Factor Reduced Matrigel (0.033 mg/ml, BD Corning) was added in order to create an overlay of Matrigel. Differentiation was initiated 24 h later (day 0) by culturing the cells in RPMI1640 medium (Life Technologies) supplemented with B27 (without insulin, Life Technologies), 2 mmol/L L-glutamine (Life technologies), 1% NEAA (Life technologies), 100 ng/mL Activin A (Miltenyi), and 10 ng/mL FGF2 for 24 hours. On the next day, the medium was replaced by RPMI1640 medium supplemented with B27 without insulin, 2 mmol/L L-glutamine, 1% NEAA, 10 ng/mL BMP4 (Miltenyi), and 5 ng/mL FGF2 for 4 days.

By day 5, cells were cultured in RPMI1640 medium supplemented with B27 complete (Life Technologies), 2 mmol/L L-glutamine and 1% NEAA, and changed every 2-3 days (Figure 24).
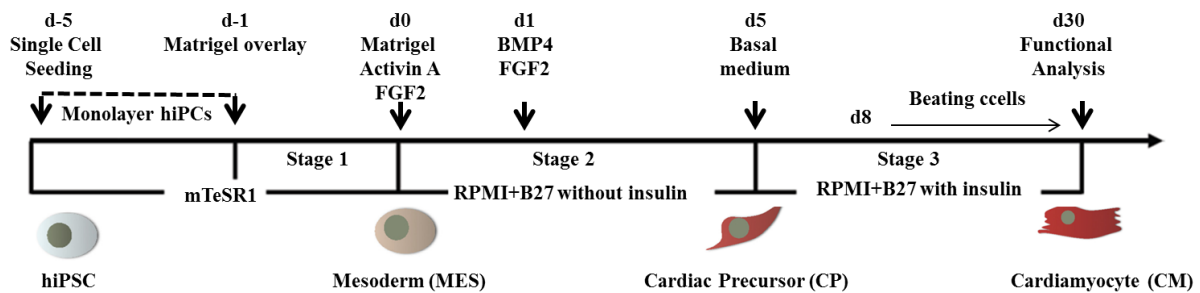
Figure 24: Detailed cardiac differentiation protocol for both urine derived hiPS cells and skin derived hiPS cells.

II.3.3 – Limitations

Beating 3 D structures are obtained starting from days 8-10, this is considered the primary sign of a successful differentiation; however, the protocol that we used have some limitations: (i) large variations remain between the cardiogenic potential of hiPS cell lines (Control/diseased), clones of the same line, and even passages of the same clones. (ii). Also the differentiated cardiomyocytes are a mixed population of: cardiac cells (atrial, nodal or ventricular) and non-differentiated cardiac cells (iii). In addition, differentiated cardiac cells have an immature phenotypes such as automaticity. Indeed, further modifications of our differentiation protocol are planned to be added.

III - Patch-clamp

III.1 – Principle

The main of objective of my thesis was to model arrhythmic disorders using hiPS-CMs. Indeed, modeling arrhythmic disease depend on the ability of recording action potentials and various ionic currents in cardiomyocytes.

In the three projects I have worked on, I used the patch-clamp technique to record action potentials and ionic currents. Patch clamp depends on the usage of a glass pipette, whose end has a diameter of about 1 micron, on a cell membrane, the pipette contacting / membrane is electrically highly resistant. This contact is enhanced by a slight suction exerted inside the pipette. When the contact resistance gigaohm reached, the contact is then called "giga-seal". This high resistance allows a perfect electrical insulation of the whole pipette cell.

At this point two types of patch clamp are differentiated. For action potential recordings, I used permeabilized patch clamp. Its defining feature is that electrical access to the cell is obtained through inclusion of a pore-forming antibiotic (in our case is amphotericin B) in the patch pipette which perforates the sealed patch of membrane in contact with the patch pipette. The antibiotic pores allow equilibration of small monovalent ions between the patch pipette and the cytosol whilst maintaining endogenous levels of divalent ions such as Ca^{+2} and signaling molecules such as cAMP. Other benefits of using perforated patch-clamp over conventional patch-clamp include reduced current rundown and stable whole-cell recording. All these conditions are crucial to record an action potential. After cell perforation the access resistance to the cell will decrease gradually, then action potential are recorded in I clamp mode.

On the other hand, to record different ionic currents, I used ruptured patch clamp. The isolated membrane fragment under the pipette is aspirated using a syringe. After piercing the cell, the resistance between the middle intra-pipette and the intracellular medium is greatly reduced, allowing electrical access to the intracellular environment. The membrane potential is then imposed and trans-membrane currents are recorded between the electrode positioned in the pipette and the reference in the bath (V clamp mode). A patch clamp amplifier (Axopatch 200A, Axon Instruments) connected to a computer with the acquisition software and Acquis-1 analysis (Bio-Logic) was used.

For LQT-2, as this syndrome is characterized with a prolongation in action potential and a reduction in I_{Kr}, action potentials and I_{Kr} were recorded. Moreover, in the second study about

modeling HIV-arrhythmic mechanisms, same measurements were done. For BrS study, sodium current, late sodium current, and action potentials were recorded.

III.2 – Cell dissociation

Regarding the cells, patch clamp measurements is only accessible in single isolated cells. For COS-7 cells, ordinary cell passage was done to ensure proper isolation of transfected cells. For hiPS-CMs, the following dissociation protocol modified form Terrenoire et al. was used (Cecile Terrenoire et al., 2013) to dissociate cardiac differentiated cells prior to patch clamp. Cardiomyocytes were dissociated around day 20 of differentiation, for 20 min in collagenase II (200 U/mL; Gibco) at 37°C. Isolated cells were then incubated at room temperature for 30 min in Kraft-Bruhe solution containing 85 mmol/L KCl, 30 mmol/L K_2HPO_4, 5 mmol/L $MgSO_4$, 1 mmol/L EGTA, 2 mmol/L Na_2-ATP, 5 mmol/L Na-pyruvate, 5 mmol/L creatine, 20 mmol/L taurine, and 20 mmol/L glucose, pH 7.2 (Figure 25).
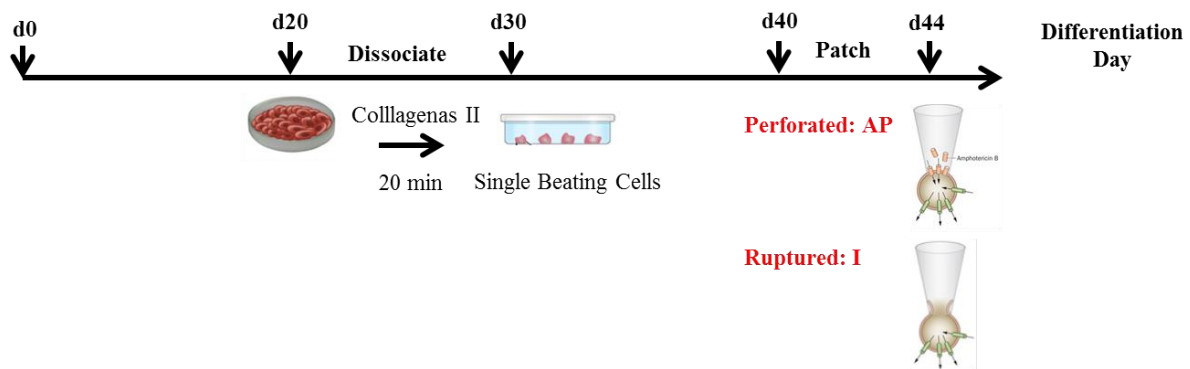
Figure 25: Detailed dissociation protocol for hiPS-CMs cells

III.3 – Solutions

Single isolated cells were selected for patch clamp. Green fluorescence cells were selected for patch clamp of COS-7 cells, while beating cells were selected for hiPS-CMs patch clamp. In both cases, cells were perfused with an extracellular solution that varies in constituent depending on the recordings done. Data were collected from a minimum of 4 independent differentiations for at two-three clones per patient.

II.3.1 – Action potential recordings

AP measurements were also performed using patch clamp (permeabilized I clamp), APs were measured at $35 \pm 2°C$ using a modified Tyrode solution containing (in mM): 140 NaCl, 5.4 KCl, 1.8 $CaCl_2$, 1.0 $MgCl_2$, 5.5 glucose, 5.0 HEPES; pH 7.4 (NaOH). The pipette solution contained (in mM): 125 K-gluconate, 20 KCl, 10 NaCl, 10 HEPES; pH 7.2 (KOH) and 0.22

amphotericin-B . Minimum diastolic potential (MDP), maximal upstroke velocity (Vmax), AP amplitude (APA), and AP duration (APD) at 20, 50 and 90% repolarization (APD20, APD50, and APD90, respectively) were analyzed. Data from 3 consecutive APs were averaged. Recorded action potentials were classified into atrial, nodal and ventricular (Ma et al., 2011).

II.3.2 – I_{Kr} recordings

The rapid component of the delayed rectifier K+ current (I_{Kr}) was recorded in the ruptured patch-clamp configurations, respectively. Cells were continuously super-fused with a Tyrode solution containing (in mmol/L): NaCl 140, KCl 4, $CaCl_2$ 1, $MgCl_2$ 1, glucose 10, HEPES 10; pH 7.4 (NaOH). During recording, a local gravity micro perfusion system allowed application of drugs, dissolved in Tyrode solution . For I_{Kr} recording, the pipette was filled with a solution containing (in mmol/L): K-gluconate 125, KCl 20, K2ATP 5, HEPES 10, EGTA 10; pH 7.2 (KOH). All products were purchased from Sigma. Data were recorded through an A/D converter (Digidata 1440A, Molecular Devices), using an Axopatch 200B amplifier (Molecular Devices). Membrane currents were analyzed with Axon pClamp 10 (Molecular Devices). Borosilicate patch pipettes had a tip resistance of 2-2.5 MΩ. All experiments were made at 35 ± 2°C. During voltage-clamp experiments, nifedipine (4 µmol/L) was added to the external solution to block the L-type calcium current ($I_{Ca,L}$).

II.3.3 – I_{Na} recordings

II.3.3.1 – I_{Na} recordings in COS-7 cells

Currents were recorded 2 days after transfection using a MultiClamp 700B amplifier and Multi Clamp Commander (Axon Instruments, Molecular Devices, Biberach van der Riss, Germany). Cells were super fused with a solution containing the following (in mmol/L): 145 NaCl, 4 CsCl, 1 $CaCl_2$, 1 $MgCl_2$, 5 HEPES, and 5 glucose, pH=7.4 with NaOH. Patch pipettes were fabricated from borosilicate glass capillaries (Module Ohm, Herlev, Denmark) and had resistances between 2.5 and 3 MΩ when filled with pipette solution (in mmol/L): 90 KCl, 45 K-gluconate, 10 NaCl and 10 HEPES, pH=7.4 with CsOH. Electronic compensation of series resistance to 65% to 70% was applied to minimize voltage errors. All analog signals were acquired at 10 to 50 kHz, filtered at 6 kHz, digitized with a Digidata 1440 converter (Axon Instruments), and stored using pClamp10 software (Axon Instruments). All recordings were made at room temperature (20°C -22°C). Data were analyzed using pClamp10 software.

II.3.3.2 – I$_{Na}$ recordings in hiPS-CMs

I$_{Na}$ measurements were recorded in the ruptured patch-clamp configuration. Cells were perfused using a Tyrode solution containing (in mM): 130 NaCl, 10 CsCl, 1.8 CaCl2, 1.2 MgCl2, 11.0 glucose and 5.0 HEPES; pH 7.3 (CsOH). The pipette solution contained (in mM): 3.0 NaCl, 133 CsCl, 2.0 MgCl2, 2.0 Na2ATP, 2.0 TEACl, 10 EGTA, 5.0 HEPES; pH 7.2 (CsOH). During recording, a local gravity micro perfusion system allowed application of an extracellular solution containing (in mM): 20 NaCl, 110 CsCl, 1.8 CoCl2, 1 MgCl2, 30 mannitol and 5.0 HEPES; pH 7.4 (CsOH) (Davis et al., 2012) (Ma et al., 2011). I$_{Na}$ densities and gating properties were measured at 35±2°C using voltage-clamp protocols shown in the relevant figures. All measurements were performed using a holding potential of -100 mV with a cycle time of 2 seconds for single step and activation, 3 seconds for inactivation and 4 seconds for recovery form inactivation. Current densities were calculated by dividing current amplitude by membrane capacitance (Cm) in (pF).

Late I$_{Na}$ was measured as a TTX-sensitive current (0.01mM) at room temperature using an ascending ramp protocol. Same intracellular and extracellular solutions were used as in the case of I$_{Na}$ peak current with a local gravity micro perfusion system of the following composition (in mM): 130 NaCl, 10 CsCl, 1.8 CoCl$_2$, 1 MgCl$_2$, 20 mannitol, 10.0 HEPES and 0.01 TTX; pH 7.4 (CsOH) (Ma et al., 2011).

III.4 – Analysis

All the measured currents are normalized by the membrane capacitance. For sodium current, the series resistance and capacitance are compensated between 60 and 70% to reduce their maximum contribution during the current measurement.

I$_{Kr}$ was measured as a 1 µmol/L E-4031-sensitive current, by digitally subtracting the current in the presence of E-4031 from that in its absence. I$_{Kr}$ densities were calculated by dividing current amplitude (pA), measured at the peak of the tail current at -60mV following a depolarization to 50 mV (prepulse), by cell membrane capacitance (pF).

The stimulation sequences allowing current measurements are presented in the manuscripts. The activation curves of I$_{Kr}$ and I$_{Na}$ (relative conductivity as a function of potential) following the waning of a sigmoid. V$_{1/2}$ activation parameters (V$_{1/2}$ act) and K are calculated by non-linear regression of the activation curve according to the Boltzmann function:

$$G / G_{max} = 1 / (1 + exp (- (V_P - V_{1/2} act) / K))$$

Or:

- G, conductance measured at V_p; $G = I / E_m\text{-}E_x$

- G_{max}, maximum conductance

- I, current measured at the peak

- E_m imposed potential

- E_x reversal potential of the ion X

- V_p pulse potential

- $V_{1/2}$ act, potential at which half of the channels are activated

- K, Boltzmann constant

Inactivation curves or availability (relative current according to the potential of the pre-stimulation) also follow a sigmoid. The parameters $V_{1/2}$ inact and K are calculated by non-linear regression of the availability curve according to Boltzman function:

$$I / I_{max} = 1 / (1 + exp\ (\text{-}\ (V_{pp}\text{-}\ V_{1/2}\ inact) / K))$$

Or:

- K, Boltzmann constant

- V_{pp}, prepulse potential

- $V_{1/2}$ inact, potential at which half of the channels are inactivated

IV – Biochemistry

IV.1 – Western blot

Western blot technique is used to assess total expression of a in a biological sample by a specific antibody of the protein of interest. This technique is semiquantitative and only allows the evaluation of the expression of a protein in comparison to another. It does not quantify precisely the amount of protein in the biological sample.

The Western blot technique is used to estimate the total expression of hERG protein in hiPC-CMs of projects 1 and 2. The cells are initially , lysed in a buffer containing 150 mM NaCl, Tris 20 mM pH 7.2, EDTA (ethylene diamine tetraacetic acid) 1 mM, Triton 1% PMSF (phenylmethanesulfonylfluoride) to 1mM taken up in absolute ethanol and a cocktail of protease inhibitors (Roche Diagnostics). The cell lysates were rotated for 20 min at 4 ° C then centrifuged at 14,000 G, 20 min at 4 ° C also. A protein assay is then carried out against a range of standard bovine serum albumin (BSA) in order to load an equivalent quantity of protein in each well. The lysates were denatured for 10 min at 50 ° C in Laemmli buffer containing 2% SDS (sodium dodecyl sulfate), 10% glycerol, 10 mM DTT (dithiothreitol), 65mm Tris, pH 6.8 and a blue peak bromophenol. 100 micrograms of each sample were

loaded onto a 10% polyacrylamide gel the proteins were separated by electrophoresis in presence of SDS. After migration, the proteins are transferred onto a nitrocellulose membrane at 4 ° C for 2 hours at 100V in a buffer containing: glycine 192mm, Tris 25 mM, SDS to 0.1% and ethanol 20%. To check the quality of the migration and transfer, the proteins are stained with ponceau red. After rinsing, the membrane is saturated for one hour in TBS-T buffer (10 mM Tris, NaCl 0.5mm and 0.1% Tween) containing 5% skimmed milk lyophilized. The membrane is then incubated with primary antibody overnight at 4 ° C in TBS-T milk. Three 5 minute washes in TBS-T milk are then made and then the membrane is incubated with the secondary antibody for 1 hour at room temperature in TBS-T milk. After 3 rinses with TBS-T for 10 minutes each, the revelation is done with an ECL plus western blotting detection system (Amersham) displayed using an imaging RT ImageQuant ECL (GE Healthcare).

IV.2 – Immunofluorescence

Immunofluorescence technique depends on the usage of a specific antibody to study, using a fluorescent microscope, the localization of a protein in the cell.

For histological analysis two cell types were analyzed: undifferentiated hiPS cells, which were cultured in 12 well plates on MEF feeders, dissociated hiPS-derived cardiomyocytes, which were plated on IBIDI plates (Biovalley) and further cultured for 6 to 10 days. For, hiPS on MEFs were fixed with 4% PFA, permeabilized with 0.5% Triton X-100 and blocked with 3% PBS-BSA. Cells were then stained with primary antibodies directed against OCT3/4 (Santa Cruz), SOX2 (Santa Cruz) and TRA1-60 (eBioscience) diluted in 1% PBS-BSA. For , after methanol fixation, cells were permeabilized with 0.1% Triton X-100, blocked with 5% PBS-BSA and stained with primary antibodies against α-Actinin (Abcam), troponin I (Santa Cruz), MLC2a (Abcam), MLC2v (Proteintech Europ), connexin 43 (Chemicon), or Nav1.5 (Alomone labs). Secondary antibody staining was performed using Alexa 488- and Alexa 568-conjugated antibodies (Molecular Probes). DAPI was used for nuclear staining.

IV. RESULTS

<u>I – Towards Personalized Medicine: Using Cardiomyocytes Differentiated from Urine derived Pluripotent Stem Cells to Recapitulate Electrophysiological Characteristics of LQT-2 syndrome</u>

Towards Personalized Medicine: Using Cardiomyocytes Differentiated from Urine derived Pluripotent Stem Cells to Recapitulate Electrophysiological Characteristics of LQT-2 syndrome

Mariam Jouni[a-e*], MSc, Karim Si-Tayeb[a-d*], PhD, Zeineb Es-Salah-Lamoureux[a-d], PhD, Xenia Latypova[a-d], MSc, Benoite Champon[a-d], BSc ,Amandine Caillaud[a-d], PhD, Anais Rungoat[a-d], BSc, Flavien Charpentier[a-d], PhD, Gildas Loussouarn[a-d], PhD, Isabelle Baró[a-d], PhD, Kazem Zibara[e], PhD, Patricia Lemarchand[a-d], MD,PhD, Nathalie Gaborit[a-d], PhD.

a. *Inserm, UMR 1087, l'institut du thorax, Nantes, France*

b. *CNRS, UMR 6291, Nantes, France*

c. *Université de Nantes, Nantes, France*

d. *CHU Nantes, l'institut du thorax, Nantes, France*

e. *ER045, PRASE, Laboratory of stem cells, Lebanese university, Beirut, Lebanon.*

*. *These authors contributed equally to this work.*

I.1 – Introduction

Despite major advances in the understanding and treatment of heart arrhythmic disorders, sudden cardiac death still represents a significant cause of morbidity and mortality worldwide. Channelopathies associated with cardiac arrhythmias have essentially been studied in heterologous systems or animal models, independently of the patients' genetic background. However, the alteration of channel functions may lead to remodeling of other proteins, which would be missed in such models. Human Induced Pluripotent stem cells (hiPS cells) offer a new paradigm for these types of studies. hiPS cells-derived cardiomyocytes (hiPS-CMs) provide researchers with cardiomyocytes (CMs) of human origin which are better-suited than CMs of animal origin or heterologous cell systems. Furthermore, hiPS-CMs provide us with the opportunity to test drugs in disease-specific CMs instead of healthy CMs. In addition, this strategy enables to generate patient-specific myocytes, which could be used to recapitulate the features of inherited arrhythmias in the context of the patient's genetic background.

Many studies have been reported on iPS-derived cardiomyocytes obtained from patients with heritable arrhythmias, where they demonstrated the applicability of this innovative approach to the study of inherited arrhythmias. From this point, fibroblasts isolated from skin biopsies have been the most commonly used primary somatic cell type for the generation of induced pluripotent stem cells. However, the required skin biopsy remains an invasive approach, representing a drawback for using fibroblasts as the starting material. More and more studies appeared over the last years, describing the reprogramming of other human somatic cell types. Cells isolated from urine, as well as more unexpected cell types, show promising characteristics for a reprogramming strategy. Here, we highlight the advantages of cells isolated from urine as a usable, noninvasive harvesting method for primary material in comparison with other commonly used cell types. We set up an experimental approach to obtain and characterize cardiomyocytes differentiated from urine-derived pluripotent stem cells (UhiPS-CMs), from a patient with Long QT syndrome. This patient presents a mutation on hERG KCNH2 gene (p.A561P).

We validated the use of cardiomyocytes differentiated from urine-derived pluripotent stem cells as a new cellular model to study patient's specific arrhythmia mechanisms.

Objective 1: To characterize and explore functional characteristics of UhiPS- CMs.

Objective 2: To characterize LQT-2 patient with hERG A561P mutation using UhiPS-CM, at molecular and functional levels.

I.2 – Article

I.2.1 – Abstract

Background: Human genetically inherited cardiac diseases have mainly been studied in heterologous systems or animal models, independently of the patients' genetic background. Since sources for human cardiomyocytes (CMs) are extremely limited, the use of urine samples to generate induced pluripotent stem (UhiPS) cell-derived CMs (UhiPS-CM) would be a non-invasive method to identify cardiac dysfunctions that lead to pathologies within the patients' specific genetic background. The objective was to validate the use of cardiomyocytes differentiated from urine-derived pluripotent stem cells as a new cellular model to study patient's specific arrhythmia mechanism.

Methods and Results: Cells obtained from urine samples of a long QT syndrome patient harboring the hERG A561P mutation and his asymptomatic non-carrier mother were reprogrammed using the episomal-based method. UhiPS cells were then differentiated into CMs using the matrix sandwich method.

UhiPS-CMs showed proper expression of atrial and ventricular myofilament proteins and ion channels. They were electrically functional; with nodal-, atrial- and ventricular-like action potentials (APs) recorded using high-throughput optical and patch-clamp techniques. Comparing hERG expression from the patient's UhiPS-CMs to the mother's UhiPS-CMs showed that the mutation led to a trafficking defect that resulted in a reduced I_{Kr} current. This phenotype gave rise to AP prolongation and arrhythmias.

Conclusions: Urine-derived iPS cells from patients carrying ion channel mutations can be used as novel tools to differentiate functional cardiomyocytes that recapitulate cardiac arrhythmia phenotypes.

Key words: Urine-derived induced pluripotent stem cells, cardiomyocyte, long QT syndrome modeling, HERG, arrhythmia.

I.2.2 – Introduction

Despite important achievements in the understanding of cardiovascular diseases over the last decade, heart disease remains the principal cause of death in developed societies. Intense research efforts have been directed at using human induced pluripotent stem (hiPS) cells to invoke cardiac regeneration for heart repair and to model human cardiac development and diseases *in vitro*. Recent studies have demonstrated that hiPS cell-derived cardiomyocytes (CMs) can be used to model several human genetically inherited cardiac diseases that manifest defects in specific cardiac structural components, signaling pathways, or electrophysiological properties[1], validating the technique as a powerful system to gain mechanistic insights into human cardiac disease. Currently, a wide variety of molecular, cellular, and physiological assays are optimized to investigate disease phenotypes in hiPS cell-derived cardiomyocytes. Experimental drugs have also been tested in this setting, inducing alleviation of the disease phenotypes, further paving the way for new therapeutic interventions for cardiac diseases. Importantly, as recently developed by S. Yamanaka, iPS cell technology can contribute to micromedicine (e.g., applied to an individual) and personalized medicine, including drug discovery based on cellular and molecular analyses. It may also contribute, in the next future, to macromedicine (e.g., applied to cohorts of individuals), including patient stratification, based on cellular and molecular analyses of participants in clinical trials or cohort studies.[2]

Nevertheless, the standard approach in which hiPS cells are generated from skin biopsy as raw material obviously limits the extensive use of this technology. Indeed, skin biopsy requires an invasive procedure, accompanied by discomforts, a risk of bleeding, infection, and permanent scars. Skin biopsy collection also raises ethical issues in the case of young children and patients' healthy relatives. Furthermore, the obtained cells expand slowly in culture and the reprogramming efficacy is low. This may require several skin samples, whereas the procedure cannot be easily performed several times on the same patient. There is a growing consensus that an ideal cell source for hiPS cells should be easily and non-invasively available, with a high reprogramming efficacy. Progress has been made regarding this issue with the reprogramming of cells from blood samples, but there is still room for improvement.

Recent reports showed that cells contained in a simple urine sample can also be an easy and non-invasive source for generating hiPS cells.[3-6] Reprogramming efficacy of urine-derived

cells is higher than for human dermal fibroblasts: the efficacy for both viral and non-integrative methods was consistently higher in urine cells as compared to dermal cells, including retroviral reprogramming that was about 50 times more efficient in urine cells [3, 7-9] and episomal reprogramming, about 10 times more efficient.[4, 10, 11] Furthermore, the cardiac molecular phenotype of a dystrophin-deficient patient was recapitulated in CMs derived from its urine cells.[12] Thus, producing urine-derived CMs from patients with genetic disorders, and also from their healthy relatives, can facilitate the study of private genetic variation impact on the risk and progression of the disease of interest.

In the present study, starting from a urine sample, we developed an *in vitro* model for a patient suffering from a mild form of type-2 long QT (LQT-2) syndrome. The long QT syndrome is an inherited cardiac channelopathy causing potentially fatal cardiac arrhythmia, and was one of the first successfully modeled human diseases using hiPS cells.[1, 13] We investigated the mutation A561P located in the *KCNH2* gene encoding the hERG channel. This mutation was the focus of a first study conducted in the laboratory.[14] The patient harboring this mutation presented arrhythmias only when treated with clobutinol, an antitussive drug. Due to the lack of cardiac cellular model, the analyses were performed in transfected COS-7 cells and the overall effects on cardiac action potential were extrapolated with an *in silico* analysis. In the present study, we have used CMs obtained from urine-derived hiPS cells (UhiPS-CM) to investigate both the molecular and functional phenotypes of the syndrome in a native cellular model. We observed AP changes, characteristic for the long QT syndrome, which were exacerbated by a hERG inhibitor, thus, modeling the patient-specific arrhythmic drug sensitivity. Overall, we demonstrated that the use of urine-derived cardiomyocytes is a convenient and powerful approach to finely model human arrhythmic diseases.

I.2.3 – Materials and methods

II.2.3.1 – Patient characteristics

The study was conducted in compliance with current Good Clinical Practice standards and in accordance with the principles set forth under the Declaration of Helsinki (1989). Institutional review board (IRB) approvals of the study were obtained before the initiation of patient enrollment. Each subject entering the study agreed to and signed an IRB-approved statement of informed consent.

Somatic cells from urine sample were obtained from a 22-year-old man who presented syncopes and *torsades de pointes* arrhythmia at the age of 13, during a treatment with an

antitussive drug, clobutinol.[14] ECG analysis showed a prolonged QT duration (QTc_{Bazett} = 628 ms and $QTc_{Fredericia}$ = 597 ms). The patient carries a missense mutation in *KCNH2* gene, encoding the hERG K^+ channel α-subunit, causing an alanine to proline substitution at position 561 (chr7: 150,648,800 G>C; NM_000238 A561P). As control, somatic cells from urine sample were also obtained from his 46 year-old mother who had no clinical symptoms, a normal ECG and was negative for the *KCNH2* mutation. An additional control, the previously described foreskin fibroblast-derived hiPS cell clone iPS.C2a (FhiPS) was also used.[15]

II.2.3.2 – Urine cell collection, isolation, culture

Urine cells were isolated and cultured as previously described.[3] Briefly, cell pellets were collected from whole urine samples (130-265 ml) via centrifugation (5 min at 1200 g) and washed with PBS. Pellets were resuspended in RE/MC medium composed of 50% of RE medium [Renal epithelial cell growth medium SingleQuot kit supplement and growth factors (Lonza, Cat#CC-3190)] and 50% of MC medium [DMEM/high glucose supplemented with 10% (vol/vol) FBS, 1% (vol/vol) GlutaMAX, 1% (vol/vol) Non-essential amino acid (NEAA), 100 U/ml penicillin, 100 μg/ml streptomycin, 5 ng/ml bFGF (Miltenyi), 5 ng/ml PDGF-AB (Cell Guidance) and 5 ng/ml EGF (Peprotech)] and cultured on 0.1% gelatin coated plates. Urine cell clusters were passaged using TripLE (Life Technologies) and characterized.

II.2.3.3– Urine cells reprogramming and UhiPS cells characterization

Urine cells were reprogrammed into urine-derived hiPS (UhiPS) cells as previously described[6]. Briefly, $3x10^5$ to $5x10^5$ urine cells were nucleofected (Lonza) with episomal vectors coding for OCT3/4, SOX2, KLF4, MYC, LIN28, NANOG and SV40LT (Addgene Cat# 20922, 20923, 20924, 20925 and 20927), and a nonepisomal vector coding for miR302/367 (System Biosciences Cat# TDH101PA-GP) and cultured 14 to 21 days with E7 medium (StemCell Technologies). UhiPS clones were manually picked on mouse embryonic fibroblasts (MEFs). Control UhiPS and A561P-UhiPS cells were characterized by RT-PCR to verify the expression of endogenous pluripotent factors OCT3/4, NANOG and SOX2 and the loss of episomal vectors (see below), immunostaining (see below), flow cytometry (see below), and their ability to form teratoma (see below).

II.2.3.4– Flow Cytometry analysis

A total of $1x10^5$ cells in suspension, for each condition, were washed 3 times with PBS/BSA 0.1%, then incubated with PE-labelled antibodies, SSEA3-PE, SSEA4-PE, TRA1-60-PE (eBioscience), for 30 minutes at 4°C in the dark and further rinsed 3 times with FACS buffer. Data acquisition was performed using FACSDiva software with LSR II instrument (Becton Dickinson, BD) or the Accury C6 (BD).

II.2.3.5– Episomal vector detection

Total RNA (tRNA) was extracted from hiPS cells at passage 10 using RNeasy mini kit (Qiagen). One µg of tRNA was reverse transcribed using High-Capacity cDNA Reverse Transcription Kit (Applied Biosystems) following manufacturer's instructions. RT-PCR studies were conducted in triplicate using the Mesa green 2X PCR Master Mix for SYBR (Eurogentec). DNA concentration was 5ng/well. Conditions were: 2 s at 90°C, followed by 40 cycles of 10 s at 95°C, 30 s at 60°C and ending by 60 s at 60°C. Cycle threshold was calculated using default settings by the real-time sequence detection software (Applied Biosystems). Primer sequences are indicated in Supplemental Table 1.

II.2.3.6– Teratoma formation

Undifferentiated UhiPS cells cultured on MEFs were mechanically dissociated with EZ Passage tools (Life Technologies), resuspended in matrigel (2 mg/mL) and injected subcutaneously into NOD/SCID IL2R gamma mice. Tumor samples were collected after 8 to 10 weeks, fixed in 4% paraformaldehyde, embedded in paraffin, sectioned and stained with hematoxylin and eosin for analysis. The animal experiments were approved by the Governmental Ethical Comity (Protocol 02017.01).

II.2.3.7– Culture of hiPS cells

Established hiPS cell lines were maintained on mitotically-inactivated MEFs in DMEM/F12 medium supplemented with 2 mmol/L L-glutamine, 0.07% β-mercaptoethanol, 20% knockout serum replacement, 5 ng/mL bFGF and 1% NEAA under low oxygen atmosphere (4% O2). Cells were passaged by manual dissection of cell clusters every 6-7 days. Before differentiation, hiPS cells were manually transferred from MEFs to matrigel-coated plates (0.05 mg/ml, BD Biosciences) and cultured on mTeSR1 medium (StemCell Technologies). Passages were performed using Gentle Cell Dissociation Buffer (StemCell Technologies).

II.2.3.8– Differentiation of hiPS cells into cardiomyocytes and dissociation

Human iPS cells were differentiated into cardiomyocytes using the established matrix sandwich method[16] with modifications. Briefly, 6 days before initiating differentiation, hiPS cell colonies were passaged on hESC-qualified matrigel-coated plates (0.05 mg/ml ; BD Biosciences) using Gentle Cell Dissociation Buffer (Stemcell Technologies) and cultured as a monolayer in mTesr1 with 1x Y-27632 Rock inhibitor (Stemcell Technologies) under normal oxygen atmosphere. When cells reached 80% confluence, cold mTesr1 with Growth Factor Reduced Matrigel (0.033 mg/ml) was added in order to create an overlay of Matrigel. Differentiation was initiated 24 h later (day 0) by culturing the cells in RPMI1640 medium (Life Technologies) supplemented with B27 (without insulin, Life Technologies), 100 ng/mL Activin A (Miltenyi), and 10 ng/mL FGF2 (Miltenyi) for 24 hours. On the next day, the medium was replaced by RPMI1640 medium supplemented with B27 without insulin, 10 ng/mL BMP4 (Miltenyi), and 5 ng/mL FGF2 for 4 days. By day 5, cells were cultured in RPMI1640 medium supplemented with B27 complete (Life Technologies) and 1% NEAA and changed every 2–3 days.

For protein and electrophysiological analyses, cardiomyocytes were dissociated around day 20 of differentiation, by a 20 min incubation with collagenase II (200 U/mL; Gibco) and 0.2 U/mL protease XIV (Sigma-Aldrich) at 37°C. Isolated cells were then incubated at room temperature for 30 min in Kraft-Bruhe solution containing 85 mmol/L KCl, 30 mmol/L K2HPO4, 5 mmol/L MgSO4, 1 mmol/L EGTA, 2 mmol/L Na2-ATP, 5 mmol/L Na-pyruvate, 5 mmol/L creatine, 20 mmol/L taurine, and 20 mmol/L glucose, pH 7.2.[17]

II.2.3.9– Gene expression analysis

Total RNA was extracted from hiPS colonies or during differentiation at day 5, 18 and 28, using RNeasy mini kit (Qiagen). One μg of tRNA was reverse transcribed using High-Capacity cDNA Reverse Transcription Kit (Applied Biosystems) following manufacturer's instructions. PCR amplification was performed using FAM labeled-TaqMan probes (Applied Biosystems; Supplemental Table 1).

II.2.3.10– Protein expression analysis

For histological analysis two cell types were analyzed: (1) undifferentiated UhiPS cells, which were cultured in 12 well plates on MEF feeders, (2) dissociated hiPS-derived cardiomyocytes, which were plated on IBIDI plates (Biovalley) and further cultured for 6 to 10 days. For (1),

UhiPS on MEFs were fixed with 4% PFA, permeabilized with 0.5% Triton X-100 and blocked with 3% PBS-BSA. Cells were then stained with primary antibodies directed against OCT3/4 (Santa Cruz) and TRA1-60 (eBioscience) diluted in 1% PBS-BSA. For (2), after methanol fixation, cells were permeabilized with 0.1% Triton X-100, blocked with 5% PBS-BSA and stained with primary antibodies against α-actinin (Abcam), troponin I (Santa Cruz), MLC2a (Abcam), MLC2v (Proteintech Europ), connexin 43 (Chemicon), hERG (Santa Cruz) or Nav1.5 (Alomone labs). Secondary antibody staining was performed using Alexa 488- and Alexa 568-conjugated antibodies (Molecular Probes). DAPI was used for nuclear staining.

For Western blot analysis, 40 µg of protein lysate from UhiPS-derived cardiomyocytes (UhiPS-CMs) were incubated with antisera against hERG (Santa Cruz) protein. Secondary antibody staining was performed using goat anti-mouse IgG-HRP antibody (Santa Cruz). Stain Free gel technology (Bio-Rad) has been used as loading control for protein normalization.[18, 19] The amount of total proteins in each lane on the blot has been calculated and used for normalization.

II.2.3.11– Cellular electrophysiology

Action potential optical recordings were performed on cardiomyocytes after 28 days of differentiation, with 5 µmol/L di-8-ANEPPS (Life Technologies) as the voltage-sensitive dye using the CellOptiq technology (Clyde Biosciences). Cells were incubated at 37°C, 5% CO2 and 20% O2 during the 2 h incubation of the dye and during the recording.

Dissociated hiPS-derived CMs were resuspended in RPMI + B27 supplemented with insulin and 1% non-essential amino acids and then plated on matrigel-coated 35-mm plastic Petri dishes. Isolated beating cells were used for patch-clamp recordings using whole-cell configuration, between day 10 and day 14 post-dissociation. The rapid component of the delayed rectifier K+ current (I_{Kr}) and action potentials (APs) were recorded in the ruptured and the permeabilized patch-clamp configurations, respectively. Cells were continuously superfused with a Tyrode solution containing (in mmol/L): NaCl 140, KCl 4, $CaCl_2$ 1, $MgCl_2$ 1, glucose 10, HEPES 10; pH 7.4 (NaOH). During recording, a local gravity microperfusion system allowed application of drugs, dissolved in Tyrode solution where glucose was replaced by mannitol 20 mM.[20] For APs recording, the pipette solution contained (in mmol/L): K-gluconate 125, KCl 20, NaCl 5, amphotericin B 0.85, HEPES 10; pH 7.2 (KOH). For I_{Kr} recording, the pipette was filled with a solution containing (in mmol/L): K-gluconate 125, KCl 20, K_2ATP 5, HEPES 10, EGTA 10; pH 7.2 (KOH).[21] All products were purchased from Sigma. Data were recorded through an A/D converter (Digidata 1440A, Molecular Devices),

using an Axopatch 200B amplifier (Molecular Devices). Membrane currents and APs were analyzed with Axon pClamp 10 (Molecular Devices). Borosilicate patch pipettes had a tip resistance of 2-2.5 MΩ. All experiments were made at 35 ± 2°C. During voltage-clamp experiments, nifedipine (4 µmol/L) was added to the external solution to block the L-type calcium current ($I_{Ca,L}$). IKr was measured as a 1 µmol/L E-4031-sensitive current, by digitally subtracting the current in the presence of E-4031 from that in its absence. I_{Kr} densities were calculated by dividing current amplitude (pA), measured at the peak of the tail current at -50mV following a depolarization to 60 mV (prepulse), by cell membrane capacitance (pF). Activation curves, determined from peak tail current normalized to the maximal value and plotted against the prepulse voltage, were fitted with a single Boltzmann function: G/Gmax = $1/(1+\exp((V_{1/2}-V)/k))$, where G/Gmax is the conductance normalized with respect to the maximal conductance, V1/2 is the half-activation potential, V is the prepulse voltage prior to the tail current measurement, and k is the slope factor. Data extracted from this equation are presented as mean ± SEM. Statistical significance of differences in current densities or activation properties was calculated using Student's t-test.

II.2.3.12– Statistical analysis

Data are expressed as mean ± S.E.M. Statistical analysis was performed with Prism5 (GraphPad Software, Inc.). Significant differences between mean values were determined with Mann-Whitney U test for comparison of two groups or paired Student's t test when appropriate. For more than two groups, 2-way ANOVA was performed. A *P* value below 0.05 was considered to indicate significance.

I.2.4 – Results

II.2.4.1– Generation of patient-specific hiPS cells from urine sample using episomal-based reprogramming

Cells isolated from urine samples from the patient carrying the hERG A561P mutation and from his healthy mother displayed a mesenchymal stem cell phenotype, including spindle-shaped morphology and expression of cell surface markers CD49a, CD73, CD90, CD105 and CD146. They did not express the hematopoietic stem cell markers CD14, CD45 and CD184 (not shown). Cells were reprogrammed upon transfection of episomal vectors. Control UhiPS clones and A561P-UhiPS clones carrying the A561P mutation were manually picked for further characterization. Endogenous expression of the pluripotent stem cell markers, *OCT3/4*, *SOX2* and *NANOG*, absent in the urine cells, was detected by qRT-PCR in both UhiPS cells types, while the loss of episomal vector expression was verified (Supplemental Figure 1B). Endogenous expression of OCT3/4 and TRA1-60 proteins was also visualized by immunofluorescence staining in control and A561P-UhiPS cells (Supplemental Figure 1A). Flow cytometry analysis showed that more than 90% of control and A561P-UhiPS cells were positive for the expression of pluripotency markers TRA1-60, SSEA4 and SSEA3 (Supplemental Figure 1C). Finally, the ability of UhiPS cells to form teratoma with all three germ layers was observed (Supplemental Figure 1D). Overall, urine cells were successfully reprogrammed into *bona fide* hiPS cells and a total of 2 to 3 clones per lines have been selected to perform the following experiments.

II.2.4.2– UhiPS cells can be differentiated into functional cardiomyocytes

Cardiomyocytes were differentiated, using the matrix sandwich method, from (1) control hiPS cells derived from foreskin fibroblasts (FhiPS-CMs), a reference tissue source that has previously been successfully used for differentiation into functional CMs (Marsman et al., 2014) [263], and from hiPS cells derived from urine samples: (2) the control healthy mother's cells (Control UhiPS-CMs) and (3) the hERG A561P-mutated cells (A561P-UhiPS-CMs). All three hiPS cells showed comparable cardiac differentiation potential (Figure 1), giving rise to spontaneously contracting cell areas after 6-8 days of differentiation. Gene expression profiling of the three hiPS cells revealed a similar differentiation pattern into cardiac cells over time, including significant reduction of pluripotent stem cell markers, *OCT3/4*, *NANOG* and *SOX2*, and progressive upregulation of a cardiac transcription factor, *NKX2-5*, connexins (*GJA1* and *GJA5*), and a regulator of calcium homeostasis, *RYR2* by day 18 (Figure 1A).

Similar gene expression profile was also observed for *SCN5A, CACNA1C, CACNA1G, KCND3, KCNQ1, KCNH2* and *KCNJ2*, the genes encoding the major cardiac ion channel α-subunits. We also analyzed the protein expression pattern of several structural and functional proteins that characterize cardiomyocytes, using immunofluorescence on cells isolated after 30 days of differentiation (Figure 1B). Cardiomyocytes displayed organized cross-striations resembling sarcomeres with proper alignment of the myofibrils, that were positive for cardiac and muscular specific cytoskeletal proteins, troponin I, α-Actinin, ventricular myosin light chain (MLC2V) and atrial myosin light chain (MLC2A). The sodium channel Nav1.5, responsible for the action potential upstroke in atrial, Purkinje and ventricular cardiomyocytes, was properly addressed at the plasma membrane (not shown). Finally, dual staining of troponin I and connexin 43, essential for coordinated cell depolarization, showed that the transmembrane proteins were located, as expected, in contact areas between CMs (Figure 1B). These results show that UhiPS cells could be differentiated into CMs using the matrix sandwich method.

II.2.4.3–Cardiomyocytes differentiated from UhiPS cells are electrically functional

Action potentials of the differentiated CMs were assessed using both patch-clamp and optical recording using the voltage-sensitive dye, di-8-ANEPPS. Isolated CMs derived from both FhiPS and UhiPS cells started beating by day 6 post-dissociation. Using the patch-clamp technique, spontaneous APs from control and A561P-UhiPS-CMs were recorded and classified as nodal-, atrial- and ventricular-like APs, based on their duration, maximum upstroke velocity (dv/dt_{max}), peak to peak duration and maximum diastolic potential (Figure 2A, Supplemental Table 2). The three types of APs were also obtained during CellOptiq AP optical recordings (Figure 2B), and their quantification showed that, irrespectively of the hiPS cell origin and genotype, ventricular-like APs were the most frequent (Figure 2C). Inversely, nodal-like APs were the less frequently recorded with none observed in A561P-UhiPS-CMs using patch-clamp technique (Figure 2A).

II.2.4.4– A561P KCNH2 mutation causes a trafficking defect of the hERG channel in human cardiomyocytes

We then investigated whether we could model and characterize LQT-2 syndrome molecular phenotype using UhiPS-CMs. The A561P mutation studied in COS-7 cells induced a decrease in plasma membrane expression of the channel that potentially causes the disease phenotype[14] We first examined cellular localization of hERG by immunofluorescence in UhiPS-CMs. As

compared to control FhiPS- and UhiPS-CMs, hERG plasma membrane expression was reduced in A561P-UhiPS-CMs (Figure 3A). Higher magnification analyses confirmed that in both FhiPS-CM and UhiPS-CMs, hERG staining was prominently observed at the cell plasma membrane (Figure 3B, arrows and plot profiles). In contrast, hERG A561P protein was detected at the plasma membrane at the same intensity as in intracellular compartments (Figure 3B, plot profile). Further analysis of hERG protein cellular localization has been performed, combining plot profile analysis of multiple cardiomyocytes differentiated from each hiPS cell line. We found a statistically significant enrichment of hERG protein at the membrane as compared to the intracellular compartment, in the two control cell lines. In opposition, the A561P-UhiPS cardiomyocytes did not show membrane enrichment of hERG protein (Figure 3C). These findings suggest a trafficking defect of hERG ion channel in UhiPS-CMs carrying the hERG A561P mutation. To further confirm this result, we investigated whether this mutation had an effect on *KCNH2* gene expression. Interestingly, the A561P mutation did not alter transcriptional expression of *KCNH2* gene (supplemental Figure 2). Using western blot analysis, the differential expression of the immature cytosolic protein was quantified as compared to the mature plasma membrane protein (Supplemental Figure 3A) [24]. The difference in hERG mature over immature forms was abolished in A561P-UhiPS-CMs (Supplemental Figure 3B), confirming a trafficking defect of mutated hERG proteins.

II.2.4.5– I_{Kr} current density is altered in patient derived UhiPS-CMs

Using patch-clamp, we investigated whether this trafficking defect had an effect on hERG-associated ionic current (I_{Kr}). As shown in Figure 4A and B, the I_{Kr} current was significantly reduced in A561P-UhiPS-CMs (p=0.007), in comparison to control UhiPS-CMs. The tail K^+ current density measured at -50 mV was markedly reduced to approximately 50-60% of the control values (Table 1). However, the activation kinetics was not modified by the A561P mutation (Figure 4C and Table 1). The current density reduction observed in A561P-UhiPS-CMs was consistent with the membrane expression reduction described above (Figure 3 and Supplemental Figure 3).

II.2.4.6– A561P hERG mutation impairs I_{Kr} contribution to the action potential in UhiPS-CMs

As expected, A561P-UhiPS-CMs had statistically significant longer ventricular-like AP durations compared to control UhiPS-CMs, mainly APD_{75} and APD_{90} (Figure 5A). In order to exclude that the AP frequency difference was responsible for these changes, we compared AP

duration in the two cell groups at comparable frequencies. To do so, we used the CellOptiq method to record a high amount of APs at spontaneous automatic rates. Action potentials were then classified and compared according to the beating frequency. The data show that A561P-UhiPS-CMs APD_{90} was significantly longer than in control cells regardless of the frequency, and that, as expected, the AP prolongation in A561P-UhiPS-CMs was potentiated at slower rates(Clancy and Rudy, 2001) (Figure 5B). Also, statistical analyses with a two-way ANOVA show that the effect of the frequency on APDs was minor as compared to the effect of the hERG mutation. Thus, the APD prolongation observed in our LQT-2 model was likely mainly due to the mutation. These data show that UhiPS-derived cardiomyocytes model the typical AP prolongation associated with LQT-2 syndrome.

II.2.4.7– UhiPS-CMs carrying the hERG A561P mutation have increased susceptibility to arrhythmia

The hERG A561P mutation carrier experienced arrhythmic episodes, namely *torsades de pointes*, when treated with a hERG channel blocker, clobutinol. As this drug is no longer available, we used the hERG blocker E-4031 to evaluate susceptibility to arrhythmia in control and A561P-UhiPS-CMs. E-4031 did not trigger any arrhythmic event in control UhiPS-CMs recorded with CellOptiq method (n = 51), but an arrhythmic event was recorded in one A561P-UhiPS-CM over 6 upon E-4031 treatment. Ventricular-like action potentials recorded with patch-clamp technique exhibited spontaneous EADs only in A561P-UiPS-CMs (in 2 among 7 cells). As shown in Figure 5C, EADs, were exacerbated in presence of E-4031, a reminiscence of the patient's phenotype, which was characterized by arrhythmias when treated with the antitussive drug clobutinol. Quantitative analysis of the prolongation of APD50, 75 and 90 showed a statically significant prolongation of APD75 and APD90 in both control and A561P-UhiPS CMs with, as expected, a greater prolongation in the mutated cells (Figure 5D).

I.2.5 – Discussion

In the present study, we demonstrated that the use of patient-specific iPS cells obtained from urine samples is a powerful approach to model the subtlety of human cardiac arrhythmic disease *in vitro*. The cells were differentiated into functional cardiomyocytes, which reproduced both phenotypic characteristics of this LQT-2 mutation, *i.e.*, (i) prolonged repolarization and (ii) increased drug-induced arrhythmogenicity.

The opportunity of producing unique patient- and disease-specific human iPS cell lines[7, 26, 27] provides genetically-defined cellular human models to study diseases, taking in consideration the patient's specific genetic background. This approach has been successfully applied to cardiac arrhythmic diseases[28], including type 2 long QT syndrome[29-32] in which human iPS cell lines were derived from dermal fibroblasts. However, owing to the complications associated with skin biopsy collection, in all these studies, control hiPS cells were derived from genetically unrelated individuals[30-32] or even from hES cell-derived fibroblasts, therefore with a different genetic context.[29] Nevertheless, direct reprogramming of somatic cells into pluripotent cells should address the need for studying patient-specific cells as well as cells derived from control subjects, of any age and, ideally, from family relatives. Indeed, this would allow testing the specific role of a mutation in a pathological phenotype, by comparing phenotypes in similar genetic backgrounds.

To avoid skin biopsy, an invasive procedure that raises ethical issues when collected from young individuals or healthy relatives, less invasive methods are required. Recently, Zhou *et al*. have been able to reprogram urine-derived cells, collected with a completely non-invasive method, into induced pluripotent stem cells.[3] Our study shows that these cells can be differentiated into cardiomyocytes and used to model an arrhythmic cardiac disease. There are, however, some limitations. First, in our laboratory seventy-nine urine samples have been collected from the same number of individuals for several ongoing studies. Using both penicillin and streptomycin in culture medium at usual concentrations, eight samples were contaminated (not shown). Cells from urine samples were isolated and expanded from only forty-five (57%) donors. These results are comparable to the ones obtained by one of the first studies on using urine cells to generate iPS cells.[3] Nevertheless, they are an important limitation as compared to PBMCs that can be usually obtained from any subject. As a result, when no urine cells can be isolated from urine samples of donors, either more urine samples need to be harvested and cultivated, or the use of PBMCs or a skin biopsy may be necessary.

Second, there was no "quarantine" time necessary to eliminate contaminated samples, but usually 2 to 3 weeks were necessary to obtain a sufficient number of cells for reprogramming. This culture duration is usual with fibroblasts from skin biopsies, but is a second limitation compared to PBMCs that can be used immediately after purification. However, urine samples are easy to obtain from any subject, including intrafamilial controls and pediatric patients. Therefore, the use of urine samples may be a good starting point to obtain iPS cells, followed by blood harvesting in case of lack of urine cells. Finally, the study has been performed on only one patient and two controls. Similar investigations on other patients with other hERG mutations would be useful to confirm the strength of this new model.

Intense research efforts have been directed at developing methods to differentiate cardiomyocytes from human iPS cells by mimicking the cell-signaling environment during early stages of cardiogenesis. We chose to use the matrix sandwich method, one of the most recent designed protocols, reported to give one of the highest differentiation efficacy.[16] However, differentiation efficacy can be iPS cell line specific. For instance, this method has been unsuccessful at differentiating cord blood-derived iPS cells, in opposition to skin fibroblasts-derived iPS cells, due to their parental source memory.[33] Thus, we tested whether this method would be efficient at differentiating urine-derived iPS cells. Here we show that urine cells reprogrammed with non-integrating episomal vectors, can be differentiated into cardiomyocytes from a monolayer cell culture, using the matrix sandwich method.

In order to validate the use of urine-derived iPS cells for modeling cardiac arrhythmic disease, we selected a mild form of type 2 long QT syndrome, related to hERG, because the LQT-2 syndrome is the reference model in studies using conventional skin fibroblast-derived iPS cells. Before the use of iPS cells, studies of hERG channel mutations, as for other channels, were conducted in heterologous expression systems, providing insights into the probable mechanism of LQT-2. Those studies have shown that defects in expression, trafficking and/or function of the mutated channels can be responsible for the diseased phenotype. However, these systems hampered the complete understanding of this disease mechanism. Indeed, they are non-cardiac cell types that do not provide a fully integrated vision and some of the disease phenotypes cannot be investigated using these systems, forcing to resort to non-cellular methods such as mathematical modeling of action potential.

The studied patient presented a QT prolongation (QTc = 597 ms) and was asymptomatic until he experienced syncope and *torsades de pointes* arrhythmias during treatment with clobutinol,

a common antitussive drug.[14] It has been proposed that the population prevalence of milder LQT syndrome mutations might be high,[34] and it is now recognized that such form of LQT syndrome could manifest itself as a predisposition to drug-induced *torsades de pointes*, as in the case of the A561P patient we present here. Also, it has been demonstrated by Moss *et al.* that mutations in different locations of the HERG potassium-channel gene are associated with different levels of risk for arrhythmic cardiac events in LQT-2, which makes it important to focus on mild phenotypes and discriminate them from severe phenotypes.[35] Interestingly, this study demonstrates that the use of urine-iPS derived models allows replicating the subtlety of a patient-specific phenotype, a result that widens the usefulness of iPS to model arrhythmogenic syndromes with complex phenotypes.

The A561P mutation has been the subject of a previous study conducted in the lab using transfected COS-7 cells.[14] This study had shown that the A561P mutation induced defects in hERG trafficking and biophysical properties. Due to the lack of cardiac cellular model, its impact on action potential duration had been tested using computer simulations.[14] In the present study, we investigated the mutation-associated disease mechanism in human cardiomyocytes differentiated from UhiPS carrying hERG A561P mutation, in comparison to two controls, one of which was UhiPS-CMs generated from a healthy family member (mother). The second one was derived from foreskin fibroblasts of a healthy individual.[15] Almost all studies that investigated the mutations associated arrhythmic diseases in hiPS-CMs recognized that those cells are immature, with electrical properties that are similar to fetal or neonatal cardiomyocytes. However, our results show that these cells are capable of capturing specific traits of LQT-2 syndrome, *i.e.,* reduced I_{Kr} current amplitude leading to a prolongation of the action potential. One discrepancy between the present study and our former one is that we did not confirm that hERG A561P mutation results in a modification of the voltage-dependence of activation, as described in COS-7 cells.[14] In COS-7 cells, this phenotype was probably due to the specific protein environment of the exogeneous channel in COS-7 that may exacerbate subtle differences that do not exist in native environment.

Our data further support the use of cardiomyocytes differentiated from iPS cells rather than non-cardiac heterologous expression systems for providing genuine knowledge of the mechanism for cardiac channelopathies. They are the closest model to human cardiomyocytes sourced directly from cardiac tissue, providing to date accurate insights into the molecular basis of disease phenotypes. Moreover, we demonstrated that iPS cells derived from a urine

sample are an alternative strategy for cardiac arrhythmic disease modeling, with the advantage to facilitate the study of familial controls compared to more invasive fibroblasts collection procedures, broadening the potentialities for iPS-guided personalized medicine.

I.2.6 – Figure legends and figures

Figure 1: Human UhiPS cells differentiated into functional cardiomyocytes. (A) Transcriptional profile of control hiPS cells derived from skin fibroblasts (control FhiPS-CMs), and from urine cells (control UhiPS-CMs and A561P-UhiPS-CMs) at days 5, 18 and 28 of cardiac differentiation. Quantitative RT-PCR analysis was performed on pluripotent stem cells markers (*OCT3/4*, *NANOG*, *SOX2*), on cardiomyocyte markers (*NKX2-5*, *GJA1*, *GJA5*, *RYR2*), and on key genes encoding cardiac ion channels (*SCN5A*, *CACNA1C*, *CACNA1G*, *KCND3*, *KCNQ1*, *KCNH2* and *KCNJ2*) to show enrichment for the cardiomyocyte population. The expression for each gene and sample (n=5 per condition) was normalized to ß-actin gene, *ACTB*, and was calculated relative to the median expression level. Raw minimum (min) and raw maximum (max) values were taken as a reference for heatmap representation. (B) Top: In control UhiPS-CMs, representative immunofluorescence images of the cardiac sarcomeric protein α-Actinin (green, left), co-staining of myosin light chain 2a (MLC2a; green; middle) and 2v (MLC2v; red, middle) and troponin I and connexin 43 (green and red, respectively, right). Bottom: In A561P-UhiPS-CMs, representative immunofluorescence images of α-Actinin (red, left), co-staining of MLC2a (red; middle) and MLC2v (green, middle) and troponin I and connexin 43 (green and red, respectively, right). Scale = 5µm.

Figure 2: Human UhiPS cells differentiated into electrically functional cardiomyocytes. Representative traces of spontaneous nodal-, atrial- and ventricular-like action potential recordings using patch-clamp (A) or optical dye (CellOptiq; B) in control UhiPS-CMs and A561P-UhiPS-CMs. (No nodal-like AP was obtained in A561P-UhiPS-CMs using patch-clamp technique.) (C) Distribution of the three types of action potentials obtained by optical measurement. Irrespectively of the hiPS cell type, the majority of the action potentials were ventricular-like. Control FhiPS-CMs: n=38, control UhiPS-CMs: n=41, and A561P-UhiPS-CMs: n=51.

Figure 3: hERG trafficking defect in A561P-UhiPS-CMs. (A) hERG protein localization (red) after cardiac differentiation of hiPS cells, highlighting the low membrane expression of hERG in A561P-UhiPS-CMs relative to intracellular signal (magnification x20) as compared to both controls (control FhiPS-CMs and UhiPS-CMs). (B) Left, specific cellular localization of hERG (red) in cardiomyocytes with counterstaining for troponin I (green, magnification

x65). Right, surface plots of hERG staining in each cell at the level of the line. (C) Statistical analysis of surface plots of hERG fluorescence intensity signal. Control FhiPS-CMs: n=12, control UhiPS-CMs: n=12, and A561P-UhiPS-CMs: n=20. The surface plot was arbitrarily segmented in three different areas: the first and last 15% of the surface plot, corresponding to plasma membrane (M1 and M2 as described in Figure 3B), and the remaining intermediate 70% of the surface plot, corresponding to the intracellular compartments (I). For each of these areas in each cell, the hERG fluorescence intensity values were averaged and normalized to the average cell hERG fluorescence intensity signal. Paired T-tests were performed between membrane and intracellular signals. *** P<0.001, for membrane vs intracellular fluorescence intensity signal.

Figure 4: Reduction of I_{Kr} current density in A561P-UhiPS-CMs. (A) Representative raw data of currents recorded from control UhiPS-CMs (left) and A561P-UhiPS-CMs (right); protocol is shown as inset (holding potential: -50 mV; stimulation frequency: 1/12.5 Hz; traces with test pulse from -40 to 0 mV are shown). Currents are shown before and after 1 μmol/L E-4031 application. E-4031-sensitive currents are considered as I_{Kr}. (B) Tail current density measurement obtained upon repolarization after test pulse at +60mV in control UhiPS-CMs (n=13) and A561P-UhiPS-CMs (n=11), highlighting a significant reduction in A561P-UhiPS-CMs. Protocol is shown in inset. ** P<0.01 *vs* control UhiPS-CMs. (C) Voltage-dependent activation curves obtained by plotting the relative E-4031-sensitive current upon repolarization at -50 mV (arrows in A) in control UhiPS-CMs (n=13) and A561P-UhiPS-CMs (n=8) (arrows in A).

Figure 5: Action potentials recorded from A561P-UhiPS-CMs model type 2 long QT syndrome. (A) Ventricular-like AP durations using patch-clamp (left, n=7 in each group) and optical measurement (right, n=27 and 30 for control and A561P cells, respectively). (B) APD_{90} at two different AP frequencies, showing a larger prolongation in A561P-UhiPS-CMs at slow rate (white circles) as compared to control UhiPS-CMs (black circles; n=13 and 6 for control and A561P cells, respectively). Statistical significance: * P<0.05, *** P<0.001, for A561P-UhiPS-CMs *vs* control UhiPS-CMs. (C) Increased arrhythmia susceptibility in A561P-UhiPS-CMs in presence of E-4031: representative action potential patch-clamp recordings before and after 1μM E-4031 treatment. (D) Quantification of the prolongation of the action potential duration (APD) after E-4031 treatment of control UhiPS-CMs (gray bars)

and A561P-UhiPS-CMs (white bars). Statistical significance of APD prolongation after E-4031 treatment in each cell type: * P<0.05.

Table 1. Effects of A561P mutation on I_{Kr} in UiPS-CMs.

	control UhiPS-CMs	A561P-UhiPS-CMs
Tail current density	1.79 ± 0.2 pA/pF	0.89 ± 0.1 pA/pF **
(n)	(13)	(11)
Activation		
$V_{1/2}$	-26.49 ± 1.7 mV	-23.81 ± 1.5 mV
k	7.75 ± 0.7	7.1 ± 0.7
(n)	(13)	(8)

V1/2: prepulse voltage for which the tail current is half of its maximal value; k: slope factor (see protocol in figure 4A). The tail current density was measured at -50 mV following a depolarization to +60 mV.
*** P<0.01 vs control UhiPS-CMs*
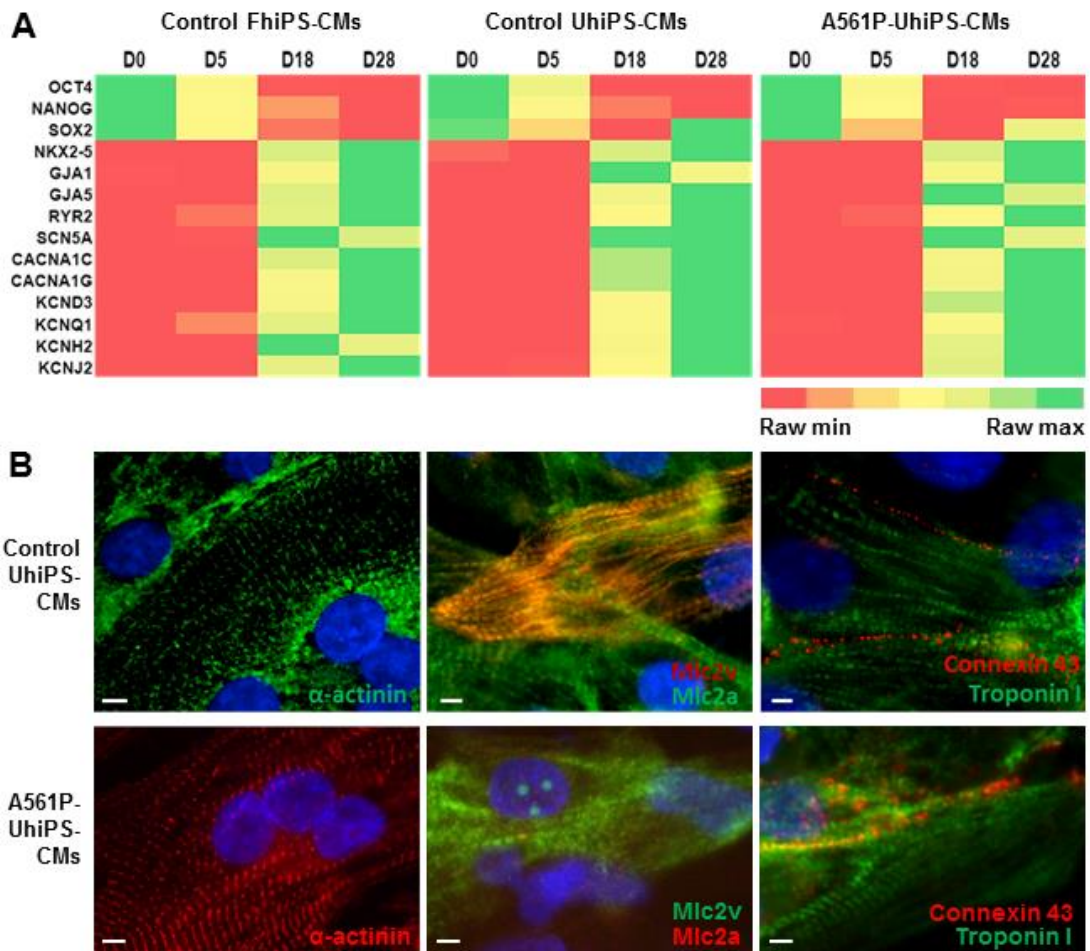
Figure 1.
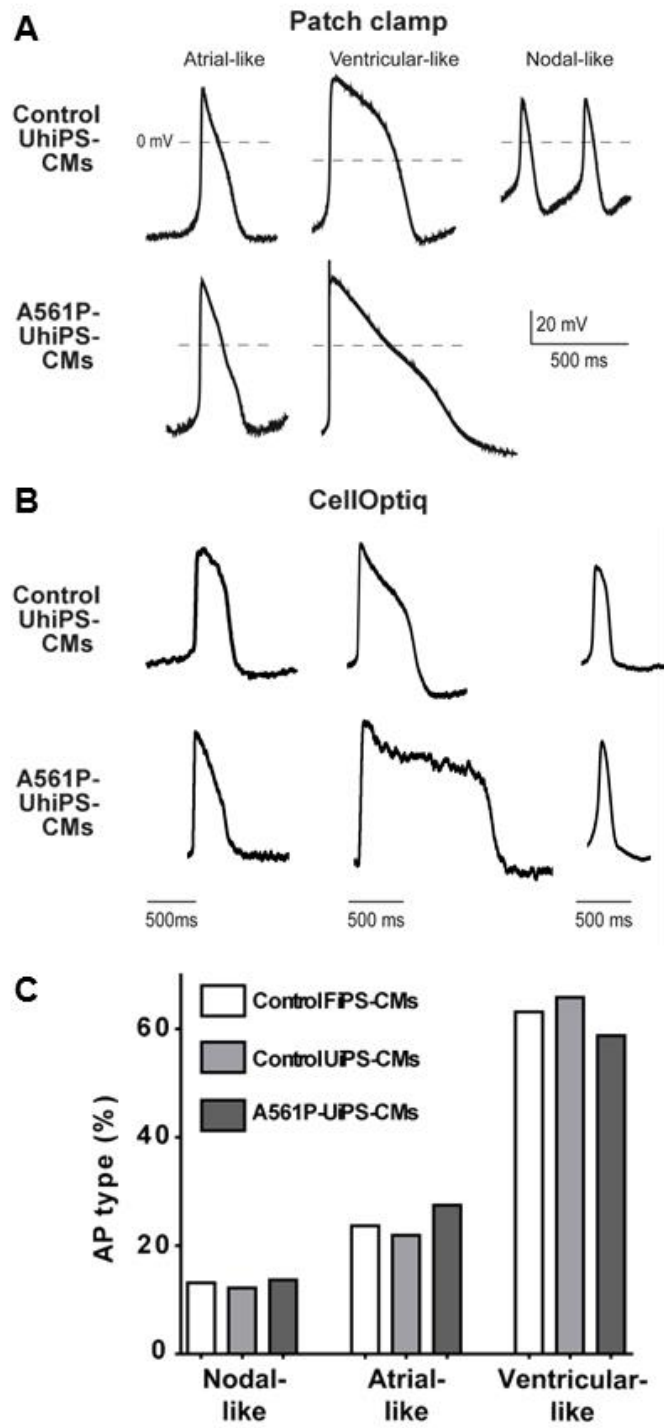
Figure 2.

II – Mechanisms of Induction of Cardiac Arrhythmias in HIV patients

In this part of the results, I am showing the results we have related to objective 2 (refer to hypothesis and objectives). This manuscript is in preparation, and will be submitted soon.

- Article 2 -

Mechanisms of induction of cardiac arrhythmias in HIV patients

Zeineb Es-Salah-Lamoureux[a-c]*, Mariam Jouni[a-d]*, Marine Gandon-Renard[a-d], Bruno Beaumelle[e], Chantal Gauthier[a-d], Albano Meli[f], Olivier Cazorla[f], Isabelle Baró[a-d], Flavien Charpentier[a-d], Kazem Zibara[g], Patricia Lemarchand[a-d], Nathalie Gaborit[a-c] [§], Gildas Loussouarn[a-d §].

To be submitted

a. *Inserm, UMR 1087, l'institut du thorax, Nantes, France*
b. *CNRS, UMR 6291, Nantes, France*
c. *Université de Nantes, Nantes, France*
d. *CHU Nantes, l'institut du thorax, Nantes, France*
e. *CPBS FRE 3689 Centre National de la Recherche Scientifique, UM Montpellier, France.*
f. *U1046 INSERM, UMR 9214 CNRS, Physiologie et Médecine Expérimentale du Cœur et des Muscles, University of Montpellier, CHRU Montpellier, Montpellier, France*
g. *ER045, PRASE, Laboratory of stem cells, Lebanese university, Beirut, Lebanon.*
*,[§]. *These authors contributed equally to this work.*

Address correspondence to:
Dr. Gildas Loussouarn
L'institut du thorax
INSERM UMR 1087 / CNRS UMR 6291
IRS-UN, 8 Quai Moncousu BP 70721
44007 Nantes cedex 1, France
Tel: +33 (0)2 2808 0150
Fax: +33 (0)2 2808 0130
E-mail: gildas.loussouarn@inserm.fr

II.1 – Article

II.1.1 – Abstract

Rationale: HIV-positive individuals are showing a mean SCD rate 4.5 fold higher than in the general population and the risk of SCD related to LQT syndrome is higher than in the general population. Several studies, using heterologous expression systems as well as *in vivo* models, have been performed in order to investigate the pathological QT prolongation observed in HIV patients, and to determine the origin of this pathological condition. Human induced pluripotent stem cells-derived cardiomyocytes may provide an alternative approach to further understand the underlying associated arrhythmic conditions.

Objective: To use cardiomyocytes derived from hiPS-CMs to decipher the mechanism of a non-genetic disease, such as cardiac arrhythmias in HIV patients.

Methods and results: Despite the proved Tat transcriptional activity and its ability to get into the both heterologous expression systems used, no modification of the hERG current was observed. On the other hand, hiPS-derived cardiomyocytes incubated with Tat had a modified electrical activity characterized by a decrease in the I_{Kr} current, and an increase in the frequency of APD alternans.

Conclusion: In conclusion, this study provides novel insights into the link between arrhythmia in HIV-positive individuals and hERG Tat-related alteration in human cardiomyocytes. Our work shows that Tat protein has a direct effect on cardiac electrical activity in the absence of the treatment or other HIV proteins.

Key words: hERG; I_{Kr}; HIV Tat protein; induced pluripotent stem cell-derived cardiomyocytes; long QT syndrome; cardiac arrhythmia.

II.1.2 – Introduction

As a consequence of the development of antiretroviral therapies (ART), life expectancy of HIV-positive individuals has greatly increased, as for many of them excess mortality is moderate in industrialized countries and comparable with patients having other chronic conditions [1] [2]. Worldwide, the increasing access of patients to ART, from 31% in 2008 to 36% in 2014 [3, 4] should lead to further increase in survival of HIV-positive individuals. This survived population will face additional pathologies that are over-represented, as pointed out by a recent study on sudden cardiac death (SCD) in HIV-positive individuals, showing a mean SCD rate 4.5 fold higher than in the general population [5]. Furthermore, up to 13.5% of the HIV patients are presenting with a long QT syndrome (LQT), and the risk of SCD related to LQT is higher than in the general population [6, 7]. However, the link between LQT and HIV remains unclear.

Many drugs and their combinations may be potential triggers of LQT through the inhibition of a major cardiac repolarizing current I_{Kr}, conducted by the voltage gated potassium channel hERG [11]. Among them, numerous drugs currently prescribed to HIV-positive individuals have been associated with a QT prolongation, such as macrolides, pentamidine, azole antifungals, fluoroquinolones [9], and methadone [10].

On the other hand, QT prolongation on ECGs from HIV-positive individuals is correlated to the duration of HIV infection rather than the anti-HIV treatment [6] and QTc prolongation is observed in non-treated HIV-positive individuals [8], suggesting a role for HIV in inducing LQT. In addition, several studies using animal models suggest a rather direct implication of HIV in LQT. Prolonged cardiac repolarization and decreased repolarizing potassium currents were observed in mice expressing the whole HIV-1 genome [12, 13]. Among the 19 proteins encoded by the virus, Tat appears as a potential candidate for inducing ventricular arrhythmias, as it prolongs the action potential of guinea-pig ventricular cardiomyocytes through a reduction in the hERG associated I_{Kr} current [15]. In addition, Tat was shown to promote bradycardia in a rat model [20]. This bradycardia may be related to the dysregulation of the autonomic nervous system, as observed in some HIV patients [21], which may favor LQT [22]. However, small animal models, especially rodents, are not the most appropriate ones to study LQT since molecular mechanisms conducting repolarizing potassium currents are different from human [14].

In face of the different hypothetical models explaining the long QT syndrome in HIV patients, we aimed at testing whether Tat alters the activity of hERG channels in human cardiomyocytes, and modifies their electrical activity. To this end, we used cardiomyocytes differentiated from human induced pluripotent stem cells (hiPS-CM).

Surprisingly, we found no effect of Tat treatment on I_{hERG} in two heterologous expression systems, whereas significant decrease of I_{Kr}, as well as impairment of the action potentials has been observed in Tat-treated hiPS-CMs. These observations suggest that a decrease in I_{Kr} activity due to Tat protein provokes the long QT syndrome in HIV patients, through abnormalities in cardiomyocytes electrical activity.

.

II.1.3 – Materials and methods

II.1.3.1 – Tat protein preparation

Recombinant Tat was purified from *Escherichia coli* as previously described [23] and suspended immediately before use in citrate buffer (110 mM sodium chloride, 30 mM sodium citrate, 20 mM sodium phosphate, pH 7.3) at concentrations of 200 ng/ml, 400 ng/ml or 600 ng/ml, which are similar to those used in previous studies and consistent with patient serum levels [15, 18]. BCA protein assay (Pierce) was used to measure Tat protein concentration.

II.1.3.2 – Cell culture and transfection

HEK293 cells stably expressing hERG (HEK-hERG; CreaCell; protein accession number: NP_000229.1) and COS-7 cells (American Type Culture Collection) were cultured in Dulbecco's modified Eagle's medium (Invitrogen) supplemented with 10% fetal calf serum (Eurobio) and antibiotics (100 international units/ml penicillin and 100 µg/ml streptomycin; Gibco) at 5% CO_2 and 37°C in a humidified incubator. For HEK-hERG cells, 1200 µg/ml G418 (Life Technologies) were used for maintenance of hERG expression.

When reaching 60–80% cell confluence, COS-7 cells were transiently transfected in 35-mm plates with 2 µg of total DNA (as described below) complexed with FuGENE 6 (Promega) according to the manufacturer's instructions. For experiments on rapidly activating delayed rectifier K^+ (hERG) channels, DNA amounts were 600 ng of pSI-hERG (protein accession number: NP_000229.1) [24] + 1.4 µg of pEGFP-C1 (Clontech). For experiments on slowly activating delayed rectifier K^+ channels, the ionic currents were obtained from a fusion protein of the human KCNE1 regulatory subunit (protein accession number: AAA58418.1) linked to the N-terminus of the human KCNQ1 channel (protein accession number: NP_000209.2), a kind gift from Dr Robert S. Kass, Columbia University, New York, NY. DNA amounts were 200 ng of pCDNA3.1-KCNE1-KCNQ1 + 1.8 µg of pEGFP-C1. Twenty-four hours post-transfection, cells were isolated using trypsin and seeded in plastic petri dishes at low density for 24 h, after which whole-cell currents were recorded.

II.1.3.3 – Tat analysis using immunofluorescence

hERG-HEK cells were treated with citrate buffer or with 200 or 400 ng/ml Tat for 24 h at 37°C. Cells were then fixed with 3.7% formaldehyde, permeabilized with 1% Saponin and blocked with 1% PBS-BSA. Cells were then stained with primary antibodies directed against HIV-1 Tat or hERG (Santa Cruz) diluted in 0.1% PBS-BSA, 1% Saponin. Secondary antibody staining was performed using Alexa 488 and Alexa 568 conjugated antibodies

(Molecular Probes) for Tat and hERG proteins respectively. DAPI was used for nuclear staining.

II.1.3.4 – Transactivation assays

Transactivation assays were performed as previously described [25]. Briefly, COS-7 cells were cultured in 24-well plates and co-transfected with 0.22 µg/well pGL3-LTR, which encodes firefly luciferase under the control of Tat-activated HIV-1-LTR promoter, and 1.78 µg/well pRL-TK (Promega), which encodes Renilla luciferase under the control of herpes simplex virus thymidine kinase promoter, to normalize results. After 24 h, 200 ng/ml recombinant Tat and 100 µM chloroquine were added. One day later, cells were lysed for dual luciferase assays (Promega), and transactivation activity was calculated using the firefly/Renilla activity ratio.

II.1.3.5 – Culture of hiPS cells

A previously described foreskin fibroblast-derived hiPS cell clone C2a (hiPS, [26]) was used to generate cardiomyocytes. Established hiPS cell line was maintained on mitotically-inactivated MEFs in DMEM/F12 medium supplemented with 2 mM L-glutamine, 0.07% β-mercaptoethanol, 20% knockout serum replacement, 5 ng/ml bFGF and 1% NEAA under low oxygen atmosphere (4% O_2). Cells were passaged by manual dissection of cell clusters every 6-7 days. Before differentiation, hiPS cells were manually transferred from MEFs to hESC-qualified matrigel-coated plates (0.05 mg/ml, BD Biosciences) and cultured on StemMACS (iPS-Brew XF) medium (Miltenyi Biotec). Passages were performed using Gentle Cell Dissociation Buffer (StemCell Technologies).

II.1.3.6 – Differentiation of hiPS cells into cardiomyocytes and dissociation

Human iPS cells were differentiated into cardiomyocytes as previously described (refer to first article). In addition, cells were dissociated with the same protocols used in article 1.

II.1.3.7 – Single-cell electrophysiology in COS-7 and HEK-hERG cells

HEK-hERG and transfected COS-7 cells were treated either with citrate buffer or with Tat for 24 h at 37°C, followed by whole-cell currents recordings at room temperature using the patch-clamp technique. The cells were continuously superfused with a HEPES buffered Tyrode solution containing (in mM): NaCl, 145; KCl, 4; $MgCl_2$, 1; $CaCl_2$, 1; HEPES, 5; glucose, 5;

pH adjusted to 7.4 with NaOH. For K^+ current recordings, pipettes (Kimble Chase; tip resistance: 1.8 to 2.5 MΩ) were filled with an intracellular medium containing (in mM): KCl, 150; $MgCl_2$, 1; EGTA, 5; HEPES, 10; pH adjusted to 7.2 with KOH. All products were purchased from Sigma. Stimulation and data recording were performed with Axon pClamp 10 (Molecular Devices) through an A/D converter (Digidata 1440A, Molecular Devices). hERG current (I_{hERG}) density was measured using a depolarization from -80 mV to +60 mV for 2 s and repolarization to -40 mV for 2 s where the tail current was measured (stimulation frequency: 0.125 Hz). Activation was evaluated by a series of 2-s depolarization from -70 to +60 mV (increment: 10 mV, same frequency as above) followed by a 2-s repolarization to -40 mV. Inactivation was studied with a three-pulse protocol: a 1-s depolarization to +40 mV was followed by a 15-ms repolarization to potentials ranging from +30 to -130 mV and a 500-ms depolarization to +40 mV where the remaining current was measured (0.2 Hz). Kinetics of deactivation were evaluated by a two-exponential regression of the decaying current recorded at various potentials from -20 to -130 mV (3 s duration), after a 2-s depolarization to +40 mV (0.125 Hz). The same protocol was used to evaluate the recovery from inactivation kinetics by fitting the rising phase of the current, before deactivation, with a single exponential function. Finally, inactivation kinetics were studied with another three-pulse protocol: a 1-s depolarization to +60 mV was followed by a 25-ms repolarization to -110 mV followed by 500-ms-depolarizations to potentials ranging from +10 to -60 mV and a 500-ms where the inactivating current was fitted with a single exponential function (0.2 Hz).

$I_{KCNE1-KCNQ1}$ current density was measured using a depolarization from -80 mV to 60mV for 4 s and repolarization to -40 mV for 1 s where the tail current was measured (stimulation frequency: 0.125 Hz). Activation was evaluated by a series of 2-s depolarization from -60 to +90 mV (increment: 10 mV, same frequency as above) followed by a 1.2-s repolarization to -40 mV.

II.1.3.8 – I_{Kr} and AP recordings in hiPS-CM

Dissociated hiPS-derived cardiomyocytes were obtained with the same protocol used in the first article (refer to article 1). Before recordings, cells were treated for 24 h either with citrate buffer or with 200 ng/ml of Tat. For the solutions used refer to article 1.

Action potentials were recorded using the perforated-patch configuration at spontaneous rate or stimulated by 1.3-1.5 ms current pulses of 300-1500 pA at various basic cycle lengths

II.1.3.9 – Data analysis

Steady-state activation and inactivation curves were fitted with a single Boltzmann function using GraphPad Prism 3.02. Data are presented as mean ± SEM or Tukey boxplots (Q1-Q3 boxes). Statistical significance was estimated using Student's t-test, Mann-Whitney test, or two-way repeated-measurement ANOVA when appropriate. Post-hoc test for multiple comparisons (Holm-Sidak method) was performed when ANOVA P value was < 0.05. A value of p<0.05 was considered significant.

II.1.4 – Results

II.1.4.1 – Tat is active in heterologous expression systems

To verify that Tat entered cells, after a 24-h incubation with recombinant Tat protein immunohistochemistry was performed on HEK-hERG cells, showing that Tat was present in most of the cells, while only background signal was observed in untreated cells or citrate buffer; Supplemental Figure 1A). As seen on confocal immunostaining images of HEK-hERG cells, Tat was observed (Supplemental Figure 1B). Similar results were also obtained with 200 ng/ml Tat treatment (data not shown). Therefore, in our experimental conditions, Tat enters the cells where it accumulates.

Tat transactivation potential was tested by measuring its activity on the Tat-activated HIV-1-LTR promoter linked to a firefly luciferase, in COS-7 cells incubated with 200 ng/ml Tat for 24 h. LTR-luciferase luminescence was increased by about 4 fold as compared to untreated cells (3.9 ± 0.3 normalized luciferase activity ($n = 3$) in Tat-incubated cells, as compared to 1 ± 0.1 normalized luciferase activity ($n = 3$) in citrate buffer incubated cells (Supplemental Figure 2)). These results confirm that Tat enters the cells and is active.

II.1.4.2 – Tat has no major effect on repolarizing currents in heterologous expression systems

Tat has been shown to delay action potential repolarization in guinea-pig cardiomyocytes [15]. Guinea-pig and human cardiomyocytes hold I_{Kr} and I_{Ks} repolarizing currents, that may be altered by Tat, provoking an action potential lengthening responsible for the QT interval prolongation [30]. Since I_{Kr} is conducted by the voltage-gated potassium channel hERG, we first evaluated the effects of Tat on hERG channel activity in HEK293 cells stably expressing hERG channels. Figure 1A shows representative hERG current recordings from cells incubated with the buffer or Tat at 200 or 400 ng/mL. Surprisingly and unlike the observation from Bai et al. [15], I_{hERG} developed similarly after 24-h Tat (200 or 400 ng/ml) or buffer treatment (Figure 1A). Quantitative analysis confirmed that Tat incubation (200 or 400 ng/ml) did not induce any significant change in hERG current density in this model (Figure 1B; Table 1). In addition, neither the steady-state activation nor the fast deactivation kinetics were modified (Figure 1C-D; Table 1). However there was a slight but significant slower late phase of deactivation when cells were incubated with the higher Tat concentration. Similarly, neither the steady-state inactivation nor the kinetics inactivation and of recovery from inactivation were modified by Tat (Figure 1E to G; Table 1). In order to evaluate whether the

cell type could explain the absence of Tat effect on I_{hERG}, this analysis was repeated in COS-7 cells transiently expressing hERG. Again, no change on the hERG current was observed after a 24-h incubation with Tat (200 ng/ml; Figure 2A-B; Table 1).

The second current involved in the action potential late repolarization, $I_{Ks,}$ is conducted by the voltage-gated potassium channel KCNQ1 associated with its regulatory subunit KCNE1. Therefore, the effect of 200 ng/ml Tat was tested on COS-7 cells transiently transfected with the human KCNE1-KCNQ1 fusion protein. Similar slowly activating and deactivating potassium currents were observed whether the cells were incubated with buffer or with Tat (Figure 2C). Indeed, no effect of a 24-h Tat incubation was observed, neither on the KCNE1-KCNQ1 current density, nor on the activation and deactivation kinetics (Figure 2D to F; Table 1).

II.1.4.3 – Tat decreases I_{Kr} repolarizing current in cardiomyocytes derived from human induced pluripotent stem cells

Cardiomyocytes differentiated from foreskin fibroblast-derived human induced pluripotent stem cells (hiPS-CMs) provided an opportunity to evaluate Tat effects on a more relevant cellular model than transfected non-cardiac cells. As shown in figure 3A, I_{Kr}, isolated as the E-4031-sensitive current, was significantly reduced hiPS-CMs incubated with 200 ng/ml Tat-treated. After full activation, the maximum tail K^+ current density measured at -50 mV was reduced by about 30% (Figure 3B; Table 1). In addition, the current activation was impaired: half-activation potential was shifted toward more negative potentials and the slope K was decreased (Table 1). The net effect of these modifications led to a decrease of the tail current (figure 3C). However, deactivation kinetics were not modified by Tat incubation (Figure 3D).

Altogether, these data show that Tat alters endogenous hERG activity in hiPS-CMs but not exogenously expressed hERG activity in COS-7 or HEK293 cells.

II.1.4.4 – Tat modifies the electrical activity of cardiomyocytes derived from human induced pluripotent stem cells

Action potentials (APs) were recorded using perforated patch-clamp configuration from hiPS-CMs. Three types of AP shapes were obtained and categorized as nodal-, atrial-, and ventricular-like APs (Supplemental Table). Since the long QT syndrome is associated with ventricular AP prolongation, we focused on ventricular-like APs. As illustrated in figure 4A, the AP duration was longer in hiPS-CMs incubated with Tat than in hiPS-CMs incubated with

buffer. AP durations (APD) at different percentages of full repolarization were quantified at two pacing cycle lengths (PCL). As shown in figure 4B, AP prolongation was larger for the late phase of repolarization than for the early phase, and this effect was more pronounced at long PCL, in accordance with the hERG-related long QT syndrome (Figure 4B).

In addition, most Tat-treated cells presented with a higher APD_{90} dispersion compared to untreated cells. As seen in Figure 5A, this dispersion resulted from AP duration and amplitude alternans. These alterations were larger in some cells (cells 2 and 3) compared to others (cell 1). APD alternans were exacerbated at faster stimulation rates (shorter PCLs; Figure 5B). Action potential prolongation and alternans were also observed in atrial-like cardiomyocytes (not shown).

II.1.5 – Disscusion

In the present study, Tat induces modifications of hiPS-derived cardiomyocyte electrical activity: decrease in the I_{Kr} current, and increase in the frequency of APD alternans. These modifications may represent the molecular and cellular background for QT prolongation in HIV patients.

Although we confirmed the presence and the transcriptional activity of the Tat protein in both heterologous expression systems, we observed only minor or no modification of the hERG current. Indeed, Tat did not lead to a decrease in hERG current in HEK-hERG cells, as previously reported in the study of Bai and collaborators [15]. In addition, Tat did not exhibit any effect on hERG expressed in COS-7 cells. Tat used in this study is 86 amino acid long, as in the study on Tat cardiac effect on rats [20]. This short form is observed in viral isolates from humans [19]. It is slightly longer than the form used by Bai and collaborators, which corresponds to the first exon of the protein only (72 amino acids). Both Tat-72 and Tat-86 contain the transactivation domain, and are frequently used for *in vitro* studies. Tat-86 is more readily taken up than Tat-72 in various cell types [36]. Thus, the origin of the difference in the effects of Tat-72 and Tat-86 is still unclear.

Nevertheless, most interestingly in the context of HIV, we observed reduction in I_{Kr} current as well as ventricular AP prolongation and alternans occurrence in hiPS-derived cardiomyocytes. This study underlines the usefulness of iPS-derived cardiomyocytes which represent a more integrated model than the heterologous expression system. The fact that we did not observe any effect of Tat on hERG stably expressed in HEK293 or transfected in COS-7 cells, but a decrease in I_{Kr} in the human cardiomyocytes suggests that Tat, which is interacting with an array of cellular processes, exhibits an indirect effect on hERG, through a molecular mechanism which is present in the cardiomyocytes, but absent in HEK293 and COS-7 cells.

Similar results were obtained in a cellular and *in silico* study regarding the effects of a hERG mutation related to the LQT syndrome *i.e.* mildly modified biophysical properties, AP prolongation at lower rate and APD alternans at elevated rate [35]. Furthermore, mild reduction in repolarization reserve due to alteration of I_{Kr} parameters led to APD alternans in an established human AP computer model of M-cells [34]. The mechanisms responsible for T wave alternans are still uncertain although regional heterogeneity of repolarization has been repeatedly proposed as one of them. In LQT patients, T-wave alternans are strongly

associated to delayed repolarization and are a known risk factor for sudden death [31, 32]. Conversely, increasing I_{Kr} by overexpression of hERG in canine cardiomyocytes suppressed AP alternans as suspected previously, using *in silico* models [37, 38].

In conclusion, this study provides novel insights into the link between arrhythmia in HIV-positive individuals and hERG Tat-related alteration in human cardiomyocytes. Tat in vivo is massively secreted by infected cells [17], and serum Tat concentration can reach hundreds of ng/ml in patients [18]. Noteworthy, serum levels of Tat remain high in treated patients, which could explain the lack of correlation between prolonged QT interval and antiretroviral therapies [18]. Our work shows that Tat protein has a direct effect on cardiac electrical activity in the absence of the treatment or other HIV proteins. At the clinical level, consideration of T wave alternans in the HIV patient's ECG may improve the patients care management.

Table 1: Biophysical characteristics of the hERG channels in HEK-hERG, COS-7 cells and hiPS-CMs, and of the KCNE1-KCNQ1 channels expressed in COS-7 cells.

	HEK-hERG			COS-7-hERG		hiPS-CMs-I_{Kr}	
	Buffer	Tat 200 ng/ml	Tat 400 ng/ml	Buffer	Tat 200 ng/ml	Buffer	Tat 200 ng/ml
Current density	(23)	(14)	(14)	(38)	(35)	(15)	(15)
at 60 mV (pA/pF)	19.5 ± 2.0	23.3 ± 3.7	18.9 ± 2.9	54.6 ± 10.9	39.9 ± 7.3	0.93 ± 0.18	0.64 ± 0.23 *
Activation	(16)	(11)	(12)	(18)	(22)	(10)	(6)
$V_{1/2}$ (mV)	-26.9 ± 1.4	-25.0 ± 2.8	-26.6 ± 1.4	-11.1 ± 1.4	-15.1 ± 1.8	-19.4 ± 2.4	-27.1 ± 2.1 *
K (mV)	7.4 ± 0.2	7.6 ± 0.3	7.5 ± 0.1	7.0 ± 0.3	6.5 ± 0.2	7.1 ± 0.6	4.7 ± 0.7 *
Inactivation	(12)	(5)	(8)	(8)	(6)	-	-
$V_{1/2}$ (mV)	-66.3 ± 1.4	-67.2 ± 3.2	71.0 ± 2.1	-54.6 ± 7.3	-57.3 ± 2.4	-	-
K (mV)	20.7 ± 0.4	20.9 ± 0.5	20.3 ± 0.7	22.6 ± 0.6	20.4 ± 0.7 *	-	-

	COS-7-KCNE1-KCNQ1	
Current density	(19)	(19)
at 60 mV (pA/pF)	31.7 ± 7.5	42.0 ± 8.6
Activation	(11)	(11)
$V_{1/2}$ (mV)	26.6 ± 4.6	26.7 ± 4.3
K (mV)	16.6 ± 1.4	15.4 ± 0.6

(n): number of cells; *: P<0.05; V1/2 and K: voltage for half-activation or -inactivation of the K^{+} currents and slope.

II.1.6 – Figure legends and figures

Figure 1: Tat has no major effect on hERG current in HEK-hERG cells. (A) Representative superimposed currents recorded from HEK293 cells stably expressing hERG, incubated with citrate buffer (left), 200 ng/ml Tat (middle) or 400 ng/ml Tat (right). (B) Tukey boxplots presenting hERG tail current densities. (C-G) Biophysical parameters in the same conditions as in (B). (C) Voltage-dependence of activation. (D) Time constants of deactivation (fast and slow) *versus* voltage. *: Buffer *versus* Tat 400 ng/ml; $: Tat 200 ng/ml *versus* Tat 400 ng/ml. *: p< 0.05, *** and $$$: p< 0.001 (Holm-Sidak test). (E) Voltage-dependence of inactivation. (F) Time constants of recovery from inactivation *versus* voltage. (G) Time constants of inactivation *versus* voltage. The protocols used are shown as insets.

Figure 2: Tat does not significantly alter hERG or human KCNE1-KCNQ1 current in COS-7 cells. (A) Tukey boxplots presenting hERG tail current densities in COS-7 cells expressing hERG channels incubated with buffer or 200 ng/ml Tat. (B) Voltage-dependence of activation. The protocols used for A and B are the same as insets in Figure 1B and A, respectively. (C) Representative human KCNE1-KCNQ1 currents after buffer or 200 ng/ml

Tat incubation. (D) Tukey boxplots presenting human KCNE1-KCNQ1 current densities. Protocol for C and D is shown in inset. (E) Voltage-dependence of activation (protocol in inset). (F) Averaged time constants of deactivation upon repolarization at -40 mV in buffer and 200 ng/ml Tat-treated cells.

Figure 3: Tat reduces I_{Kr} recorded from hiPS-CMs. (A) Representative superimposed currents recorded from hiPS-CMs incubated with buffer (left) or Tat (right), before (control) and after 1 μM E-4031 application; the E-4031-sensitive current, I_{Kr}, was obtained by digital subtraction of the current recorded after E-4031 application to the one recorded before application (inset: voltage-clamp protocol). (B) Tukey boxplots presenting I_{Kr} tail current density measured at -50 mV after depolarization at +20 mV. Mann-Whitney test: * $P<0.05$. (C) Relative I_{Kr} tail current density measured at -50 mV *versus* prepulse potential. (D) Averaged time constants of deactivation upon repolarization at -50 mV (Student t-test).

Figure 4: Tat significantly increases ventricular-like action potential durations in hiPS-CMs. (A) Left, representative ventricular-like action potentials recorded from hiPS-CMs incubated with buffer or 200 ng/ml Tat, stimulated at a pacing cycle length (PCL) of 700 ms. Right, corresponding expanded action potentials (tagged ● in left panel). Dashed line and horizontal bar: 0 mV. (B) Averaged action potential duration at 30 (APD_{30}), 50 (APD_{50}), 70 (APD_{70}) and 90% (APD_{90}) of full repolarization measured in ventricular-like cells incubated with in buffer or Tat at 2 different PCLs.*: $p < 0.05$ (Holm-Sidak test).

Figure 5: Tat treatment leads to alternans events in ventricular-like hiPS-CMs. (A) Representative ventricular-like action potentials recorded from 3 different hiPS-CMs incubated with 200 ng/ml Tat. Cell 1: APD_{90} of five consecutive APs indicated below. (B) Poincaré plots of APD_{90} (one color per cell) recorded at 3 different PCLs. The graph shows the APD_{90} of each AP (number n) *versus* the APD_{90} of its preceding one (n-1). Same color code used in A.
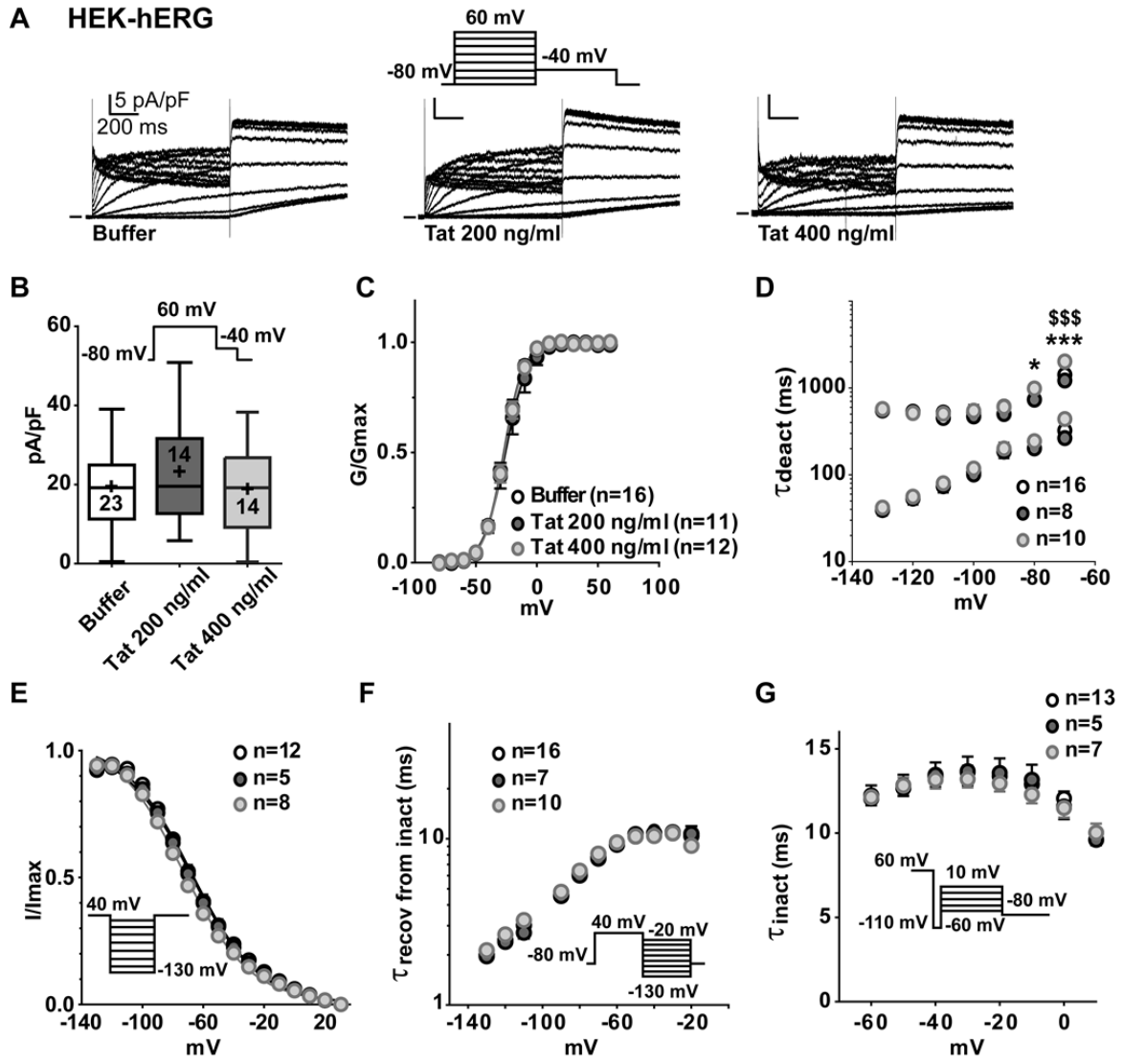
Figure 1.
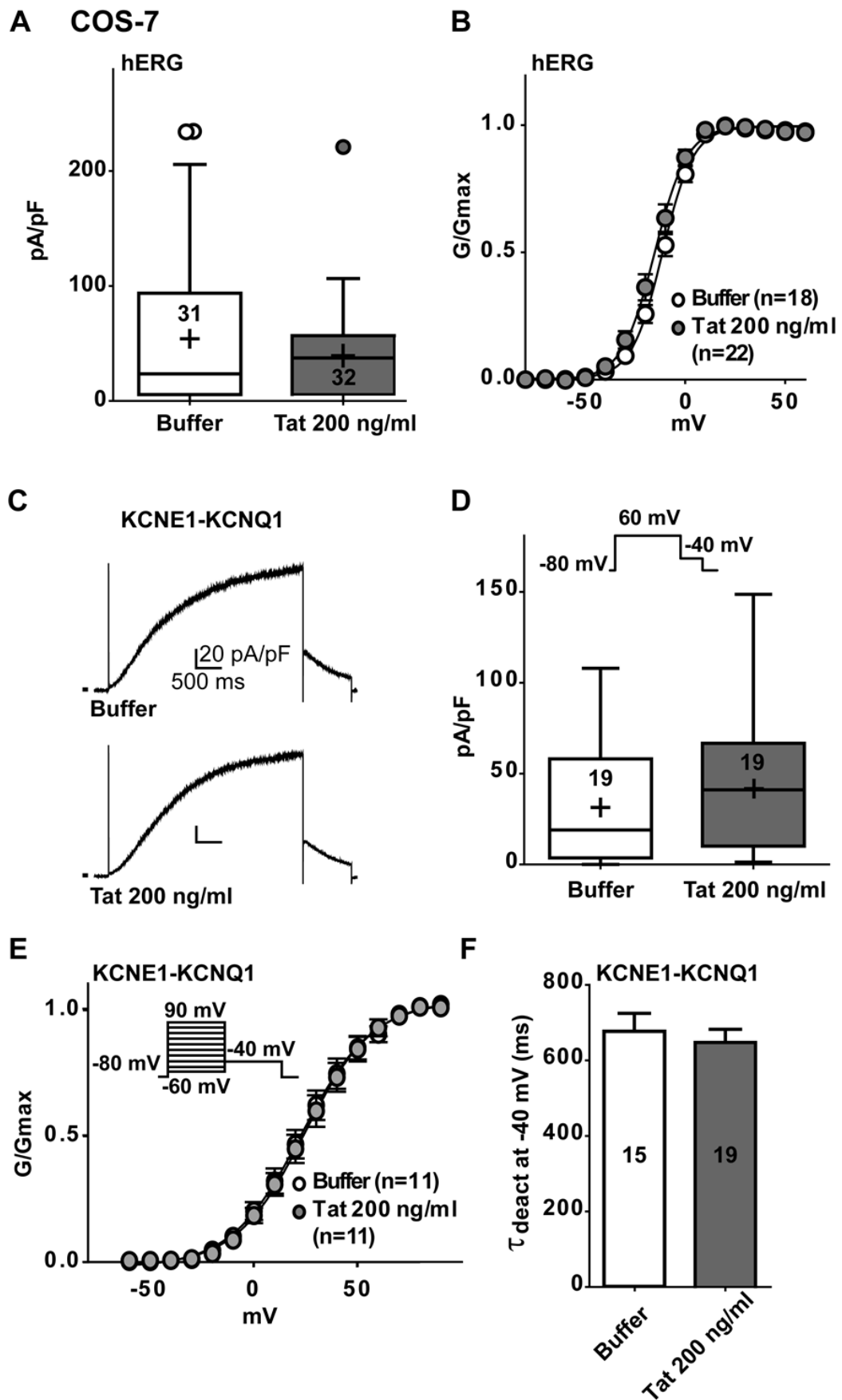
Figure 2.
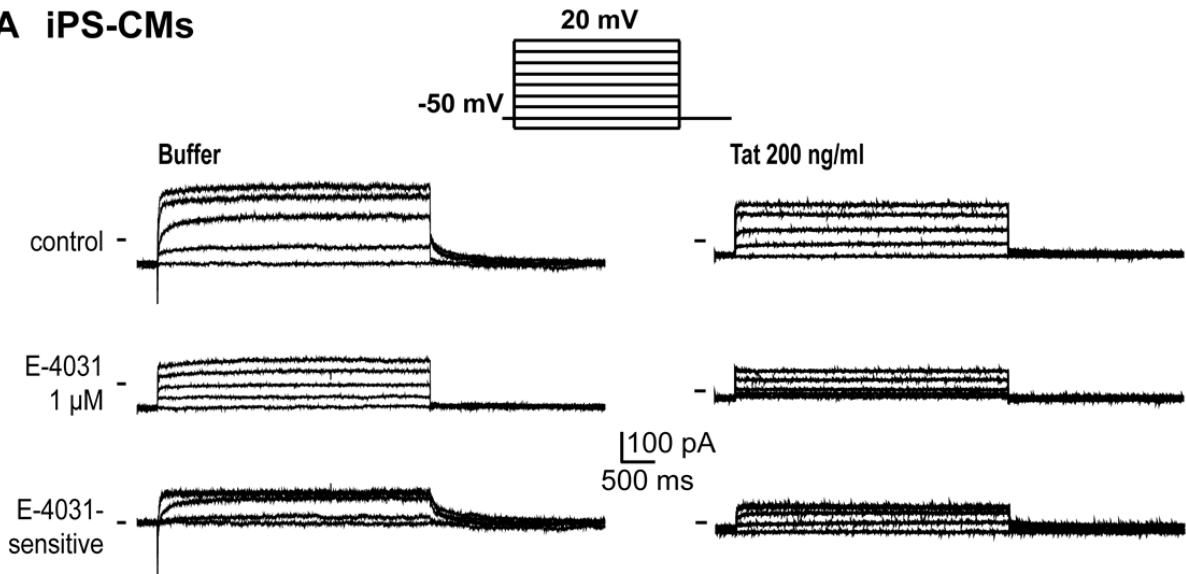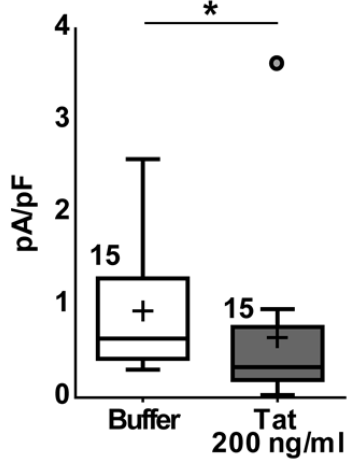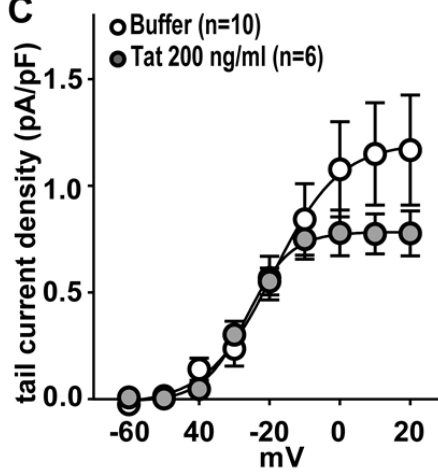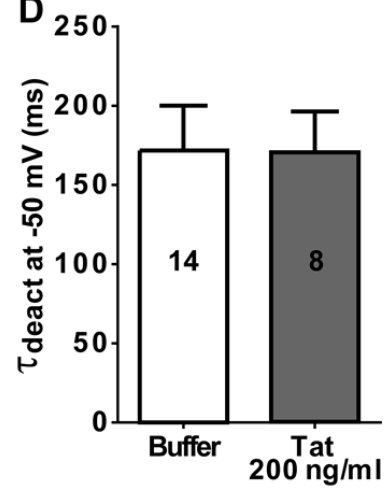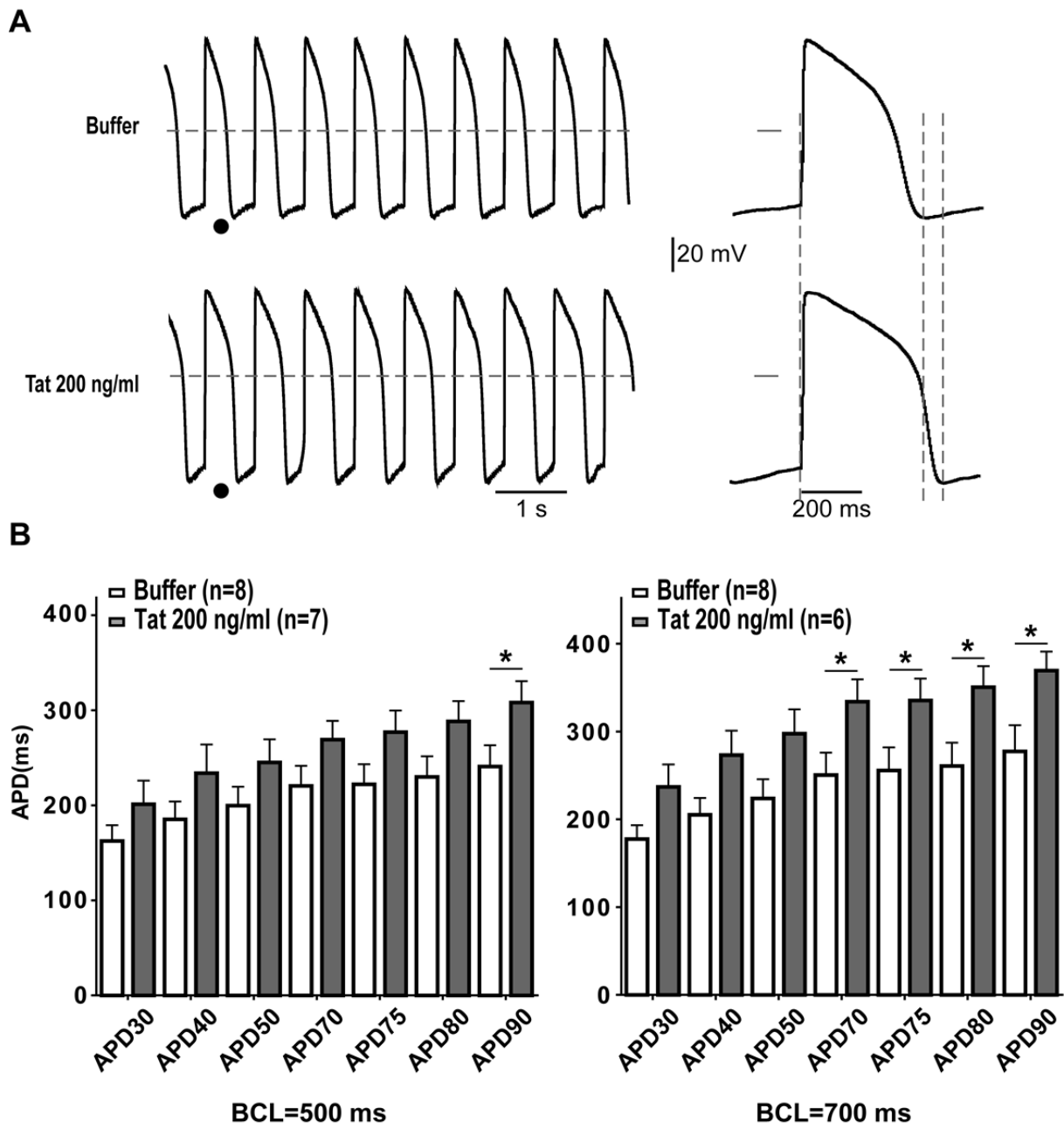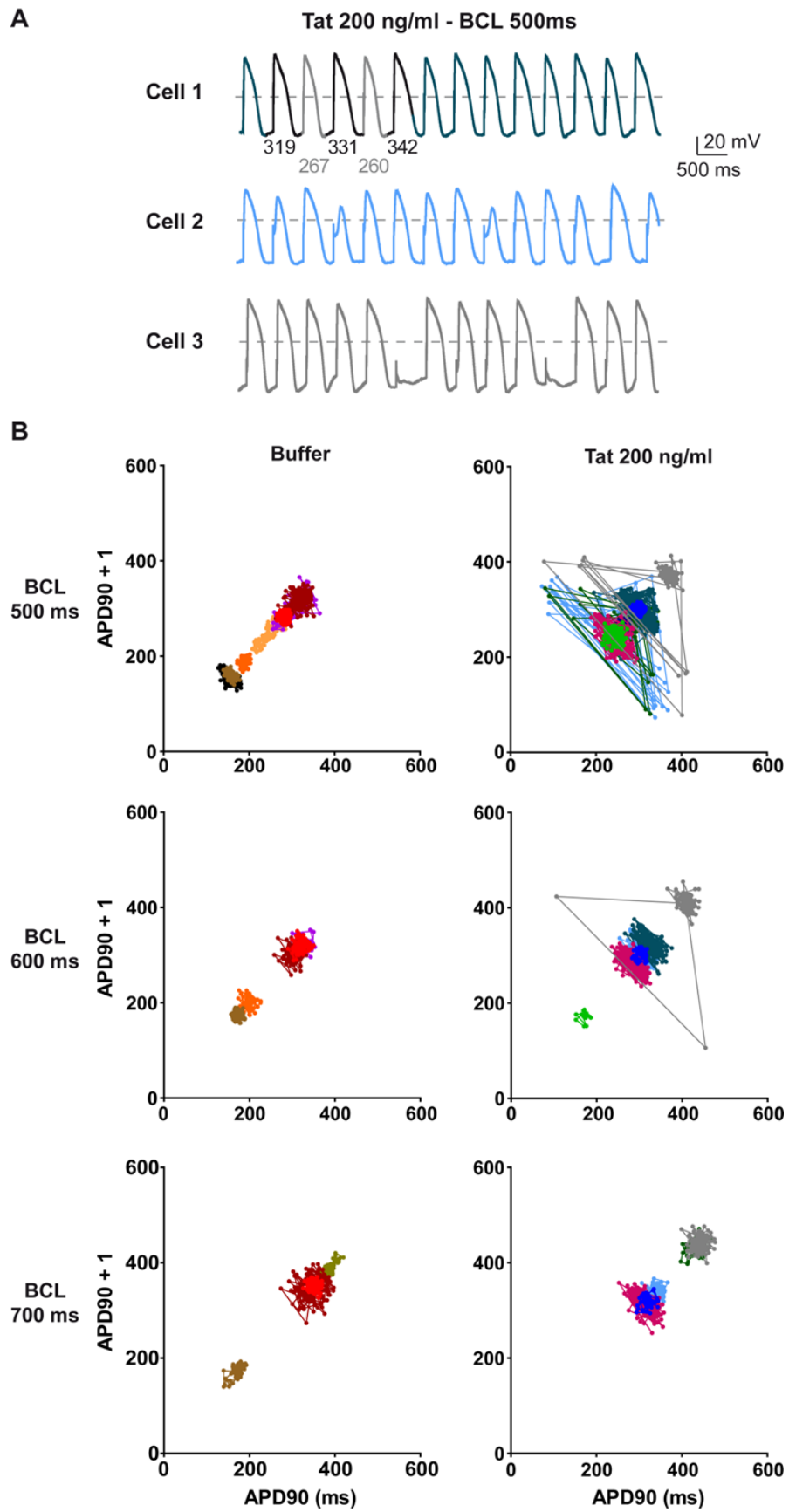
Figure 3.

Figure 4.

Figure 5.

II.1.7 – Acknowledegments

We thank the iPS cell core facility and MicroPiCell facility of SFR Santé F. Bonamy (Nantes), Patricia Charpentier from Therassay facility, and Morteza Erfanian for their technical support.

DISCLOSURES

None

II.1.8 – References

[1] Collaboration, T.A.T.C., Mortality of HIV-infected patients starting potent antiretroviral therapy: comparison with the general population in nine industrialized countries. International Journal of Epidemiology, 2009. 38(6): p. 1624-1633.

[2]. Nakagawa, F., et al., Projected life expectancy of people with HIV according to timing of diagnosis. AIDS, 2012. 26(3): p. 335-343.

[3] World Health Oganization. Towards universal access : scaling up priority HIV/AIDS interventions in the health sector : progress report 2008. 2008. 1-7-2015. Ref Type: Report

[4] World Health Oganization. Global update on the health sector response to HIV, 2014. 1-7-2014. 1-7-2015. Type: Report

[5] Tseng ZH, Secemsky EA, Dowdy D, Vittinghoff E, Moyers B, Wong JK et al. Sudden cardiac death in patients with human immunodeficiency virus infection. J Am Coll Cardiol 2012;59:1891-6.

[6] Charbit B, Rosier A, Bollens D, Boccara F, Boelle PY, Koubaa A et al. Relationship between HIV protease inhibitors and QTc interval duration in HIV-infected patients: a cross-sectional study. Br J Clin Pharmacol 2009;67:76-82.

[7] Nordin C, Kohli A, Beca S, Zaharia V, Grant T, Leider J et al. Importance of hepatitis C coinfection in the development of QT prolongation in HIV-infected patients. J Electrocardiol 2006;39:199-205.

[8] Kocheril AG, Bokhari SA, Batsford WP, Sinusas AJ. Long QTc and torsades de pointes in human immunodeficiency virus disease. Pacing Clin Electrophysiol 1997;20:2810-6.

[9]   Fantoni M, Autore C, Del BC. Drugs and cardiotoxicity in HIV and AIDS. Ann N Y Acad Sci 2001;946:179-99.

[10] Vallecillo G, Mojal S, Roquer A, Martinez D, Rossi P, Fonseca F et al. Risk of QTc prolongation in a cohort of opioid-dependent HIV-infected patients on methadone maintenance therapy. Clin Infect Dis 2013;57:1189-94.

[11] Haverkamp W, Breithardt G, Camm AJ, Janse MJ, Rosen MR, Antzelevitch C et al. The potential for QT prolongation and proarrhythmia by non-antiarrhythmic drugs: clinical and regulatory implications. Report on a policy conference of the European Society of Cardiology. Eur Heart J 2000;21:1216-31.

[12] Hanna Z, Kay DG, Cool M, Jothy S, Rebai N, Jolicoeur P. Transgenic mice expressing human immunodeficiency virus type 1 in immune cells develop a severe AIDS-like disease. J Virol 1998;72:121-32.

[13] Brouillette J, Grandy SA, Jolicoeur P, Fiset C. Cardiac repolarization is prolonged in CD4C/HIV transgenic mice. J Mol Cell Cardiol 2007;43:159-67.

[14] Nerbonne JM. Studying cardiac arrhythmias in the mouse--a reasonable model for probing mechanisms? Trends Cardiovasc Med 2004;14:83-93.

[15] Bai YL, Liu HB, Sun B, Zhang Y, Li Q, Hu CW et al. HIV Tat protein inhibits hERG K+ channels: a potential mechanism of HIV infection induced LQTs. J Mol Cell Cardiol 2011;51:876-80.

[16] Sanguinetti MC, Jiang C, Curran ME, Keating MT. A mechanistic link between an inherited and an acquired cardiac arrhythmia: HERG encodes the IKr potassium channel. Cell 1995;81:299-307.

[17] Rayne F, Debaisieux S, Yezid H, Lin YL, Mettling C, Konate K et al. Phosphatidylinositol-(4,5)-bisphosphate enables efficient secretion of HIV-1 Tat by infected T-cells. EMBO J 2010;29:1348-62.

[18] Poggi A, Carosio R, Fenoglio D, Brenci S, Murdaca G, Setti M et al. Migration of V delta 1 and V delta 2 T cells in response to CXCR3 and CXCR4 ligands in healthy

donors and HIV-1-infected patients: competition by HIV-1 Tat. Blood 2004;103:2205-13.

[19] Debaisieux S, Rayne F, Yezid H, Beaumelle B. The ins and outs of HIV-1 Tat. Traffic 2012;13:355-63.

[20] Brailoiu E, Deliu E, Sporici RA, Benamar K, Brailoiu GC. HIV-1-Tat excites cardiac parasympathetic neurons of nucleus ambiguus and triggers prolonged bradycardia in conscious rats. Am J Physiol Regul Integr Comp Physiol 2014;306:R814-R822.

[21] Chow DC, Wood R, Choi J, Grandinetti A, Gerschenson M, Sriratanaviriyakul N et al. Cardiovagal autonomic function in HIV-infected patients with unsuppressed HIV viremia. HIV Clin Trials 2011;12:141-50.

[22] Villa A, Foresti V, Confalonieri F. Autonomic neuropathy and prolongation of QT interval in human immunodeficiency virus infection. Clin Auton Res 1995;5:48-52.

[23] Vendeville A, Rayne F, Bonhoure A, Bettache N, Montcourrier P, Beaumelle B. HIV-1 Tat enters T cells using coated pits before translocating from acidified endosomes and eliciting biological responses. Mol Biol Cell 2004;15:2347-60.

[24] Rodriguez N, Amarouch MY, Montnach J, Piron J, Labro AJ, Charpentier F et al. Phosphatidylinositol-4,5-bisphosphate (PIP(2)) stabilizes the open pore conformation of the Kv11.1 (hERG) channel. Biophys J 2010;99:1110-8.

[25] Yezid H, Konate K, Debaisieux S, Bonhoure A, Beaumelle B. Mechanism for HIV-1 Tat insertion into the endosome membrane. J Biol Chem 2009;284:22736-46.

[26] Si-Tayeb K, Noto FK, Nagaoka M, Li J, Battle MA, Duris C et al. Highly efficient generation of human hepatocyte-like cells from induced pluripotent stem cells. Hepatology 2010;51:297-305.

[27] Zhang J, Klos M, Wilson GF, Herman AM, Lian X, Raval KK et al. Extracellular matrix promotes highly efficient cardiac differentiation of human pluripotent stem cells: the matrix sandwich method. Circ Res 2012;111:1125-36.

[28] Terrenoire C, Wang K, Tung KW, Chung WK, Pass RH, Lu JT et al. Induced pluripotent stem cells used to reveal drug actions in a long QT syndrome family with complex genetics. J Gen Physiol 2013;141:61-72.

[29] Loussouarn G, Baro I, Escande D. KCNQ1 K+ channel-mediated cardiac channelopathies. Methods Mol Biol 2006;337:167-83.

[30] Charpentier F, Merot J, Loussouarn G, Baro I. Delayed rectifier K(+) currents and cardiac repolarization. J Mol Cell Cardiol 2010;48:37-44.

[31] Zareba W, Moss AJ, le CS, Hall WJ. T wave alternans in idiopathic long QT syndrome. J Am Coll Cardiol 1994;23:1541-6.

[32] Platt SB, Vijgen JM, Albrecht P, Van Hare GF, Carlson MD, Rosenbaum DS. Occult T wave alternans in long QT syndrome. J Cardiovasc Electrophysiol. 1996 Feb;7(2):144-8.

[33] Laurita KR, Rosenbaum DS. Cellular mechanisms of arrhythmogenic cardiac alternans. Prog Biophys Mol Biol 2008;97:332-47.

[34] Burashnikov A, Antzelevitch C. Acceleration-induced action potential prolongation and early afterdepolarizations. J Cardiovasc Electrophysiol 1998;9:934-48.

[35] Schweigmann U, Biliczki P, Ramirez RJ, Marschall C, Takac I, Brandes RP et al. Elevated heart rate triggers action potential alternans and sudden death. translational study of a homozygous KCNH2 mutation. PLoS One 2014;9:e103150.

[36] Ma M, Nath A. Molecular determinants for cellular uptake of Tat protein of human immunodeficiency virus type 1 in brain cells. J Virol 1997;71:2495-9.

[37] Hua F, Johns DC, Gilmour RF Jr. Suppression of electrical alternans by overexpression of HERG in canine ventricular myocytes. Am J Physiol Heart CircPhysiol. 2004 Jun;286(6):H2342-51

[38] Hua F, Gilmour RF Jr. Contribution of IKr to rate-dependent action potential dynamics in canine endocardium. Circ Res. 2004 Apr 2;94(6):810-9

I.2 – Supplemental Material

Supplemental data

Es-Salah-Lamoureux *et al.*: Mechanisms of induction of cardiac arrhythmias in HIV patients
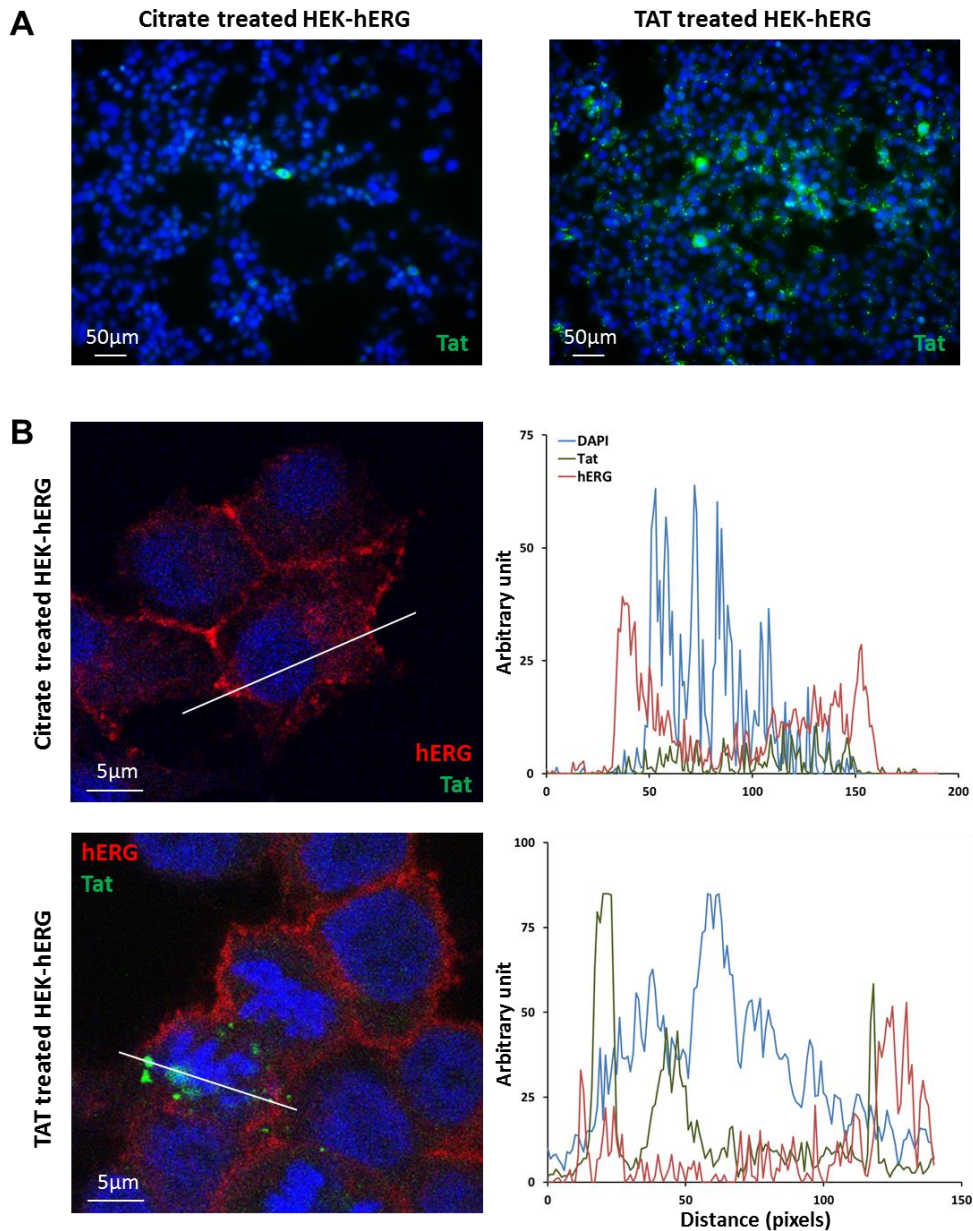
Supplemental Figure 1: Tat protein enters in HEK-hERG cells. (A) Tat protein localization (green) after treatment of HEK-hERG cells by citrate buffer (left) or 200 ng/ml Tat (right) for 24 h. (B) Left, specific localization of Tat (green) in HEK-hERG cells treated with 400 ng/ml Tat with counterstaining for hERG (red). Right, surface plots of Tat, hERG and DAPI stainings at the level of the lines.
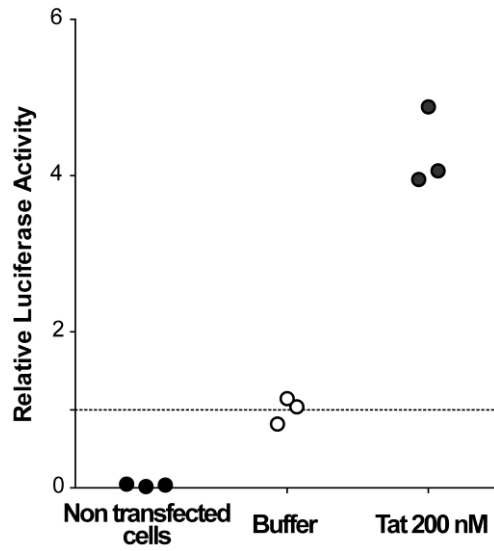
Supplemental Figure 2: Tat protein is active in COS-7 cells. Firefly/Renilla luciferase activity ratio in non-transfected, untreated (Buffer) and treated transfected COS-7 cells.

Supplemental Table. Quantitative parameters used for classification of action potentials obtained from patch-clamp experiments on buffer-treated cells.

hiPS-CMs APs (n=20)	AP amplitude (mV)	MDP (mV)	Peak to peak duration (ms)	dV/dt (V/s)	APD90 (ms)	APD30–40/ APD70–80	APD50/APD90
Nodal-like (n=4)	63.0 ± 4.4	-41.7 ± 3.7	650.1 ± 147	2.1 ± 0.4	174.4 ± 2.5	2.3 ± 0.2	0.6 ± 0.002
Atrial-like (n=7)	77.3 ± 2.2	-47.2 ± 1.5	901.2 ± 188.5	4.4 ± 0.5	215.9 ± 22.9	1.0 ± 0.1	0.6 ± 0.001
Ventricular-like (n=9)	102.6 ± 3.1	-58.6 ± 2.1	1301.2 ± 310.8	10.9 ± 1.2	269.4 ± 30.1	4.9 ± 0.7	0.8 ± 0.02

III – Induced pluripotent stem cell-derived cardiomyocytes reveal the role of depolarizing currents in Brugada syndrome

In this part of the results, I am showing the results we have related to objective 3 (refer to hypothesis and objectives). In this study, three BrS patients are included:

1. A patient with an *SCN5A* mutation, encoding Nav1.5 channel
2. A patient with un unidentified mutation
3. A patient with a *CLASP2* variant encoding the Cytoplasmic Linker Associated Protein

iPSC platform at Nantes, generated hiPS cells from the three patients. Characterization of hiPS-CMs for the first two patients was performed. On the other hand, no data are collected for hiPS-CMs from the third patient with the *CLASP2* variant. We faced some problems in amplifying hiPS cells form this patient. There is a suggestion that the mutation these cells have in *CLASP2* may affect their amplification potency. So, in the following part only data from the first two patients are presented.

Furthermore, this study includes some limitations that we are working on. First, one control is contained in the study; to better validate the obtained results a second control will be added. Furthermore, in the family of the N1722D-*SCN5A* mutated patient, another BrS-affected family member is being reprogrammed by the iPSC platform of Nantes. Interestingly, sequencing results for this patient revealed the absence of the N1722D-*SCN5A* mutation. Adding the data form hiPS-CMs from this patient may help better understand the pathological mechanisms of BrS, at least in the context of *SCN5A* mutations. Indeed, this paper is a first draft, further experiments are planned to be done in the near future.

- Article 3 -

Induced Pluripotent Stem cell-derived Cardiomyocytes Reveal the role of Depolarizing Currents in Brugada Syndrome

Mariam Jouni[a,b,c,e], Nadjet Belbachir[a-c], Aude Dervier[f] , Benoite Champon[a-c], Flavien Charpentier[a-d], Gildas Loussouarn[a-c], Isabelle Baró[a-c], Kazem Zibara[e], Patricia Lemarchand[a-d], Nathalie Gaborit[a-c]

In Preparation

a. Inserm, UMR 1087, l'institut du thorax, Nantes, France

b. CNRS, UMR 6291, Nantes, France

c. Université de Nantes, Nantes, France

d. CHU Nantes, l'institut du thorax, Nantes, France

e. ER045, PRASE, Laboratory of stem cells, Lebanese university, Beirut, Lebanon.

f. Inserm UMS 016, CNRS UMS 3556, iPS facility, SFR santé, University of Nantes, CHU Nantes, France.

III.1 – Article

III.1.1 – Abstract

Rationale: Brugada syndrome (BrS) is a hereditary cardiac disease characterized by typical electrocardiogram and ventricular tachycardia. In about 20% of the patients, mutations have been identified in the gene encoding the voltage gated Na^+ ion channel (*SCN5A*); however, more than 65% of the cases have no genetic abnormalities identified. Most genotype-phenotype studies have been performed in heterologous expression systems and animal models that lack the patients' genetic background, human induced pluripotent stem cells (hiPS) offer a new paradigm for these types of studies.

Objective: To characterize and explore functional characteristics of iPS-derived cardiomyocytes from BrS patients carrying different genetic backgrounds in order to investigate the underlying pathological mechanisms.

Methods and results: hiPS cells from two BrS affected patients, one carrying a *SCN5A*-N1722D mutation and one without identified mutation, have been generated and validated. hiPS cells from a healthy subject were used as control. Using patch clamp techniques, biophysical properties of the Na^+ channel and action potential characteristics were evaluated. Preliminary data revealed that while peak I_{Na} is only decreased in the *SCN5A* mutated hiPS cell line and both lines share a ventricular action potential arrhythmic phenotype. In this study, I_{Na} is fully characterized to investigate its role in the occurrence of these arrhythmias and observed that the late I_{Na} is altered in both Brugada patients.

Conclusion: Modeling BrS using hiPS cells-derived cardiomyocytes suggests the role of the late sodium current in the ventricular arrhythmia of the two BrS patients. Therefore, this work is a key step towards unveiling a common mechanism involved in the pathophysiology of BrS.

III.1.2 – Introduction

Brugada syndrome is a cause of sudden cardiac arrest in patients without structural cardiac abnormalities. Recognition and diagnosis of this syndrome has been slowly increasing. Syncope, ventricular dysrhythmia, or sudden cardiac arrest may be the presenting symptoms, but detection of the characteristic right precordial ST-segment elevation on ECG is the main diagnosis criteria [1] [2] [3]. However, the majority of patients with such ECG abnormalities remain completely asymptomatic [4].

Over the past years, at least 17 genes have been identified either to cause BrS or to be BrS-susceptibility genes. Mutations in *SCN5A*, which encodes the cardiac sodium channel Nav1.5, is presented as a gene 'causing' BrS, but are observed in only ∼20% of the patients [5]. Despite extensive efforts, most instances of BrS remain genetically unexplained as a monogenic disorder. Moreover, no common genetic variants in all BrS patients have been identified. Additionally, many families that carry a *SCN5A* mutation contain non-clinically affected members with the *SCN5A* mutation and clinically affected members with BrS who are not genetic carriers [30]. On the other hand, we showed that BrS patients exhibit a common ion-channel molecular expression signature that includes reduction of *SCN5A* expression irrespectively of the culprit gene [6].

Although heterologous expression systems and animal models [7] [8] [9] [10] [11] [12] have provided important insights into cardiac arrhythmic syndromes pathogenesis, the lack of *in vitro* sources for human cardiomyocytes and the inability to model patient-specific disease variations has significantly hampered the study of these diseases. Thus, there is a need for an alternative strategy to further understand the pathophysiological mechanisms associated with BrS. Human induced pluripotent stem cells derived cardiomyocytes (hiPS-CMs) [13] [14] are offering new opportunities to analyze heart rhythm disorders by enabling to study mechanisms of genetic diseases. Patient-specific hiPS cells that carry all the disease-relevant genetic alterations are important not only for understanding complex disease mechanisms in the affected cell types, but also for providing insights into factors that predispose individuals to develop these diseases. Recapitulation of cardiac diseased phenotypes by iPS-derived cardiomyocytes (hiPS-CMs) has been shown for several cardiac arrhythmias including overlap syndrome of cardiac sodium channel disease [15] but not for BrS only. Based on that, we hypothesized that hiPS-CMs may lead to novel insights in cardiac BrS pathophysiology, and offer a unique approach to improve understanding of patient-specific genotype-phenotype relationships.

In this study, we characterized and explored functional characteristics of iPS-derived cardiomyocytes from two BrS patients carrying different genetic backgrounds. Our data revealed that while peak I_{Na} is only decreased in the *SCN5A* mutated hiPS-CMs, both lines share a ventricular action potential arrhythmic phenotype. We fully characterized I_{Na} to investigate its role in the occurrence of this arrhythmia and observed that the late I_{Na} is altered in both BrS patients.

III.1.3 – Materials and methods

III.1.3.1 – *Patients selection and clinical characterization*

The study was conducted in compliance with current Good Clinical Practice standards and in accordance with the principles set forth under the Declaration of Helsinki (1989). Institutional review board approvals of the study were obtained before the initiation of patient enrollment. Each subject entering the study agreed to and signed an institutional review board-approved statement of informed consent.

Two BrS patients, originating from two families of different genetic backgrounds, were selected by the "Rhythmic Hereditary diseases" center at the University Hospital (CHU Nantes). The two families have been medically monitored at the CHU Nantes since their medical diagnosis (figures 1A and 2B). Both patients had a Brugada-specific type one ECG, with an elevation in the ST segment either at baseline or when medically challenged (figures 2A and 2B). In addition, both patients had a family history of ventricular fibrillation and syncope episodes. Using second generation sequencing based on HaloPlex technology, a list of 160 BrS candidate genes including, *SCN5A, CACNA1C, GPD1L, HCN4, KCND3, KCNH2, TRPM4* and *SCN10A*, were sequenced in both families. In the first family, a novel *SCN5A* mutation was found to segregate with the disease phenotype, while no identified mutation was identified in the second family. The *SCN5A* mutated patient is a 47 year old asymptomatic male who presented an ST elevation segment when treated with flecainide. The patient carries a missense mutation in *SCN5A* gene encoding α-subunit of the Nav1.5 sodium channel. The mutation causes an Asparagine to Aspartic acid substitution at position 1722 (chr3:38,589,553-38,674,850A>G; NM_198056.2 N1722D) (Figure 1C). The second patient, a 52 year old male, suffered from syncope at night. Skin biopsies form these two patients were processed to obtain fibroblasts, by the iPSC core facility of Nantes, to be used as somatic cells for the generation of human induced pluripotent stem cells specific for each patient.

III.1.3.2 – *Human skin fibroblast culture*

After isolation from skin biopsies, fibroblasts were kept in fibroblast media that contained: DMEM (high glucose, GlutaMAX) (Invitrogen), 10 % Fetal Bovine Serum Hyclone (Perbio), 1mM Sodium pyruvate (Invitrogen), 1 % nonessential amino acids (Invitrogen) and 10 µg/mL Gentamycin (Invitrogen). Cells were kept at 37°C and media was changed every two days.

III.1.3.3 – *Fibroblasts reprogramming and hiPS cells characterization*

III.1.3.3.a – Sendai virus (Sev) reprogramming

Fibroblasts form the patient with *SCN5A* (N1722D) mutation, were reprogrammed using Sendai virus (SeV) reprogramming. Reprogramming was performed using the Cytotune reprogramming kit (Life technologies) following the manufacturer's protocol. In brief: 80% confluent fibroblasts grown in fibroblast medium (10% FCS (Hyclone), 1% l-glutamine, 1% sodium pyruvate and 1% MEM-NEAA in high-glucose DMEM (Life technologies)) in a 6-well plate were transduced with each viruses at a multiplicity of infection (MOI) of 5 for the Klf4-Oct4-Sox2 polycystronic construct, MOI 5 for Klf4 and MOI 3 for Myc. Cells were fed every other day, plated on day 7 onto 0.1% gelatin-coated dishes containing DR4 MEFs feeders and medium was switched to hESC medium (7 μl/liter 2ME (Sigma), 20% KOSR, 2× l-Glutamine, 1× MEM-NEAA, 10 ng/ml bFGF, in DMEM/F12 (Lifetech)). Clones were picked and amplified in KSR/feeder conditions until P10, and derived on Matrigel/TeSR before being transferred to us.

III.1.3.3.b – mRNA reprogramming

Fibroblasts form the patient without any identified mutation were reprogrammed using mRNA reprogramming [16], using Stemgent mRNA reprogramming kit and pluriton medium. Briefly, fibroblasts are transfected every day with a mix of mRNA of 6 genes (Oct4, Sox2, Klf4, cMyc, Lin28, Gfp) with Lipofectamine® RNAiMAX Transfection Reagent (life technologies) for 14 days in Pluriton. Colonies were manually picked on mouse embryonic fibroblasts (MEFs). Human induced pluripotent stem cells were characterized by RT-PCR to verify the expression of endogenous pluripotent factors OCT3/4, NANOG and SOX2, immunostaining, flow cytometry, and their ability to form teratoma [17].

III.1.3.4 – *Culture of human induced pluripotent stem cells*

Established hiPS cell lines were maintained on mitotically-inactivated MEFs in DMEM/F12 medium supplemented with 2 mmol/L L-glutamine, 0.07% β-mercaptoethanol, 20% knockout serum replacement, 5 ng/mL bFGF and 1% NEAA under low oxygen atmosphere (4% O_2). Cells were passaged by manual dissection of cell clusters every 6-7 days. Before differentiation, hiPS cells were manually transferred from MEFs to matrigel-coated plates (0.05 mg/ml, BD Biosciences) and cultured on StemMACS (iPS-Brew XF). Passages were performed using Gentle Cell Dissociation Buffer (StemCell Technologies).

III.1.3.5 – *Flow Cytometry analysis*

A total of 1.10^5 cells in suspension, for each condition, were washed 3 times with PBS/BSA 0.1%, then incubated with PE-labeled antibodies, SSEA3-PE, SSEA4-PE, TRA1-60-PE (eBioscience), for 30 minutes at 4°C in the dark and further rinsed 3 times with FACS buffer. Data acquisition was performed using FACSDiva software with LSR II instrument (Becton Dickinson, BD).

III.1.3.6 – *Differentiation of hiPS cells into cardiomyocytes and dissociation*

Human iPS cells were differentiated into cardiomyocytes using the established matrix sandwich method with modifications [18]. Briefly, 6 days before initiating differentiation, hiPS cell colonies were passaged on hESC-qualified matrigel-coated plates (0.05 mg/ml, using Gentle Cell Dissociation Buffer and cultured as a monolayer in StemMACS (iPS-Brew XF) (Miltenyi), human with 1x Y-27632 Rock inhibitor (Miltenyi) under normal oxygen atmosphere. When cells reached 80% confluence, cold StemMACS with Growth Factor Reduced Matrigel (0.033 mg/ml, BD Corning) was added in order to create an overlay of Matrigel. Differentiation was initiated 24 h later (day 0) by culturing the cells in RPMI1640 medium (Life Technologies) supplemented with B27 (without insulin, Life Technologies), 2 mmol/L L-glutamine (Life technologies), 1% NEAA (Life technologies), 100 ng/mL Activin A (Miltenyi), and 10 ng/mL FGF2 for 24 hours. On the next day, the medium was replaced by RPMI1640 medium supplemented with B27 without insulin, 2 mmol/L L-glutamine, 1% NEAA, 10 ng/mL BMP4 (Miltenyi), and 5 ng/mL FGF2 for 4 days. By day 5, cells were cultured in RPMI1640 medium supplemented with B27 complete (Life Technologies), 2 mmol/L L-glutamine and 1% NEAA, and changed every 2-3 days.

For protein and electrophysiological analyses, cardiomyocytes were dissociated around day 20 of differentiation, for 20 min in collagenase II (200 U/mL; Gibco) at 37°C. Isolated cells were then incubated at room temperature for 30 min in Kraft-Bruhe solution containing 85 mmol/L KCl, 30 mmol/L K_2HPO_4, 5 mmol/L $MgSO_4$, 1 mmol/L EGTA, 2 mmol/L Na_2-ATP, 5 mmol/L Na-pyruvate, 5 mmol/L creatine, 20 mmol/L taurine, and 20 mmol/L glucose, pH 7.2 [19].

III.1.3.7 – *Gene expression analysis*

Total RNA was extracted from hiPS colonies, using RNeasy mini kit (Qiagen). One μg of tRNA was reverse transcribed using High-Capacity cDNA Reverse Transcription Kit (Applied Biosystems) following manufacturer's instructions. PCR amplification was performed using FAM labeled-TaqMan probes (Applied Biosystems).

III.1.3.8 – *Gene expression analysis*

For histological analysis two cell types were analyzed: undifferentiated hiPS cells, which were cultured in 12 well plates on MEF feeders, dissociated hiPS-derived cardiomyocytes, which were plated on IBIDI plates (Biovalley) and further cultured for 6 to 10 days. For, hiPS on MEFs were fixed with 4% PFA, permeabilized with 0.5% Triton X-100 and blocked with 3% PBS-BSA. Cells were then stained with primary antibodies directed against OCT3/4 (Santa Cruz), SOX2 (Santa Cruz) and TRA1-60 (eBioscience) diluted in 1% PBS-BSA. For , after methanol fixation, cells were permeabilized with 0.1% Triton X-100, blocked with 5% PBS-BSA and stained with primary antibodies against α-Actinin (Abcam), troponin I (Santa Cruz), MLC2a (Abcam), MLC2v (Proteintech Europ), connexin 43 (Chemicon), or Nav1.5 (Alomone labs). Secondary antibody staining was performed using Alexa 488- and Alexa 568-conjugated antibodies (Molecular Probes). DAPI was used for nuclear staining.

III.1.3.9 – *Functional analysis in COS-7 cells*

III.1.3.9.a – *Site-directed mutagenesis*

The point mutation N1722D (1859G>A) in *SCN5A* was introduced using mutated oligonucleotide extension (QuikChange II XL Site-Directed Mutagenesis Kit) in *SCN5A* isoform 2 cDNA (GenBank Acc. No. NM_000335). The mutated plasmid was verified by complete DNA sequencing of the cDNA insert by the genomics core facility.

III.1.3.9.b – *Cell culture and transfection*

The African green monkey kidney-derived cell line COS-7 cells were kept in DMEM (University of Copenhagen, Denmark) supplemented with 10% FCS (GIBCO, Invitrogen, Carlsbad, CA) and 40 mg/L L-proline at 37°C in 5% CO2. Cells were transfected with 2 μg *SCN5A* plasmid (wild type or mutant) together with 2 μg of beta subunit (*SCN1B*) plasmid. Transfections were performed using JetPI reagents (Polyplus Transfections, France)

according to the manufacturer's instructions. Enhanced green fluorescent protein GFP encoding plasmid (1.2 μg) was included to identify transfected cells.

III.1.3.9.c – Sodium current recordings (I_{Na})

Currents were recorded 2 days after transfection using an Axopatch 200A amplifier (Axon Instruments, Molecular Devices, Sunnyvale, CA, USA). Cells were super fused with a solution containing the following (in mmol/L): 145 NaCl, 4 CsCl, 1 CaCl$_2$, 1 MgCl$_2$, 5 HEPES, and 5 glucose, pH=7.4 with NaOH. Patch pipettes were fabricated from borosilicate glass capillaries (and had resistances between 1.5 and 2 MΩ when filled with pipette solution (in mmol/L): 90 KCl, 45 K-gluconate, 10 NaCl and 10 HEPES, pH=7.4 with CsOH. All recordings were made at room temperature (20°C -22°C). Data were analyzed using pClamp10 software (Axon Instruments).

III.1.3.10 – Single cell electrophysiology

Dissociated hiPS-derived cardiomyocytes were suspended in RPMI + B27 supplemented with insulin, 2 mmol/L L-glutamine and 1% NEAA and then plated on matrigel-coated 35-mm plastic Petri dishes. Isolated beating cells were used for patch-clamp recordings using whole-cell configuration, between day 10 and day 14 post-dissociation. Data were collected from a minimum of 4 independent differentiations for at two to three clones per patient.

III.1.3.10.a – Action potential recordings

Using amphotericin permeabilized patch clamp (I clamp), APs were measured at 35±0.2°C using a modified Tyrode's solution containing (in mM): 140 NaCl, 5.4 KCl, 1.8 CaCl$_2$, 1.0 MgCl$_2$, 5.5 glucose, 5.0 HEPES; pH 7.4 (NaOH). The pipette solution contained (in mM): 125 K-gluconate, 20 KCl, 10 NaCl, 10 HEPES; pH 7.2 (KOH) and 0.22 amphotericin-B [20]. Maximum diastolic potential (MDP), maximal upstroke velocity (V_{max}), AP amplitude (APA), and AP duration (APD) at 20, 50, 75 and 90% repolarization (APD$_{20}$, APD$_{50}$, APD$_{75}$ and APD$_{90}$, respectively) were analyzed. Data from 3 consecutive APs were averaged.

III.1.3.10.b – Sodium current recordings (I_{Na})

I_{Na} measurements were recorded in the ruptured patch clamp configuration. Cells were perfused using a Tyrode solution containing (in mM): 130 NaCl, 10 CsCl, 1.8 CaCl$_2$, 1.2 MgCl$_2$, 11.0 glucose and 5.0 HEPES; pH 7.3 (CsOH). The pipette solution contained (in mM): 3.0 NaCl, 133 CsCl, 2.0 MgCl$_2$, 2.0 Na$_2$ATP, 2.0 TEACl, 10 EGTA, 5.0 HEPES; pH

7.2 (CsOH). During recordings, a local gravity micro perfusion system allowed application of an extracellular solution containing (in mM): 20 NaCl, 110 CsCl, 1.8 $CoCl_2$, 1 $MgCl_2$, 30 mannitol and 5.0 HEPES; pH 7.4 (CsOH) [15] [21].

I_{Na} densities and gating properties were measured at $35 \pm 2°C$ using voltage-clamp protocols shown in the relevant figures. All measurements were performed using a holding potential of -100 mV with a cycle time of 2 seconds for single step and activation, 3 seconds for inactivation and 4 seconds for recovery form inactivation. Current densities were calculated by dividing current amplitude by membrane capacitance (Cm) in (pF). Voltage-dependence of activation and inactivation curves were fitted with a Boltzmann function ($y=[1+exp\{(V-V_{1/2})/K\}]-1$), where $V_{1/2}$ is the half-maximal voltage of (in)activation and K is the slope factor. Recovery from inactivation was assessed with a double pulse protocol. Data were normalized to the current elicited by the first pulse (P1) and fitted with a bi-exponential function ($y=y0+A_f\{1-exp[-t/\tau_f]\}+A_s\{1- exp[-t/\tau_s]\}$), where A_f and A_s represent the amplitudes of the fast and the slow components of recovery from inactivation, and τ_f and τ_s are their respective recovery time constants.

Late I_{Na} was measured as a TTX-sensitive current (Tetrodotoxine Citrate 1069 mg, TOCRIS Bioscience) at room temperature using an ascending ramp protocol. Same intracellular and extracellular solutions were used as in the case of I_{Na} peak current with a local gravity micro perfusion system of the following composition (in mM): 130 NaCl, 10 CsCl, 1.8 $CoCl_2$, 1 $MgCl_2$, 20 mannitol, 10.0 HEPES and 0.01 TTX; pH 7.4 (CsOH) [21].

III.1.3.10.c – L type Calcium current recordings ($I_{Ca,L}$)

$I_{Ca,L}$ measurements were recorded in the ruptured patch-clamp configuration. Cells were perfused using a Tyrode solution containing (in mM): 140 NaCl, KCl 4, 1.0 $CaCl_2$, 0.5 $MgCl_2$, 10.0 glucose and 10.0 HEPES; pH 7.4 (NaOH). The pipette solution contained (in mM): 5.0 NaCl, 145 CsCl, 2.0 $CaCl_2$, 5.0 EGTA, 5.0 MgATP, 5.0 HEPES; pH 7.2 (CsOH). During recording, a local gravity micro perfusion system allowed application of an extracellular solution containing (in mM): 160 TEA-Cl, 5.0 $CaCl_2$, 1.0 $MgCl_2$, 1 $MgCl_2$, 10 glucose and 5.0 HEPES and 0.01 TTX; pH 7.4 (CsOH). $I_{Ca,L}$ densities and gating properties were measured at room temperature using voltage-clamp protocols shown in the relevant figures [21].

III.1.3.10 – Statistical analysis

Results are expressed as mean ± SEM. Comparisons were made by use of an unpaired Mann Whitney t-test, one-way ANOVA, or two-way repeated measures ANOVA. Values of $P <$ 0.05 were considered statistically significant. Statistical analyses were performed with GraphPad software.

III.1.4 – Results

III.1.4.1 – *Generation and Characterization of N1722D-hiPS-CMs and Um-hiPS-CMs*

Skin fibroblasts were obtained from two patients with clinical symptoms of Brugada syndrome: one carrying the N1722D-*SCN5A* mutation and the other with an unidentified mutation (Um). Fibroblasts were reprogrammed using non integrative methods to generate the corresponding hiPS cell lines. Ten independent clones for each patient were manually picked. A previously described foreskin fibroblast-derived hiPS cell clone C2a (Control-hiPS) was used as a control [22]. Endogenous expression of the pluripotent stem cell markers, *OCT3/4*, *SOX2* and *NANOG*, absent in the fibroblasts, were detected by qRT-PCR in hiPS cells of both patients (figure 3A). Endogenous expression of OCT3/4 and TRA1-60 proteins was also visualized by immunofluorescence staining in hiPS cells of both patients (figure 3B). Flow cytometry analysis showed that N1722D-hiPS cells and Um-hiPS cells were positive for the expression of pluripotency markers TRA1-60, SSEA4 and SSEA3 (figure 3C). Moreover, N1722D heterozygous mutation in the *SCN5A* locus was confirmed to be present in the N1722D-hiPS cells but not in control-hiPS cells (figure 3D). Overall, the adult somatic cells were successfully reprogrammed into induced pluripotent stem cells and a total of 2 to 3 clones per lines have been selected to perform the following experiments.

III.1.4.2 – *N1722D-hiPS and Um-hiPS can be differentiated into cardiomyocytes*

Cardiomyocytes were differentiated, using the matrix sandwich method from control-hiPS cells, N1722D-hiPS cells and Um-hiPS cells. All three hiPS cells showed comparable cardiac differentiation potential (figure 4), giving rise to spontaneously contracting cell areas after 8-10 days of differentiation. Cardiomyocytes isolated from Control-hiPS cells, N1722D-hiPS cells and Um-hiPS cells displayed organized cross-striations with proper alignment of the myofibrils that were positive for cardiac and muscular specific cytoskeletal proteins, troponin I, α-Actinin, and both MLC2A and MLC2V. In addition RyR2, an actor of calcium homeostasis was expressed in the three cell lines (Figure 4). These results suggest that Control-, N1722D- and Um-hiPS cells have similar cardiac differentiation potentials.

III.1.4.3 – I_{Na} *current density is reduced in N1722D-hiPS-CMs but not in Um-hiPS-CMs*

Using whole cell patch-clamp we investigated whether hiPS-CMs of both patients had a similar reduction in *SCN5A*-conducted current, I_{Na}. Representative traces of I_{Na} recordings obtained from N1722D-hiPS-CMs and Um-hiPS-CMs as well as control-hiPS-CMs are shown in figure 5A. As shown in Figure 5A, B and C, I_{Na} current was significantly reduced in N1722D-hiPS-CMs (p=0.0077), in comparison to Control-hiPS-CMs. In contrast, no similar reduction was observed in the second patient. Activation, inactivation and recovery form inactivation kinetics were not modified in hiPS-CMs of both patients, in comparison with the control (Figure 5D, E and G) and (Table 1 of supplementary data). Interestingly, similar data were also obtained in COS-7 cells transfected with plasmids expressing either Control-*SCN5A* or N1722D- *SCN5A*, as indicated in figures 6A, 6B and 6C. Indeed, a significant reduction of I_{Na} (p=0.0002) was also observed without any modifications in activation and inactivation kinetics (Figures 6D and 6E).

III.1.4.4 – *N1722D-SCN5A alters ventricular action potential parameters*

To investigate whether the BrS-hiPS-CMs had other alterations at the functional level, action potentials were recorded using perforated patch clamp (I-clamp). Action potential recordings provide a whole image of the potential altered functions of ionic channels involved in its generation. All recoded action potential were classified into nodal, atrial and ventricular, based on the maximum slope rise (dv/dt_{max}) and action potential duration at 90% of repolarization (APD 90) [21] (values are indicated in Table 2 in supplementary data). Comparable proportions of the different types of action potentials were obtained from the three cell types. In the context of BrS, a ventricular arrhythmic disease, we focused on ventricular action potentials, and included only this type in the following figures. In accordance with the I_{Na} reduction observed solely in N1722D-hiPS-CMs, the maximum slope rise (dv/ dt_{max}) and peak amplitude were significantly reduced in these cells (p=0.0095 and p=0.0104 for maximum slope rise and peak amplitude respectively), but not in Um-hiPS-CMs (Figure 7A and 7B). On the other hand, likewise the patient's electrocardiographic phenotype (normal QTc), no significant differences in APD at 30, 50, 75 and 90% repolarization were observed in hiPS-CMs from both patients (Figure 7C).

III.1.4.5 – *N1722D-hiPS-CMs and Um-hiPS-CMs have increased susceptibility to arrhythmia*

Action potential data revealed a common arrhythmic phenotype in the hiPS-CMs from both patients. Early afterdepolarizations (EADs) were observed in approximately 30% of the ventricular cells of N1722D-hiPS-CMs and Um-hiPS-CMs (Figure 8B), while none of these events were observed in atrial or nodal cells (figure 8A). Interestingly, EADs in N1722D-hiPS-CMs were more pronounced than the ones observed in Um-hiPS-CMs (arrows in Figure 8B).

III.1.4.6 – *Late sodium current I_{Na} and L type calcium current ($I_{Ca,L}$) are implicated in the action potential arrhythmic events*

The mechanism underlying the observed EADs was then investigated through the analysis of depolarizing currents (late sodium current and L-type calcium current ($I_{Ca,L}$), as alterations in these currents may lead to arrhythmic incidents such as EADs [23] [24] [25] [26].

Late sodium current was measured as a 0.01 mM Tetrodotoxine (TTX)-sensitive current using an ascending voltage ramp protocol. Representative examples of traces obtained from N1722D-, Um- and control-hiPS-CMs, illustrating the difference in late I_{Na} after application of Tetrodotoxine along with the corresponding recording ramp protocol are shown in Figure 9A. Interestingly, in 30% of the measured cells in both BrS hiPS-CMs, the late I_{Na} density was significantly increased as compared to the control (p=0.0052 for N1722D-hiPS-CMs and, p=0.0027 for Um-hiPS-CMs) (Figure 9B). This suggests that late I_{Na} may participate to the EAD phenotype commonly observed in both cell types.

Calcium current, $I_{Ca,L}$, was also characterized using whole cell ruptured patch clamp. Representative traces are shown in Figure 9C. $I_{Ca,L}$ was significantly increased in N1722D-hiPS-CMs (p=0.00089), in comparison to control-hiPS-CMs (figure 9D), however, no modifications were observed in Um-hiPS-CMs cells. Kinetics of activation and inactivation were not modified in both hiPS-CMs (figure 9E). These data suggest that the persistent sodium current observed in the hiPS-CMs from both patients could be the substrate of the EADs while the increase in the $I_{Ca,L}$ observed solely in N1722D-hiPS-CMs may be the trigger for the more severe EADs phenotype observed in these cells.

III.1.5 – Discussion

In this study, we characterized and explored functional characteristics of iPS-derived cardiomyocytes from two BrS patients carrying different genetic backgrounds. We fully characterized I_{Na} to investigate its role in the pathophysiology of this disease and showed that alteration in persistent I_{Na} in both cell lines may be the substrate of arrhythmic incidents observed in hiPS-CMs in both patients.

Since the identification of BrS in 1992 [27], even though huge work has been performed to further understand the pathophysiological bases of this disease, many questions remain unresolved and the cellular basis of the BrS is still not completely understood [28]. Several theories have been proposed, either based on abnormal electrical transmural gradient or on abnormal electrical impulse propagation or linked to minor abnormalities of cardiac structure [29]. At the genetic level, *SCN5A*, the gene that encodes the voltage-gated sodium channel, presents 20-30 % of mutations identified in BrS. However, more than 65 % of the disease cases remain genetically unidentified [5]. Moreover, our group suggested that *SCN5A* mutations may not be directly causal to the occurrence of the disease and that genetic background may play a powerful role in the pathophysiology of BrS [30]. Furthermore, Bezzina et al [31] showed that a number of other genetic variations are also associated in the pathophysiology of BrS. In brief, BrS has been proven to be an oligogenic, complex disease with a variety of genetic mutations and variants that are linked to its pathophysiology. In this context, heterologous expression systems and transgenic animals available may not be fully adequate to explain the pathophysiological mechanisms associated with BrS. In the present study we showed that human induced pluripotent stem cell-derived cardiomyocytes (hiPS-CMs) [13] [14] provide an alternative approach to improve our knowledge on BrS in the context of the patients' genetic background.

With this study, we made the first electrophysiological characterization of a BrS-specific *SCN5A* mutation using cardiomyocytes differentiated from induced pluripotent stem cells. Indeed, one of the selected patients carries a mutation in the *SCN5A* gene that has not been previously characterized. Comparative analysis of this mutation in COS-7 cells, a more usual cellular model, as well as in hiPS-CMs was also performed. Similar results from both models at the level of I_{Na} current characterization were observed, suggesting that heterologous expression systems are sufficient for modeling single ion channel mutations. However, as BrS is a complex disease that cannot be explained solely by *SCN5A* mutations, COS-7 cellular model may not provide a full picture of its mechanism. In opposition, hiPS-CMs provide is a

multiple approach investigating system, suitable for the study of Brugada syndrome. It allows analysis of other functional levels such as action potential measurements, as well as pathophysiological characterization of patients without any identified mutations.

Based on previously published transcriptomic data [6], I_{Na} in both *SCN5A* mutated and not mutated CMs was characterized using patch clamp, but the expected common current reduction in the two cell lines was not observed. These data suggest that *SCN5A* is not the major contributor of the occurrence of BrS and that the pathophysiology of BrS includes other players beyond mutant sodium channels. Interestingly, early afterdepolarizations (EADs) were detected in 30% of ventricular action potentials of both hiPS-CM lines. EADs observed in the N1722D-hiPS-CMs were more severe than the ones observed in the Um-hiPS-CMs. EADs have been reported as a result of possible occurrence of abnormal depolarizing currents such as persistent I_{Na} and /or $I_{Ca,L}$ [26] [24] [32] [33] [34] [35]. In 30% of total cells recorded from both hiPS-CM lines, a significant increase in late I_{Na} was observed. In contrast, $I_{Ca, L}$ was only found to be increased in *SCN5A* mutated-CMs, along with the more severe EAD phenotype. With these data, we suggest that increase in late I_{Na} act as a substrate for the occurrence of the EADs in the two cell lines, and that $I_{Ca,L}$ triggers the severe EAD phenotype.

III.1.6 – Conclusion

In this study, we showed for the first time that hiPS-CMs can (1) identify various features of an un-described BrS-associated *SCN5A* mutation, and (2) provide global analysis of CMs derived from a BrS patient without any identified mutation. We also unveiled in the two hiPS-CMs of both patients a common electrophysiological phenotype that, to our best knowledge, had not been previously reported in BrS studies. Such model could thus prove beneficial for testing and developing novel pharmacological treatments for BrS patients.

III.1.7 – Figure legends and figures

Figure 1: Clinical and genetic profile of the first BrS patient, carrying N1722D-*SCN5A* mutation (patient is indicated with a black arrow). (A) Genotype of BrS and *SCN5A* of each family member of the N1722D-*SCN5A* patient. (B) 12 leads electrocardiography of the patient challenged with flecainide and showing an ST elevation segment and T wave conversion in leads V1-V2-V3. (C) The N1722D mutation (red dot) is located in domain four of the Nav1.5 protein, which is made of 6 trans-membrane segments (S1-S6).

Figure 2: Clinical and genetic profile of the second BrS patient with an unidentified mutation (patient is indicated with a black arrow). (A) Pedigree of the patient's family. (B) 12 leads electrocardiography for the patient at baseline showing an ST elevation segment and T wave conversion in lead V1.

Figure 3: Characterization of hiPS cells. (A) Expression level of additional endogenous pluripotent stem cell marker (*OCT3/4, NANOG and SOX2*) genes by qRT-PCR in N1722D-hiPS cells and Um-hiPS cells as compared to fibroblasts (B) Endogenous pluripotent stem cell marker (OCT3/4, SOX2 and TRA1-60) visualization by immunofluorescence staining of two N1722D-hiPS clones and three Um -hiPS clones. (C) Percentage of N1722D-hiPS cells and Um -hiPS cells expressing the SSEA4, SSEA3 and TRA1-60 pluripotency genes measured by flow cytometry. (D) Representative images of teratoma following injection of undifferentiated hiPS cells in NOD/SCID mice. The presence of neural tissue (ectoderm, top), intestinal epithelium (endoderm, middle) and immature bone tissue and cartilage (mesoderm, bottom) is shown. (E) Genetic screening in the patient N1722D-hiPS cells revealed the heterozygous single-nucleotide mutation A-G of the *SCN5A* gene, in position 1859 of the coding sequence, resulting in the substitution of an asparagine with an aspartic acid at position 1722 of the protein.

Figure 4: Human hiPS cells differentiated into functional cardiomyocytes. Representative immunofluorescence images of the cardiac sarcomeric protein α-Actinin (green, left), RyR2 (red, middle), troponin I (green, middle) and co-staining of myosin light chain 2a (MLC2a; green; right) and 2v (MLC2v; red, right) in control-hiPS-CMs, N1722D-hiPS-CMs and Um-hiPS-CMs. Scale = 5µm.

Figure 5: Electrophysiological characterization of I$_{Na}$ N1722D-hiPS-CMs and Um-hiPS-CMs. (A) Representative whole cell current recordings for control-hiPS-CMs, N1722D-hiPS-CMs and Um-hiPS-CMs. Currents were activated by the depicted voltage-clamp protocol. (B) I$_{Na}$ density, measured at -30 mV showing a significant reduction in N1722D-hiPS-CMs. (C) Peak current density plotted as a function of voltage demonstrating a reduction in current for N1722D-hiPS-CMs (D) and (E) Average voltage dependence of activation and voltage dependence of inactivation respectively.(F) recovery from inactivation and (G) time constant (slow and fast) of recovery form inactivation. Statistical significance * P<0.05, *** P<0.001

Figure 6: Electrophysiological characterization of N1722D in COS-7 cells. (A) Representative whole cell current recordings in COS-7 cells overexpressing *SCN5A* wild type (WT; n=10) and N1722D (n=9) cDNAs. Currents were activated by the depicted voltage-clamp protocol. (B) I$_{Na}$ density, measured at -30 mV in COS-7+*SCN5A*-WT and COS-7 +*SCN5A*-N1722D, showing a significant reduction in the *SCN5A*-N1722D. (C) Peak current density plotted as a function of voltage demonstrating a reduction in current for N1722D. (D) and (E). Average voltage dependence of activation and voltage dependence of inactivation respectively.

Figure 7: Analysis of Action potentials recorded from N1722D-hiPS-CMs and Um-hiPS-CMs. (A) peak amplitude, (B) dv/dt$_{max}$, and (C) AP duration using patch-clamp measured in N1722D-hiPS-CMs and Um-hiPS-CMs. Statistical significance, * P<0.05, *** P<0.001

Figure 8: Increased arrhythmia susceptibility in N1722D-hiPS-CMs and UmhiPS-CMs. Representative action potential recordings using patch clamp showing early after depolarization that happened specifically in 30% of ventricular cells of N1722D-hiPS-CMs and Um-hiPS-CMs, incidents were more prone in N1722D-hiPS-CMs.

Figure 9 :(1) Late sodium current recorded in N1722D-hiPS-CMs and Um-hiPS-CMs. (A) Example of ramp current traces elicited with an ascending ramp depolarization protocol. The protocol is shown at the bottom. (B) The currents recorded during the ramp expressed as current densities. **(2) Electrophysiological characterization of I$_{CA,L}$ in N1722D-hiPS-CMs and Um-hiPS-CMs.** (A) Representative whole cell current recordings for control-hiPS-CMs, N1722D-hiPS-CMs and Um-hiPS-CMs. Currents were activated by the depicted voltage-clamp protocol. (B) Peak current density plotted as a function of voltage demonstrating an

increase in current for N1722D. (C) and (D) Average voltage dependence of activation and voltage dependence of inactivation respectively. Statistical significance, * P<0.05, ** P<0.01 and *** P<0.001.
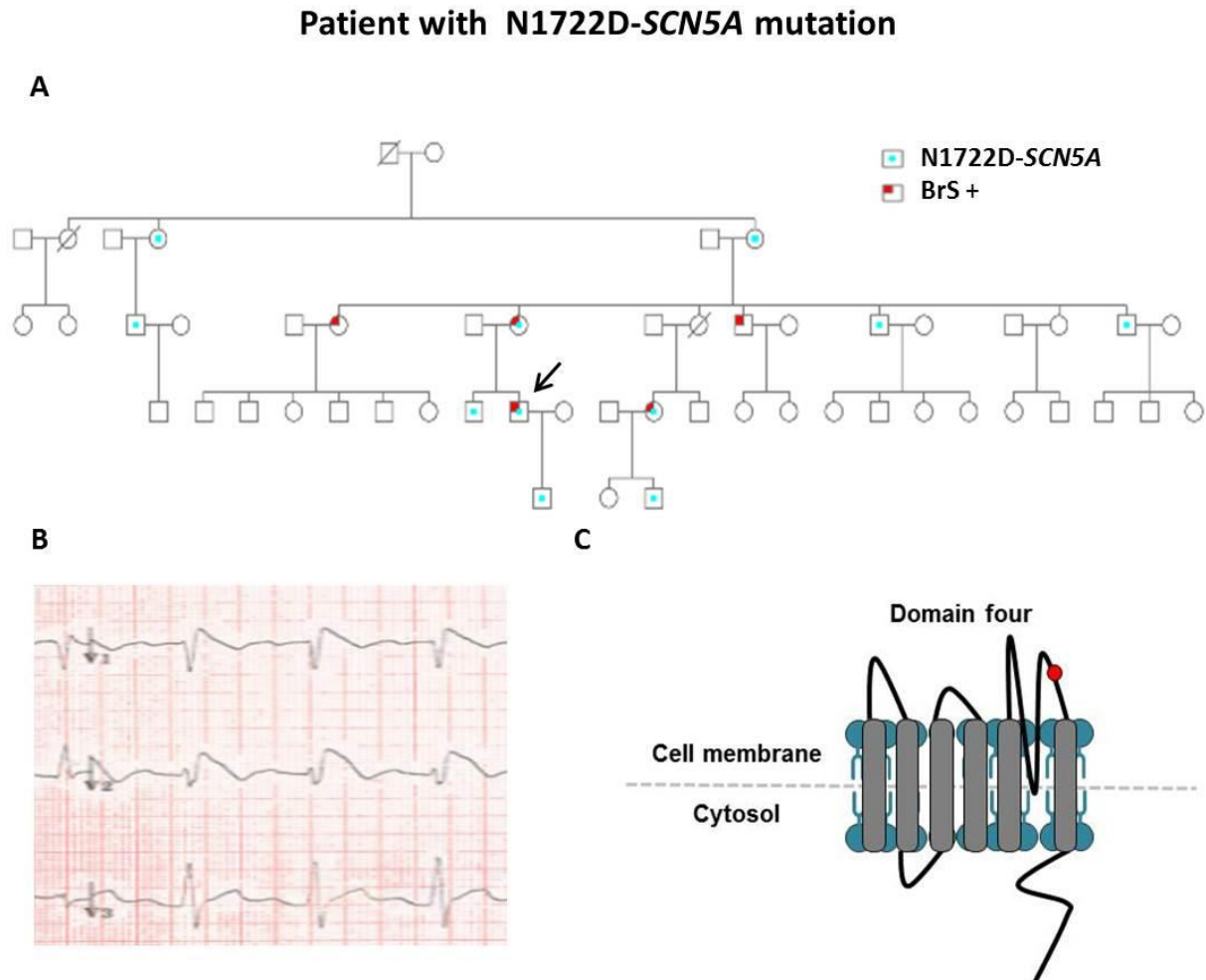
Figure 1.

Patient with Unidentified mutation

A
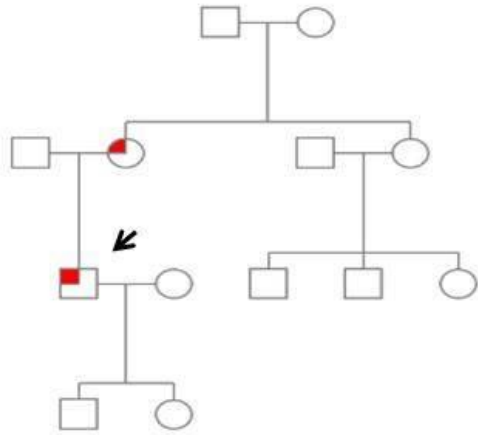
B
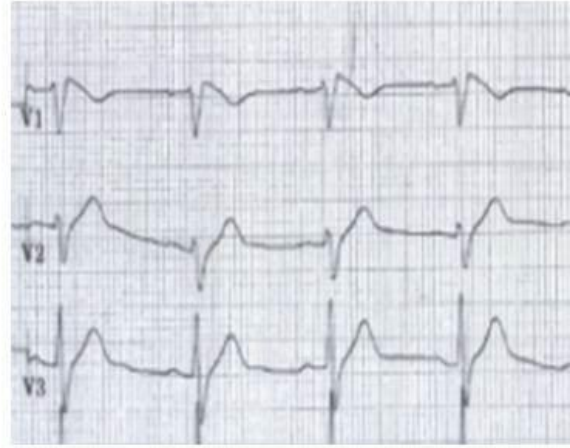
Figure 2.
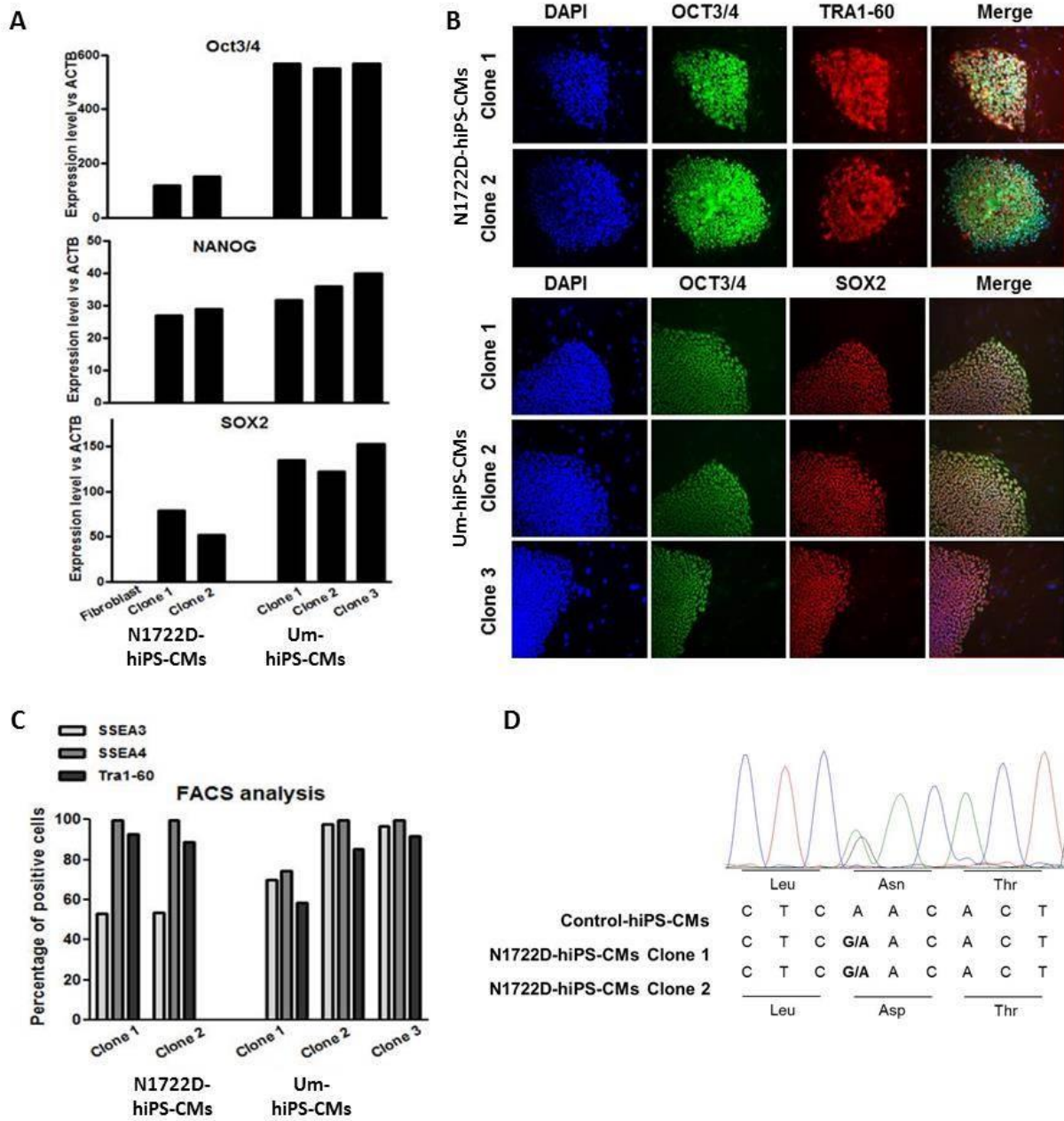
Figure 3.
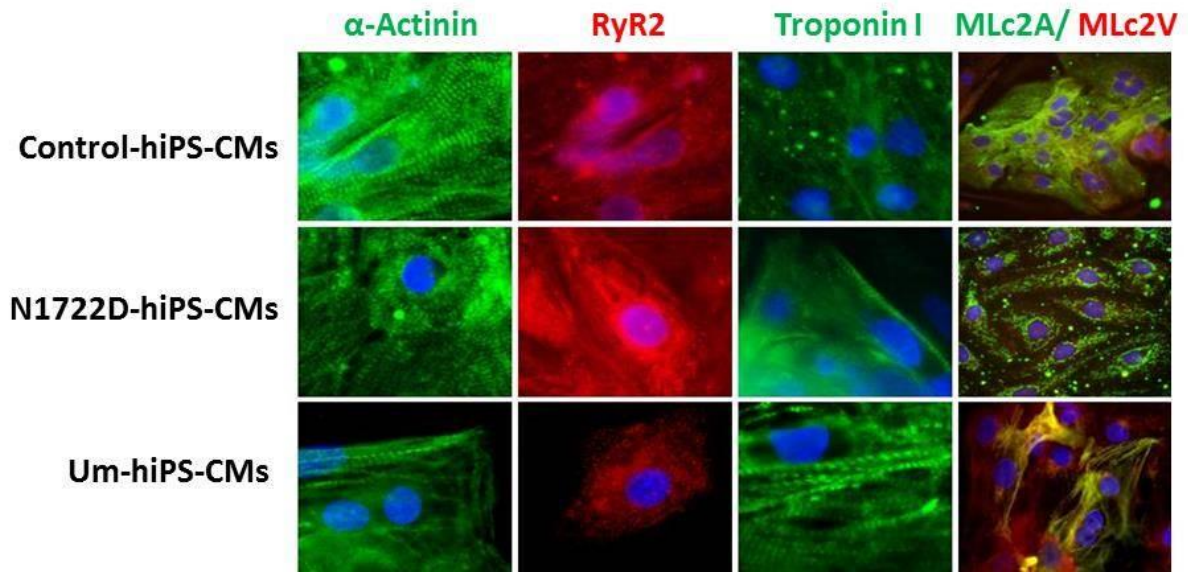
Figure 4.
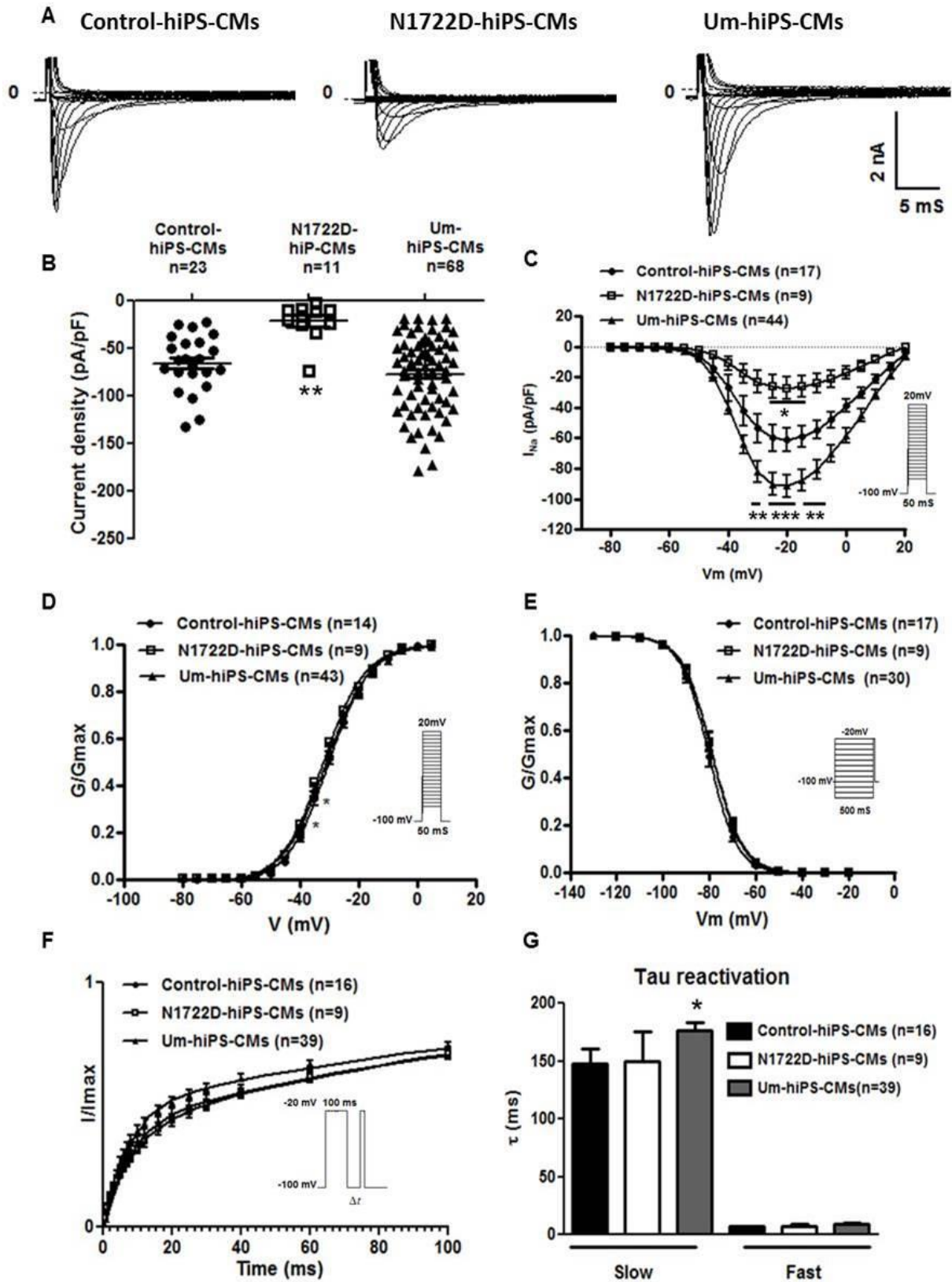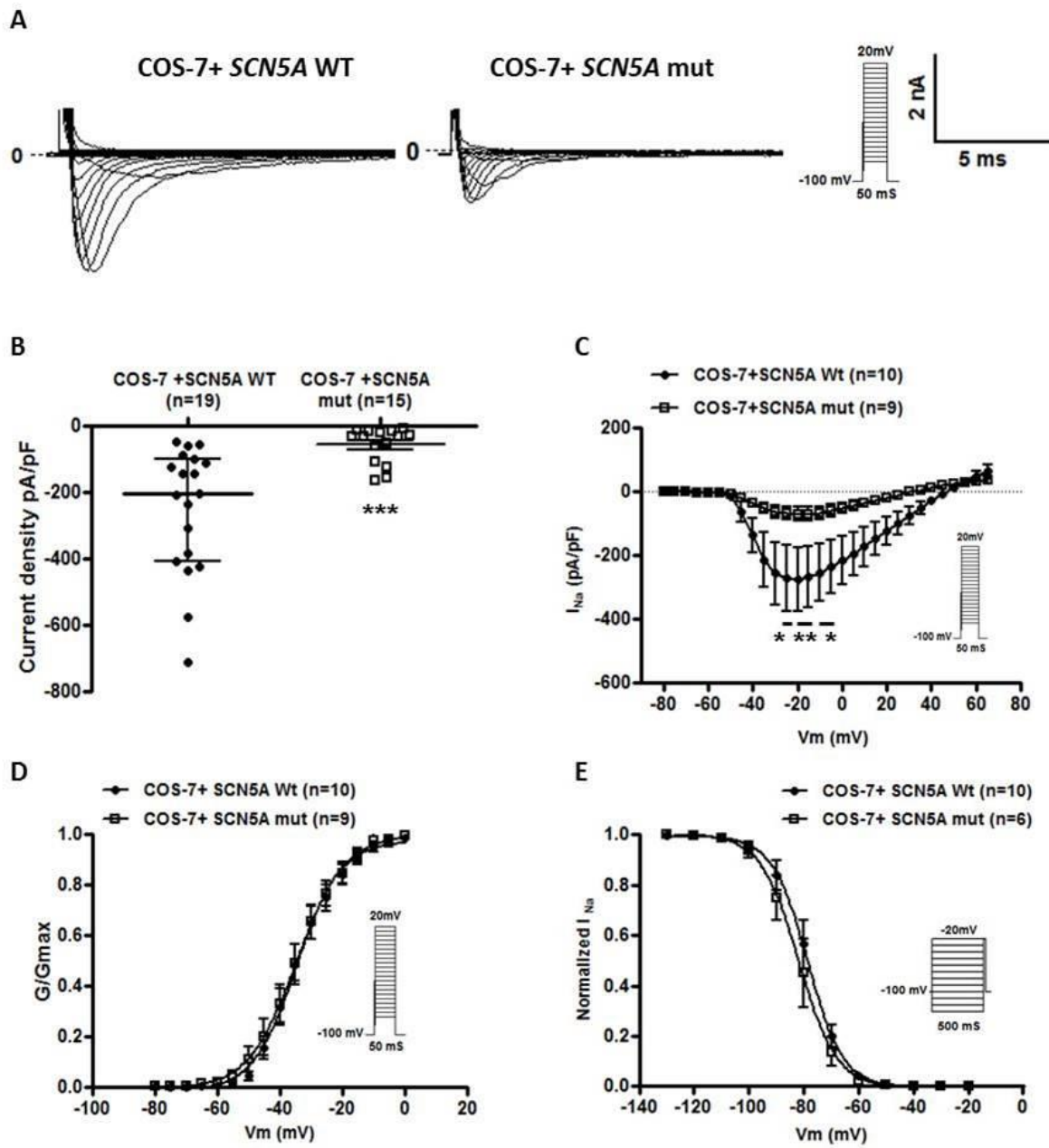
Figure 5.

Figure 6.
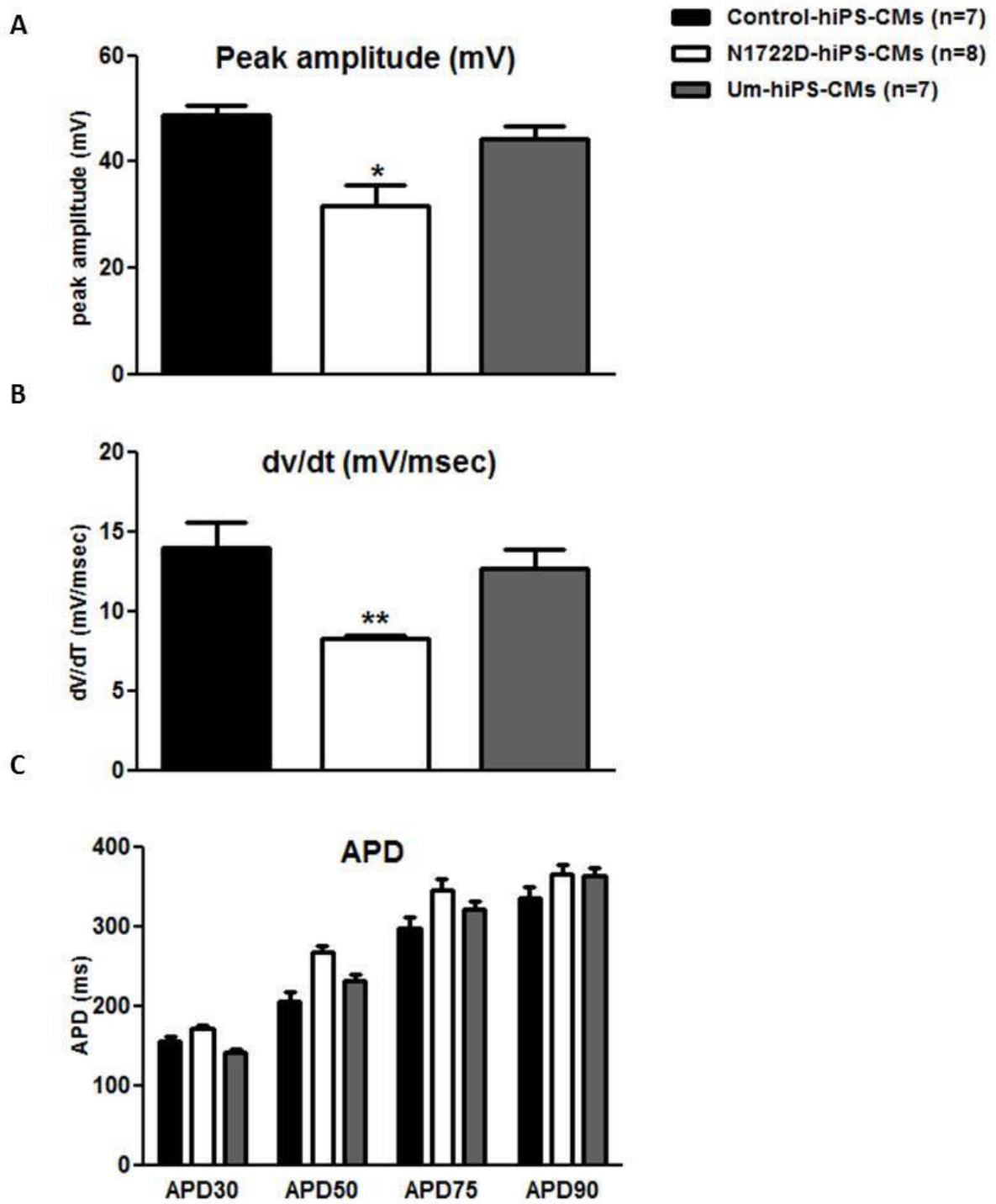
Figure 7.
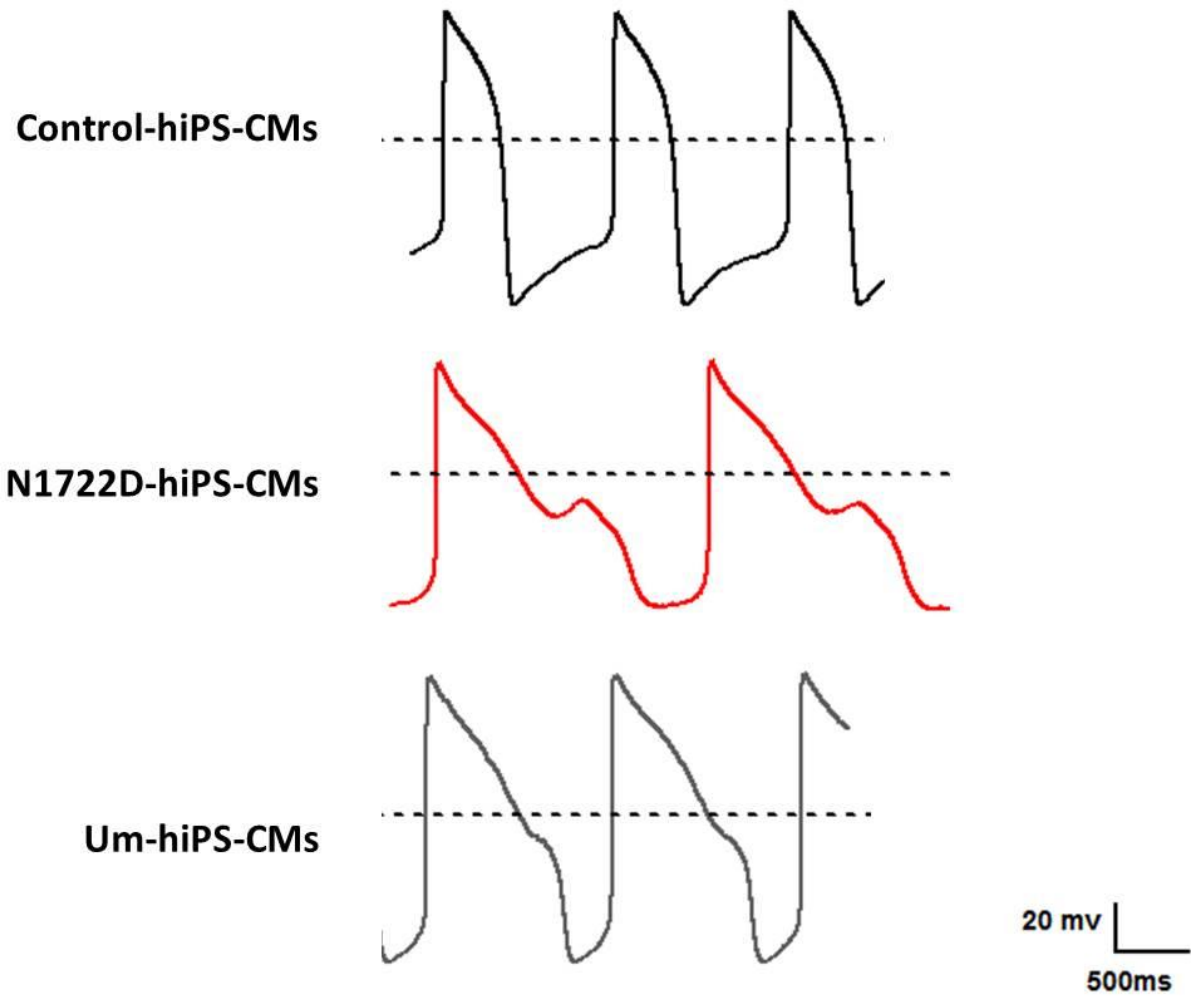
Figure 8.
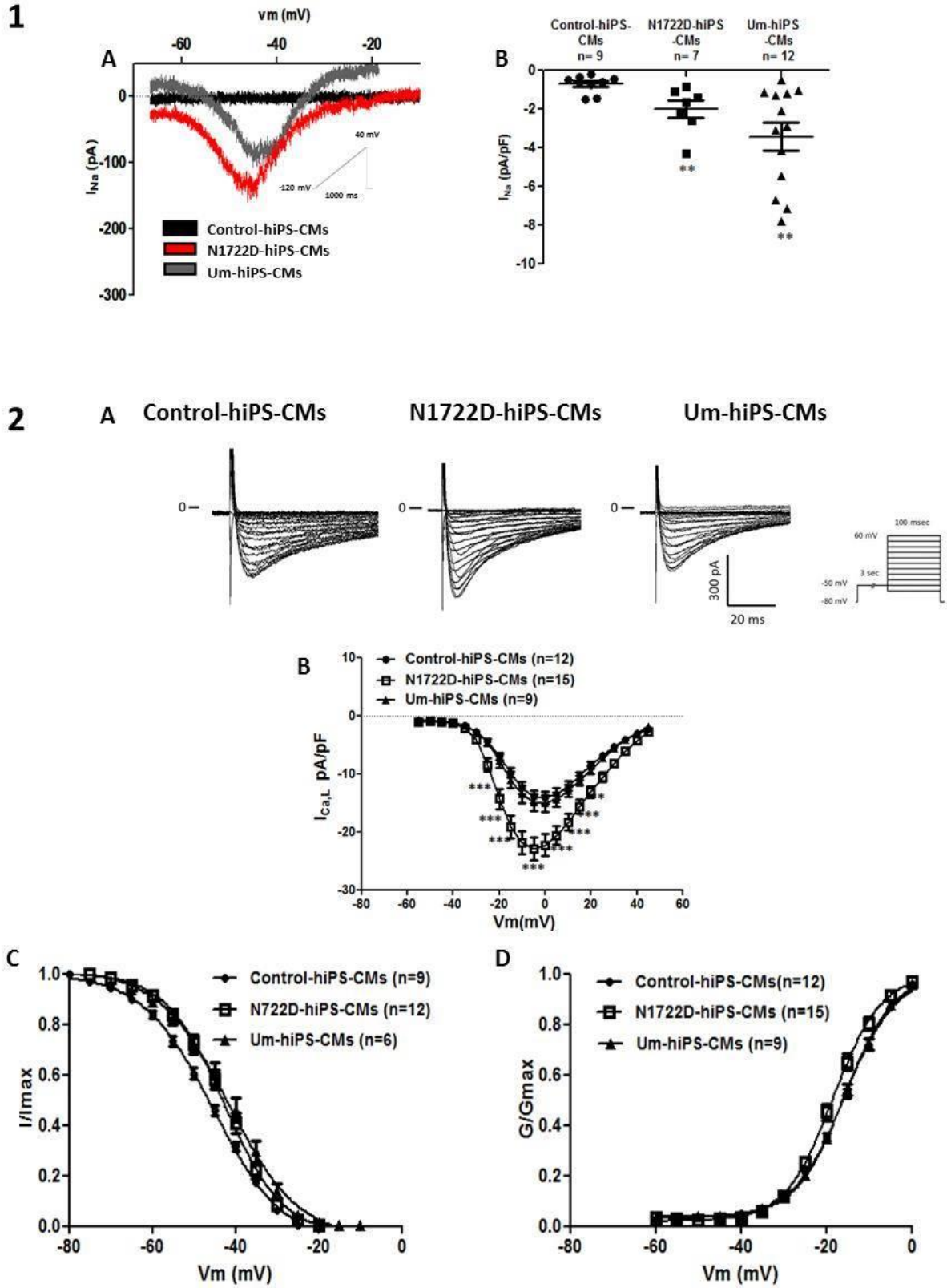
Figure 9.

III.1.8 – References

[1] J. Steinfurt, J. Biermann, C. Bode and K.E. Odening, *The Diagnosis, Risk Stratification, and Treatment of Brugada Syndrome*, Dtsch Arztebl International. 112 (2015) 394-401.

[2] M.W. Nielsen, A.G. Holst, S.-P. Olesen and M.S. Olesen, *The genetic component of Brugada Syndrome*, Frontiers in Physiology. 4 (2013)

[3] H. Abriel, *Genetic background of Brugada syndrome is more complex than what we would like it to be!* ed.), 2015.

[4] R. Brugada, O. Campuzano, G. Sarquella-Brugada, J. Brugada and P. Brugada, *BRUGADA SYNDROME*, Methodist DeBakey Cardiovascular Journal. 10 (2014) 25-28.

[5] O. Campuzano, R. Brugada and A. Iglesias, *Genetics of Brugada syndrome*, Current Opinion in Cardiology. 25 (2010) 210-215.

[6] N. Gaborit, 1, 3†, Thomas Wichter4,5†, Andras Varro6,7, Viktoria Szuts7,, Guillaume Lamirault1, Lars Eckardt4, Matthias Paul4, Gu¨nter Breithardt4, and D.E. Eric Schulze-Bahr4, 2,3, Stanley Nattel8, and Sophie Demolombe1,2,3*, *Transcriptional profiling of ion channel genes in Brugada syndrome and other right ventricular arrhythmogenic diseases*, European Heart Journal. (2008) 487-496.

[7] M. Derangeon, J. Montnach, I. Baró and F. Charpentier, *Mouse Models of SCN5A-Related Cardiac Arrhythmias*, Frontiers in Physiology. 3 (2012) 210.

[8] I. Rivolta, H. Abriel, M. Tateyama, H. Liu, M. Memmi, P. Vardas, C. Napolitano, S.G. Priori and R.S. Kass, *Inherited Brugada and Long QT-3 Syndrome Mutations of a Single Residue of the Cardiac Sodium Channel Confer Distinct Channel and Clinical Phenotypes*, Journal of Biological Chemistry. 276 (2001) 30623-30630.

[9] J.R. Giudicessi, D. Ye, D.J. Tester, L. Crotti, A. Mugione, V.V. Nesterenko, R.M. Albertson, C. Antzelevitch, P.J. Schwartz and M.J. Ackerman, *Transient outward current (Ito) gain-of-function mutations in the KCND3-encoded Kv4.3 potassium channel and Brugada syndrome*, Heart rhythm. 8 (2011) 1024-1032.

[10] K. Calloe, M.M. Refaat, S. Grubb, J. Wojciak, J. Campagna, N.M. Thomsen, R.L. Nussbaum, M.M. Scheinman and N. Schmitt, *Characterization and Mechanisms of Action of Novel NaV1.5 Channel Mutations Associated With Brugada Syndrome*, Circulation: Arrhythmia and Electrophysiology. 6 (2013) 177-184.

[11] P.J. Mohler, I. Rivolta, C. Napolitano, G. LeMaillet, S. Lambert, S.G. Priori and V. Bennett, *Nav1.5 E1053K mutation causing Brugada syndrome blocks binding to ankyrin-G and expression of Nav1.5 on the surface of cardiomyocytes*, Proceedings of the National Academy of Sciences of the United States of America. 101 (2004) 17533-17538.

[12] T. Ishikawa, N. Takahashi, S. Ohno, H. Sakurada, K. Nakamura, Y.K. On, J.E. Park, T. Makiyama, M. Horie, T. Arimura, N. Makita and A. Kimura, *Novel SCN3B Mutation Associated With Brugada Syndrome Affects Intracellular Trafficking and Function of Nav1.5*, Circulation Journal. 77 (2013) 959-967.

[13] K. Takahashi, K. Tanabe, M. Ohnuki, M. Narita, T. Ichisaka, K. Tomoda and S. Yamanaka, *Induction of Pluripotent Stem Cells from Adult Human Fibroblasts by Defined Factors*, Cell. 131 (2007) 861-872.

[14]   J. Zhang, G.F. Wilson, A.G. Soerens, C.H. Koonce, J. Yu, S.P. Palecek, J.A. Thomson and T.J. Kamp, *Functional Cardiomyocytes Derived from Human Induced Pluripotent Stem Cells*, Circulation Research. 104 (2009) e30-e41.

[15]   R.P. Davis, S. Casini, C.W. van den Berg, M. Hoekstra, C.A. Remme, C. Dambrot, D. Salvatori, D.W.-v. Oostwaard, A.A.M. Wilde, C.R. Bezzina, A.O. Verkerk, C. Freund and C.L. Mummery, *Cardiomyocytes Derived From Pluripotent Stem Cells Recapitulate Electrophysiological Characteristics of an Overlap Syndrome of Cardiac Sodium Channel Disease*, Circulation. 125 (2012) 3079-3091.

[16]   L. Warren, Y. Ni, J. Wang and X. Guo, *Feeder-Free Derivation of Human Induced Pluripotent Stem Cells with Messenger RNA*, Sci. Rep. 2 (2012)

[17]   T.M. Schlaeger, L. Daheron, T.R. Brickler, S. Entwisle, K. Chan, A. Cianci, A. DeVine, A. Ettenger, K. Fitzgerald, M. Godfrey, D. Gupta, J. McPherson, P. Malwadkar, M. Gupta, B. Bell, A. Doi, N. Jung, X. Li, M.S. Lynes, E. Brookes, A.B.C. Cherry, D. Demirbas, A.M. Tsankov, L.I. Zon, L.L. Rubin, A.P. Feinberg, A. Meissner, C.A. Cowan and G.Q. Daley, *A comparison of non-integrating reprogramming methods*, Nature Biotechnology. 33 (2014) 58-63.

[18]   J. Zhang, M. Klos, G.F. Wilson, A.M. Herman, X. Lian, K.K. Raval, M.R. Barron, L. Hou, A.G. Soerens, J. Yu, S.P. Palecek, G.E. Lyons, J.A. Thomson, T.J. Herron, J. Jalife and T.J. Kamp, *Extracellular Matrix Promotes Highly Efficient Cardiac Differentiation of Human Pluripotent Stem Cells: The Matrix Sandwich Method*, Circulation Research. 111 (2012) 1125-1136.

[19]   Cecile Terrenoire, Kai Wang, Kelvin W. Chan Tung, Wendy K. Chung, Robert H. Pass, , Jonathan T. Lu, Jyh-Chang Jean, Amel Omari, Kevin J. Sampson, Darrell N. Kotton, Gordon Keller and a.R.S. Kass1, *Induced pluripotent stem cells used to reveal drug actions in a long QT syndrome family with complex genetics.*, The Journal of General Physiology. 141 (2013) 61-72.

[20]   M. Bellin, S. Casini, R.P. Davis, C. D'Aniello, J. Haas, D. Ward-van Oostwaard, L.G.J. Tertoolen, C.B. Jung, D.A. Elliott, A. Welling, K.-L. Laugwitz, A. Moretti and C.L. Mummery, *Isogenic human pluripotent stem cell pairs reveal the role of a KCNH2 mutation in long-QT syndrome*, The EMBO Journal. 32 (2013) 3161-3175.

[21]   J. Ma, L. Guo, S.J. Fiene, B.D. Anson, J.A. Thomson, T.J. Kamp, K.L. Kolaja, B.J. Swanson and C.T. January, *High purity human-induced pluripotent stem cell-derived cardiomyocytes: electrophysiological properties of action potentials and ionic currents* ed.), 2011.

[22]   K. Si-Tayeb, F.K. Noto, M. Nagaoka, J. Li, M.A. Battle, C. Duris, P.E. North, S. Dalton and S.A. Duncan, *Highly Efficient Generation of Human Hepatocyte–like Cells from Induced Pluripotent Stem Cells*, Hepatology (Baltimore, Md.). 51 (2010) 297-305.

[23]   A.G. Edwards, E. Grandi, J.E. Hake, S. Patel, P. Li, S. Miyamoto, J.H. Omens, J. Heller Brown, D.M. Bers and A.D. McCulloch, *Nonequilibrium Reactivation of Na+ Current Drives Early Afterdepolarizations in Mouse Ventricle*, Circulation: Arrhythmia and Electrophysiology. 7 (2014) 1205-1213.

[24]   S. Wagner, L.S. Maier and D.M. Bers, *Role of Sodium and Calcium Dysregulation in Tachyarrhythmias in Sudden Cardiac Death* Circ Res. 116 (2015) 1956-1970.

[25]   H.E. Driessen, V.J.A. Bourgonje, T.A.B. van Veen and M.A. Vos, *New antiarrhythmic targets to control intracellular calcium handling*, Neth Heart J. 22 (2014) 198-213.

[26] N.V. Antzelevitch C1, Shryock JC, Rajamani S, Song Y, Belardinelli L., *The role of late I Na in development of cardiac arrhythmias.*, Handb Exp Pharmacol. 221 (2014) 137-168.

[27] P. Brugada and J. Brugada, *Right bundle branch block, persistent ST segment elevation and sudden cardiac death: a distinct clinical and electrocardiographic syndrome. A multicenter report*, J Am Coll Cardiol. 20 (1992) 1391 - 1396.

[28] H. Morita, D.P. Zipes and J. Wu, *Brugada syndrome: Insights of ST elevation, arrhythmogenicity, and risk stratification from experimental observations*, Heart rhythm. 6 (2009) S34-S43.

[29] N.K. Veerakul G1, *Brugada syndrome: two decades of progress.*, Circ J. . 76 (2012) 2713-2722.

[30] V. Probst, A.A.M. Wilde, J. Barc, F. Sacher, D. Babuty, P. Mabo, J. Mansourati, S. Le Scouarnec, F. Kyndt, C. Le Caignec, P. Guicheney, L. Gouas, J. Albuisson, P.G. Meregalli, H. Le Marec, H.L. Tan and J.-J. Schott, *SCN5A Mutations and the Role of Genetic Background in the Pathophysiology of Brugada Syndrome*, Circulation: Cardiovascular Genetics. 2 (2009) 552-557.

[31] C.R. Bezzina, J. Barc, Y. Mizusawa, C.A. Remme, J.-B. Gourraud, F. Simonet, A.O. Verkerk, P.J. Schwartz, L. Crotti, F. Dagradi, P. Guicheney, V. Fressart, A. Leenhardt, C. Antzelevitch, S. Bartkowiak, M. Borggrefe, R. Schimpf, E. Schulze-Bahr, S. Zumhagen, E.R. Behr, R. Bastiaenen, J. Tfelt-Hansen, M.S. Olesen, S. Kaab, B.M. Beckmann, P. Weeke, H. Watanabe, N. Endo, T. Minamino, M. Horie, S. Ohno, K. Hasegawa, N. Makita, A. Nogami, W. Shimizu, T. Aiba, P. Froguel, B. Balkau, O. Lantieri, M. Torchio, C. Wiese, D. Weber, R. Wolswinkel, R. Coronel, B.J. Boukens, S. Bezieau, E. Charpentier, S. Chatel, A. Despres, F. Gros, F. Kyndt, S. Lecointe, P. Lindenbaum, V. Portero, J. Violleau, M. Gessler, H.L. Tan, D.M. Roden, V.M. Christoffels, H. Le Marec, A.A. Wilde, V. Probst, J.-J. Schott, C. Dina and R. Redon, *Common variants at SCN5A-SCN10A and HEY2 are associated with Brugada syndrome, a rare disease with high risk of sudden cardiac death*, Nat Genet. 45 (2013) 1044-1049.

[32] L. Belardinelli, W.R. Giles, S. Rajamani, H.S. Karagueuzian and J.C. Shryock, *Cardiac late Na+ current: Proarrhythmic effects, roles in long QT syndromes, and pathological relationship to CaMKII and oxidative stress*, Heart rhythm. 12 (2015) 440-448.

[33] B. Horvath, T. Banyasz, Z. Jian, B. Hegyi, K. Kistamas, P.P. Nanasi, L.T. Izu and Y. Chen-Izu, *Dynamics of the Late Na(+) current during cardiac action potential and its contribution to afterdepolarizations*, Journal of Molecular and Cellular Cardiology. 64 (2013) 10.1016/j.yjmcc.2013.1008.1010.

[34] C.M. Sag, S. Wagner and L.S. Maier, *Role of oxidants on calcium and sodium movement in healthy and diseased cardiac myocytes*, Free Radical Biology and Medicine. 63 (2013) 338-349.

[35] S. Viatchenko-Karpinski, D. Kornyeyev, N. El-Bizri, G. Budas, P. Fan, Z. Jiang, J. Yang, M.E. Anderson, J.C. Shryock, C.-P. Chang, L. Belardinelli and L. Yao, *Intracellular Na+ overload causes oxidation of CaMKII and leads to Ca2 + mishandling in isolated ventricular myocytes*, Journal of Molecular and Cellular Cardiology. 76 (2014) 247-256.

[36] Y. Mimori-Kiyosue, I. Grigoriev, H. Sasaki, C. Matsui, A. Akhmanova, S. Tsukita and I. Vorobjev, *Mammalian CLASPs are required for mitotic spindle organization and kinetochore alignment*, Genes to Cells. 11 (2006) 845-857.

[37]   P.J. Mohler and V. Bennett, *Ankyrin-based cardiac arrhythmias: a new class of channelopathies due to loss of cellular targeting*, Current Opinion in Cardiology. 20 (2005) 189-193.

[38]   M. Liu, K.-C. Yang and S.C. Dudley Jr, *Cardiac sodium channel mutations: why so many phenotypes?*, Nat Rev Cardiol. 11 (2014) 607-615.

[39]   K. Drabek, L. Gutiérrez, M. Vermeij, T. Clapes, Sunita R. Patel, J.-C. Boisset, J. van Haren, Ana L. Pereira, Z. Liu, U. Akinci, T. Nikolic, W. van Ijcken, M. van den Hout, M. Meinders, C. Melo, C. Sambade, D. Drabek, Rudi W. Hendriks, S. Philipsen, M. Mommaas, F. Grosveld, H. Maiato, Joseph E. Italiano Jr, C. Robin and N. Galjart, *The Microtubule Plus-End Tracking Protein CLASP2 Is Required for Hematopoiesis and Hematopoietic Stem Cell Maintenance*, Cell Reports. 2 (2012) 781-788.

III.2 – Supplemental materials

Supplemental Table 1. Biophysical characteristics of the Nav1.5 channels in control-hiPS-CMs, N1722D-hiPS-CMs and Um-hiPS-CMs.

	Activation		Inactivation	
	$V_{1/2}$ (mV)	K	$V_{1/2}$ (mV)	K
Control-hiPS-CMs	-31.3± 1.06	6.21± 0.26	-80.39± 1.01	-5.9± 0.37
	(n=17)		*(n=17)*	
N1722D-hiPS-CMs	-29.21± 0.7	7.04 ± 0.33	-78.47± 1.45	-5.53± 0.39
	(n=9)		*(n=9)*	
Um-hiPS-CMs	-30.58±0.6	6.46± 0.12	-79± 0.71	-5.748± 0.249
	(n=44)		*(n=30*	

Supplemental Table 2. Quantitative parameters used for classification of action potentials obtained from patch-clamp experiments on control cells.

Control-hiPS-CMs APs (n=17)	AP amplitude (mV)	MDP (mV)	Peak to peak duration (ms)	dv/dt$_{max}$ (mV/msec)	APD90 (ms)
Nodal like (n=4)	31.4± 5.5	-44.65± 1.65	604± 25.9	5± 0.51	90± 13.77
Atrial like (n=6)	41.82± 2.1	-50± 1.25	1051± 173	14.02± 0.814	187± 13..26
Ventricular like (n=7)	49.52± 3.5	-54.02±3.4	1263± 69.02	14.1± 1.533	351± 32.72

V. GENERAL DISCUSSION AND CONCLUSION

V.1. – General discussion

Despite major advances in understanding and treatment of heart arrhythmic disorders, sudden cardiac death still represents a significant cause of morbidity and mortality worldwide. Sudden cardiac death is the cause of about half of deaths due to cardiovascular disease or about 15% of all deaths globally. About 80% of sudden cardiac death is the result of ventricular arrhythmias (Mehra, 2007).

Much progress has been made in identifying the clinical phenotypes, cellular and genetic mechanisms underlying the various arrhythmic syndromes, including LQT and BrS (Scicluna et al., 2008). Studying the electrophysiological and molecular consequences of a mutation associated with cardiac arrhythmia should ideally be done in native cardiomyocytes (CMs). However, obtaining ventricular cardiac biopsies from patients is a highly invasive procedure with significant risks. Consequently, the majority of functional studies on specific mutations associated with arrhythmic disorders relied on heterologous expression systems in which the mutated ion channel of interest is expressed. Such cellular models have significant shortcomings since they lack important constituents of cardiac ion channel macromolecular complexes that might be required to reproduce the exact molecular and electrophysiological phenotype of the mutation. One way to overcome this has been to generate transgenic mice for specific mutations (Derangeon et al., 2012). However, generation of these models are not practical for high-throughput screening of rare inherited arrhythmia mutations. Moreover, remains crucial differences between mouse and human cardiac electrophysiological characteristics. In addition, these models are limited in the case of unidentified mutations.

Discovery of somatic cell reprogramming to generate induced pluripotent stem cells (Takahashi and Yamanaka, 2006) (Takahashi et al., 2007) has created much excitement because of the possibility to produce unique patient- and disease-specific human iPS cell lines. Zhang et al. (Zhang et al., 2009) were the first to show that hiPS cells can differentiate into functional cardiomyocytes, making it possible to generate patient-specific human cardiomyocytes that have the patient genetic background integrity. hiPS-CMs therefore represent a new model system for studying inherited arrhythmia disorders (Hoekstra et al., 2012).

Patient-specific hiPS-CMs have now been shown to provide valuable models of heritable cardiac arrhythmias, including congenital LQT syndrome and other diseases. Although the first hiPS cell lines were derived from dermal fibroblasts (Takahashi et al., 2007) hiPS cells

can now be generated from a wide variety of somatic cells including urine derived cells (Zhou et al., 2012). Cells isolated from urine show promising characteristics for a reprogramming strategy.

In this work, three main studies are included:

1. In the first study: we used cardiomyocytes obtained from urine-derived hiPS cells (UhiPS-CM) to investigate both the molecular and functional phenotypes of the syndrome in an integrated cellular model. Overall, we demonstrated that the use of urine-derived cardiomyocytes is a convenient and powerful approach to model human arrhythmic diseases.

2. In the second study: we were interested in modeling an acquired form of LQT-2 using hiPS-CMs. AIDS patients have an increased risk of cardiovascular events, including LQT-2. The cardiac arrhythmic incidents observed maybe a result of the drugs used to treat the disease and/or the viral proteins associated with the virus itself. In this study we investigated the possible mechanisms by which one of the HIV-viral proteins, Tat, may lead to arrhythmias in HIV-infected patients.

3. In the third study, we were interested in modeling BrS, a second and more complex example of cardiac arrhythmic diseases. Despite extensive work in genetic testing, BrS pathology is still unclear; we aimed to use hiPS-CMs to further model this disease in the context of patients' genetic backgrounds.

Despite the massive progress the usage of human induced pluripotent stem cells derived cardiomyocytes is witnessing, this model need to be evaluated at different levels.

The striking advantage of using iPS cells rather than embryonic stem cell-based approaches is that iPS cells can be derived from any individual with relative ease, thereby allowing development of a personalized study platform on individual genomic information. iPS and differentiated cells from the iPS cells retain their personal identity, suggesting that iPS technology can be applied to disease-, patient-, and finally person-specific approaches to examine the individual differences in pharmacokinetic/pharmacodynamic features. Given that everyone will almost certainly become a patient at least once in his or her lifetime, individual iPS cells-based predictive therapeutic and toxicity profiling of all drugs available in multiple cell types will be a logical and attractive approach. This "pharmaco-iPSCellomic" analysis could eventually be available in an array-based format for high-throughput assay before

specific drug therapy is prescribed for a particular disease condition (Inoue and Yamanaka, 2011).

Moreover, although most of the diseases studied so far using iPS cells-derived somatic cells were monogenetic diseases; one of the strengths of the iPS cell system is the ability to study a disease phenotype even if the genetic background is unknown. BrS is known to be caused by mutations of the cardiac sodium channel, voltage-gated, type V, α-subunit. However, these mutations account for 20-30% of cases. Moreover, a highly varying degree of penetrance exists among patients with known mutation status, and the typical ECG pattern is present more often in men than in women, suggesting that other genetic factors might play an important role for the precipitation of the phenotype (Campuzano et al., 2010). Cardiomyocytes generated from iPS cells derived from patients with and without known mutations as well as from mutation carriers with and without clinical symptoms might provide a tool to define a functional BrS phenotype and to identify novel molecular compounds involved in the pathophysiology of this disease. An example of this approach is what we did in the BrS study (refer to study #3).One of the patients that we had, was without an identified mutation. Using hiPS-CMs from this patient, we were able to start to analyze the underlying pathophysiological mechanisms with different levels of complexity.

On the other hand, despite the fast advances we are witnessing, limitations and challenges remain before this model can be widely used to develop regenerative medicine strategies for treating cardiovascular disease. Challenges and limitations include:

V.1.1 – Cardiomyocyte purification

Despite considerable progress in improving the efficiency of cardiac differentiation, the isolation of cardiomyocytes or the removal of unwanted cell populations may be required. Genetic selection of cells based on the expression of a selectable marker driven by a lineage-restricted promoter such as *NKX2-5* (Elliott et al., 2011), *MYH6* (Anderson et al., 2007) and *MLC2V* (Huber et al., 2007) offers the possibility of isolating myocardial precursors at high purity; when this process is coupled with antibiotic selection, it is possible to generate cells at greater than 99% purity. Although early studies were commonly based on either small plasmid based reporter constructs or transgenesis using bacterial artificial chromosomes, more recent studies have focused on the use of reporter lines that are established by gene targeting. Gene targeting is achieved in hiPS cells using technologies that are based on zinc-finger

nucleases, transcription activator-like effector nucleases (TALENs) or clustered regularly interspaced short palindromic repeats (CRISPRs) (Tabar and Studer, 2014). The principal drawback of genetic selection is the necessity of inserting a selection cassette into the host genome, which may increase the risk of tumor genesis and is therefore unsuitable for clinical practice. Antibodies to cell surface markers have the advantage of not requiring genetic modification of stem cell populations, and therefore may be applicable to all hiPS cell lines. FACS has the ability to analyze multiple surface markers simultaneously, and it has been used to isolate cardiac progenitor populations based on the expression of markers expressed specifically on cardiomyocytes, including EMILIN2 (Van Hoof et al., 2010), SIRPA (Elliott et al., 2011) (Dubois et al., 2011), and VCAM (Elliott et al., 2011) (Uosaki et al., 2011), and made it possible to isolate highly enriched populations of these cells.

Another non-genetic method for isolating hiPS cells-derived cardiomyocytes is based on the use of the mitochondrial dye tetramethylrhodamine methyl ester perchlorate (TMRM) (Hattori et al., 2010). Because this dye only functions in cells with high mitochondrial density such as cardiomyocytes, it does not detect the most immature cells that develop in the cultures (Dubois et al., 2011). Moreover, a non-genetic method for mass-producing cardiomyocytes from mouse and human pluripotent stem cell derivatives is based on the marked biochemical differences in glucose and lactate metabolism between cardiomyocytes and non-cardiomyocytes, including undifferentiated cells. hiPS-CMs were cultured with glucose-depleted culture medium containing abundant lactate. Using this approach, cardiomyocytes of up to 99% purity were obtained (Tohyama et al., 2013).

There has been extensive progress in developing genetic reporter lines to optimize directed differentiation and to prospectively purify defined cell types for downstream applications. Collectively, these recent discoveries have provided tools and reagents for the generation of highly enriched populations of hiPS-CMs.

V.1.2 – Cardiomyocyte maturation

One of the remaining challenges associated with the use of hiPS-CMs for cardiac repair as well as for *in vitro* drug discovery and disease modeling applications is their relative immature phenotype. Although hiPS-CMs have been demonstrated to possess cardiac-like molecular, ultra-structural, electrophysiological and excitation-contraction coupling characteristics, these properties were shown to be relatively immature. From the electrophysiological angle, such early-stage properties include the presence of spontaneous automaticity and a relatively depolarized resting membrane potential. Potential strategies to

induce human embryonic stem cells-derived cardiomyocytes or hiPS cells- techniques that can induce maturation include the use of small molecules such as tri-iodothyronine binding thyroid hormone receptors (Lee et al., 2010), overexpression or down regulation of specific genes (Yamanaka et al., 2008), and extrinsic cues from other non-cardiac cells, including endothelial cells (Kim et al., 2009). Exercise via mechanical force (Tulloch et al., 2011) has also been demonstrated to enhance maturation (Burridge and 2012) (Zwi-Dantsis and Gepstein, 2012).

V.1.3 – Intrinsic variability and control definition

hiPS-CMs offer a valuable approach to model various disorders, however, there are some limitations. In comparative studies, the different genetic backgrounds of the control hiPS-CMs lines may induce variability at molecular and/or functional levels that may hamper revelation of subtle disease-related phenotypic abnormalities in the diseased lines. In addition, phenotypic intra-variability between clones generated form the same donor (patient or control) also exists. Several approaches are now considered to overcome these inter- and intra-variations. First, to overcome intra-variability multiple clones must be analyzed to identify outlier clones even in the control lines. Regarding, inter-variability, some studies use healthy siblings as controls, however, only ~50% of the genome is shared between siblings, so that phenotypic differences could result from DNA variants in the other ~50% of the genome, rather than the disease-associated mutations. Furthermore, a number of studies have documented that the process of generating, expanding and passaging hiPS cell lines can lead to the accumulation of a variety of genetic alterations, ranging from single-nucleotide variants to copy-number variants and to chromosomal amplifications, deletions and rearrangements (Mayshar et al., 2010) (Laurent et al., 2011) (Hussein et al., 2011) (Gore et al., 2011) (Taapken et al., 2011) (Howden et al., 2011). Another significant aspect is epigenetic state. A number of studies have documented that iPS cells vary widely with respect to genomic methylation patterns, in some cases seeming to retain epigenetic "memory" of the somatic cell from which the iPS cells were reprogrammed. Some iPS cells seem to retain this memory indefinitely, whereas others gradually lose this memory as they go through many passages in culture (Kim et al., 2010) (Polo et al., 2010). Other potential confounders include unmatched age, gender and ethnicity between the patients and control individuals; differences in the reprogramming methodology (e.g. lentivirus versus RNA transfection); and differences in passage number and adaptation to culture of the iPS cell lines.

The most rigorous possible comparisons would be between cell lines that differ only with respect to disease mutations. In this issue Wang et al. (Wang et al., 2014b) (Wang et al., 2014a) proposed an approach in which genetic mutations are directly introduced by genome engineering in generic embryonic stem cells or non-diseased iPS cell lines. The engineered pluripotent cells can then be differentiated into cardiomyocytes, and display disease features as compared with the unedited cell lines (so-called isogenic controls). Isogenic controls would also eliminate, or at least limit, all of the other confounders (age, gender and ethnicity), allowing investigators to directly connect genotype to phenotype to establish causality. Such a strategy requires the ability to efficiently introduce specific genetic alterations into the genomes of hiPS cells known as in site-specific "genome editing". This approach is supported by recent developments with the use of designer nucleases (molecular scissors) that cut DNA sequences within the chromosome that then can be replaced by another sequence template. Three different types of molecular scissors have been developed to cut at specific sites: 1) zinc finger nucleases (ZFN); 2) transcription activator-like effector nuclease (TALENS); and 3) clustered regularly inter-spaced short palindromic repeats (CRISPR). These designer nucleases each have unique features, but the capability of each one to target specific DNA sequences makes them a very useful tool for manipulating pluripotent cells (Hajjar and Hulot, 2014) (Burridge and 2012). In the context of the present work, Bellin et al (Bellin et al., 2013) demonstrated in a study about LQT-2, that isogenic pairs of hiPS cells can be used (1) to prove the authenticity of the genotype-phenotype correlation and (2) to unravel the pathophysiological mechanism seen in a genetically inherited cardiac disease.

V.2. – Conclusion

In conclusion, the ability to generate cardiomyocytes de novo has progressed rapidly and an increasing number of potential sources of cells have become viable. The three major applications of these cardiomyocytes, in regenerative medicine, drug testing, and disease modeling, have their own specific requirements in terms of number of cells, speed of derivation, characterization, and similarity to adult cardiomyocytes. It is likely that a variety of approaches for making cardiomyocytes will be used in the future, depending on the specific parameters set by the application. Certainly, for applications in genetic disease modeling or personalized therapies, hiPS cells are an obvious choice. Such questions should not obscure the exciting prospect that, for the first time, it is possible to envisage overcoming the significant hurdles that have blocked the path to successful clinical application of de novo generated cardiomyocytes.

VI.   BIBLIOGRAPHY

Aasen, T., A. Raya, M.J. Barrero, E. Garreta, A. Consiglio, F. Gonzalez, R. Vassena, J. Bilic, V. Pekarik, G. Tiscornia, M. Edel, S. Boue, and J.C.I. Belmonte. 2008. Efficient and rapid generation of induced pluripotent stem cells from human keratinocytes. *Nat Biotech*. 26:1276-1284.

Abriel, H., and E.V. Zaklyazminskaya. 2013. Cardiac channelopathies: Genetic and molecular mechanisms. *Gene*. 517:1-11.

Addis, R.C., and J.A. Epstein. 2013. Induced regeneration—the progress and promise of direct reprogramming for heart repair. *Nature medicine*. 19:829-836.

Aiba, T., W. Shimizu, I. Hidaka, K. Uemura, T. Noda, C. Zheng, A. Kamiya, M. Inagaki, M. Sugimachi, and K. Sunagawa. 2006. Cellular Basis for Trigger and Maintenance of Ventricular Fibrillation in the Brugada Syndrome Model: High-Resolution Optical Mapping Study. *Journal of the American College of Cardiology*. 47:2074-2085.

Aistrup, G.L., Y. Shiferaw, S. Kapur, A.H. Kadish, and J.A. Wasserstrom. 2009. Mechanisms Underlying the Formation and Dynamics of Subcellular Calcium Alternans in the Intact Rat Heart. *Circulation Research*. 104:639-649.

Amin, A.S., A. Asghari-Roodsari, and H.L. Tan. 2010. Cardiac sodium channelopathies. *Pflugers Archiv*. 460:223-237.

Anderson, D., T. Self, I.R. Mellor, G. Goh, S.J. Hill, and C. Denning. 2007. Transgenic Enrichment of Cardiomyocytes From Human Embryonic Stem Cells. *Mol Ther*. 15:2027-2036.

Antoons, G., P.G. Volders, T. Stankovicova, V. Bito, M. Stengl, M.A. Vos, and K.R. Sipido. 2007. Window Ca2+ current and its modulation by Ca2+ release in hypertrophied cardiac myocytes from dogs with chronic atrioventricular block. *J Physiol*. 579:147-160.

Antzelevitch, C. 2005. In vivo human demonstration of phase 2 reentry. *Heart rhythm*. 2:804-806.

Antzelevitch, C., and L. Belardinelli. 2006. The Role of Sodium Channel Current in Modulating Transmural Dispersion of Repolarization and Arrhythmogenesis. *Journal of Cardiovascular Electrophysiology*. 17:S79-S85.

Antzelevitch, C., P. Brugada, M. Borggrefe, J. Brugada, R. Brugada, D. Corrado, I. Gussak, H. LeMarec, K. Nademanee, A.R. Perez Riera, W. Shimizu, E. Schulze-Bahr, H. Tan, and A. Wilde. 2005. Brugada Syndrome: Report of the Second Consensus Conference: Endorsed by the Heart Rhythm Society and the European Heart Rhythm Association. *Circulation*. 111:659-670.

Antzelevitch, C., G.D. Pollevick, J.M. Cordeiro, O. Casis, M.C. Sanguinetti, Y. Aizawa, A. Guerchicoff, R. Pfeiffer, A. Oliva, B. Wollnik, P. Gelber, E.P. Bonaros, Jr., E. Burashnikov, Y. Wu, J.D. Sargent, S. Schickel, R. Oberheiden, A. Bhatia, L.F. Hsu, M. Haissaguerre, R. Schimpf, M. Borggrefe, and C. Wolpert. 2007. Loss-of-function mutations in the cardiac calcium channel underlie a new clinical entity characterized by ST-segment elevation, short QT intervals, and sudden cardiac death. *Circulation*. 115:442-449.

Armoundas, A.A., G.F. Tomaselli, and H.D. Esperer. 2002. Pathophysiological basis and clinical application of T-wave alternans. *Journal of the American College of Cardiology*. 40:207-217.

Bai, Y.-L., H.-B. Liu, B. Sun, Y. Zhang, Q. Li, C.-W. Hu, J.-X. Zhu, D.-M. Gong, X. Teng, Q. Zhang, B.-F. Yang, and D.-L. Dong. 2011. HIV Tat protein inhibits hERG K+ channels: A potential mechanism of HIV infection induced LQTs. *Journal of Molecular and Cellular Cardiology*. 51:876-880.

Baroudi, G., V. Pouliot, I. Denjoy, P. Guicheney, A. Shrier, and M. Chahine. 2001. Novel Mechanism for Brugada Syndrome: Defective Surface Localization of an SCN5A Mutant (R1432G). *Circulation Research*. 88:e78-e83.

Bassani, R.A., and D.M. Bers. 1995. Rate of diastolic Ca release from the sarcoplasmic reticulum of intact rabbit and rat ventricular myocytes. *Biophysical Journal*. 68:2015-2022.

Bébarová, M. 2013. Arrhythmogenesis in Brugada syndrome: Impact and constrains of current concepts. *International Journal of Cardiology*. 167:1760-1771.

Belevych, A.E., D. Terentyev, S. Viatchenko-Karpinski, R. Terentyeva, A. Sridhar, Y. Nishijima, L.D. Wilson, A.J. Cardounel, K.R. Laurita, C.A. Carnes, G.E. Billman, and S. Gyorke. 2009. Redox modification of ryanodine receptors underlies calcium alternans in a canine model of sudden cardiac death. 387-395 pp.

Bellin, M., S. Casini, R.P. Davis, C. D'Aniello, J. Haas, D. Ward-van Oostwaard, L.G. Tertoolen, C.B. Jung, D.A. Elliott, A. Welling, K.L. Laugwitz, A. Moretti, and C.L. Mummery. 2013. Isogenic human pluripotent stem cell pairs reveal the role of a KCNH2 mutation in long-QT syndrome. *EMBO J*. 32:3161-3175.

Bellocq, C., R. Wilders, J.J. Schott, B. Louerat-Oriou, P. Boisseau, H. Le Marec, D. Escande, and I. Baro. 2004. A common antitussive drug, clobutinol, precipitates the long QT syndrome 2. *Mol Pharmacol*. 66:1093-1102.

Benito, B., J. Brugada, R. Brugada, and P. Brugada. 2009. Brugada Syndrome. *Revista Española de Cardiología (English Edition)*. 62:1297-1315.

Berne, P., and J. Brugada. 2012. Brugada Syndrome 2012. *Circulation Journal*. 76:1563-1571.

Bers, D.M. 2002. Cardiac excitation-contraction coupling. *Nature*. 415:198-205.

Bers, D.M. 2014. Cardiac Sarcoplasmic Reticulum Calcium Leak: Basis and Roles in Cardiac Dysfunction. *Annual Review of Physiology*. 76:107-127.

Bers, D.M., and E. Perez-Reyes. 1999. Ca channels in cardiac myocytes: structure and function in Ca influx and intracellular Ca release. 339-360 pp.

Beuckelmann, D.J., M. Näbauer, and E. Erdmann. 1993. Alterations of K+ currents in isolated human ventricular myocytes from patients with terminal heart failure. *Circulation Research*. 73:379-385.

Béziau, D., J. Barc, T. O'Hara, L. Le Gloan, M. Amarouch, A. Solnon, D. Pavin, S. Lecointe, P. Bouillet, J.-B. Gourraud, P. Guicheney, I. Denjoy, R. Redon, P. Mabo, H. le Marec, G. Loussouarn, F. Kyndt, J.-J. Schott, V. Probst, and I. Baró. 2014. Complex Brugada syndrome inheritance in a family harbouring compound SCN5A and CACNA1C mutations. *Basic Res Cardiol*. 109:1-15.

Bezzina, C., M.W. Veldkamp, M.P. van den Berg, A.V. Postma, M.B. Rook, J.-W. Viersma, I.M. van Langen, G. Tan-Sindhunata, M.T.E. Bink-Boelkens, A.H. van der Hout, M.M.A.M. Mannens, and A.A.M. Wilde. 1999. A Single Na+ Channel Mutation Causing Both Long-QT and Brugada Syndromes. *Circulation Research*. 85:1206-1213.

Bezzina, C.R., J. Barc, Y. Mizusawa, C.A. Remme, J.-B. Gourraud, F. Simonet, A.O. Verkerk, P.J. Schwartz, L. Crotti, F. Dagradi, P. Guicheney, V. Fressart, A. Leenhardt, C. Antzelevitch, S. Bartkowiak, M. Borggrefe, R. Schimpf, E. Schulze-Bahr, S. Zumhagen, E.R. Behr, R. Bastiaenen, J. Tfelt-Hansen, M.S. Olesen, S. Kaab, B.M. Beckmann, P. Weeke, H. Watanabe, N. Endo, T. Minamino, M. Horie, S. Ohno, K. Hasegawa, N. Makita, A. Nogami, W. Shimizu, T. Aiba, P. Froguel, B. Balkau, O. Lantieri, M. Torchio, C. Wiese, D. Weber, R. Wolswinkel, R. Coronel, B.J. Boukens, S. Bezieau, E. Charpentier, S. Chatel, A. Despres, F. Gros, F. Kyndt, S. Lecointe, P. Lindenbaum, V. Portero, J. Violleau, M. Gessler, H.L. Tan, D.M. Roden, V.M. Christoffels, H. Le Marec, A.A. Wilde, V. Probst, J.-J. Schott, C. Dina, and R. Redon. 2013. Common variants at SCN5A-SCN10A and HEY2 are associated with Brugada syndrome, a rare disease with high risk of sudden cardiac death. *Nat Genet*. 45:1044-1049.

Bhuiyan, M.Z.A., S. Al-Shahrani, J. Al-Aama, A. Wilde, and T.S. Momenah. 2013. Congenital Long QT Syndrome: An Update and Present Perspective in Saudi Arabia. *Frontiers in Pediatrics*. 1.

Bongianino, R., and S.G. Priori. 2015. Gene therapy to treat cardiac arrhythmias. *Nat Rev Cardiol*. advance online publication.

Brailoiu, E., E. Deliu, R.A. Sporici, K. Benamar, and G.C. Brailoiu. 2014. HIV-1-Tat excites cardiac parasympathetic neurons of nucleus ambiguus and triggers prolonged bradycardia in conscious rats. R814-R822 pp.

Brouillette, J., S.A. Grandy, P. Jolicoeur, and C. Fiset. 2007. Cardiac repolarization is prolonged in CD4C/HIV transgenic mice. *Journal of Molecular and Cellular Cardiology*. 43:159-167.

Brugada, J., R. Brugada, C. Antzelevitch, J. Towbin, K. Nademanee, and P. Brugada. 2002. Long-term follow-up of individuals with the electrocardiographic pattern of right bundle-branch block and ST-segment elevation in precordial leads V1 to V3. *Circulation*. 105:73-78.

Brugada, R., J. Brugada, C. Antzelevitch, G.E. Kirsch, D. Potenza, J.A. Towbin, and P. Brugada. 2000. Sodium channel blockers identify risk for sudden death in patients with ST-segment elevation and right bundle branch block but structurally normal hearts. *Circulation*. 101:510-515.

Brugada, R., O. Campuzano, G. Sarquella-Brugada, J. Brugada, and P. Brugada. 2014. BRUGADA SYNDROME. *Methodist DeBakey Cardiovascular Journal*. 10:25-28.

Burashnikov, A., and C. Antzelevitch. 1998. Acceleration-Induced Action Potential Prolongation and Early Afterdepolarizations. *Journal of Cardiovascular Electrophysiology*. 9:934-948.

Burashnikov, E., R. Pfeiffer, H. Barajas-Martinez, E. Delpon, D. Hu, M. Desai, M. Borggrefe, M. Haissaguerre, R. Kanter, G.D. Pollevick, A. Guerchicoff, R. Laino, M. Marieb, K. Nademanee, G.B. Nam, R. Robles, R. Schimpf, D.D. Stapleton, S. Viskin, S. Winters, C. Wolpert, S. Zimmern, C. Veltmann, and C. Antzelevitch. 2010. Mutations in the cardiac L-type calcium channel associated with inherited J-wave syndromes and sudden cardiac death. *Heart Rhythm*. 7:1872-1882.

Burridge, P.W., and , 2 Gordon Keller,3 Joseph D. Gold, 4 and Joseph C. Wu 1 ,2 ,*. 2012. Production of De Novo Cardiomyocytes:Human Pluripotent Stem Cell Differentiation and Direct Reprogramming. *Cell Press*. 10:16-28.

Burridge, Paul W., G. Keller, Joseph D. Gold, and Joseph C. Wu. 2012. Production of De Novo Cardiomyocytes: Human Pluripotent Stem Cell Differentiation and Direct Reprogramming. *Cell Stem Cell*. 10:16-28.

Calloe, K., M.M. Refaat, S. Grubb, J. Wojciak, J. Campagna, N.M. Thomsen, R.L. Nussbaum, M.M. Scheinman, and N. Schmitt. 2013. Characterization and Mechanisms of Action of Novel NaV1.5 Channel Mutations Associated With Brugada Syndrome. *Circulation: Arrhythmia and Electrophysiology*. 6:177-184.

Campuzano, O., R. Brugada, and A. Iglesias. 2010. Genetics of Brugada syndrome. *Current Opinion in Cardiology*. 25:210-215.

Cecile Terrenoire, Kai Wang, Kelvin W. Chan Tung, Wendy K. Chung, 3 Robert H. Pass,6, Jonathan T. Lu, Jyh-Chang Jean, Amel Omari, Kevin J. Sampson, Darrell N. Kotton, Gordon Keller, and a.R.S. Kass1. 2013. Induced pluripotent stem cells used to reveal drug actions in a long QT syndrome family with complex genetics. *The Journal of General Physiology*. 141:61-72.

Charbit, B., A. Rosier, D. Bollens, F. Boccara, P.-Y. Boelle, A. Koubaa, P.-M. Girard, and C. Funck-Brentano. 2009. Relationship between HIV protease inhibitors and QTc interval duration in HIV-infected patients: a cross-sectional study. *British Journal of Clinical Pharmacology*. 67:76-82.

Chen, Q., G.E. Kirsch, D. Zhang, R. Brugada, J. Brugada, P. Brugada, D. Potenza, A. Moya, M. Borggrefe, G. Breithardt, R. Ortiz-Lopez, Z. Wang, C. Antzelevitch, R.E. O'Brien, E. Schulze-Bahr, M.T. Keating, J.A. Towbin, and Q. Wang. 1998. Genetic basis and molecular mechanism for idiopathic ventricular fibrillation. *Nature*. 392:293-296.

Chiang, K.-C., L.-P. Lai, and R.-C. Shieh. 2009. Characterization of a novel Nav1.5 channel mutation, A551T, associated with Brugada syndrome. *Journal of Biomedical Science*. 16:76.

Choi, B.-R., F. Burton, and G. Salama. 2002. Cytosolic Ca2+ triggers early afterdepolarizations and torsade de pointes in rabbit hearts with type 2 long QT syndrome. *The Journal of Physiology*. 543:615-631.

Chow, D.C., R. Wood, J. Choi, A. Grandinetti, M. Gerschenson, N. Sriratanaviriyakul, B. Nakamoto, C. Shikuma, and P. Low. 2011. Cardiovagal Autonomic Function in HIV-Infected Patients with Unsuppressed HIV Viremia. *HIV Clinical Trials*. 12:141-150.

Christini, D.J., M.L. Riccio, C.A. Culianu, J.J. Fox, A. Karma, and R.F. Gilmour. 2006. Control of Electrical Alternans in Canine Cardiac Purkinje Fibers. *Physical Review Letters*. 96:104101.

Clancy, C.E., and Y. Rudy. 2001. Cellular consequences of HERG mutations in the long QT syndrome: precursors to sudden cardiac death. *Cardiovasc Res*. 50:301-313.

Cook, S.A., P.H. Sugden, and A. Clerk. 1999. Activation of c-Jun N-Terminal Kinases and p38-Mitogen-activated Protein Kinases in Human Heart Failure Secondary to Ischaemic Heart Disease. *Journal of Molecular and Cellular Cardiology*. 31:1429-1434.

Coronel, R., S. Casini, T.T. Koopmann, F.J.G. Wilms-Schopman, A.O. Verkerk, J.R. de Groot, Z. Bhuiyan, C.R. Bezzina, M.W. Veldkamp, A.C. Linnenbank, A.C. van der Wal, H.L. Tan, P. Brugada, A.A.M. Wilde, and J.M.T. de Bakker. 2005. Right Ventricular Fibrosis and Conduction Delay in a Patient With Clinical Signs of Brugada Syndrome: A Combined Electrophysiological, Genetic, Histopathologic, and Computational Study. *Circulation*. 112:2769-2777.

Crotti, L., C.A. Marcou, D.J. Tester, S. Castelletti, J.R. Giudicessi, M. Torchio, A. Medeiros-Domingo, S. Simone, M.L. Will, F. Dagradi, P.J. Schwartz, and M.J. Ackerman. 2012. Spectrum and Prevalence of Mutations Involving BrS1- Through BrS12-Susceptibility Genes in a Cohort of Unrelated Patients Referred for Brugada Syndrome Genetic Testing: Implications for Genetic Testing. *Journal of the American College of Cardiology*. 60:1410-1418.

Davis, R.P., S. Casini, C.W. van den Berg, M. Hoekstra, C.A. Remme, C. Dambrot, D. Salvatori, D.W.-v. Oostwaard, A.A.M. Wilde, C.R. Bezzina, A.O. Verkerk, C. Freund, and C.L. Mummery. 2012. Cardiomyocytes Derived From Pluripotent Stem Cells Recapitulate Electrophysiological Characteristics of an Overlap Syndrome of Cardiac Sodium Channel Disease. *Circulation*. 125:3079-3091.

Debaisieux, S., F. Rayne, H. Yezid, and B. Beaumelle. 2012. The Ins and Outs of HIV-1 Tat. *Traffic*. 13:355-363.

Delisle, B.P., B.D. Anson, S. Rajamani, and C.T. January. 2004. Biology of Cardiac Arrhythmias: Ion Channel Protein Trafficking. *Circulation Research*. 94:1418-1428.

Delpon, E., J.M. Cordeiro, L. Nunez, P.E. Thomsen, A. Guerchicoff, G.D. Pollevick, Y. Wu, J.K. Kanters, C.T. Larsen, J. Hofman-Bang, E. Burashnikov, M. Christiansen, and C. Antzelevitch. 2008. Functional effects of KCNE3 mutation and its role in the development of Brugada syndrome. *Circ Arrhythm Electrophysiol*. 1:209-218.

Derangeon, M., J. Montnach, I. Baró, and F. Charpentier. 2012. Mouse Models of SCN5A-Related Cardiac Arrhythmias. *Frontiers in Physiology*. 3:210.

Despa, S., M.A. Islam, C.R. Weber, S.M. Pogwizd, and D.M. Bers. 2002. Intracellular Na+ Concentration Is Elevated in Heart Failure But Na/K Pump Function Is Unchanged. *Circulation*. 105:2543-2548.

Dick, E., D. Rajamohan, J. Ronksley, and C. Denning. 2010. Evaluating the utility of cardiomyocytes from human pluripotent stem cells for drug screening. 1037-1045 pp.

Drouin, E., G. Lande, and F. Charpentier. 1998. Amiodarone reduces transmural heterogeneity of repolarization in the human heart. *Journal of the American College of Cardiology*. 32:1063-1067.

Dubois, N.C., A.M. Craft, P. Sharma, D.A. Elliott, E.G. Stanley, A.G. Elefanty, A. Gramolini, and G. Keller. 2011. SIRPA is a specific cell-surface marker for isolating cardiomyocytes derived from human pluripotent stem cells. *Nat Biotech*. 29:1011-1018.

Edwards, A.G., E. Grandi, J.E. Hake, S. Patel, P. Li, S. Miyamoto, J.H. Omens, J. Heller Brown, D.M. Bers, and A.D. McCulloch. 2014. Nonequilibrium Reactivation of Na+ Current Drives Early Afterdepolarizations in Mouse Ventricle. *Circulation: Arrhythmia and Electrophysiology*. 7:1205-1213.

Egashira, T., S. Yuasa, T. Suzuki, Y. Aizawa, H. Yamakawa, T. Matsuhashi, Y. Ohno, S. Tohyama, S. Okata, T. Seki, Y. Kuroda, K. Yae, H. Hashimoto, T. Tanaka, F. Hattori, T. Sato, S. Miyoshi, S. Takatsuki, M. Murata, J. Kurokawa, T. Furukawa, N. Makita, T. Aiba, W. Shimizu, M. Horie, K. Kamiya, I. Kodama, S. Ogawa, and K. Fukuda. 2012. Disease characterization using LQTS-specific induced pluripotent stem cells. 419-429 pp.

Elizari, M.V., R. Levi, R.S. Acunzo, P.A. Chiale, M.M. Civetta, M. Ferreiro, and S. Sicouri. 2007. Abnormal expression of cardiac neural crest cells in heart development: A different hypothesis for the etiopathogenesis of Brugada syndrome. *Heart rhythm*. 4:359-365.

Elliott, D.A., S.R. Braam, K. Koutsis, E.S. Ng, R. Jenny, E.L. Lagerqvist, C. Biben, T. Hatzistavrou, C.E. Hirst, Q.C. Yu, R.J.P. Skelton, D. Ward-van Oostwaard, S.M. Lim, O. Khammy, X. Li, S.M. Hawes, R.P. Davis, A.L. Goulburn, R. Passier, O.W.J. Prall, J.M. Haynes, C.W. Pouton, D.M. Kaye, C.L. Mummery, A.G. Elefanty, and E.G. Stanley. 2011. NKX2-5eGFP/w hESCs for isolation of human cardiac progenitors and cardiomyocytes. *Nat Meth*. 8:1037-1040.

Fantoni, M., C. Autore, and C. Del Borgo. 2001. Drugs and Cardiotoxicity in HIV and AIDS. *Annals of the New York Academy of Sciences*. 946:179-199.

Fatima, A., G. Xu, K. Shao, S. Papadopoulos, M. Lehmann, J.J. Arnáiz-Cot, A.O. Rosa, F. Nguemo, M. Matzkies, S. Dittmann, S.L. Stone, M. Linke, U. Zechner, V. Beyer, H.C. Hennies, S. Rosenkranz, B. Klauke, A.S. Parwani, W. Haverkamp, G. Pfitzer, M. Farr, L. Cleemann, M. Morad, H. Milting, J. Hescheler, and T. Šaric. 2011. *In vitro* Modeling of Ryanodine

Receptor 2 Dysfunction Using Human Induced Pluripotent Stem Cells. *Cellular Physiology and Biochemistry*. 28:579-592.

Florea, S.M., and L.A. Blatter. 2010. The role of mitochondria for the regulation of cardiac alternans. *Frontiers in Physiology*. 1.

Fredj, S., N. Lindegger, K.J. Sampson, P. Carmeliet, and R.S. Kass. 2006. Altered Na+ Channels Promote Pause-Induced Spontaneous Diastolic Activity in Long QT Syndrome Type 3 Myocytes. *Circulation Research*. 99:1225-1232.

Freund, C., D. Ward-van Oostwaard, J. Monshouwer-Kloots, S. van den Brink, M. van Rooijen, X. Xu, R. Zweigerdt, C. Mummery, and R. Passier. 2008. Insulin Redirects Differentiation from Cardiogenic Mesoderm and Endoderm to Neuroectoderm in Differentiating Human Embryonic Stem Cells. *Stem Cells*. 26:724-733.

Gaborit, N., 1, 3†, Thomas Wichter4,5†, Andras Varro6,7, Viktoria Szuts7,, Guillaume Lamirault1, Lars Eckardt4, Matthias Paul4, Gu¨nter Breithardt4,, and D.E. Eric Schulze-Bahr4, 2,3, Stanley Nattel8, and Sophie Demolombe1,2,3*. 2008. Transcriptional profiling of ion channel genes in Brugada syndrome and other right ventricular arrhythmogenic diseases. *European Heart Journal*:487-496.

Gaborit, N., S. Le Bouter, V. Szuts, A. Varro, D. Escande, S. Nattel, and S. Demolombe. 2007. Regional and tissue specific transcript signatures of ion channel genes in the non-diseased human heart. *The Journal of Physiology*. 582:675-693.

George, A.L. 2005. Inherited disorders of voltage-gated sodium channels. *Journal of Clinical Investigation*. 115:1990-1999.

Gerbal-Chaloin, S., N. Funakoshi, A. Caillaud, C. Gondeau, B. Champon, and K. Si-Tayeb. 2014. Human induced pluripotent stem cells in hepatology: beyond the proof of concept. *Am J Pathol*. 184:332-347.

Gherghiceanu, M., L. Barad, A. Novak, I. Reiter, J. Itskovitz-Eldor, O. Binah, and L.M. Popescu. 2011. Cardiomyocytes derived from human embryonic and induced pluripotent stem cells: comparative ultrastructure. *Journal of Cellular and Molecular Medicine*. 15:2539-2551.

Giudicessi, J.R., and a.M.J. Ackerman. 2012. Potassium-channel mutations and cardiac arrhythmias-diagnosis and therapy. *Nature Review Cardiology* 3:319-332.

Giudicessi, J.R., D. Ye, D.J. Tester, L. Crotti, A. Mugione, V.V. Nesterenko, R.M. Albertson, C. Antzelevitch, P.J. Schwartz, and M.J. Ackerman. 2011. Transient outward current (I(to)) gain-of-function mutations in the KCND3-encoded Kv4.3 potassium channel and Brugada syndrome. *Heart Rhythm*. 8:1024-1032.

Gore, A., Z. Li, H.-L. Fung, J.E. Young, S. Agarwal, J. Antosiewicz-Bourget, I. Canto, A. Giorgetti, M.A. Israel, E. Kiskinis, J.-H. Lee, Y.-H. Loh, P.D. Manos, N. Montserrat, A.D. Panopoulos, S. Ruiz, M.L. Wilbert, J. Yu, E.F. Kirkness, J.C.I. Belmonte, D.J. Rossi, J.A. Thomson, K. Eggan, G.Q. Daley, L.S.B. Goldstein, and K. Zhang. 2011. Somatic coding mutations in human induced pluripotent stem cells. *Nature*. 471:63-67.

Grilo, L.S., P.-A. Carrupt, and H. Abriel. 2010. Stereoselective Inhibition of the hERG1 Potassium Channel. *Frontiers in Pharmacology*. 1:137.

Guan, X., D.L. Mack, C.M. Moreno, J.L. Strande, J. Mathieu, Y. Shi, C.D. Markert, Z. Wang, G. Liu, M.W. Lawlor, E.C. Moorefield, T.N. Jones, J.A. Fugate, M.E. Furth, C.E. Murry, H. Ruohola-Baker, Y. Zhang, L.F. Santana, and M.K. Childers. 2014. Dystrophin-deficient cardiomyocytes derived from human urine: new biologic reagents for drug discovery. *Stem Cell Res*. 12:467-480.

Gurtler, A., N. Kunz, M. Gomolka, S. Hornhardt, A.A. Friedl, K. McDonald, J.E. Kohn, and A. Posch. 2013. Stain-Free technology as a normalization tool in Western blot analysis. *Anal Biochem*. 433:105-111.

Gussak, I., C. Antzelevitch, P. Bjerregaard, J. Towbin, and B. Chaitman. 1999. The Brugada syndrome: clinical, electrophysiologic and genetic aspects. *Journal of the American College of Cardiology*. 33:5-15.

Gutstein, D.E., G.E. Morley, D. Vaidya, F. Liu, F.L. Chen, H. Stuhlmann, and G.I. Fishman. 2001. Heterogeneous Expression of Gap Junction Channels in the Heart Leads to Conduction Defects and Ventricular Dysfunction. *Circulation*. 104:1194-1199.

Hajjar, R.J., and J.-S. Hulot. 2014. Modeling CVD in Human Pluripotent Cells by Genome Editing∗. *Journal of the American College of Cardiology*. 64:460-462.

Hallaq, H., D.W. Wang, J.D. Kunic, A.L. George, K.S. Wells, and K.T. Murray. 2012. Activation of protein kinase C alters the intracellular distribution and mobility of cardiac Na+ channels. H782-H789 pp.

Hanna, Z., D.G. Kay, M. Cool, S. Jothy, N. Rebai, and P. Jolicoeur. 1998. Transgenic Mice Expressing Human Immunodeficiency Virus Type 1 in Immune Cells Develop a Severe AIDS-Like Disease. *Journal of Virology*. 72:121-132.

Hattori, F., H. Chen, H. Yamashita, S. Tohyama, Y.-s. Satoh, S. Yuasa, W. Li, H. Yamakawa, T. Tanaka, T. Onitsuka, K. Shimoji, Y. Ohno, T. Egashira, R. Kaneda, M. Murata, K. Hidaka, T. Morisaki, E. Sasaki, T. Suzuki, M. Sano, S. Makino, S. Oikawa, and K. Fukuda. 2010. Nongenetic method for purifying stem cell-derived cardiomyocytes. *Nat Meth*. 7:61-66.

Haverkamp, W., G. Breithardt, A.J. Camm, M.J. Janse, M.R. Rosen, C. Antzelevitch, D. Escande, M. Franz, M. Malik, A. Moss, and R. Shah. 2000. The potential for QT prolongation and proarrhythmia by non-antiarrhythmic drugs: clinical and regulatory implications. Report on a Policy Conference of the European Society of Cardiology. 1216-1231 pp.

He, J.-Q., Y. Ma, Y. Lee, J.A. Thomson, and T.J. Kamp. 2003. Human Embryonic Stem Cells Develop Into Multiple Types of Cardiac Myocytes: Action Potential Characterization. *Circulation Research*. 93:32-39.

Hoekstra, M., C.L. Mummery, A.A.M. Wilde, C.R. Bezzina, and A.O. Verkerk. 2012. Induced pluripotent stem cell derived cardiomyocytes as models for cardiac arrhythmias. *Frontiers in Physiology*. 3.

Howden, S.E., A. Gore, Z. Li, H.-L. Fung, B.S. Nisler, J. Nie, G. Chen, B.E. McIntosh, D.R. Gulbranson, N.R. Diol, S.M. Taapken, D.T. Vereide, K.D. Montgomery, K. Zhang, D.M. Gamm, and J.A. Thomson. 2011. Genetic correction and analysis of induced pluripotent stem cells from a patient with gyrate atrophy. *Proceedings of the National Academy of Sciences*. 108:6537-6542.

Hu, D., H. Barajas-Martinez, E. Burashnikov, M. Springer, Y. Wu, A. Varro, R. Pfeiffer, T.T. Koopmann, J.M. Cordeiro, A. Guerchicoff, G.D. Pollevick, and C. Antzelevitch. 2009. A mutation in the beta 3 subunit of the cardiac sodium channel associated with Brugada ECG phenotype. *Circ Cardiovasc Genet*. 2:270-278.

Huber, I., I. Itzhaki, O. Caspi, G. Arbel, M. Tzukerman, A. Gepstein, M. Habib, L. Yankelson, I. Kehat, and L. Gepstein. 2007. Identification and selection of cardiomyocytes during human embryonic stem cell differentiation. *The FASEB Journal*. 21:2551-2563.

Huffaker, R., S.T. Lamp, J.N. Weiss, and B. Kogan. 2004. Intracellular calcium cycling, early afterdepolarizations, and reentry in simulated long QT syndrome. *Heart rhythm*. 1:441-448.

Huikuri, H.V., A. Castellanos, and R.J. Myerburg. 2001. Sudden Death Due to Cardiac Arrhythmias. *New England Journal of Medicine*. 345:1473-1482.

Hüser, J., Y.G. Wang, K.A. Sheehan, F. Cifuentes, S.L. Lipsius, and L.A. Blatter. 2000. Functional coupling between glycolysis and excitation—contraction coupling underlies alternans in cat heart cells. *The Journal of Physiology*. 524:795-806.

Hussein, S.M., N.N. Batada, S. Vuoristo, R.W. Ching, R. Autio, E. Narva, S. Ng, M. Sourour, R. Hamalainen, C. Olsson, K. Lundin, M. Mikkola, R. Trokovic, M. Peitz, O. Brustle, D.P. Bazett-Jones, K. Alitalo, R. Lahesmaa, A. Nagy, and T. Otonkoski. 2011. Copy number variation and selection during reprogramming to pluripotency. *Nature*. 471:58-62.

Inoue, H., N. Nagata, H. Kurokawa, and S. Yamanaka. 2014. iPS cells: a game changer for future medicine. *EMBO J*. 33:409-417.

Inoue, H., and S. Yamanaka. 2011. The Use of Induced Pluripotent Stem Cells in Drug Development. *Clinical Pharmacology & Therapeutics*. 89:655-661.

Iost, N., L. Virág, M. Opincariu, J. Szécsi, András Varró, and J.G. Papp. 1998. Delayed rectifier potassium current in undiseased human ventricular myocytes. 508-515 pp.

Ishikawa, T., N. Takahashi, S. Ohno, H. Sakurada, K. Nakamura, Y.K. On, J.E. Park, T. Makiyama, M. Horie, T. Arimura, N. Makita, and A. Kimura. 2013. Novel SCN3B Mutation Associated With Brugada Syndrome Affects Intracellular Trafficking and Function of Nav1.5. *Circulation Journal*. 77:959-967.

Itoh, H., T. Sakaguchi, T. Ashihara, W.-G. Ding, I. Nagaoka, Y. Oka, Y. Nakazawa, T. Yao, H. Jo, M. Ito, K. Nakamura, T. Ohe, H. Matsuura, and M. Horie. 2009. A novel KCNH2 mutation as a modifier for short QT interval. *International Journal of Cardiology*. 137:83-85.

Itzhaki, I., L. Maizels, I. Huber, L. Zwi-Dantsis, O. Caspi, A. Winterstern, O. Feldman, A. Gepstein, G. Arbel, H. Hammerman, M. Boulos, and L. Gepstein. 2011a. Modelling the long QT syndrome with induced pluripotent stem cells. *Nature*. 471:225-229.

Itzhaki, I., S. Rapoport, I. Huber, I. Mizrahi, L. Zwi-Dantsis, G. Arbel, J. Schiller, and L. Gepstein. 2011b. Calcium Handling in Human Induced Pluripotent Stem Cell Derived Cardiomyocytes. *PLoS ONE*. 6:e18037.

Jansen, J.A., M. Noorman, H. Musa, M. Stein, S. de Jong, R. van der Nagel, T.J. Hund, P.J. Mohler, M.A. Vos, T.A. van Veen, J.M. de Bakker, M. Delmar, and H.V. van Rijen. 2012. Reduced heterogeneous expression of Cx43 results in decreased Nav1.5 expression and reduced sodium current that accounts for arrhythmia vulnerability in conditional Cx43 knockout mice. *Heart rhythm*. 9:600-607.

January, C.T., and J.M. Riddle. 1989. Early afterdepolarizations: mechanism of induction and block. A role for L-type Ca2+ current. *Circulation Research*. 64:977-990.

Jonsson, M.K.B., M.A. Vos, G.R. Mirams, G. Duker, P. Sartipy, T.P. de Boer, and T.A.B. van Veen. 2012. Application of human stem cell-derived cardiomyocytes in safety pharmacology requires caution beyond hERG. *Journal of Molecular and Cellular Cardiology*. 52:998-1008.

Jung, C.B., A. Moretti, M. Mederos y Schnitzler, L. Iop, U. Storch, M. Bellin, T. Dorn, S. Ruppenthal, S. Pfeiffer, A. Goedel, R.J. Dirschinger, M. Seyfarth, J.T. Lam, D. Sinnecker, T. Gudermann, P. Lipp, and K.-L. Laugwitz. 2012. Dantrolene rescues arrhythmogenic RYR2 defect in a patient-specific stem cell model of catecholaminergic polymorphic ventricular tachycardia. *EMBO Molecular Medicine*. 4:180-191.

Kääb, S., H.B. Nuss, N. Chiamvimonvat, B. O'Rourke, P.H. Pak, D.A. Kass, E. Marban, and G.F. Tomaselli. 1996. Ionic Mechanism of Action Potential Prolongation in Ventricular Myocytes From Dogs With Pacing-Induced Heart Failure. *Circulation Research*. 78:262-273.

Kamp, T.J. 2011. An Electrifying iPSC Disease Model: Long QT Syndrome Type 2 and Heart Cells in a Dish. *Cell Stem Cell*. 8:130-131.

Kannankeril, P., D.M. Roden, and D. Darbar. 2010. Drug-Induced Long QT Syndrome. *Pharmacological Reviews*. 62:760-781.

Kattygnarath, D., S. Maugenre, N. Neyroud, E. Balse, C. Ichai, I. Denjoy, G. Dilanian, R.P. Martins, V. Fressart, M. Berthet, J.J. Schott, A. Leenhardt, V. Probst, H. Le Marec, B. Hainque, A. Coulombe, S.N. Hatem, and P. Guicheney. 2011. MOG1: A New Susceptibility Gene for Brugada Syndrome. *Circulation: Cardiovascular Genetics*. 4:261-268.

Kehat, I., D. Kenyagin-Karsenti, M. Snir, H. Segev, M. Amit, A. Gepstein, E. Livne, O. Binah, J. Itskovitz-Eldor, and L. Gepstein. 2001. Human embryonic stem cells can differentiate into myocytes with structural and functional properties of cardiomyocytes. *Journal of Clinical Investigation*. 108:407-414.

Keller, D.I., J.-S. Rougier, J.P. Kucera, N. Benammar, V. Fressart, P. Guicheney, A. Madle, M. Fromer, J. Schläpfer, and H. Abriel. 2005. Brugada syndrome and fever: Genetic and molecular characterization of patients carrying SCN5A mutations. 510-519 pp.

Kim, C., M. Majdi, P. Xia, K.A. Wei, M. Talantova, S. Spiering, B. Nelson, M. Mercola, and H.-s.V. Chen. 2009. Non-Cardiomyocytes Influence the Electrophysiological Maturation of Human Embryonic Stem Cell-Derived Cardiomyocytes During Differentiation. *Stem Cells and Development*. 19:783-795.

Kim, K., A. Doi, B. Wen, K. Ng, R. Zhao, P. Cahan, J. Kim, M.J. Aryee, H. Ji, L.I.R. Ehrlich, A. Yabuuchi, A. Takeuchi, K.C. Cunniff, H. Hongguang, S. McKinney-Freeman, O. Naveiras, T.J. Yoon, R.A. Irizarry, N. Jung, J. Seita, J. Hanna, P. Murakami, R. Jaenisch, R. Weissleder, S.H. Orkin, I.L. Weissman, A.P. Feinberg, and G.Q. Daley. 2010. Epigenetic memory in induced pluripotent stem cells. *Nature*. 467:285-290.

Kocheril, A.G., S.A.J. Bokhari, W.P. Batsford, and A.J. Sinusas. 1997. Long QTc and Torsades de Pointes in Human Immunodeficiency Virus Disease. *Pacing and Clinical Electrophysiology*. 20:2810-2816.

Laflamme, M.A., K.Y. Chen, A.V. Naumova, V. Muskheli, J.A. Fugate, S.K. Dupras, H. Reinecke, C. Xu, M. Hassanipour, S. Police, C. O'Sullivan, L. Collins, Y. Chen, E. Minami, E.A. Gill, S. Ueno, C. Yuan, J. Gold, and C.E. Murry. 2007. Cardiomyocytes derived from human embryonic stem cells in pro-survival factors enhance function of infarcted rat hearts. *Nat Biotech*. 25:1015-1024.

Lahti, A.L., V.J. Kujala, H. Chapman, A.-P. Koivisto, M. Pekkanen-Mattila, E. Kerkelä, J. Hyttinen, K. Kontula, H. Swan, B.R. Conklin, S. Yamanaka, O. Silvennoinen, and K. Aalto-Setälä. 2012. Model for long QT syndrome type 2 using human iPS cells demonstrates arrhythmogenic characteristics in cell culture. *Disease Models & Mechanisms*. 5:220-230.

Lambiase, P.D., A.K. Ahmed, E.J. Ciaccio, R. Brugada, E. Lizotte, S. Chaubey, R. Ben-Simon, A.W. Chow, M.D. Lowe, and W.J. McKenna. 2009. High-Density Substrate Mapping in Brugada Syndrome: Combined Role of Conduction and Repolarization Heterogeneities in Arrhythmogenesis. *Circulation*. 120:106-117.

Laurent, L.C., I. Ulitsky, I. Slavin, H. Tran, A. Schork, R. Morey, C. Lynch, J.V. Harness, S. Lee, M.J. Barrero, S. Ku, M. Martynova, R. Semechkin, V. Galat, J. Gottesfeld, J.C.I. Belmonte, C. Murry, H.S. Keirstead, H.-S. Park, U. Schmidt, A.L. Laslett, F.-J. Muller, C.M. Nievergelt, R. Shamir, and J.F. Loring. 2011. Dynamic Changes in the Copy Number of Pluripotency and Cell Proliferation Genes in Human ESCs and iPSCs during Reprogramming and Time in Culture. *Cell Stem Cell*. 8:106-118.

Lee, K.I., H.T. Kim, and D.Y. Hwang. 2014. Footprint- and xeno-free human iPSCs derived from urine cells using extracellular matrix-based culture conditions. *Biomaterials*. 35:8330-8338.

Lee, Y.-K., K.-M. Ng, Y.-C. Chan, W.-H. Lai, K.-W. Au, C.-Y.J. Ho, L.-Y. Wong, C.-P. Lau, H.-F. Tse, and C.-W. Siu. 2010. Triiodothyronine Promotes Cardiac Differentiation and Maturation of Embryonic Stem Cells via the Classical Genomic Pathway. *Molecular Endocrinology*. 24:1728-1736.

Lee, Y.-K., K.-M. Ng, W.-H. Lai, Y.-C. Chan, Y.-M. Lau, Q. Lian, H.-F. Tse, and C.-W. Siu. 2011. Calcium Homeostasis in Human Induced Pluripotent Stem Cell-Derived Cardiomyocytes. *Stem Cell Rev and Rep*. 7:976-986.

Li, A., M.M. Saba, and E.R. Behr. 2013. Genetic biomarkers in Brugada syndrome. *Biomarkers Med*. 7:535–546.

Liu, H., S. Chatel, C. Simard, N. Syam, L. Salle, V. Probst, J. Morel, G. Millat, M. Lopez, H. Abriel, J.-J. Schott, R. Guinamard, and P. Bouvagnet. 2013. Molecular Genetics and Functional Anomalies in a Series of 248 Brugada Cases with 11 Mutations in the TRPM4 Channel. *PLoS ONE*. 8:e54131.

Liu, M., K.-C. Yang, and S.C. Dudley Jr. 2014. Cardiac sodium channel mutations: why so many phenotypes? *Nat Rev Cardiol*. 11:607-615.

Loh, Y.-H., S. Agarwal, I.-H. Park, A. Urbach, H. Huo, G.C. Heffner, K. Kim, J.D. Miller, K. Ng, and G.Q. Daley. 2009. Generation of induced pluripotent stem cells from human blood. *Blood*. 113:5476-5479.

London, B., M. Michalec, H. Mehdi, X. Zhu, L. Kerchner, S. Sanyal, P.C. Viswanathan, A.E. Pfahnl, L.L. Shang, M. Madhusudanan, C.J. Baty, S. Lagana, R. Aleong, R. Gutmann, M.J. Ackerman, D.M. McNamara, R. Weiss, and S.C. Dudley, Jr. 2007. Mutation in glycerol-3-phosphate dehydrogenase 1 like gene (GPD1-L) decreases cardiac Na+ current and causes inherited arrhythmias. *Circulation*. 116:2260-2268.

Loussouarn, G., I. Baro, and D. Escande. 2006. KCNQ1 K+ channel-mediated cardiac channelopathies. *Methods Mol Biol*. 337:167-183.

Lu, J.T., and R.S. Kass. 2010. Recent progress in congenital long QT syndrome. *Current Opinion in Cardiology*. 25:216-221.

Ma, J., L. Guo, S.J. Fiene, B.D. Anson, J.A. Thomson, T.J. Kamp, K.L. Kolaja, B.J. Swanson, and C.T. January. 2011. High purity human-induced pluripotent stem cell-derived cardiomyocytes: electrophysiological properties of action potentials and ionic currents. H2006-H2017 pp.

Magyar, J., N. Iost, Á. Körtvély, T. Bányász, L. Virág, P. Szigligeti, A. Varró, M. Opincariu, J. Szécsi, J.G. Papp, and P.P. Nánási. 2000. Effects of endothelin-1 on calcium and potassium currents in undiseased human ventricular myocytes. *Pflugers Archiv*. 441:144-149.

Maltsev, V.A., and A.I. Undrovinas. 2006. A multi-modal composition of the late Na+ current in human ventricular cardiomyocytes. 116-127 pp.

Marjamaa, A., V. Salomaa, C. Newton-Cheh, K. Porthan, A. Reunanen, H. Karanko, A. Jula, P. Lahermo, H. Vaananen, L. Toivonen, H. Swan, M. Viitasalo, M.S. Nieminen, L. Peltonen, L. Oikarinen, A. Palotie, and K. Kontula. 2009. High prevalence of four long QT syndrome founder mutations in the Finnish population. *Ann Med*. 41:234-240.

Marsman, R.F., H.L. Tan, and C.R. Bezzina. 2014. Genetics of sudden cardiac death caused by ventricular arrhythmias. *Nat Rev Cardiol*. 11:96-111.

Maruyama, M., S.-F. Lin, Y. Xie, S.-K. Chua, B. Joung, S. Han, T. Shinohara, M.J. Shen, Z. Qu, J.N. Weiss, and P.-S. Chen. 2011. Genesis of Phase 3 Early Afterdepolarizations and Triggered Activity in Acquired Long-QT Syndrome. *Circulation: Arrhythmia and Electrophysiology*. 4:103-111.

Mashar, M., A.J. Kwok, R. Pinder, and I. Sabir. 2014. The Brugada syndrome revisited. *Trends in Cardiovascular Medicine*. 24:191-196.

Matsa, E., D. Rajamohan, E. Dick, L. Young, I. Mellor, A. Staniforth, and C. Denning. 2011. Drug evaluation in cardiomyocytes derived from human induced pluripotent stem cells carrying a long QT syndrome type 2 mutation. 952-962 pp.

Maury, P., A. Moreau, F. Hidden-Lucet, A. Leenhardt, V. Fressart, M. Berthet, I. Denjoy, N. Bennamar, A. Rollin, C. Cardin, P. Guicheney, and M. Chahine. 2013. Novel SCN5A mutations in two families with "Brugada-like" ST elevation in the inferior leads and conduction disturbances. *J Interv Card Electrophysiol*. 37:131-140.

Mayshar, Y., U. Ben-David, N. Lavon, J.-C. Biancotti, B. Yakir, A.T. Clark, K. Plath, W.E. Lowry, and N. Benvenisty. 2010. Identification and Classification of Chromosomal Aberrations in Human Induced Pluripotent Stem Cells. *Cell Stem Cell*. 7:521-531.

Medeiros-Domingo, A., B.H. Tan, L. Crotti, D.J. Tester, L. Eckhardt, A. Cuoretti, S.L. Kroboth, C. Song, Q. Zhou, D. Kopp, P.J. Schwartz, J.C. Makielski, and M.J. Ackerman. 2010. Gain-of-function mutation S422L in the KCNJ8-encoded cardiac K(ATP) channel Kir6.1 as a pathogenic substrate for J-wave syndromes. *Heart Rhythm*. 7:1466-1471.

Mehra, R. 2007. Global public health problem of sudden cardiac death. *Journal of Electrocardiology*. 40:S118-S122.

Mehta, A., G.L. Sequiera, C.J.A. Ramachandra, Y. Sudibyo, Y. Chung, J. Sheng, K.Y. Wong, T.H. Tan, P. Wong, R. Liew, and W. Shim. 2014. Re-trafficking of hERG reverses long QT syndrome 2 phenotype in human iPS-derived cardiomyocytes. 497-506 pp.

Meregalli, P.G., J.M. Ruijter, N. Hofman, C.R. Bezzina, A.A. Wilde, and H.L. Tan. 2006. Diagnostic value of flecainide testing in unmasking SCN5A-related Brugada syndrome. *J Cardiovasc Electrophysiol*. 17:857-864.

Meregalli, P.G., H.L. Tan, V. Probst, T.T. Koopmann, M.W. Tanck, Z.A. Bhuiyan, F. Sacher, F. Kyndt, J.-J. Schott, J. Albuisson, P. Mabo, C.R. Bezzina, H. Le Marec, and A.A.M. Wilde. 2009. Type of SCN5A mutation determines clinical severity and degree of conduction slowing in loss-of-function sodium channelopathies. *Heart rhythm*. 6:341-348.

Meregalli, P.G., A.A.M. Wilde, and H.L. Tan. 2005. Pathophysiological mechanisms of Brugada syndrome: Depolarization disorder, repolarization disorder, or more? 367-378 pp.

Mewes, T., and U. Ravens. 1994. L-type Calcium Currents of Human Myocytes from Ventricle of Non-failing and Failing Hearts and from Atrium. *Journal of Molecular and Cellular Cardiology*. 26:1307-1320.

Mironov, S., J. Jalife, and E.G. Tolkacheva. 2008. Role of Conduction Velocity Restitution and Short-Term Memory in the Development of Action Potential Duration Alternans in Isolated Rabbit Hearts. *Circulation*. 118:17-25.

Miyoshi, K., D. Tsuji, K. Kudoh, K. Satomura, T. Muto, K. Itoh, and T. Noma. 2010. Generation of human induced pluripotent stem cells from oral mucosa. *Journal of Bioscience and Bioengineering*. 110:345-350.

Mizusawa, Y., and A.A.M. Wilde. 2012. Brugada Syndrome. *Circulation: Arrhythmia and Electrophysiology*. 5:606-616.

Mohamed, U., M.H. Gollob, R.M. Gow, and A.D. Krahn. 2006. Sudden cardiac death despite an implantable cardioverter-defibrillator in a young female with catecholaminergic ventricular tachycardia. *Heart rhythm*. 3:1486-1489.

Moreno, J.D., and C.E. Clancy. 2012. Pathophysiology of the cardiac late Na current and its potential as a drug target. *Journal of Molecular and Cellular Cardiology*. 52:608-619.

Moretti, A., M. Bellin, A. Welling, C.B. Jung, J.T. Lam, L. Bott-Flügel, T. Dorn, A. Goedel, C. Höhnke, F. Hofmann, M. Seyfarth, D. Sinnecker, A. Schömig, and K.-L. Laugwitz. 2010. Patient-Specific Induced Pluripotent Stem-Cell Models for Long-QT Syndrome. *New England Journal of Medicine*. 363:1397-1409.

Morita, H., D.P. Zipes, and J. Wu. 2009. Brugada syndrome: Insights of ST elevation, arrhythmogenicity, and risk stratification from experimental observations. *Heart rhythm*. 6:S34-S43.

Moss, A.J., W. Zareba, E.S. Kaufman, E. Gartman, D.R. Peterson, J. Benhorin, J.A. Towbin, M.T. Keating, S.G. Priori, P.J. Schwartz, G.M. Vincent, J.L. Robinson, M.L. Andrews, C. Feng, W.J. Hall, A. Medina, L. Zhang, and Z. Wang. 2002. Increased risk of arrhythmic events in long-QT syndrome with mutations in the pore region of the human ether-a-go-go-related gene potassium channel. *Circulation*. 105:794-799.

Muller, M., T. Seufferlein, A. Illing, and J. Homann. 2013. Modelling human channelopathies using induced pluripotent stem cells: a comprehensive review. *Stem Cells Int*. 2013:496501.

Mummery, C., D. Ward-van Oostwaard, P. Doevendans, R. Spijker, S. van den Brink, R. Hassink, M. van der Heyden, T. Opthof, M. Pera, A.B. de la Riviere, R. Passier, and L. Tertoolen. 2003. Differentiation of Human Embryonic Stem Cells to Cardiomyocytes: Role of Coculture With Visceral Endoderm-Like Cells. *Circulation*. 107:2733-2740.

Muslin, Anthony J. 2008. MAPK signalling in cardiovascular health and disease: molecular mechanisms and therapeutic targets. 203-218 pp.

Myles, R.C., L. Wang, D.M. Bers, and C.M. Ripplinger. 2015. Decreased inward rectifying K+ current and increased ryanodine receptor sensitivity synergistically contribute to sustained focal arrhythmia in the intact rabbit heart. *The Journal of Physiology*. 593:1479-1493.

Myles, R.C., L. Wang, C. Kang, D.M. Bers, and C.M. Ripplinger. 2012. Local β-Adrenergic Stimulation Overcomes Source-Sink Mismatch to Generate Focal Arrhythmia. *Circulation Research*. 110:1454-1464.

Nabauer, M., D.J. Beuckelmann, P. Uberfuhr, and G. Steinbeck. 1996. Regional differences in current density and rate-dependent properties of the transient outward current in subepicardial and subendocardial myocytes of human left ventricle. *Circulation*. 93:168-177.

Nagase, S., K.F. Kusano, H. Morita, Y. Fujimoto, M. Kakishita, K. Nakamura, T. Emori, H. Matsubara, and T. Ohe. 2002. Epicardial electrogram of the right ventricular outflow tract in patients with the brugada syndrome: Using the epicardial lead. *Journal of the American College of Cardiology*. 39:1992-1995.

Nagase, S., K.F. Kusano, H. Morita, N. Nishii, K. Banba, A. Watanabe, S. Hiramatsu, K. Nakamura, S. Sakuragi, and T. Ohe. 2008. Longer Repolarization in the Epicardium at the Right Ventricular Outflow Tract Causes Type 1 Electrocardiogram in Patients With Brugada Syndrome. *Journal of the American College of Cardiology*. 51:1154-1161.

Napolitano, C., and C. Antzelevitch. 2011. Phenotypical manifestations of mutations in the genes encoding subunits of the cardiac voltage-dependent L-type calcium channel. *Circulation Research*. 108:607-618.

Narayan, S.M. 2006. T-Wave Alternans and the Susceptibility to Ventricular Arrhythmias. *Journal of the American College of Cardiology*. 47:269-281.

Naseef, A., E.R. Behr, and V.N. Batchvarov. 2015. Electrocardiographic methods for diagnosis and risk stratification in the Brugada syndrome. *Journal of the Saudi Heart Association*. 27:96-108.

Nerbonne, J.M. 2004. Studying Cardiac Arrhythmias in the Mouse—A Reasonable Model for Probing Mechanisms? *Trends in Cardiovascular Medicine*. 14:83-93.

Nerbonne, J.M., and R.S. Kass. 2005. Molecular Physiology of Cardiac Repolarization. 1205-1253 pp.

Nielsen, M.W., A.G. Holst, S.-P. Olesen, and M.S. Olesen. 2013. The genetic component of Brugada Syndrome. *Frontiers in Physiology*. 4.

Novak, A., L. Barad, N. Zeevi-Levin, R. Shick, R. Shtrichman, A. Lorber, J. Itskovitz-Eldor, and O. Binah. 2012. Cardiomyocytes generated from CPVTD307H patients are arrhythmogenic in response to β-adrenergic stimulation. *Journal of Cellular and Molecular Medicine*. 16:468-482.

Ohno, S., D.P. Zankov, W.G. Ding, H. Itoh, T. Makiyama, T. Doi, S. Shizuta, T. Hattori, A. Miyamoto, N. Naiki, J.C. Hancox, H. Matsuura, and M. Horie. 2011. KCNE5 (KCNE1L) variants are novel modulators of Brugada syndrome and idiopathic ventricular fibrillation. *Circ Arrhythm Electrophysiol*. 4:352-361.

Okita, K., and S. Yamanaka. 2011. Induced pluripotent stem cells: opportunities and challenges. *Philos Trans R Soc Lond B Biol Sci*. 366:2198-2207.

Passier, R., D.W.-v. Oostwaard, J. Snapper, J. Kloots, R.J. Hassink, E. Kuijk, B. Roelen, A.B. de la Riviere, and C. Mummery. 2005. Increased Cardiomyocyte Differentiation from Human Embryonic Stem Cells in Serum-Free Cultures. *Stem Cells*. 23:772-780.

Pastore, J.M., S.D. Girouard, K.R. Laurita, F.G. Akar, and D.S. Rosenbaum. 1999. Mechanism Linking T-Wave Alternans to the Genesis of Cardiac Fibrillation. *Circulation*. 99:1385-1394.

Patterson, E., B. Szabo, B.J. Scherlag, and R. Lazzara. 1990. Early and Delayed Afterdepolarizations Associated with Cesium Chloride-Induced Arrhythmias in the Dog. *Journal of Cardiovascular Pharmacology*. 15:323-331.

Petitprez, S., T. Jespersen, E. Pruvot, D. Keller, C. Corbaz, J. Schlapfer, H. Abriel, and J. Kucera. 2008. Analyses of a novel SCN5A mutation (C1850S): conduction vs. repolarization disorder hypotheses in the Brugada syndrome. *Cardiovasc Res*. 78:494 - 504.

Petitprez, S., A.F. Zmoos, J. Ogrodnik, E. Balse, N. Raad, S. El-Haou, M. Albesa, P. Bittihn, S. Luther, S.E. Lehnart, S.N. Hatem, A. Coulombe, and H. Abriel. 2011. SAP97 and dystrophin macromolecular complexes determine two pools of cardiac sodium channels Nav1.5 in cardiomyocytes. *Circ Res*. 108:294-304.

Pfahnl, A.E., P.C. Viswanathan, R. Weiss, L.L. Shang, S. Sanyal, V. Shusterman, C. Kornblit, B. London, and S.C. Dudley Jr. 2007. A sodium channel pore mutation causing Brugada syndrome. *Heart rhythm*. 4:46-53.

Piacentino, V., C.R. Weber, X. Chen, J. Weisser-Thomas, K.B. Margulies, D.M. Bers, and S.R. Houser. 2003. Cellular Basis of Abnormal Calcium Transients of Failing Human Ventricular Myocytes. *Circulation Research*. 92:651-658.

Pieske, B., L.S. Maier, V. Piacentino, J. Weisser, G. Hasenfuss, and S. Houser. 2002. Rate Dependence of [Na+]i and Contractility in Nonfailing and Failing Human Myocardium. *Circulation*. 106:447-453.

Poggi, A., R. Carosio, D. Fenoglio, S. Brenci, G. Murdaca, M. Setti, F. Indiveri, S. Scabini, E. Ferrero, and M.R. Zocchi. 2004. Migration of Vδ1 and Vδ2 T cells in response to CXCR3 and CXCR4 ligands in healthy donors and HIV-1–infected patients: competition by HIV-1 Tat. 2205-2213 pp.

Pogwizd, S.M., K. Schlotthauer, L. Li, W. Yuan, and D.M. Bers. 2001. Arrhythmogenesis and Contractile Dysfunction in Heart Failure: Roles of Sodium-Calcium Exchange, Inward Rectifier Potassium Current, and Residual β-Adrenergic Responsiveness. *Circulation Research*. 88:1159-1167.

Polo, J.M., S. Liu, M.E. Figueroa, W. Kulalert, S. Eminli, K.Y. Tan, E. Apostolou, M. Stadtfeld, Y. Li, T. Shioda, S. Natesan, A.J. Wagers, A. Melnick, T. Evans, and K. Hochedlinger. 2010. Cell type of origin influences the molecular and functional properties of mouse induced pluripotent stem cells. *Nat Biotech*. 28:848-855.

Potet, F., P. Mabo, G. Le Coq, V. Probst, J.-J. Schott, F. Airaud, G. Guihard, J.-C. Daubert, D. Escande, and H. Le Marec. 2003. Novel Brugada SCN5A Mutation Leading to ST Segment Elevation in the Inferior or the Right Precordial Leads. *Journal of Cardiovascular Electrophysiology*. 14:200-203.

Priori, S.G., C. Napolitano, E. Di Pasquale, and G. Condorelli. 2013. Induced pluripotent stem cell-derived cardiomyocytes in studies of inherited arrhythmias. *J Clin Invest*. 123:84-91.

Priori, S.G., C. Napolitano, M. Gasparini, C. Pappone, P. Della Bella, U. Giordano, R. Bloise, C. Giustetto, R. De Nardis, M. Grillo, E. Ronchetti, G. Faggiano, and J. Nastoli. 2002. Natural

history of Brugada syndrome: insights for risk stratification and management. *Circulation*. 105:1342-1347.

Priori, S.G., C. Napolitano, P.J. Schwartz, R. Bloise, L. Crotti, and E. Ronchetti. 2000. The Elusive Link Between LQT3 and Brugada Syndrome: The Role of Flecainide Challenge. *Circulation*. 102:945-947.

Probst, V., C. Veltmann, L. Eckardt, P.G. Meregalli, F. Gaita, H.L. Tan, D. Babuty, F. Sacher, C. Giustetto, E. Schulze-Bahr, M. Borggrefe, M. Haissaguerre, P. Mabo, H. Le Marec, C. Wolpert, and A.A.M. Wilde. 2010. Long-Term Prognosis of Patients Diagnosed With Brugada Syndrome: Results From the FINGER Brugada Syndrome Registry. *Circulation*. 121:635-643.

Probst, V., A.A. Wilde, J. Barc, F. Sacher, D. Babuty, P. Mabo, J. Mansourati, S. Le Scouarnec, F. Kyndt, C. Le Caignec, P. Guicheney, L. Gouas, J. Albuisson, P.G. Meregalli, H. Le Marec, H.L. Tan, and J.J. Schott. 2009. SCN5A mutations and the role of genetic background in the pathophysiology of Brugada syndrome. *Circ Cardiovasc Genet*. 2:552-557.

Pruvot, E.J., R.P. Katra, D.S. Rosenbaum, and K.R. Laurita. 2004. Role of Calcium Cycling Versus Restitution in the Mechanism of Repolarization Alternans. *Circulation Research*. 94:1083-1090.

Puri, R., K.C. Roberts-Thomson, and G.D. Young. 2009. HIV and Long QT syndrome—Cause or coincidence. *International Journal of Cardiology*. 133:e9-e10.

Qu, Z., H.S. Karagueuzian, A. Garfinkel, and J.N. Weiss. 2004. Effects of Na+ channel and cell coupling abnormalities on vulnerability to reentry: a simulation study. H1310-H1321 pp.

Qu, Z., M. Nivala, and J.N. Weiss. 2013. Calcium alternans in cardiac myocytes: Order from disorder. *Journal of Molecular and Cellular Cardiology*. 58:100-109.

Qu, Z., Y. Xie, A. Garfinkel, and J.N. Weiss. 2010. T-wave Alternans and Arrhythmogenesis in Cardiac Diseases. *Frontiers in Physiology*. 1.

Rayne, F., S. Debaisieux, H. Yezid, Y.L. Lin, C. Mettling, K. Konate, N. Chazal, S.T. Arold, M. Pugnière, F. Sanchez, A. Bonhoure, L. Briant, E. Loret, C. Roy, and B. Beaumelle. 2010. Phosphatidylinositol-(4,5)-bisphosphate enables efficient secretion of HIV-1 Tat by infected T-cells. 1348-1362 pp.

Reinsch, N., C. Buhr, P. Krings, H. Kaelsch, K. Neuhaus, H. Wieneke, R. Erbel, T. Neumann, and t.G.H.F. Network. 2009. Prevalence and Risk Factors of Prolonged QTc Interval in HIV-Infected Patients: Results of the HIV-HEART Study. *HIV Clinical Trials*. 10:261-268.

Remme, C.A., and A.A.M.W. , and Connie R. Bezzina. 2008. Cardiac sodium channel overlap syndromes: different faces of SCN5A mutations. *Trends Cardiovasc Med*. 18:78-87.

Remme, C.A., B.P. Scicluna, A.O. Verkerk, A.S. Amin, S. van Brunschot, L. Beekman, V.H.M. Deneer, C. Chevalier, F. Oyama, H. Miyazaki, N. Nukina, R. Wilders, D. Escande, R. Houlgatte, A.A.M. Wilde, H.L. Tan, M.W. Veldkamp, J.M.T. de Bakker, and C.R. Bezzina. 2009. Genetically Determined Differences in Sodium Current Characteristics Modulate Conduction Disease Severity in Mice With Cardiac Sodium Channelopathy. *Circulation Research*. 104:1283-1292.

Riuró, H., P. Beltran-Alvarez, A. Tarradas, E. Selga, O. Campuzano, M. Vergés, S. Pagans, A. Iglesias, J. Brugada, P. Brugada, F.M. Vázquez, G.J. Pérez, F.S. Scornik, and R. Brugada. 2013. A Missense Mutation in the Sodium Channel β2 Subunit Reveals SCN2B as a New Candidate Gene for Brugada Syndrome. *Human Mutation*. 34:961-966.

Rivero-Gutierrez, B., A. Anzola, O. Martinez-Augustin, and F.S. de Medina. 2014. Stain-free detection as loading control alternative to Ponceau and housekeeping protein immunodetection in Western blotting. *Anal Biochem*. 467:1-3.

Rosenbaum, D.S., L.E. Jackson, J.M. Smith, H. Garan, J.N. Ruskin, and R.J. Cohen. 1994. Electrical Alternans and Vulnerability to Ventricular Arrhythmias. *New England Journal of Medicine*. 330:235-241.

Ruan, Y., N. Liu, and S. Priori. 2009. Sodium channel mutations and arrhythmias. *Nat Rev Cardiol*. 6:337 - 348.

Sabir, I.N., M.J. Killeen, A.A. Grace, and C.L.H. Huang. 2008. Ventricular arrhythmogenesis: Insights from murine models. *Progress in Biophysics and Molecular Biology*. 98:208-218.

Saint, D.A., Y.K. Ju, and P.W. Gage. 1992. A persistent sodium current in rat ventricular myocytes. *The Journal of Physiology*. 453:219-231.

Sakakibara, Y., T. Furukawa, D.H. Singer, H. Jia, C.L. Backer, C.E. Arentzen, and J.A. Wasserstrom. 1993. Sodium current in isolated human ventricular myocytes. H1301-H1309 pp.

Sanguinetti, M.C., C. Jiang, M.E. Curran, and M.T. Keating. 1995. A mechanistic link between an inherited and an acquird cardiac arrthytmia: HERG encodes the IKr potassium channel. *Cell*. 81:299-307.

Sartiani, L., E. Bettiol, F. Stillitano, A. Mugelli, E. Cerbai, and M.E. Jaconi. 2007. Developmental Changes in Cardiomyocytes Differentiated from Human Embryonic Stem Cells: A Molecular and Electrophysiological Approach. *Stem Cells*. 25:1136-1144.

Satoh, H. 1999. Taurine modulates IKr but not IKs in guinea-pig ventricular cardiomyocytes. *British Journal of Pharmacology*. 126:87-92.

Scicluna, B.P., A.W. Wilde, and C.R. Bezzina. 2008. The Primary Arrhythmia Syndromes: Same Mutation, Different Manifestations. Are We Starting to Understand Why? *Journal of Cardiovascular Electrophysiology*. 19:445-452.

Si-Tayeb, K., F.K. Noto, M. Nagaoka, J. Li, M.A. Battle, C. Duris, P.E. North, S. Dalton, and S.A. Duncan. 2010. Highly efficient generation of human hepatocyte-like cells from induced pluripotent stem cells. *Hepatology*. 51:297-305.

Sinnecker, D., A. Goedel, T. Dorn, R.J.D.A. Moretti&, and K.-L. Laugwitz. 2013. Modeling Long-QT Syndromes with iPS Cells. *J. of Cardiovasc. Trans. Res*. 6:31-36.

Smits, J.P.P., L. Eckardt, V. Probst, C.R. Bezzina, J.J. Schott, C.A. Remme, W. Haverkamp, G. Breithardt, D. Escande, E. Schulze-Bahr, H. LeMarec, and A.A.M. Wilde. 2002. Genotype-phenotype relationship in Brugada syndrome: electrocardiographic features differentiate SCN5A-related patients from non–SCN5A-related patients. *Journal of the American College of Cardiology*. 40:350-356.

Sommariva, E., C. Pappone, F. Martinelli Boneschi, C. Di Resta, M. Rosaria Carbone, E. Salvi, P. Vergara, S. Sala, D. Cusi, M. Ferrari, and S. Benedetti. 2013. Genetics can contribute to the prognosis of Brugada syndrome: a pilot model for risk stratification. *Eur J Hum Genet*. 21:911-917.

Song, Y., J.C. Shryock, S. Wagner, L.S. Maier, and L. Belardinelli. 2006. Blocking Late Sodium Current Reduces Hydrogen Peroxide-Induced Arrhythmogenic Activity and Contractile Dysfunction. *Journal of Pharmacology and Experimental Therapeutics*. 318:214-222.

Sossalla, S., S. Wagner, E.C.L. Rasenack, H. Ruff, S.L. Weber, F.A. Schöndube, T. Tirilomis, G. Tenderich, G. Hasenfuss, L. Belardinelli, and L.S. Maier. 2008. Ranolazine improves diastolic dysfunction in isolated myocardium from failing human hearts — Role of late sodium current and intracellular ion accumulation. *Journal of Molecular and Cellular Cardiology*. 45:32-43.

Steinfurt, J., J. Biermann, C. Bode, and K.E. Odening. 2015. The Diagnosis, Risk Stratification, and Treatment of Brugada Syndrome. *Dtsch Arztebl International*. 112:394-401.

Sun, N., N.J. Panetta, D.M. Gupta, K.D. Wilson, A. Lee, F. Jia, S. Hu, A.M. Cherry, R.C. Robbins, M.T. Longaker, and J.C. Wu. 2009. Feeder-free derivation of induced pluripotent stem cells from adult human adipose stem cells. *Proceedings of the National Academy of Sciences of the United States of America*. 106:15720-15725.

Taapken, S.M., B.S. Nisler, M.A. Newton, T.L. Sampsell-Barron, K.A. Leonhard, E.M. McIntire, and K.D. Montgomery. 2011. Karyotypic abnormalities in human induced pluripotent stem cells and embryonic stem cells. *Nat Biotech*. 29:313-314.

Tabar, V., and L. Studer. 2014. Pluripotent stem cells in regenerative medicine: challenges and recent progress. *Nat Rev Genet*. 15:82-92.

Takahashi, K., K. Tanabe, M. Ohnuki, M. Narita, T. Ichisaka, K. Tomoda, and S. Yamanaka. 2007. Induction of Pluripotent Stem Cells from Adult Human Fibroblasts by Defined Factors. *Cell*. 131:861-872.

Takahashi, K., and S. Yamanaka. 2006. Induction of Pluripotent Stem Cells from Mouse Embryonic and Adult Fibroblast Cultures by Defined Factors. *Cell*. 126:663-676.

Tamaoki, N., K. Takahashi, T. Tanaka, T. Ichisaka, H. Aoki, T. Takeda-Kawaguchi, K. Iida, T. Kunisada, T. Shibata, S. Yamanaka, and K. Tezuka. 2010. Dental Pulp Cells for Induced Pluripotent Stem Cell Banking. *Journal of Dental Research*. 89:773-778.

Terrenoire, C., D. Simhaee, and R.S. Kass. 2007. Role of Sodium Channels in Propagation in Heart Muscle: How Subtle Genetic Alterations Result in Major Arrhythmic Disorders. *Journal of Cardiovascular Electrophysiology*. 18:900-905.

Terrenoire, C., K. Wang, K.W. Chan Tung, W.K. Chung, R.H. Pass, J.T. Lu, J.-C. Jean, A. Omari, K.J. Sampson, D.N. Kotton, G. Keller, and R.S. Kass. 2013. Induced pluripotent stem cells used to reveal drug actions in a long QT syndrome family with complex genetics. *The Journal of General Physiology*. 141:61-72.

Tohyama, S., F. Hattori, M. Sano, T. Hishiki, Y. Nagahata, T. Matsuura, H. Hashimoto, T. Suzuki, H. Yamashita, Y. Satoh, T. Egashira, T. Seki, N. Muraoka, H. Yamakawa, Y. Ohgino, T. Tanaka, M. Yoichi, S. Yuasa, M. Murata, M. Suematsu, and K. Fukuda. 2013. Distinct Metabolic Flow Enables Large-Scale Purification of Mouse and Human Pluripotent Stem Cell-Derived Cardiomyocytes. *Cell Stem Cell*. 12:127-137.

Tukkie, R., P. Sogaard, J. Vleugels, I.K.L.M. de Groot, A.A.M. Wilde, and H.L. Tan. 2004. Delay in Right Ventricular Activation Contributes to Brugada Syndrome. *Circulation*. 109:1272-1277.

Tulloch, N.L., V. Muskheli, M.V. Razumova, F.S. Korte, M. Regnier, K.D. Hauch, L. Pabon, H. Reinecke, and C.E. Murry. 2011. Growth of Engineered Human Myocardium with Mechanical Loading and Vascular Co-culture. *Circulation Research*. 109:47-59.

Uosaki, H., H. Fukushima, A. Takeuchi, S. Matsuoka, N. Nakatsuji, S. Yamanaka, and J.K. Yamashita. 2011. Efficient and Scalable Purification of Cardiomyocytes from Human Embryonic and Induced Pluripotent Stem Cells by VCAM1 Surface Expression. *PLoS ONE*. 6:e23657.

Ursitti, J.A., B.G. Petrich, P.C. Lee, W.G. Resneck, X. Ye, J. Yang, W.R. Randall, R.J. Bloch, and Y. Wang. 2007. Role of an alternatively spliced form of αII-spectrin in localization of connexin 43 in cardiomyocytes and regulation by stress-activated protein kinase. *Journal of Molecular and Cellular Cardiology*. 42:572-581.

Valdivia, C.R., D.J. Tester, B.A. Rok, C.-b.J. Porter, T.M. Munger, A. Jahangir, J.C. Makielski, and M.J. Ackerman. 2004. A trafficking defective, Brugada syndrome-causing SCN5A mutation rescued by drugs. 53-62 pp.

Vallecillo, G., S. Mojal, A. Roquer, D. Martinez, P. Rossi, F. Fonseca, R. Muga, and M. Torrens. 2013. Risk of QTc Prolongation in a Cohort of Opioid-Dependent HIV-Infected Patients on Methadone Maintenance Therapy. *Clinical Infectious Diseases*. 57:1189-1194.

van Bemmelen, M.X., J.-S. Rougier, B. Gavillet, F. Apothéloz, D. Daidié, M. Tateyama, I. Rivolta, M.A. Thomas, R.S. Kass, O. Staub, and H. Abriel. 2004. Cardiac Voltage-Gated Sodium Channel Nav1.5 Is Regulated by Nedd4-2 Mediated Ubiquitination. *Circulation Research*. 95:284-291.

Van Hoof, D., W. Dormeyer, S.R. Braam, R. Passier, J. Monshouwer-Kloots, D. Ward-van Oostwaard, A.J.R. Heck, J. Krijgsveld, and C.L. Mummery. 2010. Identification of Cell Surface Proteins for Antibody-Based Selection of Human Embryonic Stem Cell-Derived Cardiomyocytes. *Journal of Proteome Research*. 9:1610-1618.

van Rijen, H.V.M., D. Eckardt, J. Degen, M. Theis, T. Ott, K. Willecke, H.J. Jongsma, T. Opthof, and J.M.T. de Bakker. 2004. Slow Conduction and Enhanced Anisotropy Increase the Propensity for Ventricular Tachyarrhythmias in Adult Mice With Induced Deletion of Connexin43. *Circulation*. 109:1048-1055.

Vandenberg, J.I., M.D. Perry, M.J. Perrin, S.A. Mann, Y. Ke, and A.P. Hill. 2012. hERG K+ Channels: Structure, Function, and Clinical Significance. 1393-1478 pp.

Veerakul G1, N.K. 2012. Brugada syndrome: two decades of progress. *Circ J.* . 76:2713-2722.

Veldkamp, M.W., P.C. Viswanathan, C. Bezzina, A. Baartscheer, A.A.M. Wilde, and J.R. Balser. 2000. Two Distinct Congenital Arrhythmias Evoked by a Multidysfunctional Na+ Channel. *Circulation Research*. 86:e91-e97.

Venetucci, L., M. Denegri, C. Napolitano, and S.G. Priori. 2012. Inherited calcium channelopathies in the pathophysiology of arrhythmias. *Nat Rev Cardiol*. 9:561-575.

Verkerk, A.O., R. Wilders, E. Schulze-Bahr, L. Beekman, Z.A. Bhuiyan, J. Bertrand, L. Eckardt, D. Lin, M. Borggrefe, G. Breithardt, M.M. Mannens, H.L. Tan, A.A. Wilde, and C.R. Bezzina. 2005. Role of sequence variations in the human ether-a-go-go-related gene (HERG, KCNH2) in the Brugada syndrome. *Cardiovasc Res*. 68:441-453.

Villa, A., V. Foresti, and F. Confalonieri. 1995. Autonomic neuropathy and prolongation of QT interval in human immunodeficiency virus infection. *Clinical Autonomic Research*. 5:48-52.

Virág, L., N. Iost, M. Opincariu, J. Szolnoky, J. Szécsi, G. Bogáts, P. Szenohradszky, A. Varró, and J.G. Papp. 2001. The slow component of the delayed rectifier potassium current in undiseased human ventricular myocytes. 790-797 pp.

Volders, P.G.A., M.A. Vos, B. Szabo, K.R. Sipido, S.H.M. de Groot, A.P.M. Gorgels, H.J.J. Wellens, and R. Lazzara. 2000. Progress in the understanding of cardiac early afterdepolarizations and torsades de pointes: time to revise current concepts. 376-392 pp.

Wagner, S., L.S. Maier, and D.M. Bers. 2015. Role of Sodium and Calcium Dysregulation in Tachyarrhythmias in Sudden Cardiac Death. *Circulation Research*. 116:1956-1970.

Wagner, S., H.M. Ruff, S.L. Weber, S. Bellmann, T. Sowa, T. Schulte, M.E. Anderson, E. Grandi, D.M. Bers, J. Backs, L. Belardinelli, and L.S. Maier. 2011. Reactive Oxygen Species–Activated Ca/Calmodulin Kinase IIδ Is Required for Late INa Augmentation Leading to Cellular Na and Ca Overload. *Circulation Research*. 108:555-565.

Wang, D.W., N. Makita, A. Kitabatake, J.R. Balser, and A.L. George. 2000. Enhanced Na+ Channel Intermediate Inactivation in Brugada Syndrome. *Circulation Research*. 87:e37-e43.

Wang, T., J.J. Wei, D.M. Sabatini, and E.S. Lander. 2014a. Genetic Screens in Human Cells Using the CRISPR-Cas9 System. *Science*. 343:80-84.

Wang, Y., P. Liang, F. Lan, H. Wu, L. Lisowski, M. Gu, S. Hu, M.A. Kay, F.D. Urnov, R. Shinnawi, J.D. Gold, L. Gepstein, and J.C. Wu. 2014b. Genome Editing of Isogenic Human Induced Pluripotent Stem Cells Recapitulates Long QT Phenotype for Drug Testing. *Journal of the American College of Cardiology*. 64:451-459.

Watanabe, H., T.T. Koopmann, S. Le Scouarnec, T. Yang, C.R. Ingram, J.-J. Schott, S. Demolombe, V. Probst, F. Anselme, D. Escande, A.C.P. Wiesfeld, A. Pfeufer, S. Kääb, H.E. Wichmann, C. Hasdemir, Y. Aizawa, A.A.M. Wilde, D.M. Roden, and C.R. Bezzina. 2008. Sodium channel β1 subunit mutations associated with Brugada syndrome and cardiac conduction disease in humans. *The Journal of Clinical Investigation*. 118:2260-2268.

Wettwer, E., G.J. Amos, H. Posival, and U. Ravens. 1994. Transient outward current in human ventricular myocytes of subepicardial and subendocardial origin. *Circ Res*. 75:473-482.

Wilde, A.A.M., and E.R. Behr. 2013. Genetic testing for inherited cardiac disease. *Nat Rev Cardiol*. 10:571-583.

Xie, Y., D. Sato, A. Garfinkel, Z. Qu, and J.N. Weiss. 2010. So Little Source, So Much Sink: Requirements for Afterdepolarizations to Propagate in Tissue. *Biophysical Journal*. 99:1408-1415.

Xue, Y., X. Cai, L. Wang, B. Liao, H. Zhang, Y. Shan, Q. Chen, T. Zhou, X. Li, J. Hou, S. Chen, R. Luo, D. Qin, D. Pei, and G. Pan. 2013. Generating a non-integrating human induced pluripotent stem cell bank from urine-derived cells. *PLoS One*. 8:e70573.

Yamanaka, S., I. Zahanich, R.P. Wersto, and K.R. Boheler. 2008. Enhanced Proliferation of Monolayer Cultures of Embryonic Stem (ES) Cell-Derived Cardiomyocytes Following Acute Loss of Retinoblastoma. *PLoS ONE*. 3:e3896.

Yan, G.-X., W. Shimizu, and C. Antzelevitch. 1998. Characteristics and Distribution of M Cells in Arterially Perfused Canine Left Ventricular Wedge Preparations. *Circulation*. 98:1921-1927.

Yan, G.X., and C. Antzelevitch. 1999. Cellular basis for the Brugada syndrome and other mechanisms of arrhythmogenesis associated with ST-segment elevation. *Circulation*. 100:1660-1666.

Yanagita, T., H. Kobayashi, Y. Uezono, H. Yokoo, T. Sugano, T. Saitoh, S.-I. Minami, S. Shiraishi, and A. Wada. 2003. Destabilization of Nav1.7 Sodium Channel α-Subunit mRNA by Constitutive Phosphorylation of Extracellular Signal-Regulated Kinase: Negative Regulation of Steady-State Level of Cell Surface Functional Sodium Channels in Adrenal Chromaffin Cells. *Molecular Pharmacology*. 63:1125-1136.

Yap, Y.G., E.R. Behr, and A.J. Camm. 2009. Drug-induced Brugada syndrome. 989-994 pp.

Yazawa, M., B. Hsueh, X. Jia, A.M. Pasca, J.A. Bernstein, J. Hallmayer, and R.E. Dolmetsch. 2011. Using iPS cells to investigate cardiac phenotypes in patients with Timothy Syndrome. *Nature*. 471:230-234.

Ye, L., S. Zhang, L. Greder, J. Dutton, S.A. Keirstead, M. Lepley, L. Zhang, D. Kaufman, and J. Zhang. 2013. Effective cardiac myocyte differentiation of human induced pluripotent stem cells requires VEGF. *PLoS One*. 8:e53764.

Yu, J., K.F. Chau, M.A. Vodyanik, J. Jiang, and Y. Jiang. 2011. Efficient feeder-free episomal reprogramming with small molecules. *PLoS One*. 6:e17557.

Yu, J., M.A. Vodyanik, K. Smuga-Otto, J. Antosiewicz-Bourget, J.L. Frane, S. Tian, J. Nie, G.A. Jonsdottir, V. Ruotti, R. Stewart, I.I. Slukvin, and J.A. Thomson. 2007. Induced Pluripotent Stem Cell Lines Derived from Human Somatic Cells. *Science*. 318:1917-1920.

Yuan, W., K.S. Ginsburg, and D.M. Bers. 1996. Comparison of sarcolemmal calcium channel current in rabbit and rat ventricular myocytes. *The Journal of Physiology*. 493:733-746.

Zanella, F., R.C. Lyon, and F. Sheikh. 2014. Modeling heart disease in a dish: from somatic cells to disease-relevant cardiomyocytes. *Trends Cardiovasc Med*. 24:32-44.

Zhang, J., M. Klos, G.F. Wilson, A.M. Herman, X. Lian, K.K. Raval, M.R. Barron, L. Hou, A.G. Soerens, J. Yu, S.P. Palecek, G.E. Lyons, J.A. Thomson, T.J. Herron, J. Jalife, and T.J. Kamp. 2012. Extracellular matrix promotes highly efficient cardiac differentiation of human pluripotent stem cells: the matrix sandwich method. *Circ Res*. 111:1125-1136.

Zhang, J., G.F. Wilson, A.G. Soerens, C.H. Koonce, J. Yu, S.P. Palecek, J.A. Thomson, and T.J. Kamp. 2009. Functional Cardiomyocytes Derived from Human Induced Pluripotent Stem Cells. *Circulation Research*. 104:e30-e41.

Zhang, Q., J. Jiang, P. Han, Q. Yuan, J. Zhang, X. Zhang, Y. Xu, H. Cao, Q. Meng, L. Chen, T. Tian, X. Wang, P. Li, J. Hescheler, G. Ji, and Y. Ma. 2011. Direct differentiation of atrial and ventricular myocytes from human embryonic stem cells by alternating retinoid signals. *Cell Res*. 21:579-587.

Zhang, Z., Y. Xu, H. Song, J. Rodriguez, D. Tuteja, Y. Namkung, H.-S. Shin, and N. Chiamvimonvat. 2002. Functional Roles of Cav1.3 (α1D) Calcium Channel in Sinoatrial Nodes: Insight Gained Using Gene-Targeted Null Mutant Mice. *Circulation Research*. 90:981-987.

Zhou, J., H.-G. Shin, J. Yi, W. Shen, C.P. Williams, and K.T. Murray. 2002. Phosphorylation and Putative ER Retention Signals Are Required for Protein Kinase A-Mediated Potentiation of Cardiac Sodium Current. *Circulation Research*. 91:540-546.

Zhou, T., C. Benda, S. Dunzinger, Y. Huang, J.C. Ho, J. Yang, Y. Wang, Y. Zhang, Q. Zhuang, Y. Li, X. Bao, H.F. Tse, J. Grillari, R. Grillari-Voglauer, D. Pei, and M.A. Esteban. 2012. Generation of human induced pluripotent stem cells from urine samples. *Nat Protoc*. 7:2080-2089.

Zhou, Z., Q. Gong, B. Ye, Z. Fan, J.C. Makielski, G.A. Robertson, and C.T. January. 1998. Properties of HERG channels stably expressed in HEK 293 cells studied at physiological temperature. *Biophys J*. 74:230-241.

Zwi-Dantsis, L., and L. Gepstein. 2012. Induced pluripotent stem cells for cardiac repair. *Cell. Mol. Life Sci.* 69:3285-3299.

Etude de Maladies du Rythme Cardiaque à l'aide de Cellules Souches Pluripotentes Induites

Les troubles du rythme sont des maladies cardiaques fréquentes et sont une cause majeure de mort subite par anomalie de l'excitabilité du cœur. L'étude de ces dysfonctionnements est essentielle pour comprendre les mécanismes responsables de ces maladies cardiaques et mettre au point de nouveaux traitements. La technologie des cellules souches pluripotentes induites (iPS) permet de générer, à partir de cellules somatiques d'un patient, des cellules souches pluipotentes spécifiques de ce patient, qui peuvent ensuite être différenciées en tout type cellulaire, dont les cardiomyocytes. Lorsqu'elles sont obtenues à partir de patients souffrant d'un trouble du rythme, elles permettent la modélisation du trouble du rythme cardiaque du patient. Ce travail a permis la caractérisation moléculaire et fonctionnelle de troubles du rythme cardiaque génétiques héréditaires, syndrome du QT long et syndrome de Brugada, grâce à la différenciation en cardiomyocytes d'iPS provenant de patients atteints de ces arythmies.

Analysis of Heart Rhythm Disorders using Induced Pluripotent Stem Cells

Heart rhythm disorders are frequent heart diseases and are a major cause of sudden cardiac death from abnormal excitability of the heart. Studying these dysfunctions is essential to understand the mechanisms of these cardiac diseases and develop new treatments. The technology of induced pluripotent stem cells (iPS) allows generation, from a patient's somatic cells, of pluripotent stem cells specific for this patient, which can be differentiated in any type cell, including cardiomyocytes. When obtained from a patient suffering from an arrhythmic syndrome, these cells will thus allow the modeling of the patient's cardiac rhythm disorder. In this thesis, we characterized at molecular and functional levels, genetically inherited cardiac arryhthmias, long QT and Brugada syndrome (BrS), using cardiomyocytes differentiated from induced pluripotent stem cells derived from patients suffering from these genetically inherited arrhythmias.